UNIVERSITY OF CALIFORNIA,
IRVINE

A General Mixture Model for Nonlinear Heterogeneous Tumor Growth

DISSERTATION

submitted in partial satisfaction of the requirements
for the degree of

DOCTOR OF PHILOSOPHY

in Mathematics

by

Andrew Thomas

Dissertation Committee:
Professor John Lowengrub, Chair
Professor Jun Allard
Professor Frederic Wan

2017

DEDICATION

To my wife

TABLE OF CONTENTS

LIST OF FIGURES

LIST OF TABLES

ACKNOWLEDGMENTS

I would like to thank my advisor John Lowengrub. I have learned so much from him about what it means to be a mathematician and what it takes to do research. Without his guidance this thesis would not have been possible. I would also like to thank Huaming Yan for his invaluable support and time spent being a constant resource for the computational aspects of my work.

I am also indebted to the faculty and staff of the mathematics department for their help, support, and service. In particular, my committee members Jun Allard and Frederic Wan, who have provided many useful comments and suggestions and have taken the time to read my work.

I would also like to thank all my friends I have made in the mathematics department both past and present. They have been an integral part of my education and their support has been invaluable. Lastly, and most importantly, I want to thank my wife, Elizabeth Holmes. She has been very supportive of my work and my constant source of energy that kept me motivated. I can never repay her for all the sacrifices she has made and I will always be eternally grateful.

CURRICULUM VITAE

Andrew Thomas

EDUCATION

Doctor of Philosophy in Mathematics **2017**
Thesis Title:A General Mixture Model for Nonlinear Heterogeneous Tumor Growth
Advisor: John Lowengrub
University of California, Irvine *Irvine, CA*

Masters of Science in Mathematics **2009**
Thesis Title: On the Mean Curvature Flow
Advisor: Yu Ding
California State University, Long Beach *Long Beach, CA*

Bachelor of Arts in Mathematics **2007**
University of California, Berkeley *Berkeley, CA*

RESEARCH EXPERIENCE

Research Assistant **2014-2017**
University of California, Irvine *Irvine, CA*

TEACHING EXPERIENCE

Adjunct Professor **2016**
Orange Coast Community College *Costa Mesa, CA*

Teaching Assistant **2010–2017**
University of California, Irvine *Irvine, CA*

Teaching Assistant **2007–2009**
California State University, Long Beach *Long Beach, CA*

ACADEMIC HONORS

Pedagogical Fellowship	**2014-2015**
Nicholas Endowment Fellowship	**2012**

DEPARTMENTAL SERVICE

TA Training for Incoming Engineering Graduate Students	**2016**
TA Training for Incoming Mathematics Graduate Students	**2014, 20015**

ABSTRACT OF THE DISSERTATION

A General Mixture Model for Nonlinear Heterogeneous Tumor Growth

By

Andrew Thomas

Doctor of Philosophy in Mathematics

University of California, Irvine, 2017

Professor John Lowengrub, Chair

In this paper we develop a general mixture model that incorporates a non-constant water fraction. A novel energy for the system is devised that allows for different water levels to be considered in the host and viable cell regions. For the first time the energy provides a way to flux the water out of the necrotic core and produce stable tumor spheroids with liquid centers. The model is also capable of producing invasive tumors with a detailed morphology.

Parameter studies are performed to characterize the model. The parameters that can influence the size of the stable tumor and the growth rate are identified and the parameter regimes that can destabilize the tumor are explored. We demonstrate that this model is able to capture a wide range of tumor behavior.In particular, water fraction parameters for the host and viable cell regions allows us to consider the effects of different water fraction levels in the host and viable cell regions.

Finally, the non-constant water fraction model is extended to describe hierarchical structures that incorporate cancer stem cells. This model is capable of producing a detailed invasive morphology that has hierarchical and heterogeneous cell distributions and develops necrotic cores. The model is also capable of forming stable tumors with heterogeneous cell distributions. A parameter study on the positive and negative feedback rates for the stem cell differentiation rate shows how the morphology of the tumor is dependent on the sensitivity

to these parameters and possible avenues for therapy are seen.

Chapter 1

Introduction

1.1 Motivation

In 2012 about 14.1 million new cases of cancer were diagnosed globally [53, Ch.1.1] and it was responsible for 14.6 percent of all deaths or about 8.2 million deaths worldwide [53, Ch.1.3][52]. Of the 14.1 million new cases, 165,000 were children under 15 years of age [53, Ch.6.7]. Additionally, the financial cost of cancer worldwide has been estimated at 1.16 trillion US dollars per year. For the past several decades there has been extraordinary focus on understanding, identifying causes and developing effective treatments for cancer. However, as the numbers above suggest, there is still a considerable amount of work that needs to be done help eradicate this deadly disease.

At its most basic, cancer is a family of diseases that are marked by abnormal cell growth with the potential to spread to other parts of the body [53, 32]. In particular, ten characteristics of cancer have been proposed [25]:

1. Sustaining proliferative signaling

2. Evading growth suppressors
3. Avoiding immune destruction
4. Enabling replicative immortality
5. Tumor promoting inflammation
6. Activating invasion and metastasis
7. Inducing angiogensis
8. Genome instability and mutation
9. Resisting cell death
10. Deregulating cellular energetics.

The tumor microenvironment (stromal, immune, endothelial, and other accessory cells in the extracellular matrix) is now recognized as a facilitator of tumor growth and metastasis [24, 50]. Further, the recognition that tumors consist of heterogeneous compartments including stem cells, transit-amplifying or committed progenitor cells, and terminally differentiated cells has implicated both endogenous and exogenous signaling from the tumor microenviroment in promoting and maintaining the spatial heterogeneity that is optimal for tumor spread [64]. It is clear that cancer progression involves many events that occur at multiple time and space scales. Further, what occurs at the scale of molecules and the scale of cells effects the behavior of the tumor on the tissue scale. In order to understand how these different scales interact we employ mathematical models and simulations to study tumor behavior. In particular, the close connection between the tumor morphology and the cellular/molecular dynamics are studied in the hopes of determining the key factors involved in tumor progression. The ultimate goal of mathematical modeling of cancer is the prevention, early diagnosis, and effective treatment of this complex disease. Theory and simulations will

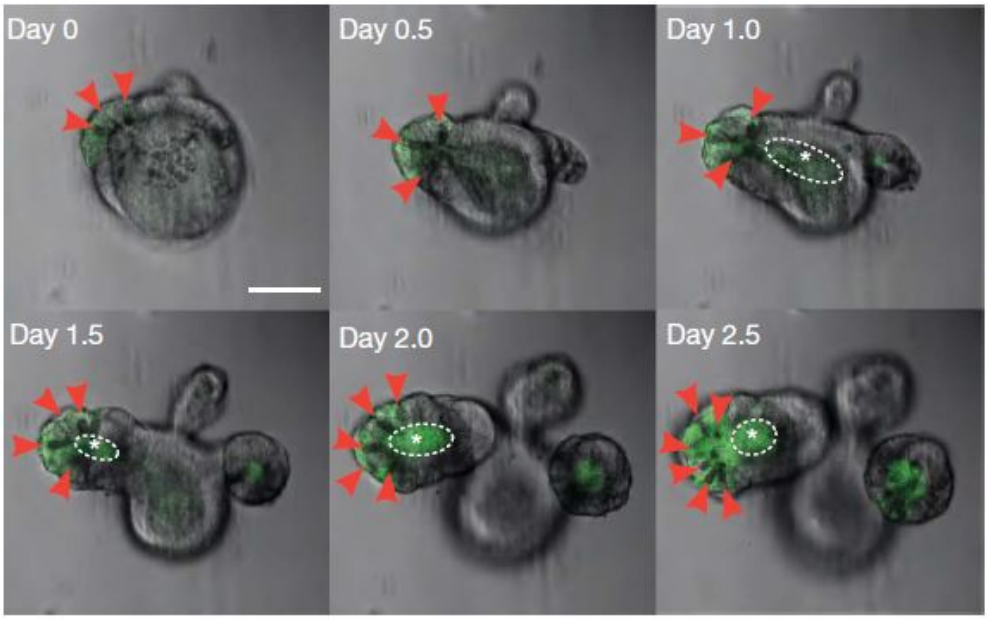

Figure 1.1: Time course of crypt organoid growth. Differential interference contrast image reveals granule containing Paneth cells (red arrowheads) at the site of budding where a new crypt forms. Lgr5GFP (green) stem cells expand at the crypt base in close proximity to Paneth cells. Asterisk and dotted oval indicate autofluorescence.[65] Scale bar: 50 mm.

help aid in developing individualized patient therapy that minimizes patient suffering and maximizes treatment effectiveness.

In addition, the same mathematical models that simulate cancer growth can also be used to model the morphology of healthy cells and tissues. In 2013 one of the runners up for breakthrough of the year in Science magazine was growing mini-organs from stem cells. One of the the organs they grew included a rudimentary human brain [40]. Once the cells were the size of an apple seed the cells at the core started to die out from lack of nutrients and formed a necrotic core. However, even at this size the researchers were able to gain insights into the brain disease microcephaly [40]. In the future the researchers hope to use these mini-organs and mathematical models as a way to investigate other diseases. A different set of experiments along the same lines has demonstrated that intestinal crypts (mini-guts) can be grown from a single stem cell [62, 65]. In figure 1.1 and figure 1.2 the evolution of an Lgr5 stem cell into a self-organized mini-gut is shown. Note the similarities here between

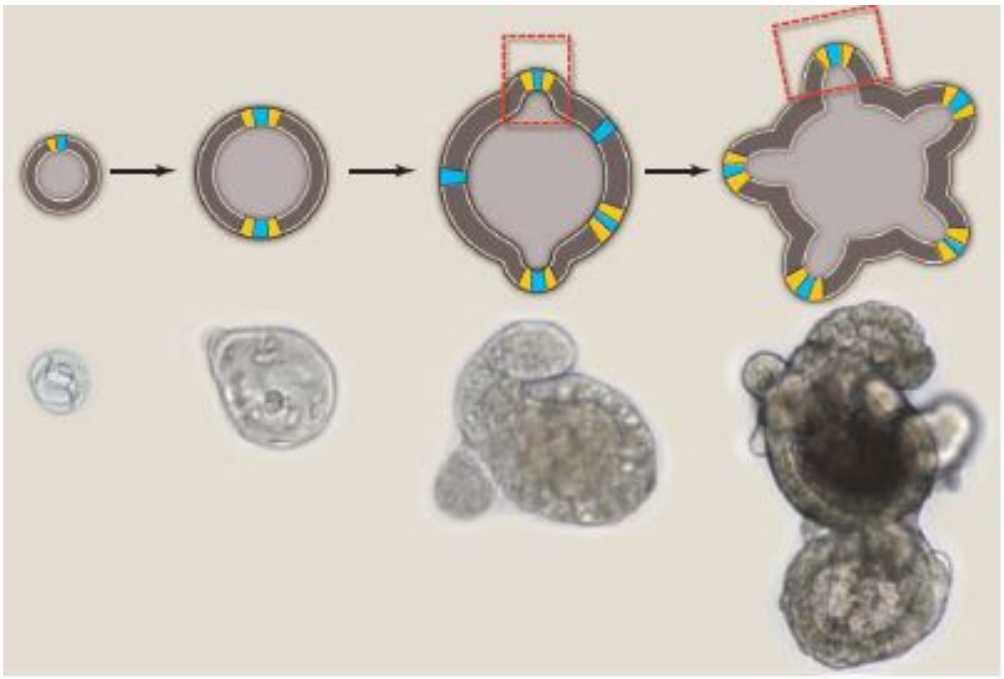

Figure 1.2: Time course of organoid growth. A single stem cell forms a symmetric cyst structure. The symmetry is broken by bud formation. The budding structure resembles a crypt. Lgr5+ CBC cells are depicted in yellow, and Paneth cells are shown in blue.[62]

avascular tumor growth and the evolution of mini-organs from stem as seen in figures (1.1) and (D.1). In particular, they have a strikingly similar morphology. This is because cancer cells typically use the same pathways and mechanisms as healthy cells to develop. The difference between the cancer tissue and healthy tissue is that the mechanisms that control growth in cancer are unregulated. Thus, the cancer models herein can also be used to model healthy organ tissue development by altering the model parameters to match the regulated healthy tissue. Protocols have already been established to grow human epithelial mini-guts from biopsies [65]. Because of this it is possible to obtain a "bio bank" and make a side by side comparison of the disease tissue with the healthy tissue. Then computational models can be used to try to bridge the gap between experiment and patient treatment and outcome. Thus the need to develop accurate and efficient mathematical models of tumor growth is clear.

1.2 Background

In this paper, a continuum model that treats the tumor as a collection of tissue cells is used. This approach uses principles from continuum mechanics to describe the variables as continuous fields by means of partial differential equations. The model variables include cell volume fractions or densities and cell substrate concentrations, e.g. nutrient, oxygen and growth factors. Although continuum models are appropriate at the tissue scale where gross tumor behavior can be quantified, the limitations in scale prevents such models from simulating individual cells and discrete events. This may be important when studying the effect of genetic, cellular and microenvironment characteristics on overall tumour behaviour. Discrete models can translate biological processes into model rules more easily than the continuum approach but, they can be difficult to study analytically and the computational costs increases rapidly as the number of cells modeled grows. In general it is difficult to simulate a tumor greater than 1mm in size using discrete models. For larger scale systems, such as the one considered here, the continuum model is more appropriate and in particular, the continuum mixture models are capable of simulating the details of the interactions among cell species. A combination of these two, known as hybrid continuum-discrete models, are promising and have the potential to combine the best features of both the models. However, more work is necessary to make these hybrid models competitive with the continuum models at large scales and is the subject of ongoing work. For more information about discrete and continuum models consult [34].

The model presented here is an adaptation of the model presented in [71, 23]. This model is a diffuse interface continuum model of multispecies tumor growth. In the diffuse interface approach the sharp interfaces are replaced by narrow transition layers that arise from the different adhesive forces among the cell species. This approach eliminates the need to enforce complicated boundary conditions across the tumor/host interface that would have to be satisfied if the interface were sharp. Additionally, the diffuse interface approach eliminates

the need to explicitly track the boundary as in the sharp interface case. The diffuse interface model is related to recently developed multicomponent mixture models [3, 8]. The model is well posed and involves fourth order nonlinear advection-reaction-diffusion equation of Cahn-Hillard type for the cell species volume fractions coupled with reaction-diffusion equations for the substrates. Until recently the numerical simulations of mixture models have been limited to one-dimension or symmetric tumor configurations [15]. This is due largely to the complicated governing nonlinear partial differential equations and the fact that some of the equations that regulate the adhesive forces are unregularized backwards diffusion equations that may lead to ill-posedness. This is problematic in higher dimensions where the spatial discretization may lead to false instabilities. In this paper, the approach to deriving the model is based on energy variation. The energy variation is used to derive the appropriate diffuse interface equations that account for all the cell species interactions that are modeled. This model is also thermodynamically consistent and capable of giving a detailed description of tumor progression. The main focus in this model is on interactions between the species and it leads to a well-posed fourth order nonlinear partial differential equation that eliminates the problem of the previous mixture models. This model also accounts for hydrostatic pressure and the cell velocity is found through a generalized Darcy's law. It is possible to account for elastic and viscolastic effects [47, 59] by incorporating the relevant energies in the system energy and performing energy variation [4]. This is an avenue for possible future work. We also include the spatiotemporally heterogeneous growth factors supplied by the microenvironment. Further, we incorporate the nonhomogeneous interstitial fluid fraction found in the tumor microenvironment.

In previous works [23, 71] the fluid fraction in the system is treated as constant with zero flux. This is done to greatly simplify the computations and the analysis of the model. However, there are several reasons the consider a non-constant water fraction. The primary reason is to make the simulations more consistent with the underlying biology. For example, the water fraction in the necrotic core of the tumor is generally much higher than in the viable region

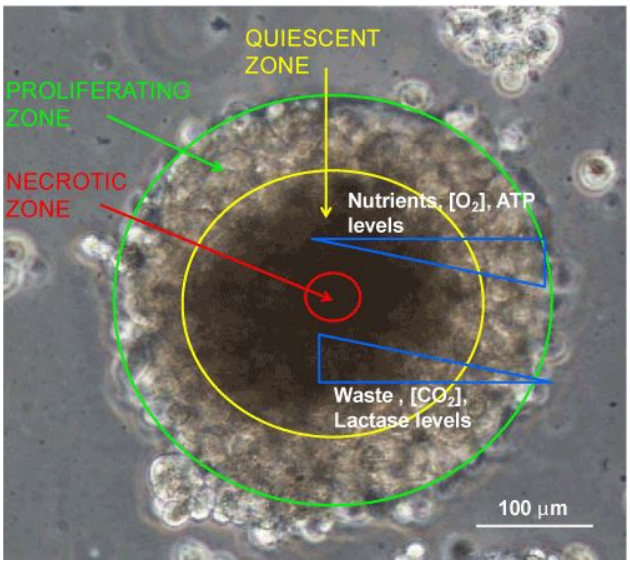

Figure 1.3: In vitro tumor spheroid [11]

and surrounding tissue (see figure 1.3). In the necrotic core the dead cells are degrading and the extracellular fluid is being released. Further, there are no viable cells in the core that uptake the water fraction. Thus, to capture the fluid distribution in a solid tumor a non-constant water fraction is necessary.

Secondly, the interstitial fluid fraction is known to play a crucial role in tumor development and treatment [46, 35]. The the composition of the fluid in tumor is significantly different than the fluid in host tissue due to the absence of a well defined lymphatic network. This unordered structure is produced by the tumors rapid proliferation and results in higher interstitial fluid pressure and diffusion rates compared to the host tissue. These differences have important consequences for the treatment of tumors. Approximately 85% of human cancer involves solid tumors and current therapies depend on the delivery of the agents to the tumor [58, 73]. However, high fluid pressure inside the tumor and heterogeneous fluid levels impede the delivery and transport of agents to the viable rim of the tumor. The concentration of the drug is highest closest to the rim of the tumor but very little of the drug reaches 90% of the tumor and if any of the cancer cells remain the tumor can eventually regrow [61, 22]. Therefore, it is important to incorporate the fluid fraction into previous

tumor models to investigate drug delivery mechanisms.

It is also useful to consider a non-constant water fraction when considering tumor development in different tissue types. In particular, once the tumor is advanced enough to metastasize, a secondary tumor will develop at a secondary site that could have a different level of interstitial fluid than the primary site. For instance, hepatic cancer can metastasize and migrate to the brain which would have a higher water fraction or it could migrate to bone which would have a lower water fraction that the original host tissue. It is clear that different water fractions and densities of the host tissues can impact the growth rates and morphologies of tumors [54]. A non-constant water fraction provides the necessary framework to begin exploring these different cases. A particularly important case we can now consider is growing tumor spheroids in-vitro. Tumor spheroids provide an alternative way to study tumors that is realistic and biologically meaningful without the complexity and cost of in-vivo whole organism approaches [2, 44]. We will see that the non-constant water faction model that is developed here is capable of producing stable tumor spheroids. Thus, the in-vitro case will give a way to calibrate the model and perform the necessary validation to begin applying the results in a clinical setting.

The non-constant water fraction model developed in this paper also allows us to extend the model given in [23]. This extension considers the viable cells of the tumor as a composition of cells at different stages of differentiation. Tumor cells as well as healthy tissue cells progress through lineage stages. The existence of cancer stem cells, or the cells capable of initiating cancer, was first demonstrated in leukemia by showing that transplanting only a certain type of cell consistently resulted in leukemia in healthy animals [18, 6]. Stem cells have also been located in the solid tumors of other cancers [16, 13, 30]. A cell lineage is a set of progenitor-progeny relationships such that progressive changes in cell character occur. The lineage can be traced back to the self-perpetuating stem cell and ends with the terminally differentiated cells that either divides slowly compared to its lifespan or doesn't divide at all. In between,

there are committed progenitor cells or transit-amplifying cells. Every population of dividing cell at a given stage in the lineage has a parameter P that gives the fraction of daughter cells that remain at the same lineage stage after division. If $P = 0.5$ then the populations of the cell lineage would stay the same, this is characteristic of stem cells. If $P < 0.5$ then the lineage will eventually die out, this is characteristic of committed progenitor cells.

It has been demonstrated that the growth and division of the stem cells and committed progenitor cells are controlled by feedback signals [7]. In particular, the control of the cell population involves feedback loops that determine mitosis rates and the self-renewal fraction P [72, 38]. For instance, TGF-β factors have been shown to decrease self-renewal and differentiation rates of stem cells in cancerous and healthy tissues [48]. Other factors, such as Wnts, Notch, Shh, and FGF upregulate stem and committed progenitor cell renewal and proliferation rates in healthy and cancerous tissue [39]. The relationship between the feedback factors and the cell lineages in this model are seen in figure 1.4. Using mathematical models it was shown that the feedback regulation of the P values by more differentiated cells explains many tissue behaviors such as regeneration of tissue in response to injury and insensitivity of tissue size to perturbations in P [41, 43]. Further, these models suggest that feedback mechanisms are the reason why stem and committed progenitor cell behaviors emerge in tissue. Thus it is of crucial importance to incorporate these feedback factors and cell lineages into the modeling of cancer. We will show in chapter 6 that the non-constant water fraction model extended to include the cancer stem cells and their progeny is capable of produces tumors that develop necrotic cores and an invasive morphology.

This thesis is organized as follows, in chapter 2 the mixture model is derived where all the species are assumed to be non-constant. The derivation is similar in nature to the one presented in [71]. The main contribution in this chapter is the new choice of the energy for the system that governs the flux and velocity of the species. New terms are introduced to enforce the water fractions in the host and the viable cells. We also propose a way to model

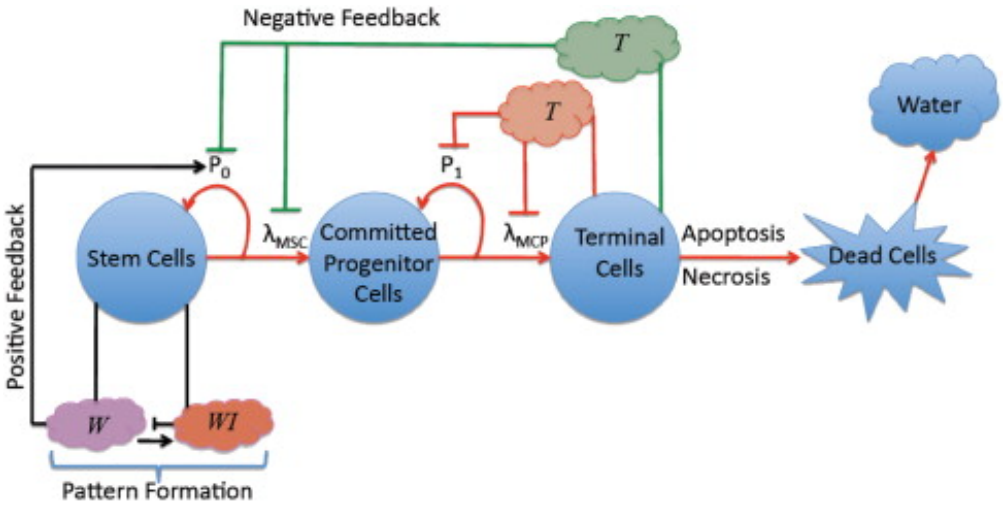

Figure 1.4: A schematic of a cell lineage with positive and negative feedback factors affecting the self-renewal and mitosis rates of cancer stem cells and committed progenitor cells. Terminally differentiated cells produce soluble factors T that reduce the self-renewal fraction and mitosis rates of less differentiated cells (e.g. members of TGFb family). Note that the T factors that act on the committed progenitor and stem cells may be different [21, 72]. Additional feedback factors W produced by cancer stem cells (e.g. Wnt) promote self-renewal and increase mitosis rates of cancer stem cells. The self-renewing promoters may also be inhibited by other factors WI (e.g. Dkk, SFRPs), which can lead to pattern formation and spatiotemporally heterogeneous cell distributions.

the fluid flux out of the necrotic core that produces stable tumors. In chapter 3 we analyze the behavior of the model for a fixed set of parameters that constitute the base case for the remainder of the paper. We consider tumor evolution from a symmetric initial condition and from and non-symmetric initial conditions. In the symmetric case we see the tumor forms a stable tumor spheroid and the non-symmetric case elongates and develops typical invasive behaviors. In chapter 4 a parameter study is performed on the model with a symmetric initial condition. We investigate how the physical and model parameters can impact the growth of the tumor and the size of the stable spheroids. The parameter regimes that produce an unstable tumor are also investigated. In chapter 5 is a similar parameter variation performed on the model with a non-symmetric initial condition. We determine which parameters affect the growth and morphology of the tumor. Parameters that can stabilize the non-symmetric tumor or increase the invasiveness of the tumor are given special attention. In chapter 6 the non-constant water fraction model developed here is extended to incorporate the cancer stem cells in a similar fashion as [23]. We show that this model can produce invasive tumors that are also capable of developing a necrotic core. In chapter 7 the main contributions of this work are summarized and future work is discussed.

Chapter 2

Model Equations

2.1 Mass Conservation Equation

We begin by formulating the mass conservation equations for a general multispecies model that accounts for the mass/momentum exchange interactions among the different species. The primary variables in the $(N+1)$-species model are, the volume fractions of the cell species $\phi_0, \ldots, \phi_N$, the densities of the components $\rho_0, \ldots, \rho_N$, and the component velocities $\mathbf{u}_0, \ldots, \mathbf{u}_N$.

We assume that the densities are constant and there are no voids in the tissue. This last condition implies the sum of the volume fractions is 1. Without loss of generality we may let ϕ_0 be the water component and ϕ_N be the host component. The volume fractions are assumed to be continuous in a domain Ω that contains both the tumor and host.

Now we derive the equation that determines the evolution of the cell species. Let m_i be the mass of cell-species i inside some imaginary surface S and let $\mathbf{j}_i$ be the flux of the cells

through the surface S. The mass m_i can be written in terms of the dependent variables as

$$m_i = \iiint_V \phi_i \rho_i dV.$$

The only way to introduce to increase the mass of the i-species in the surface S is for additional ϕ_i to flux into the surface or for ϕ_i to be created inside the region. We know the surface integral of the flux over the surface S is equal to the rate of cells passing through the surface S. Thus, the continuity equation reads

$$\frac{dm_i}{dt} + \iint_S \mathbf{j}_i \cdot d\mathbf{S} = \Sigma_i \tag{2.1}$$

where Σ_i is the rate that m_i is generated inside V. By the divergence theorem we can write the surface integral as $\iint_S \mathbf{j}_i \cdot d\mathbf{S} = \iiint_V \nabla \cdot \mathbf{j}_i dV$. Therefore, we have

$$\iiint_V \frac{\partial \phi_i \rho_i}{\partial t} dV + \iiint_V \nabla \cdot \mathbf{j}_i dV = \Sigma_i$$

where $\Sigma_i = \iiint_V S_i dV$. Hence the differential form of (2.1) is

$$\frac{\partial \phi_i \rho_i}{\partial t} + \nabla \cdot \mathbf{j}_i = S_i.$$

Next, we suppose the two sources of cell flux are the diffusive flux and the advective flux. We can write the advective flux as

$$\mathbf{j}_{adv} = \mathbf{u}_i \phi_i \rho_i$$

where $\mathbf{u}_i$ is the velocity of the species. We write the flux term as

$$\mathbf{j}_i = \mathbf{J}_i + \mathbf{u}_i \phi_i \rho_i$$

where $\mathbf{J}_i$ is the diffusion term. Therefore each cell type can be determined by the following conservation equation,

$$\rho_i \left(\frac{\partial \phi_i}{\partial t} + \nabla \cdot (\mathbf{u}_i \phi_i) \right) = -\nabla \cdot \mathbf{J}_i + S_i \tag{2.2}$$

with the Neumann boundary condition

$$\omega_\infty \cdot \nabla \phi_i = 0. \tag{2.3}$$

Here equation (2.2) is on a domain Ω with boundary Σ_∞ and ω_∞ is the outward normal vector on the boundary Σ_∞. The $\mathbf{J}_i$'s are the fluxes that account the mechanical interactions among the cell species. Define the density of the mixture as $\rho = \sum_{i=0}^{N} \rho_i \phi_i$ and define the mass averaged velocity of the mixture as $\mathbf{u} = \frac{1}{\rho} \sum_{i=0}^{N} \rho_i \phi_i \mathbf{u}_i$. Summing equation (2.2) from 0 to N we see

$$\frac{\partial \rho}{\partial t} + \nabla \cdot (\mathbf{u}\rho) = -\sum_{i=0}^{N} \nabla \cdot \mathbf{J}_i + \sum_{i=0}^{N} S_i.$$

So the mass is conserved only if $-\sum_{i=0}^{N} \nabla \cdot \mathbf{J}_i + \sum_{i=0}^{N} S_i = 0$. Therefore we impose the condition

$$\sum_{i=0}^{N} \mathbf{J}_i = 0 \tag{2.4}$$

$$\sum_{i=0}^{N} S_i = 0 \tag{2.5}$$

as a consistency constraint for the fluxes and sources. Note that we could make $\sum_{i=0}^{N} \mathbf{J}_i = C$ for some constant C and for simplicity we let $C = 0$. In the next section we introduce an energy to motivate our choices for the flux terms and the component velocities.

2.2 Energy

In order to determine the generalized diffusion terms and the velocities of the components we follow [71] and consider the energy for the system. The energy we consider focuses on interactions between the species. We do not consider elastic and viscoelastic effects here. The diffusion and velocity terms will be chosen to decrease the energy of the system so it is thermodynamically consistent. That is, the free energy functional derived below is non-increasing in time which is equivalent to nondecreasing entropy in an isothermal system. To describe the energy associated with the interactions among the different components we introduce the Helmholtz free energy of component interactions as in [60]. This is a thermodynamic potential that measures the useful work obtainable from a closed thermodynamic system at a constant temperature. We define the energy of each component as

$$E_i = U_i - \theta s_i$$

where U_i is the energy that results from interaction forces between the ith component and the other components, s_i is the entropy of mixing, and θ is the temperature of the system which is assumed to be constant. Introducing the interaction potential U_{ij} between the ith and jth conponents, we can write

$$U_i = \frac{1}{2}\sum_{j\neq i}\iint U_{ij}(x-y)\phi_i(x)\phi_j(y)d\mathbf{x}d\mathbf{y}$$

and the entropy can be written as

$$s_i = -R\int \phi_i \log\left(\frac{1}{\phi_i}\right) d\mathbf{x}$$

where R is a fixed constant [60]. Thus the free energy of adhesion of the ith component is given by

$$E_i = \iint \frac{1}{2} \sum_{j \neq i} U_{ij}(x-y)\phi_i(x)\phi_j(y)d\mathbf{x}d\mathbf{y} + R\theta \int \phi_i \log(\phi_i)d\mathbf{x}.$$

The total energy of the system is $E = \sum_{i=0}^{N} E_i$. For simplicity assume that $U_{ij} = U_{ji}$ and supposed that U_{ij} is radially symmetric and localized (i.e., $U_{ij} = \epsilon_{ij}^{-d} U_{ij}\left(\frac{|x|}{\epsilon_{ij}}\right)$ were d is the dimension). Thus,

$$E_i = \iint \sum_{j \neq i} \epsilon_{ij}^{-d} U_{ij}\left(\frac{|x-y|}{\epsilon_{ij}}\right)\phi_i(x)\phi_j(y)d\mathbf{x}d\mathbf{y} + R\theta \int \phi_i \log(\phi_i)d\mathbf{x}.$$

Let $z = \frac{x-y}{\epsilon_{ij}}$, then the first term is

$$\iint \sum_{j \neq i} U_{ij}\left(|z|\right)\phi_i(\epsilon_{ij}z + y)\phi_j(y)d\mathbf{z}d\mathbf{y}.$$

Taking the Taylor expansion for ϕ_i about ϵ_{ij} gives

$$\iint \sum_{j \neq i} U_{ij}\left(|z|\right)\Big[\phi_i(y) + \epsilon_{ij}\nabla\phi_i(y)\cdot z + \frac{\epsilon_{ij}^2}{2} z^T\nabla^2\phi_i(y)z + \frac{\epsilon_{ij}^3}{6}\nabla^3\phi_i(y)z^3 + O(\epsilon_{ij}^4))\Big]\phi_j(y)d\mathbf{z}d\mathbf{y}.$$

Next using the radial symmetry and dropping the $O(\epsilon_{ij}^4)$ term we get

$$\iint \sum_{j \neq i} U_{ij}\left(|z|\right)\left[\phi_i(y) + \frac{\epsilon_{ij}^2}{2} z^T\nabla^2\phi_i(y)z)\right]\phi_j(y)d\mathbf{z}d\mathbf{y}.$$

Let

$$U_{ij}^0 = \int U_{ij}(|z|)d\mathbf{z}$$
$$U_{ij}^1 = \int U_{ij}(|z|)|z|^2 d\mathbf{z}.$$

Thus we get

$$E_i = \int \sum_{j\neq i} U_{ij}^0 \phi_i(y)\phi_j(y) + \frac{\epsilon_{ij}^2}{2} U_{ij}^1 \nabla^2\phi_i(y)\phi_j(y)d\mathbf{y} + R\theta\phi_i(y)\log(\phi_i(y))d\mathbf{y}.$$

Integrating by parts we find,

$$E_i = \int \sum_{j\neq i} U_{ij}^0 \phi_i(y)\phi_j(y) - \frac{\epsilon_{ij}^2}{2} U_{ij}^1 \nabla\phi_i(y)\cdot\nabla\phi_j(y) + R\theta\phi_i(y)\log(\phi_i(y))d\mathbf{y}.$$

Now we consider the term $A_i = \sum_{j\neq i} -\frac{\epsilon_{ij}^2}{2} U_{ij}^1 \nabla\phi_i(y)\cdot\nabla\phi_j(y)$ and define $\bar{\epsilon}_{ij}^2 = \epsilon_{ij}^2 U_{ij}^1$ (we drop the bar notation). We first consider the A_0 term,

$$\begin{aligned} A_0 &= -\sum_{i=1}^{N} \frac{\epsilon_{0i}^2}{2}\nabla\phi_0\cdot\nabla\phi_i = -\sum_{i=1}^{N-1} \frac{\epsilon_{0i}^2}{2}\nabla\phi_0\cdot\nabla\phi_i + \frac{\epsilon_{0N}^2}{2}\sum_{i=0}^{N-1}\nabla\phi_0\cdot\nabla\phi_i \\ &= \sum_{i=1}^{N-1}\left(\frac{\epsilon_{0N}^2}{2} - \frac{\epsilon_{0i}^2}{2}\right)\nabla\phi_0\cdot\nabla\phi_i + \frac{\epsilon_{0N}^2}{2}\nabla\phi_0\cdot\nabla\phi_0 \end{aligned}$$

where the second equality is from $1 = \sum_{i=0}^{N}\phi_i$. Now we let $\epsilon_{0N} = \epsilon_0$ and $\epsilon_{0i} = \epsilon_0$ for $1 \leq i \leq N-1$. This choice of epsilons eliminates the non-squared terms. Thus,

$$A_0 = \frac{\epsilon_0^2}{2}|\nabla\phi_0|^2.$$

Similarly, for the A_N term,

$$A_N = -\sum_{i=0}^{N-1} \frac{\epsilon_{Ni}^2}{2} \nabla\phi_N \cdot \nabla\phi_i = -\sum_{i=1}^{N-1} \frac{\epsilon_{Ni}^2}{2} \nabla\phi_N \cdot \nabla\phi_i + \frac{\epsilon_{N0}^2}{2} \sum_{i=1}^{N} \nabla\phi_N \cdot \nabla\phi_i$$
$$= \sum_{i=1}^{N-1} \left(\frac{\epsilon_{N0}^2}{2} - \frac{\epsilon_{Ni}^2}{2} \right) \nabla\phi_N \cdot \nabla\phi_i + \frac{\epsilon_{N0}^2}{2} \nabla\phi_N \cdot \nabla\phi_N$$

where the second equality is again from $1 = \sum_{i=0}^{N} \phi_i$. Now we let $\epsilon_{N0} = \epsilon_N$ and $\epsilon_{Ni} = \epsilon_N$ for $1 \leq i \leq N-1$. This choice of epsilons also eliminates the non-squared terms. Thus,

$$A_N = \frac{\epsilon_N^2}{2} |\nabla\phi_N|^2.$$

For the intermediate terms we calculate,

$$A_i = \sum_{j=0, j\neq i}^{N} -\frac{\epsilon_{ij}^2}{2} \nabla\phi_i \cdot \nabla\phi_j = \sum_{j=0, j\neq i}^{N-1} -\frac{\epsilon_{ij}^2}{2} \nabla\phi_i \cdot \nabla\phi_j + \sum_{j=0}^{N-1} \frac{\epsilon_{iN}^2}{2} \nabla\phi_i \cdot \nabla\phi_j.$$

Now let $\epsilon_{iN} = \epsilon_{i0} = \epsilon_T$ and $\epsilon_{ij} = 0$ for $1 \leq j \leq N-1$. Therefore,

$$A_i = \frac{\epsilon_T^2}{2} \nabla\phi_i \cdot \nabla\phi_T, \text{ for } 1 \leq i \leq N-1.$$

The choice of epsilons is equivalent to keeping only the squared terms and considering the tumor as single component instead of as the sum of different cell species. Note that,

$$\sum_{i=1}^{N-1} A_i = \frac{\epsilon_T^2}{2} |\nabla\phi_T|^2.$$

With this simplification we obtain the following nonlocal model of the Helmholtz free energy,

$$E = \sum_{i=0}^{N} E_i$$

where the ith component is given by,

$$\begin{aligned} E_0 &= \int \left(F_0(\phi_0, \ldots, \phi_N) + \frac{\epsilon_0^2}{2} |\nabla \phi_0|^2 \right) dx \\ E_i &= \int \left(F_i(\phi_0, \ldots, \phi_N) + \frac{\epsilon_T^2}{2} \nabla \phi_i \cdot \nabla \phi_T \right) dx, \text{ for } 1 \leq i \leq N-1 \\ E_N &= \int \left(F_N(\phi_0, \ldots, \phi_N) + \frac{\epsilon_N^2}{2} |\nabla \phi_N|^2 \right) dx. \end{aligned} \tag{2.6}$$

The first term models the bulk energy of the components due to local interactions while the gradient terms model longer range interactions.

2.2.1 Model Derivation

Next we take the time derivative of the energy to get

$$\begin{aligned} \frac{dE}{dt} = &\sum_{i=0}^{N} \frac{dE_i}{dt} = \int_\Omega \left(\sum_{i=0}^{N} \sum_{j=0}^{N} \frac{\partial F_i}{\partial \phi_j} \frac{\partial \phi_j}{\partial t} + \epsilon_0^2 \nabla \phi_0 \cdot \nabla \frac{\partial \phi_0}{\partial t} \right. \\ &\left. + \epsilon_T^2 \nabla \phi_T \cdot \nabla \frac{\partial \phi_T}{\partial t} + \epsilon_N^2 \nabla \phi_N \cdot \nabla \frac{\partial \phi_N}{\partial t} \right) dx. \end{aligned}$$

Integrating by parts we get,

$$\begin{aligned} \frac{dE}{dt} = &\int_\Omega \left(\left(\sum_{i=0}^{N} \frac{\partial F_i}{\partial \phi_0} - \epsilon_0^2 \nabla \cdot \nabla \phi_0 \right) \frac{\partial \phi_0}{\partial t} + \sum_{j=1}^{N-1} \left(\sum_{i=0}^{N} \frac{\partial F_i}{\partial \phi_j} - \epsilon_T^2 \nabla \cdot \nabla \phi_T \right) \frac{\partial \phi_j}{\partial t} \right. \\ &\left. + \left(\sum_{i=0}^{N} \frac{\partial F_i}{\partial \phi_N} - \epsilon_N^2 \nabla \cdot \nabla \phi_N \right) \frac{\partial \phi_N}{\partial t} \right) dx + \sum_{i=0}^{N} \int_{\partial \Omega} \left(\epsilon_0^2 \frac{\partial \phi_0}{\partial t} \nabla \phi_0 \cdot \omega_\infty \right. \\ &\left. + \epsilon_T^2 \frac{\partial \phi_T}{\partial t} \nabla \phi_T \cdot \omega_\infty + \epsilon_N^2 \frac{\partial \phi_N}{\partial t} \nabla \phi_N \cdot \omega_\infty \right) ds. \end{aligned}$$

Note the boundary terms are zero by (2.3). Define

$$\begin{aligned}
\frac{\delta E_i}{\delta \phi_0} &= \frac{\partial F_i}{\partial \phi_0} - \frac{\epsilon_0^2}{N} \nabla \cdot \nabla \phi_0 \\
\frac{\delta E_i}{\delta \phi_j} &= \frac{\partial F_i}{\partial \phi_j} - \frac{\epsilon_T^2}{N} \nabla \cdot \nabla \phi_T, \quad 1 \leq j \leq N-1 \\
\frac{\delta E_i}{\delta \phi_N} &= \frac{\partial F_i}{\partial \phi_N} - \frac{\epsilon_N^2}{N} \nabla \cdot \nabla \phi_N \\
\frac{\delta E}{\delta \phi_j} &= \sum_{i=0}^{N} \frac{\delta E_i}{\delta \phi_j}.
\end{aligned}$$

Thus,

$$\frac{dE}{dt} = \sum_{j=0}^{N} \int_\Omega \frac{\delta E}{\delta \phi_j} \frac{\partial \phi_j}{\partial t} dx.$$

Using equation (2.2) with $S_i = 0$ we see

$$\frac{dE}{dt} = -\sum_{j=0}^{N} \int_\Omega \frac{\delta E}{\delta \phi_j} \left(\frac{1}{\rho_j} \nabla \cdot \mathbf{J}_j + \nabla \cdot (\mathbf{u}_j \phi_j) \right) dx.$$

Integrating by parts again,

$$\frac{dE}{dt} = \sum_{j=0}^{N} \left(\int_\Omega \phi_j \nabla \frac{\delta E}{\delta \phi_j} \cdot \mathbf{u}_j + \nabla \left(\frac{1}{\rho_j} \frac{\delta E}{\delta \phi_j} \right) \cdot \mathbf{J}_j dx - \int_{\partial \Omega} \frac{\delta E}{\delta \phi_j} \left(\frac{1}{\rho_j} \mathbf{J}_j + \mathbf{u}_j \phi_j \right) \cdot \omega_\infty ds \right).$$

Choose the boundary conditions such that the last term is zero. Now we can sum from $0 \leq j \leq N$ over equation (2.2) and see

$$\sum_{j=0}^{N} \nabla \cdot (\mathbf{u}_j \phi_j) + \sum_{j=0}^{N} \frac{1}{\rho_j} \nabla \cdot \mathbf{J}_j = 0.$$

Hence we can introduce a function $\tilde{p}$ such that

$$\sum_{j=0}^{N} \int_{\Omega} \nabla \tilde{p} \left(\mathbf{u}_j \phi_j + \frac{1}{\rho_j} \mathbf{J}_j \right) dx = 0. \tag{2.7}$$

Therefore adding these terms won't change the energy. So,

$$\frac{dE}{dt} = \sum_{j=0}^{N} \int_{\Omega} \phi_j \nabla \left(\frac{\delta E}{\delta \phi_j} + \tilde{p} \right) \cdot \mathbf{u}_j + \nabla \left(\frac{1}{\rho_j} \frac{\delta E}{\delta \phi_j} + \frac{1}{\rho_j} \tilde{p} \right) \cdot \mathbf{J}_j dx.$$

Further, we supposed that $\mathbf{J}_N = -\sum_{j=0}^{N-1} \mathbf{J}_j$. Hence we need to add some terms to remove $\mathbf{J}_N$ from the above equation. Thus,

$$\begin{aligned} \frac{dE}{dt} = & \int_{\Omega} \sum_{j=0}^{N} \phi_j \nabla \left(\frac{\delta E}{\delta \phi_j} + \tilde{p} \right) \cdot \mathbf{u}_j \\ & + \sum_{j=0}^{N-1} \nabla \left(\frac{1}{\rho_j} \frac{\delta E}{\delta \phi_j} - \frac{1}{\rho_N} \frac{\delta E}{\delta \phi_N} + \left(\frac{1}{\rho_j} - \frac{1}{\rho_N} \right) \tilde{p} \right) \cdot \mathbf{J}_j dx. \end{aligned} \tag{2.8}$$

We will choose $\mathbf{u}_j$ and $\mathbf{J}_j$ to decrease the energy. Now consider the velocity terms and suppose all the non-liquid and non-dead species move with the same velocity. That is all species but the dead cells and water move with velocity $\mathbf{u}_j = \mathbf{u}_s$ for $j \geq 2$. Also let ϕ_1 be the volume fraction for the dead cells. The first term gives

$$\begin{aligned} & \sum_{j=0}^{N} \int_{\Omega} \left(\phi_j \nabla \left(\frac{\delta E}{\delta \phi_j} + \tilde{p} \right) \cdot \mathbf{u}_j dx \right) = \int_{\Omega} \phi_0 \nabla \left(\frac{\delta E}{\delta \phi_0} + \tilde{p} \right) \cdot \mathbf{u}_0 dx \\ & + \int_{\Omega} \phi_1 \nabla \left(\frac{\delta E}{\delta \phi_1} + \tilde{p} \right) \cdot \mathbf{u}_1 dx + \sum_{j=2}^{N} \int_{\Omega} \left(\phi_j \nabla \left(\frac{\delta E}{\delta \phi_j} + \tilde{p} \right) \cdot \mathbf{u}_s dx \right) \\ & = \int_{\Omega} \phi_0 \nabla \left(\frac{\delta E}{\delta \phi_0} + \tilde{p} \right) \cdot \mathbf{u}_0 dx + \int_{\Omega} \phi_1 \nabla \left(\frac{\delta E}{\delta \phi_1} + \tilde{p} \right) \cdot \mathbf{u}_1 dx \\ & + \int_{\Omega} \left(\sum_{j=2}^{N} \phi_j \nabla \frac{\delta E}{\delta \phi_j} + \phi_s \nabla \tilde{p} \right) \cdot \mathbf{u}_s dx \end{aligned}$$

where we have used the product rule and $\sum_{j=2}^{N}\phi_j = \phi_s$. Define $p = \frac{\delta E}{\delta \phi_0} + \tilde{p}$ and set

$$\mathbf{u}_s = -k_s\left(\phi_s\nabla\tilde{p} + \sum_{j=2}^{N}\phi_j\nabla\frac{\delta E}{\delta\phi_j}\right) = -k_s\left(\phi_s\nabla p - \phi_s\nabla\frac{\delta E}{\delta\phi_0} + \sum_{j=2}^{N}\phi_j\nabla\frac{\delta E}{\delta\phi_j}\right). \tag{2.9}$$

Now write $\mathbf{u}_j = \mathbf{u}_s + \mathbf{w}_j$ for $j \geq 2$ where $\mathbf{u}_s$ is the mass averaged velocity of the tumor cells and the host and $\mathbf{w}_j$ is the deviation from this velocity. Plugging these definitions in equation (2.8) above,

$$\begin{aligned}\frac{dE}{dt} = &\int_\Omega \phi_0\nabla p\cdot\mathbf{u}_0 dx + \int_\Omega \phi_1\nabla\left(\frac{\delta E}{\delta\phi_1} - \frac{\delta E}{\delta\phi_0} + p\right)\cdot\mathbf{u}_1 dx\\ &+\left(\sum_{j=2}^{N}\phi_j\nabla\frac{\delta E}{\delta\phi_j} - \phi_s\frac{\delta E}{\delta\phi_0} + \phi_s\nabla p\right)\cdot\mathbf{u}_s + \int_\Omega\sum_{j=2}^{N}\phi_j\nabla\left(\frac{\delta E}{\delta\phi_j} - \frac{\delta E}{\delta\phi_0} + p\right)\cdot\mathbf{w}_j\\ &+\sum_{j=0}^{N}\int_\Omega\nabla\left(\frac{1}{\rho_j}\frac{\delta E}{\delta\phi_j} - \frac{1}{\rho_N}\frac{\delta E}{\delta\phi_N} + \left(\frac{1}{\rho_j} - \frac{1}{\rho_N}\right)\left(p - \frac{\delta E}{\delta\phi_0}\right)\right)\cdot\mathbf{J}_j dx.\end{aligned} \tag{2.10}$$

Now let

$$\mathbf{u}_0 = -k_0\phi_0\nabla p \tag{2.11}$$

$$\mathbf{u}_1 = -k_1\phi_1\nabla\left(p + \frac{\delta E}{\delta\phi_1} - \frac{\delta E}{\delta\phi_0}\right) \tag{2.12}$$

$$\mathbf{w}_j = -k_j\phi_j\nabla\left(p + \frac{\delta E}{\delta\phi_j} - \frac{\delta E}{\delta\phi_0}\right), j \geq 2 \tag{2.13}$$

$$\mathbf{J}_j = -M_j\nabla\left(\frac{1}{\rho_j}\frac{\delta E}{\delta\phi_j} - \frac{1}{\rho_N}\frac{\delta E}{\delta\phi_N} + \left(\frac{1}{\rho_j} - \frac{1}{\rho_N}\right)\left(p - \frac{\delta E}{\delta\phi_0}\right)\right). \tag{2.14}$$

Here M_j is a positive definite matrix representing the diffusive mobility of the jth component and k_s, k_j are nonnegative cell motilities that reflect the response of the average and individual motions of cells to pressure and interaction forces. Equations (2.13) and (2.9)

combine to give

$$\mathbf{u}_j = -k_s \left(\phi_s \nabla p - \phi_s \nabla \frac{\delta E}{\delta \phi_0} + \sum_{j=2}^{N} \phi_j \nabla \frac{\delta E}{\delta \phi_j} \right) - k_j \phi_j \nabla \left(p + \frac{\delta E}{\delta \phi_j} - \frac{\delta E}{\delta \phi_0} \right), j \geq 2. \tag{2.15}$$

Plugging (2.13), (2.9) and (2.14) into (2.10) we see

$$\frac{dE}{dt} = -\int_\Omega \frac{1}{k_0}|\mathbf{u}_0|^2 + \frac{1}{k_1}|\mathbf{u}_1|^2 + \frac{1}{k}|\mathbf{u}_\mathbf{l}|^2 + \sum_{j=2}^{N} \frac{1}{k_j}|\mathbf{w}_j|^2 + \sum_{j=0}^{N} \frac{1}{M_j}|\mathbf{J}_j|^2 dx.$$

Hence with our choice of the flux and velocity above we see that the energy of the system is non-increasing in time and thus our model is consistent with the second law of thermodynamics.

The energy E has a central role in the model and the numerical simulations. From a biological prospective the energy gives a way to model the multiple cell species through cell interaction. This also controls the extent which the tumor and host cells intermix. From the numerical perspective the energy is a way to keep the structure of the diffuse interface and the cell fractions realistic.

2.3 Tumor Model

The general model above will now be adapted to a specific model we will analyze. The tumor is composed of viable tumor cells, dead cells, host and water. The local volume fractions of the species are denoted by,

$$\phi_V, \phi_D, \phi_H, \phi_W$$

respectively. We define $\phi_T = \phi_V + \phi_D$ and make the simplifying approximation that all the densities are matched (i.e., $\rho_i = \rho$).

We suppose that the tumor cells prefer to adhere to one another rather than the host and we do not distinguish between adhesive properties of the viable and dead cells. To formulate the $F_i(\phi_0, \ldots, \phi_N)$ term in equation (2.6) that models the bulk energy we take $F_i(\phi_0, \ldots, \phi_N) = f(\phi_W, \phi_D, \phi_V)$ where $f(x, y, z)$ is a sum of interaction potentials. In particular, we use a polynomial approximation of the local interaction energy

$$\begin{aligned} f(\phi_W, \phi_D, \phi_V) =& \frac{1}{4}\phi_T^2\phi_H^2 + \frac{\alpha_{HW}}{2}\phi_H^2(\phi_W - \bar{\phi}_W^H)^2 + \frac{\alpha_{VW}}{2}\phi_V^2(\phi_W - \bar{\phi}_W^V)^2 \\ &+ \frac{\alpha_{Vitro}}{2}\phi_W^2\phi_H^2 + \frac{\kappa}{2}(C_0 - 1.0)^2\phi_W^2 + \frac{\alpha_{WDH}}{2}\phi_W^2\phi_D^2\phi_H^2 \\ &+ \frac{\alpha_{VWDH}}{2}\phi_V^2\phi_W^2\phi_D^2\phi_H^2 + \frac{\alpha_V}{2}\phi_V^2\mathcal{H}(-\phi_V) + \frac{\alpha_W}{2}\phi_W^2\mathcal{H}(-\phi_W) \\ &+ \frac{\alpha_D}{2}\phi_D^2\mathcal{H}(-\phi_D) + \frac{\alpha_H}{2}\phi_H^2\mathcal{H}(-\phi_H). \end{aligned} \tag{2.16}$$

where $\bar{\phi}_W^H, \bar{\phi}_W^V$ are the water levels in the host cells and viable cells respectively. The α parameters are available to weight the various interaction potentials. Additionally, this energy can be written just in terms of ϕ_V, ϕ_W, and ϕ_D by using, $\phi_H = 1 - \phi_V - \phi_W - \phi_D$. Similar bulk energy terms have also been used to describe multiphase systems and modeling multicomponent alloys [26], [31], [29], [28], [27].

The first term in the energy gives a well-delineated phase separation between the tumor and host tissue. The next two terms with the α_{HW} and α_{VW} parameters maintain the water levels set by $\bar{\phi}_W^H$ and $\bar{\phi}_W^V$ respectively. The necessity of these terms will be seen in section 4.4 when the variations of the model parameters are discussed. We will demonstrate that the water fraction can produce unphysical behaviors without these parameters. The term with the α_{Vitro} parameter is only necessary when we consider the in vitro case (i.e., $\bar{\phi}_W^H = 1.0$). In section 4.2 we show the introduction of this term eliminates the host fraction build up in the in-vitro case where this behavior is not physical. The α_{Vitro} term enforces a phase

separation between the host and water fractions and since the water fraction is present in the entire domain the host is phased out. The κ term determines the water diffusion rate out of the necrotic core of the tumor and will be discussed greater depth in section 2.3.4. The α_{WDH} term prevents unphysical build up of host in the necrotic core of the tumor and the α_{VWHD} term prevents the unphysical generation of a phase in an interfacial region. The last three terms with Heaviside functions compel the volume fractions to remain positive as the tumor develops. Similar terms have been added in models of composition materials [26], [31], [29]. We further define $\epsilon_0 = \epsilon_T = \epsilon_N = \epsilon$. Thus,

$$\begin{aligned} E = \sum_{i=0}^{3} E_i &= \int_\Omega f(\phi_W, \phi_D, \phi_V) + \frac{\epsilon_0^2}{2}|\nabla\phi_0|^2 + \frac{\epsilon_T^2}{2}|\nabla\phi_T|^2 + \frac{\epsilon_N^2}{2}|\nabla\phi_N|^2 dx \\ &= \int_\Omega f(\phi_W, \phi_D, \phi_V) + \frac{\epsilon^2}{2}\left(|\nabla\phi_W|^2 + |\nabla\phi_T|^2 + |\nabla\phi_H|^2\right) dx \\ &= \int_\Omega f(\phi_W, \phi_D, \phi_V) + \frac{\epsilon^2}{2}\left(|\nabla\phi_W|^2 + |\nabla\phi_T|^2 + |\nabla(\phi_W + \phi_D + \phi_V)|^2\right) dx \end{aligned}$$

where we have used $\phi_H = 1 - \phi_W - \phi_D - \phi_V$. Hence we write the energy as

$$E = \int_\Omega f(\phi_W, \phi_D, \phi_V) + \frac{\epsilon^2}{2}\left(|\nabla\phi_W|^2 + |\nabla\phi_T|^2 + |\nabla(\phi_W + \phi_D + \phi_V)|^2\right) dx.$$

Note that this interaction energy does not depend on the host.

2.3.1 Generalized Diffusion Term

From equation (2.14) have

$$\mathbf{J}_i = -M_i\nabla\left(\frac{\delta E}{\delta\phi_i} - \frac{\delta E}{\delta\phi_N}\right), 0 \leq i \leq N-1$$

and $\mathbf{J}_N = -\sum_{i=0}^{N-1} \mathbf{J}_i$, where $M_i > 0$ is the motility. Specializing to the tumor case and taking the motilities $M_i = -\bar{M}_i \phi_i$ for $0 \leq i \leq 2$ where $\bar{M}_i$ is constant we see

$$\mathbf{J}_i = -\bar{M}_i \phi_i \nabla \frac{\delta E}{\delta \phi_i}$$

where we have used that the energy does not depend on ϕ_3. Further,

$$\begin{aligned}
\frac{\delta E}{\delta \phi_0} &= \frac{\delta E}{\delta \phi_W} = \frac{\partial f(\phi_W, \phi_D, \phi_V)}{\partial \phi_W} - \epsilon^2 \nabla^2 \phi_V - 2\epsilon^2 \nabla^2 \phi_W - \epsilon^2 \nabla^2 \phi_D \\
\frac{\delta E}{\delta \phi_1} &= \frac{\delta E}{\delta \phi_D} = \frac{\partial f(\phi_W, \phi_D, \phi_V)}{\partial \phi_D} - 2\epsilon^2 \nabla^2 \phi_V - \epsilon^2 \nabla^2 \phi_W - 2\epsilon^2 \nabla^2 \phi_D \\
\frac{\delta E}{\delta \phi_2} &= \frac{\delta E}{\delta \phi_V} = \frac{\partial f(\phi_W, \phi_D, \phi_V)}{\partial \phi_V} - 2\epsilon^2 \nabla^2 \phi_V - \epsilon^2 \nabla^2 \phi_W - 2\epsilon^2 \nabla^2 \phi_D.
\end{aligned}$$

Hence, the flux term for the components is given by,

$$\begin{aligned}
\mathbf{J}_0 &= -M_W \phi_W \nabla \nu \\
\mathbf{J}_D &= -M_D \phi_D \nabla \delta \\
\mathbf{J}_V &= -M_V \phi_V \nabla \mu \\
\nu &= \frac{\delta E}{\delta \phi_W} = \frac{\partial f}{\partial \phi_W}(\phi_W, \phi_D, \phi_V) - \epsilon^2 \nabla^2 \phi_V - 2\epsilon^2 \nabla^2 \phi_W - \epsilon^2 \nabla^2 \phi_D \\
\delta &= \frac{\delta E}{\delta \phi_D} = \frac{\partial f}{\partial \phi_D}(\phi_W, \phi_D, \phi_V) - 2\epsilon^2 \nabla^2 \phi_V - \epsilon^2 \nabla^2 \phi_W - 2\epsilon^2 \nabla^2 \phi_D \\
\mu &= \frac{\delta E}{\delta \phi_V} = \frac{\partial f}{\partial \phi_V}(\phi_W, \phi_D, \phi_V) - 2\epsilon^2 \nabla^2 \phi_V - \epsilon^2 \nabla^2 \phi_W - 2\epsilon^2 \nabla^2 \phi_D.
\end{aligned}$$

Thus, the flux is a fourth order nonlinear advection-diffusion of Cahn-Hilliard type [10]. The flux is for the host component is

$$\mathbf{J}_H = -\sum_{i=0}^{2} \mathbf{J}_i = M_W \phi_W \nabla \nu + M_D \phi_D \nabla \delta + M_V \phi_V \nabla \mu.$$

2.3.2 Advection

From equations (2.11), (2.12), (2.15) we know the resulting generalized Darcy laws for the velocity of components are given by

$$\begin{aligned}
\mathbf{u}_0 &= -\, k_0\phi_0\nabla p \\
\mathbf{u}_1 &= -\, k_1\phi_1\nabla\left(p + \frac{\delta E}{\delta\phi_1} - \frac{\delta E}{\delta\phi_0}\right) \\
\mathbf{u}_j &= -\, k\left(\phi_s\nabla p - \phi_s\nabla\frac{\delta E}{\delta\phi_0} + \sum_{j=2}^{N}\phi_j\nabla\frac{\delta E}{\delta\phi_j}\right) - k_j\phi_j\nabla\left(p + \frac{\delta E}{\delta\phi_j} - \frac{\delta E}{\delta\phi_0}\right), j \geq 2.
\end{aligned} \tag{2.17}$$

Further for $1 \leq j \leq 3$ we have

$$\mathbf{u}_0 = -\, k_0\phi_0\nabla p \tag{2.18}$$

$$\mathbf{u}_1 = -\, k_1\phi_1\nabla\left(p + \delta - \nu\right) \tag{2.19}$$

$$\mathbf{u}_2 = -\, k_s\left(\phi_s\nabla p - \phi_s\nabla\nu + \phi_V\nabla\mu\right) - k_2\phi_V\nabla\left(p + \mu - \nu\right) \tag{2.20}$$

$$\mathbf{u}_3 = -\, k_s\left(\phi_s\nabla p - \phi_s\nabla\nu + \phi_V\nabla\mu\right) - k_3\phi_H\nabla\left(p - \nu\right). \tag{2.21}$$

Here we again use that the energy does not depend on ϕ_H. The coefficients k, k_j are motilities that reflect the response of the water and the cells to the pressure gradients. As a further simplifying assumption we take $k_j = 0$ for $j \geq 1$ which is consistent with assuming the host and tumor cells are tightly packed and march together. Thus the viable cells and host component have the velocity

$$\mathbf{u}_s = -k_s\left(\phi_s\nabla p - \phi_s\nabla\nu + \phi_V\nabla\mu\right). \tag{2.22}$$

Note that $k_s > 0$ may depend on ϕ_i for $0 \leq i \leq 3$ and other variables. This constitutive law for velocity assumes the tumor can be treated as a viscous, inertialess fluid and models this flow through a porous medium.

Now we write the continuity equation for the ϕ_i for $0 \leq i \leq 3$

$$\frac{\partial \phi_i}{\partial t} + \nabla \cdot (\mathbf{u}_i \phi_i) = -\nabla \cdot \mathbf{J}_i + S_i$$

where ρ is absorbed into the motility constant for $\mathbf{J}$ and the source term. Assuming the source term for the host tissue is 0 (i.e., $S_H = 0$), the continuity equations for $0 \leq i \leq 3$ can be summed to yield

$$0 + \nabla \cdot (\phi_s \mathbf{u}_s + \phi_D \mathbf{u}_1 + \phi_W \mathbf{u}_0) = -\nabla \cdot \sum_{i=0}^{3} \mathbf{J}_i + \sum_{i=0}^{3} S_i.$$

Thus by equations (2.4) and (2.5),

$$\nabla \cdot (\phi_s \mathbf{u}_s + \phi_D \mathbf{u}_1 + \phi_W \mathbf{u}_0) = 0.$$

This equation with (6.8). (6.3). and (6.4) can be used to solve for the pressure (a linear elliptic equation for p). This closes the system and it remains to account for the source terms.

2.3.3 Source/Mass-Exchange

Assume that the viable cells mitosis rate is linearly proportional to the level of oxygen, glucose, and other survival promoting factors that are modeled as a single concentration C_0. We also assume that the mitosis rate is linearly proportional to amount of water in the system and water is depleted during mitosis. Death of the cells may occur by apoptosis or by necrosis if the nutrient levels are too low to support cell viability. After the cells die the dead cells are converted to water through lysis, a process of cell degradation clearance. The

source terms are given by,

$$\begin{aligned} S_V =& \lambda_M \phi_V \phi_W C_0 - \lambda_N \phi_V \mathcal{H}(\bar{C}_0 - C_0) - \lambda_A \phi_V \\ S_W =& -\lambda_M \phi_V \phi_W C_0 + \lambda_l \phi_D \mathcal{H}(\bar{\phi}_D - \phi_D) \\ S_D =& \lambda_A \phi_V + \lambda_N \phi_V \mathcal{H}(\bar{C}_0 - C_0) - \lambda_l \phi_D \mathcal{H}(\bar{\phi}_D - \phi_D) \\ S_H =& 0 \end{aligned} \tag{2.23}$$

where $\lambda_M, \lambda_A, \lambda_N$ denote mitosis, apoptosis, and necrosis rates of the viable cells. $\bar{C}_0$ is the minimum level of oxygen, glucose, and growth promoting factors required for cell viability and $\bar{\phi}_D$ is the minimal level of necrotic dead cells needed to initiate lysis.

Now, everything in the source terms above is a parameter or dependent variable except for C_0. Denote oxygen, glucose, and other growth promoting factors as O. Assume the uptake of O is negligible in the host domain compared to the uptake by the tumor cells. On the time scale of cell proliferation the diffusion of O is rapid and the time derivatives and advection terms can be neglected. Therefore the concentration of O is given by,

$$0 = \nabla \cdot (D_0 \nabla C_0) - \nu_{UOV} \phi_V C_0 + \nu_{PO}(\bar{C}_{AO} - C_0) Q(\phi_T). \tag{2.24}$$

Here D_0 is the diffusion coefficient and ν_{UOV} is the uptake rate of oxygen by the viable tumor cells and ν_{PO} is the rate that O is supplied to the microenvironment. $\bar{C}_{AO}$ is the concentration of O in the blood (in vivo) or in the medium (in vitro) far from the tumor. The function $Q(\phi_T)$ approximates the characteristic function of the host domain and models the source of O as being external to the tumor (i.e., the tumor is avascular). More specifically the function Q can be taken to be,

$$Q(\phi_T) = \begin{cases} 0 & \text{if } \phi_T > 0.01 \\ 1 & \text{if } \phi_T \leq 0.01 \end{cases}$$

The uptake of O in the host domain is assumed to be negligible compared to the uptake in the viable tumor domain. Thus, the PDE for C_0 is given the Dirichlet boundary condition $C_0 = \bar{C}_{AO}$ on Σ_∞.

2.3.4 Water Diffusion

In order for a symmetric initial tumor seed to grow to a stable tumor spheroid we need to introduce a way to flux the water out from the center of the tumor. In the constant water fraction case this was done with lysis to provide a sink for solid materials. For the non-constant water fraction case considered here, the water fraction is part of the system and lysing the dead cells produces a build up of water in the necrotic core and the tumor does not stabilize. Thus, in the non-constant water fraction case we use water diffusion to flux the water out of the center of the tumor. The nutrient variable includes oxygen, glucose and other growth promoting factors that are non-polar molecules. Outside the tumor the nutrient concentration is higher than inside the necrotic core by $(1/\bar{C}_0 - 1)\%$. This difference establishes an osmotic pressure gradient from the necrotic core to the environment outside the tumor. Additionally, there will also be a diffusion effect from higher water concentrations to lower concentrations. This can be seen in the diffusion coefficient necessary to stabilize the tumor for different water levels in the host. The in vivo case we consider in the next chapter has the water fraction in the host set to around 20% [55] and a much smaller diffusion coefficient is needed than in the in vitro case where we assume the tumor is surrounded by 100% water. This can be interpreted as the increased water diffusion gradient is acting opposite the osmotic pressure gradient. This is modeled in the energy by,

$$\kappa \int_\Omega (C_0 - 1)^2 \phi_W^2 dx.$$

This double well potential has a well at $C_0 = 1.0$ and $\phi_W = 0.0$. Once the tumor develops a necrotic core we will see that outside the tumor the C_0 level is near 1.0 and inside the tumor the viable cells uptake the nutrients and the nutrient level is reduced to $\bar{C}_0$. Thus, outside the tumor this energy term will not contribute to the interaction energy and the water will not experience any diffusion. As C_0 is consumed by the viable cells the nutrient level begins to fall. To minimize the contribution of this term to the interaction energy the water fraction decreases to approach its well value of 0.0 and the water will flux out of the center of the tumor. Thus, as the nutrient level drops inside the tumor the water fraction also begins to diffuse and the lower the nutrient level the greater the water diffusion. Therefore, as the nutrient level decreases water begins to diffuse out of the tumor and inside the necrotic core the water diffusion is the greatest. This diffusion potential is a quantitative way to incorporate the diffusion effect with the osmotic pressure gradient. The κ perimeter will determine the magnitude of the diffusion.

Thus, the full model is given by,

$$
\begin{aligned}
\partial_t \phi_V =& M_V \nabla \cdot (\phi_V \nabla \mu) + S_V - \nabla \cdot (\phi_V \mathbf{u}_s) \\
\partial_t \phi_W =& M_W \nabla \cdot (\phi_W \nabla \nu) + S_W - \nabla \cdot (\phi_W \mathbf{u}_w) \\
\partial_t \phi_D =& M_D \nabla \cdot (\phi_D \nabla \delta) + S_D - -\nabla \cdot (\phi_D \mathbf{u}_1) \\
\mu =& \frac{\delta E}{\delta \phi_V} = \frac{\partial f}{\partial \phi_V}(\phi_W, \phi_D, \phi_V) - 2\epsilon^2 \Delta \phi_V - \epsilon^2 \Delta \phi_W - 2\epsilon^2 \Delta \phi_D \\
\nu =& \frac{\delta E}{\delta \phi_W} = \frac{\partial f}{\partial \phi_W}(\phi_W, \phi_D, \phi_V) - 2\epsilon^2 \Delta \phi_W - \epsilon^2 \Delta \phi_V - \epsilon^2 \Delta \phi_D \\
\delta =& \frac{\delta E}{\delta \phi_D} = \frac{\partial f}{\partial \phi_D}(\phi_W, \phi_D, \phi_V) - 2\epsilon^2 \Delta \phi_V - \epsilon^2 \Delta \phi_W - 2\epsilon^2 \Delta \phi_D \\
\mathbf{u}_s =& - k_s(\phi_s \nabla p + \phi_V \nabla \mu - \phi_s \nabla \nu) \\
\mathbf{u}_1 =& - k_1 \phi_1 \nabla (p + \delta - \nu) \\
\mathbf{u}_w =& - k_w \phi_W \nabla p \\
0 =& \nabla \cdot ((k_s \phi_s^2 + k_w \phi_W^2 + k_1 \phi_D^2) \nabla p) + k_s \nabla \cdot (\phi_s \phi_V \nabla \mu - \phi_s^2 \nabla \nu) \\
& + k_1 \nabla \cdot (\phi_D \nabla \delta - \phi_D \nabla \nu) \\
S_V =& \lambda_M \phi_V \phi_W C_0 - \lambda_N \phi_V \mathcal{H}(\bar{C}_0 - C_0) - \lambda_A \phi_V \\
S_W =& - \lambda_M \phi_V \phi_W C_0 + \lambda_l \phi_D \mathcal{H}(\bar{\phi}_D - \phi_D) \\
S_D =& \lambda_N \phi_V \mathcal{H}(\bar{C}_0 - C_0) - \lambda_l \phi_D \mathcal{H}(\bar{\phi}_D - \phi_D) + \lambda_A \phi_V \\
0 =& D_0 \nabla^2 C_0 - C_0 \nu_{UOT} \phi_V + \nu_{PO}(\bar{C}_{AO} - C_0) Q(\phi_T).
\end{aligned}
$$

2.4 Model Simplification and Nondimensional Equations

To simplify the model we neglect the effects of apoptosis on the viable cells since the apoptosis rate the tumor cells should be very small compared to the time scales we consider. We also assume the dead cells have no mobility and no velocity (i.e., $M_D = 0, \mathbf{u}_1 = 0$). This implies

that the change in the dead cells is only due to the source term. Indeed the movement of the dead cells should be dominated by the necrosis of the viable cells and the lysis rate.

Following [15] we nondimensionalize the governing equations using the oxygen diffusion length scale and the mitosis rate of the viable cells time scale in table 2.1. These can be estimated as $l \approx 200\mu m$ and $\tau \approx 1$ day. The oxygen concentration is measured against the concentration in the blood or in the medium in the vitro case. The dimensional simplified model is given by,

$$
\begin{aligned}
\partial_t \phi_V =& M_V \nabla \cdot (\phi_V \nabla \mu) + S_V - \nabla \cdot (\phi_V \mathbf{u}_l) \\
\partial_t \phi_W =& M_W \nabla \cdot (\phi_W \nabla \nu) + S_W - \nabla \cdot (\phi_W \mathbf{u}_w) \\
\partial_t \phi_D =& S_D \\
\mu =& \frac{\delta E}{\delta \phi_V} = \frac{\partial f}{\partial \phi_V}(\phi_W, \phi_D, \phi_V) - 2\epsilon^2 \Delta \phi_V - \epsilon^2 \Delta \phi_W - 2\epsilon^2 \Delta \phi_D \\
\nu =& \frac{\delta E}{\delta \phi_W} = \frac{\partial f}{\partial \phi_W}(\phi_W, \phi_D, \phi_V) - 2\epsilon^2 \Delta \phi_W - \epsilon^2 \Delta \phi_V - \epsilon^2 \Delta \phi_D \\
\mathbf{u}_s =& - k_s(\phi_s \nabla p + \phi_V \nabla \mu - \phi_s \nabla \nu) \\
\mathbf{u}_w =& - k_w \phi_W \nabla p \\
0 =& \nabla \cdot ((k_s \phi_s^2 + k_w \phi_W^2) \nabla p) + k_s \nabla \cdot (\phi_s \phi_V \nabla \mu - \phi_s^2 \nabla \nu) \\
S_V =& \lambda_M \phi_V \phi_W C_0 - \lambda_N \phi_V \mathcal{H}(\bar{C}_0 - C_0) \\
S_W =& - \lambda_M \phi_V \phi_W C_0 + \lambda_l \phi_D \mathcal{H}(\bar{\phi}_D - \phi_D) \\
S_D =& \lambda_N \phi_V \mathcal{H}(\bar{C}_0 - C_0) - \lambda_l \phi_D \mathcal{H}(\bar{\phi}_D - \phi_D) \\
0 =& D_0 \nabla^2 C_0 - C_0 \nu_{UOT} \phi_V + \nu_{PO}(\bar{C}_{AO} - C_0) Q(\phi_T)
\end{aligned}
$$

with energy

$$
E = \int_\Omega f(\phi_W, \phi_D, \phi_V) + \frac{\epsilon^2}{2} \left(|\nabla \phi_W|^2 + |\nabla \phi_T|^2 + |\nabla(\phi_W + \phi_D + \phi_V)|^2 \right) dx
$$

and interaction potential

$$\begin{aligned} f(\phi_W, \phi_D, \phi_V) =& \frac{1}{4}\phi_T^2\phi_H^2 + \frac{\alpha_{HW}}{2}\phi_H^2(\phi_W - \bar{\phi}_W^H)^2 + \frac{\alpha_{VW}}{2}\phi_V^2(\phi_W - \bar{\phi}_W^V)^2 \\ &+ \frac{\alpha_{Vitro}}{2}\phi_W^2\phi_H^2 + \frac{\kappa}{2}(C_0 - 1.0)^2\phi_W^2 + \frac{\alpha_{WDH}}{2}\phi_W^2\phi_D^2\phi_H^2 \\ &+ \frac{\alpha_{VWDH}}{2}\phi_V^2\phi_W^2\phi_D^2\phi_H^2 + \frac{\alpha_V}{2}\phi_V^2\mathcal{H}(-\phi_V) + \frac{\alpha_W}{2}\phi_W^2\mathcal{H}(-\phi_W) \\ &+ \frac{\alpha_D}{2}\phi_D^2\mathcal{H}(-\phi_D) + \frac{\alpha_H}{2}\phi_H^2\mathcal{H}(-\phi_H). \end{aligned} \tag{2.25}$$

To nondimensionalize we set $\mathbf{x} = \mathcal{L}\mathbf{x}'$ and $t = \mathcal{T}t'$ where $\mathcal{L}$ and $\mathcal{T}$ are scaling factors. This gives the relationship,

$$\begin{aligned} \partial_t &= \frac{1}{\mathcal{T}}\partial_{t'} \\ \nabla &= \frac{1}{\mathcal{L}}\nabla'. \end{aligned}$$

Note that the prime notation will denote a function or operator in the scaled coordinates.

Plugging the scaled coordinates into the system gives,

$$
\begin{aligned}
\partial_{t'}\phi'_V =& \frac{\mathcal{T}}{\mathcal{L}^2} M_V \nabla' \cdot (\phi'_V \nabla' \mu') + \mathcal{T} S'_V - \frac{\mathcal{T}}{\mathcal{L}} \nabla' \cdot (\phi'_V \mathbf{u}'_s) \\
\partial_{t'}\phi'_W =& \frac{\mathcal{T}}{\mathcal{L}^2} M_W \nabla' \cdot (\phi'_W \nabla' \nu') + \mathcal{T} S'_W - \frac{\mathcal{T}}{\mathcal{L}} \nabla' \cdot (\phi'_W \mathbf{u}'_w) \\
\partial_{t'}\phi'_D =& \mathcal{T} S'_D \\
\mu' =& \frac{\partial f}{\partial \phi'_V}(\phi'_W, \phi'_D, \phi'_V) - \frac{1}{\mathcal{L}^2} 2\epsilon^2 \Delta' \phi'_V - \frac{1}{\mathcal{L}^2} \epsilon^2 \Delta' \phi'_W - \frac{1}{\mathcal{L}^2} 2\epsilon^2 \Delta' \phi'_D \\
\nu' =& \frac{\partial f}{\partial \phi'_W}(\phi'_W, \phi'_D, \phi'_V) - \frac{1}{\mathcal{L}^2} 2\epsilon^2 \Delta' \phi'_W - \frac{1}{\mathcal{L}^2} \epsilon^2 \Delta' \phi'_V - \frac{1}{\mathcal{L}^2} \epsilon^2 \Delta' \phi'_D \\
\mathbf{u}'_s =& \frac{-k_s}{\mathcal{L}} (\phi'_s \nabla' p' + \phi'_V \nabla' \mu' - \phi'_s \nabla' \nu') \\
\mathbf{u}'_w =& \frac{-k_w}{\mathcal{L}} \phi'_W \nabla' p' \\
0 =& \frac{1}{\mathcal{L}^2} \nabla' \cdot ((k_s {\phi'_s}^2 + k_w {\phi'_W}^2) \nabla' p') + \frac{k_s}{\mathcal{L}^2} \nabla' \cdot (\phi'_s \phi'_V \nabla' \mu' - {\phi'_s}^2 \nabla' \nu') \\
S'_V =& \lambda_M \phi'_V \phi'_W C'_0 - \lambda_n \mathcal{H}(\bar{C}'_0 - C_0) \phi'_V \\
S'_W =& -\lambda_M \phi'_V \phi'_W C'_0 + \lambda_l \phi'_D \\
S'_D =& \lambda_n \mathcal{H}(\bar{C}'_0 - C_0) \phi'_V - \lambda_l \phi'_D \\
0 =& \frac{D_0}{\mathcal{L}^2} \nabla'^2 C'_0 - C'_0 \nu_{UOT} \phi'_V + \nu_{PO} (\bar{C}_{AO} - C'_0) Q(\phi'_T).
\end{aligned}
$$

Now we are free to choose $\mathcal{T}$, $\mathcal{L}$, define new parameters, or scale the functions. Let's rewrite

the system without the primes.

$$
\begin{aligned}
\partial_t \phi_V =& \frac{\mathcal{T}}{\mathcal{L}^2} M_V \nabla \cdot (\phi_V \nabla \mu) + \mathcal{T} S_V - \frac{\mathcal{T}}{\mathcal{L}} \nabla \cdot (\phi_V \mathbf{u}_s) \\
\partial_t \phi_W =& \frac{\mathcal{T}}{\mathcal{L}^2} M_W \nabla \cdot (\phi_W \nabla \nu) + \mathcal{T} S_W - \frac{\mathcal{T}}{\mathcal{L}} \nabla \cdot (\phi_W \mathbf{u}_w) \\
\partial_t \phi_D =& \mathcal{T} S_D \\
\mu =& \frac{\partial f}{\partial \phi_V}(\phi_W, \phi_D, \phi_V) - \frac{2\epsilon^2}{\mathcal{L}^2} \Delta \phi_V - \frac{\epsilon^2}{\mathcal{L}^2} \Delta \phi_W - \frac{2\epsilon^2}{\mathcal{L}^2} \Delta \phi_D \\
\nu =& \frac{\partial f}{\partial \phi_W}(\phi_W, \phi_D, \phi_V) - \frac{2\epsilon^2}{\mathcal{L}^2} \Delta \phi_W - \frac{\epsilon^2}{\mathcal{L}^2} \Delta \phi_V - \frac{\epsilon^2}{\mathcal{L}^2} \Delta \phi_D \\
\mathbf{u}_s =& \frac{-k_s}{\mathcal{L}} (\phi_s \nabla p + \phi_V \nabla \mu - \phi_s \nabla \nu) \\
\mathbf{u}_w =& \frac{-k_w}{\mathcal{L}} \phi_W \nabla p \\
0 =& \frac{1}{\mathcal{L}^2} \nabla \cdot ((k_s {\phi_s}^2 + k_w {\phi_W}^2) \nabla p) + \frac{k_s}{\mathcal{L}^2} \nabla \cdot (\phi_s \phi_V \nabla \mu - {\phi_s}^2 \nabla \nu) \\
S_V =& \lambda_M \phi_V \phi_W C_0 - \lambda_n \mathcal{H}(\bar{C}_0 - C_0) \phi_V \\
S_W =& -\lambda_M \phi_V \phi_W C_0 + \lambda_l \phi_D \\
S_D =& \lambda_n \mathcal{H}(\bar{C}_0 - C_0) \phi_V - \lambda_l \phi_D \\
0 =& \frac{D_0}{\mathcal{L}^2} \nabla^2 C_0 - C_0 \nu_{UOT} \phi_V + \nu_{PO} (\bar{C}_{AO} - C_0) Q(\phi_T).
\end{aligned}
$$

Dividing the nutrient equation by $\bar{C}_{AO}$ and ν_{UOT} we can define $C_0' = C_0/\bar{C}_{AO}$ to get,

$$
0 = \frac{D_0}{\nu_{UOT} \mathcal{L}^2} \nabla^2 C_0' - C_0' \nu_{UOT} \phi_V + \nu_{PO} (1 - C_0') Q(\phi_T).
$$

From here we can define,

$$
\mathcal{L} = \sqrt{D_0/\nu_{UOT}}
$$

that is, the length scale is the diffusion scale for the nutrients. Thus, the nutrient equation becomes,

$$
0 = \nabla^2 C_0' - C_0' \phi_V + \nu_{PO}' (1 - C_0') Q(\phi_T)
$$

where and $\nu'_{PO} = \frac{\nu_{PO}}{\nu_{UOT}}$.

Now let's look at the source terms,

$$\begin{aligned}
\mathcal{T}S_V =& \mathcal{T}\lambda_M\phi_V\phi_W C'_0\bar{C}_{AO} - \mathcal{T}\lambda_n\mathcal{H}(\bar{C}_0 - C'_0\bar{C}_{AO})\phi_V \\
\mathcal{T}S_W =& -\mathcal{T}\lambda_M\phi_V\phi_W C'_0\bar{C}_{AO} + \mathcal{T}\lambda_l\phi_D\mathcal{H}(\bar{\phi}_D - \phi_D) \\
\mathcal{T}S_D =& \mathcal{T}\lambda_n\mathcal{H}(\bar{C}_0 - C'_0\bar{C}_{AO})\phi_V - \mathcal{T}\lambda_l\phi_D\mathcal{H}(\bar{\phi}_D - \phi_D).
\end{aligned}$$

We can define the time scale as

$$\mathcal{T} = \frac{1}{\lambda_M\bar{C}_{AO}}$$

that is the time scale is the mitosis rate for the tumor. We can also scale the other rates by the time factor, $\lambda'_n = \mathcal{T}\lambda_n$ and $\lambda'_l = \mathcal{T}\lambda_l$ gives,

$$\begin{aligned}
\mathcal{T}S_V =& \phi_V\phi_W C'_0 - \lambda'_n\mathcal{H}(\bar{C}_0 - C'_0\bar{C}_{AO})\phi_V \\
\mathcal{T}S_W =& -\phi_V\phi_W C'_0 + \lambda'_l\phi_D\mathcal{H}(\bar{\phi}_D - \phi_D) \\
\mathcal{T}S_D =& \lambda'_n\mathcal{H}(\bar{C}_0 - C'_0\bar{C}_{AO})\phi_V - \lambda'_l\phi_D\mathcal{H}(\bar{\phi}_D - \phi_D).
\end{aligned}$$

Additionally, the coefficients of the diffusion terms in the species equations can be written as,

$$M'_V = \frac{\mathcal{T}}{\mathcal{L}^2}M_V,\ M'_W = \frac{\mathcal{T}}{\mathcal{L}^2}M_W$$

and from the μ and ν equations we see

$$\epsilon' = \frac{\epsilon}{\mathcal{L}}.$$

Further, we can redefine the velocities as,

$$\mathbf{u}_s' = \frac{\mathcal{T}}{\mathcal{L}}\mathbf{u}_s$$
$$\mathbf{u}_w' = \frac{\mathcal{T}}{\mathcal{L}}\mathbf{u}_w.$$

Thus, the water velocity equation gives,

$$\frac{\mathcal{L}}{\mathcal{T}}\mathbf{u}_w' = \frac{-k_w}{\mathcal{L}}\phi_W \nabla p$$
$$\mathbf{u}_w' = \frac{-k_w \mathcal{T}}{\mathcal{L}^2}\phi_W \nabla p.$$

So we can define $p' = \frac{\mathcal{T}}{\mathcal{L}^2}p$. Using this p in the equation for the tumor and host velocity we get,

$$\mathbf{u}_s' = -k_s(\phi_s \nabla p' + \frac{\mathcal{T}}{\mathcal{L}^2}\phi_V \nabla \mu - \frac{\mathcal{T}}{\mathcal{L}^2}\phi_l \nabla \nu).$$

Now we can write $\frac{\mathcal{T}}{\mathcal{L}^2}$ in terms of ϵ' and a new variable γ' where $\gamma' = \frac{\mathcal{T}\epsilon}{\mathcal{L}^3}$. Hence,

$$\frac{\gamma'}{\epsilon'} = \frac{\mathcal{T}}{\mathcal{L}^2}$$

and

$$\mathbf{u}_s' = -k_s(\phi_s \nabla p' + \frac{\gamma'}{\epsilon'}\phi_V \nabla \mu - \frac{\gamma'}{\epsilon'}\phi_s \nabla \nu).$$

Finally, using the definition of p' and $\frac{\gamma'}{\epsilon'}$ the pressure equation becomes,

$$0 = \nabla \cdot ((k_s {\phi_s}^2 + k_w {\phi_W}^2)\nabla p') + k_s \frac{\gamma'}{\epsilon'} \nabla \cdot (\phi_s \phi_V \nabla \mu - {\phi_s}^2 \nabla \nu).$$

Dropping the primes again the nondimensionalized system is given by,

$$
\begin{aligned}
\partial_t \phi_V =& M_V \nabla \cdot (\phi_V \nabla \mu) + S_V - \nabla \cdot (\phi_V \mathbf{u}_s) \\
\partial_t \phi_W =& M_W \nabla \cdot (\phi_W \nabla \nu) + S_W - \nabla \cdot (\phi_W \mathbf{u}_w) \\
\partial_t \phi_D =& S_D \\
\mu =& \alpha_{VW} \phi_V (\phi_W - \bar{\phi}_W^V)^2 - \alpha_{HW} (\phi_W - \bar{\phi}_W^H)^2 \phi_H - \frac{1}{2} \phi_T^2 \phi_H + \frac{1}{2} \phi_T \phi_H^2 \\
& - \alpha_{Vitro} \phi_W^2 \phi_H - \alpha_{WDH} \phi_W^2 \phi_D^2 \phi_H + \alpha_{VWDH} \phi_V \phi_W^2 \phi_D^2 \phi_H^2 \\
& - \alpha_{VWDH} \phi_V^2 \phi_W^2 \phi_D^2 \phi_H + \alpha_V \phi_V \mathcal{H}(-\phi_V) - \alpha_H \phi_H \mathcal{H}(-\phi_H) \\
& - 2\epsilon^2 \Delta \phi_V - \epsilon^2 \Delta \phi_W - 2\epsilon^2 \Delta \phi_D \\
\nu =& \alpha_{VW} (\phi_W - \bar{\phi}_W^V) \phi_V^2 + \alpha_{HW} (\phi_W - \bar{\phi}_W^H) \phi_H^2 - \alpha_{HW} (\phi_W - \bar{\phi}_W^H)^2 \phi_H \\
& + \alpha_{Vitro} \phi_W \phi_H^2 - \alpha_{Vitro} \phi_W^2 \phi_H - \frac{1}{2} \phi_T^2 \phi_H - \kappa (C_0 - 1)^2 \phi_W \\
& + \alpha_{WDH} \phi_W \phi_D^2 \phi_H^2 - \alpha_{WDH} \phi_W^2 \phi_D^2 \phi_H + \alpha_{VWDH} \phi_V^2 \phi_W \phi_D^2 \phi_H^2 \\
& - \alpha_{VWDH} \phi_V^2 \phi_W^2 \phi_D^2 \phi_H + \alpha_W \phi_W \mathcal{H}(-\phi_W) - \alpha_H \phi_H \mathcal{H} \\
& - 2\epsilon^2 \Delta \phi_D - \epsilon^2 \Delta \phi_W - 2\epsilon^2 \Delta \phi_V \\
\mathbf{u}_s =& - k_s (\phi_s \nabla p + \frac{\gamma}{\epsilon} \phi_V \nabla \mu - \frac{\gamma}{\epsilon} \phi_s \nabla \nu) \\
\mathbf{u}_w =& - k_w \phi_W \nabla p \\
0 =& \nabla \cdot ((k_s \phi_s^2 + k_w \phi_W^2) \nabla p) + k_s \frac{\gamma}{\epsilon} \nabla \cdot (\phi_s \phi_V \nabla \mu - \phi_s^2 \nabla \nu) \\
S_V =& \phi_V \phi_W C_0 - \lambda_N \phi_V \mathcal{H}(\bar{C}_0 - C_0) \\
S_W =& - \phi_V \phi_W C_0 + \lambda_l \phi_D \mathcal{H}(\bar{\phi}_D - \phi_D) \\
S_D =& \lambda_N \phi_V \mathcal{H}(\bar{C}_0 - C_0) - \lambda_l \phi_D \mathcal{H}(\bar{\phi}_D - \phi_D) \\
0 =& \nabla^2 C_0 - C_0 \phi_V + \nu_{PO} (1 - C_0) Q(\phi_T)
\end{aligned}
\tag{2.26}
$$

with the following parameters,

$\mathcal{T} = 1/(\lambda_M \bar{C}_{AO})$	Time Scale
$\mathcal{L} = \sqrt{D_0/\nu_{UOT}}$	Length Scale
$M'_V = M_V \mathcal{T}/\mathcal{L}^2$	Viable Cell Mobility
$M'_W = M_W \mathcal{T}/\mathcal{L}^2$	Water Mobility
$\mathbf{u}'_l = \mathbf{u}_l \mathcal{T}/\mathcal{L}$	Living Cell Velocity
$\mathbf{u}'_w = \mathbf{u}_w \mathcal{T}/\mathcal{L}$	Water Velocity
$\epsilon' = \epsilon/\mathcal{L}$	Interface Thickness
$\lambda'_n = \mathcal{T}\lambda_n$	Necrosis Rate
$\lambda'_l = \mathcal{T}\lambda_l$	Lysis Rate
$D'_0 = 1/\nu_{UOT}$	Nutrient Diffusion
$\nu'_{PO} = \nu_{PO}/\nu_{UOT}$	Nutrient Production
$\gamma' = \mathcal{T}\epsilon/\mathcal{L}^3$	Adhesion Force
$p' = p\mathcal{T}/\mathcal{L}^2$	Pressure

Table 2.1: nondimensionalized parameters

2.5 Comparison with Constant Water Fraction Model

We now compare the non-constant water fraction model we derived above with the constant water fraction model found in [71]. The constant water fraction model is given by,

$$
\begin{aligned}
\partial_t \phi_V &= M\nabla \cdot (\phi_V \nabla \mu) + S_V - \nabla \cdot (\phi_V \mathbf{u}_s) \\
\partial_t \phi_D &= M\nabla \cdot (\phi_D \nabla \mu) + S_D - \nabla \cdot (\phi_D \mathbf{u}_s) \\
\mu &= 2\phi_T(2\phi_T^2 - 3\phi_T + 1) - \epsilon^2 \Delta \phi_T \\
S_V &= \lambda_M \phi_V C_0 - \lambda_N \phi_V \mathcal{H}(\bar{C}_0 - C_0) - \lambda_A \phi_V \\
S_D &= \lambda_A \phi_V + \lambda_N \phi_V \mathcal{H}(\bar{C}_0 - C_0) - \lambda_l \phi_D \\
0 &= \nabla^2 C_0 - C_0 \phi_V + \nu_{PO}(1 - C_0) Q(\phi_T) \\
\mathbf{u}_s &= -k(\nabla p - \frac{\gamma}{\epsilon}\mu \nabla \phi_T) \\
\nabla \cdot (k \nabla p) &= \frac{\gamma}{\epsilon} \nabla \cdot (k\mu \nabla \phi_T) - S_T \\
\mathbf{u}_W &= -k_w \nabla q \\
\nabla \cdot (k_w \nabla q) &= \frac{1}{\tilde{\phi}_W} S_T
\end{aligned}
$$

here $\phi_T = \phi_V + \phi_D$ and $S_T = S_V + S_D$. Also note the water source term is given by,

$$S_W = -(S_V + S_D + S_H) = -\lambda_M \phi_V C_0 + \lambda_l \phi_D.$$

The first difference we note is the increase in the number of potentials in the model with a non-constant water fraction. That is, the non-constant water fraction model has three potentials (μ, ν, δ) before the simplification and the constant water fraction model has one (μ). This due to the different model energies. The non-constant water model has the energy given by (6.1) and the constant water model uses the energy

$$\tilde{E} = \int_\Omega \phi_T^2 \phi_H^2 + \frac{\epsilon^2}{2} |\nabla \phi_T|^2 dx.$$

This energy only enforces the separation between the tumor and the host. Notice that $\frac{\delta \tilde{E}}{\delta \phi_V} = \frac{\delta \tilde{E}}{\delta \phi_D}$ and so the dead cell potential is equal to the viable cell potential. For the non-constant case we see, $\frac{\delta E}{\delta \phi_V} \neq \frac{\delta E}{\delta \phi_D} \neq \frac{\delta E}{\delta \phi_W}$ necessitating three different potentials.

Another difference is our modeling choice of the dead cells. The constant case assumes the dead cells have the same mobility coefficient as the viable cells and they both move with the same velocity. For the non-constant case all the species have independent mobility rates and we assume the dead cells have zero mobility. This assumes that the dead cells cannot actively move within the tumor. Indeed, the dead cell movement is dominated by the necrosis of viable cells and the lysis rate. Without the smoothing effects of the diffusion terms the dead cell continuity equation becomes unstable with just the velocity and source terms. To simplify the problem further we assume the dead cells also have no velocity. The solid velocity is two orders of magnitude smaller than the necrosis and lysis rates so dropping the dead cell velocity is a suitable approximation. However, we do assume that viable and host cells move with the same velocity.

Further, the different models also have different velocities and pressures. In the constant

case the water and solid components have different pressures while in the non-constant case there is a single bulk pressure for the entire system. This difference is a manifestation of the water fraction and hence solid fractions being constant in the constant water model. If we let the source terms be zero (i.e., $S_i = 0$) then water and solid fraction ($\tilde{\phi}_s = 1 - \tilde{\phi}_W$) continuity equation read,

$$0 = \frac{\partial \tilde{\phi}_W}{\partial t} = -\nabla \cdot (\tilde{\phi}_W \mathbf{u}_W)$$
$$0 = \frac{\partial \tilde{\phi}_s}{\partial t} = -\nabla \cdot (\tilde{\phi}_s \mathbf{u}_s).$$

Notice that the water fraction and water velocity are independent from the solid fraction and solid velocity. This gives different Lagrange multipliers for the velocities equations that result in different pressures for the solid and water velocities similar to equation (2.7). In the non-constant case, the continuity equations cannot be separated in this fashion. Summing all volume fractions together we get,

$$0 = \frac{\partial 1}{\partial t} = -\nabla \cdot (\phi_W \mathbf{u}_W + \phi_s \mathbf{u}_s).$$

Thus, in this case we only introduce one Lagrange multiplier that results in a single bulk pressure. In the non-constant case we can also see the pressure equation contains the water potential and the water fraction. In the constant case the water pressure only depends of the water fraction and the solid pressure depends only on the solid components. This is consequence of the separability of the solid and water fractions in the constant case.

Another difference between the models is the inclusion of the water fraction in the growth term and the minimum level of dead cells necessary to initial lysis. The constant model does not explicitly include the water faction. However, since the water fraction is constant anyway it can be absorbed into the mitosis rate. The non-constant model includes the water fraction in the growth term and this assumes that water is up-taken during the mitosis process.

This also implies that a lower water level would imply slow the growth of the tumor and without water the tumor would not be able to grow. The non-constant model also included a assumption on the lysis rate. We assume that there is a minimum fraction of dead cells necessary to initial lysis. This implies that there is always some concentration of dead cells in the necrotic core as the tumor evolves. Without this level the entire necrotic core would convert entirely into water in some cases and this may not be physically realistic. This level provides a way to model the amount of dead cell that do not entirely degrade in the necrotic core. In the constant case there can be no buildup of water in the center of the cell as the water level is constant so this assumption in not needed.

Perhaps the largest difference between the two models in the introduction of the water diffusion terms in the water potential in the non-constant model. As discussed the section 2.3.4 in order for a symmetric initial tumor seed to grow to a stable tumor spheroid we need to introduce a way to flux the water out from the center of the tumor. In the constant water fraction case this was done with the lysis term in the dead cell source term. In section 4.2 we will see that the lysis rate in the non-constant water fraction model is a sensitive parameter and increasing lysis rate can affect the level of viable cells in the necrotic core as the viable cell source term now includes the water fraction. Thus, a new way to flux the water of of the center of the tumor is necessary and the water diffusion term developed here is an effective way to achieve the water flux.

Chapter 3

Numerical Results

3.1 Introduction

In this chapter we consider an avascular in-vivo tumor in two dimensions with symmetric and non-symmetric initial conditions. We demonstrate the spherical initial condition grows to stable steady state with a mostly liquid necrotic core. The non-symmetric initial condition produces an elongated tumor that is typical of behaviors in the preliminary stage of malignant cancer development. We also show that the development of a non-symmetric tumor is dependent on the size of the initial non-symmetric tumor seed. As the tumor develops it smooths out perturbations in the viable cell rim and grows more circular. The closer the tumor becomes to the stable steady state the less pronounced the inhomogeneity in the proliferating rim will be and the longer it will take for this instability to elongate the tumor.

3.2 Spherically Symmetric Initial Condition

In figure 3.1 the evolution of a spherically symmetric initial condition with radius, $r = \sqrt{3}$ to a stable steady state is shown. The simulation is done by solving the system of equations (2.26) in two dimensions with the parameters given in table 3.1. The problem is solved on the computational domain $[0, 40] \times [0, 40]$ and the one dimensional results are shown by taking a slice of the two dimensional results in the middle of the grid at $y = 20$. Further details on the numerical method are found in section 3.4.

Initially the the tumor is composed only of viable cells (80%) and water (20%) [55]. As the tumor develops nutrients are uptaken by the viable cells and as the nutrient level drops below the level needed for viability a necrotic core develops. By time $t = 25$ (figure 3.1b) we can see a necrotic core has developed in the center of the tumor and the water in the core has been exhausted. Additionally, we can see a dip in the water fraction as the tumor advances and the host is increased. Water peaks appear at the tumor-host interface as the tumor advances since the tumor cells and the host do not overlap exactly in the interface and the water fills in this gap.

As the tumor expands, the necrotic core also expands and we can see the dead cell fraction inside the necrotic core begins to decrease as the dead cells undergo lysis and raise the water level (figure 3.1c). This increase in the water fraction is then uptaken by the proliferating cells at the edge of the necrotic core. This behavior coupled with water diffusion creates a flux of water outward from the center of the tumor. As cellular and water mass is lost from center of the tumor the viable cells in the proliferating rim are fluxed toward the center of the tumor. This dynamic eventually leads to a tumor that grows to a stable size when these two fluxes are in balance. The tumor in this case stabilizes with a radius of $r \approx 4.75$ where r is defined by $\phi_V(r) = 0.5$. This radius is consistent with tumor spheroid observations [49, 44]. We can also observe that as the tumor approaches the steady state the water fraction

stabilizes in the host region and the host fraction is no longer raised. After the initial rapid expansion of the tumor we see a gradual decline in the enlargement rate. This behavior can be seen in the evolution of radius of the tumor in figure (3.1h).

Another way to see how fast the tumor reaches the steady state is to analyze the volume plots. In figure (3.2) we can see that for before $t = 20$ the viable cells rapidly proliferate and no dead cells are present. We also see a sharp decrease in the water volume as the water fraction is uptaken by the proliferating cells. After $t = 20$ the nutrient concentration falls below the viability level for the viable cells and a necrotic core beings to form. Note that the water fraction continues to decrease for a short time after the formation of the necrotic core as the water released by lysis does not overtake the uptake by mitosis until the core is large enough. The formation of the necrotic core also decreases the volume of the viable cells as they begin to necrose in the hypoxic region. After time $t = 60$ the dead cell volume begins to stabilize as the lysis rate of the dead cells balances the necrosis rate. When the dead cells begin to accumulate and start to lyse, the water volume increases inside the necrotic core. The water released by the degraded dead cells begins to accumulate in the necrotic core and raise the water volume. As the water fraction increases it begins to diffuses out of the core to the host region. After $t = 80$ the diffusion rate of the water balances the lysis rate of the dead cells. The water diffusion from the center of the tumor fluxes the viable cells toward the center of the tumor and the proliferation rate of the viable cells balances the necrosis rate and the tumor volume stabilizes.

In the constant water model [71] the tumor stabilizes at $t \approx 10$. The non-constant water model presented here does not approach the steady state radius until $t \approx 50$. After $t = 50$ the main change in the tumor morphology is the water and dead cell levels reaching equilibrium. This increase in time is a result of diffusing the water out of the center of the tumor instead of lysing it out of the system as in the non-constant water model. In the next chapter we will look at how the different parameters effect the size of the stable tumor and how fast the

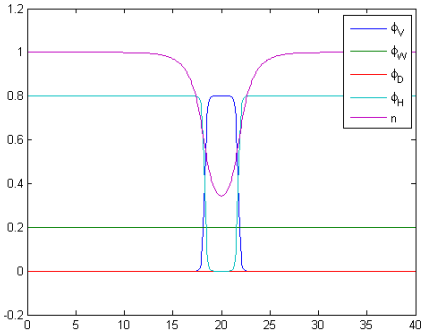

(a) $t = 0$

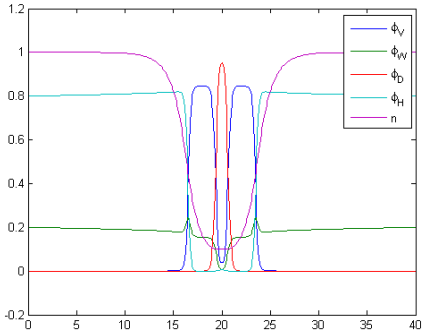

(b) $t = 25$

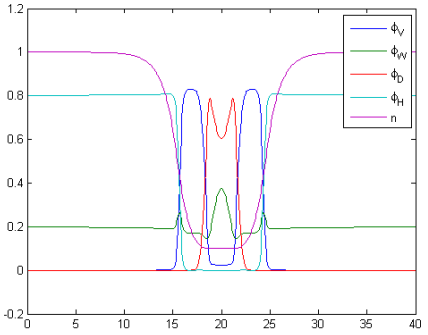

(c) $t = 50$

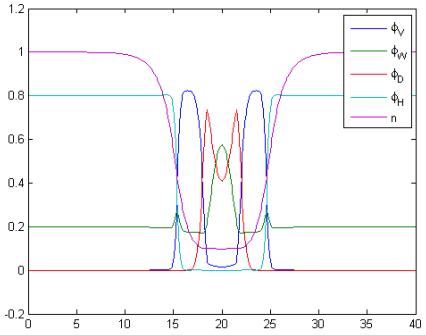

(d) $t = 75$

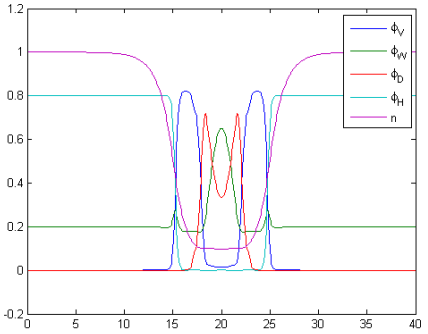

(e) $t = 100$

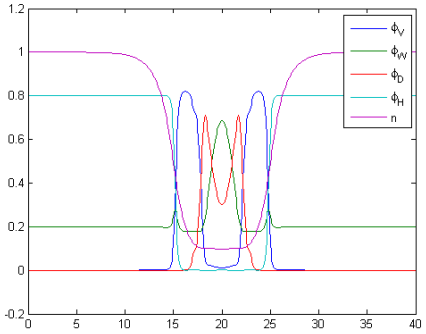

(f) $t = 125$

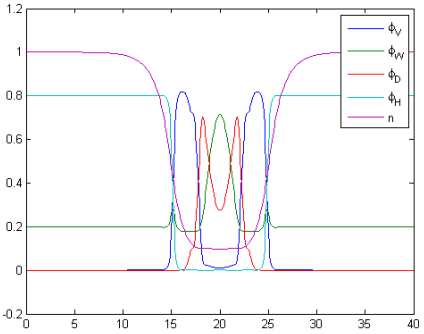

(g) $t = 200$

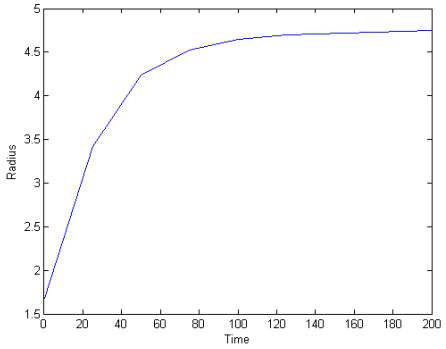

(h) radius of the tumor

Figure 3.1: The evolution to a stable tumor spheroid for a spherically symmetric initial condition with $r = \sqrt{3}$

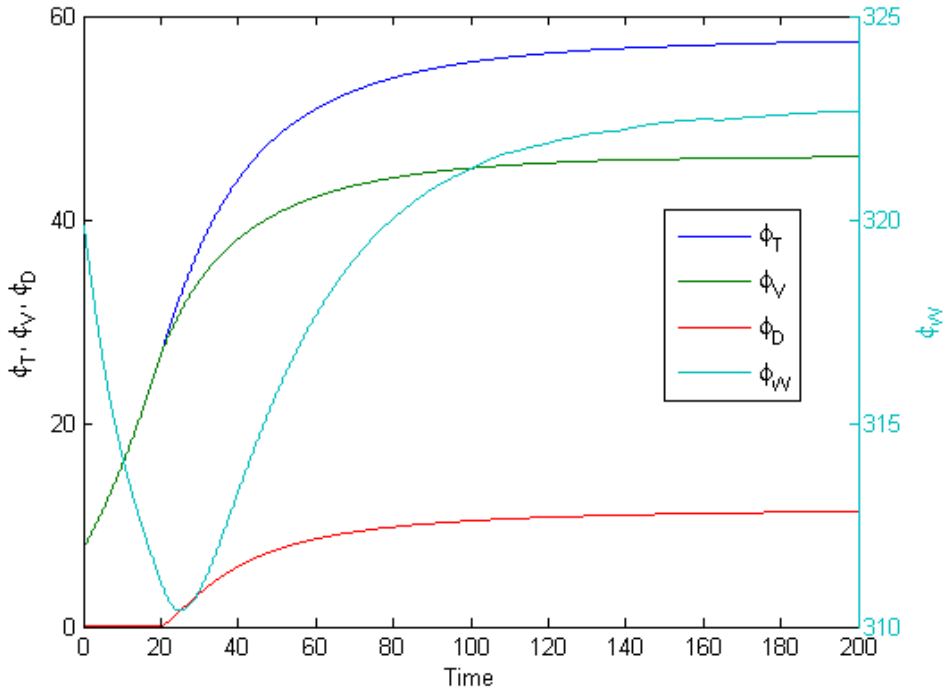

Figure 3.2: Total volume for the different cell species for the symmetric initial condition that evolves to a stable tumor spheroid

tumor stabilizes.

We observe in figures 3.3a and 3.3b that at the steady state the velocities $\mathbf{u}_s$, $\mathbf{u}_w$ and the fluxes $\mathbf{J}_W$, $\mathbf{J}_V$ are zero at the tumor-host interface. Inside the tumor we see the fluxes of the viable cells and the water fraction are equal and opposite and thus they are balanced. In the right half of tumor we see the water fraction fluxing to the right, out of the tumor, and the viable cells fluxing to the left, into the tumor. In the left half of the tumor we see the flux has opposite signs implying the opposite direction of the fluxes. Thus, we can see that water is diffusing out of the tumor and the viable cells are fluxing into the center of the tumor. Notice the fluxes are greatest for the water fraction and the viable cells at the necrotic core interface. In figure (3.1g) we see the highest dead cell fraction is at this interface. Therefore, in this interface more dead cells are lysing and increasing the water fraction which in turn increases the water flux rate. The water fluxing out of the tumor causes the viable cells to

flux inwards.

The velocities inside the tumor are opposite signs and are symmetric about the center of the tumor. In the necrotic core the water has no velocity, it rapidly increases at the necrotic interface and then linearly decreases to near zero at the tumor-host interface. This shows that water is flowing against the flux into the viable cells and the rate increases for the water fraction in the quiescent zone. Inside the necrotic core the water has no velocity and its movement is influenced entirely by the lysis rate and flux. The solid velocity of the tumor and host species is nonzero inside the necrotic core (except the very center) since there is still a small level of viable cells there. The velocity increases until the necrotic interface when it decreases to a near zero level at the tumor-host interface. This shows the greatest cell flow occurs at the necrotic interface and the viable cells are flowing against the flux of the viable cells. Thus, in this case the velocities are acting against the fluxes. In section 4.3 we will see that the direction and magnitude of the velocities is controlled by the parameter γ and increasing this parameter decreases the radius of the stable tumor. However, the velocity of the species is two orders of magnitude smaller than the flux so varying γ does not significantly influence the radius of the stable tumor spheroid.

It is important to note that this steady state is a dynamic one. There is still proliferation of viable cells near the tumor boundaries, but only enough to balance the loss of cells due to death and lysis. Lastly, in the steady state the pressure is zero outside the tumor and it becomes negative inside the proliferating rim and levels out to a constant value inside the necrotic core. Therefore, the pressure of the system is lowest inside the necrotic core and highest outside the tumor in the host.

At the steady state, the interface between the necrotic core ($\phi_V \leq 0.03$ and $\phi_D \geq 0.25$) and the proliferating rim ($\phi_V \geq 0.6$ and $\phi_D \approx 0$) is not well delineated for this set of parameters. The viable cells do not become necrotic instantly, but at the the rate λ_N. Indeed, there is a small percentage of viable cells inside the hypoxic region where $C_0 < \bar{C}_0$ in the steady state.

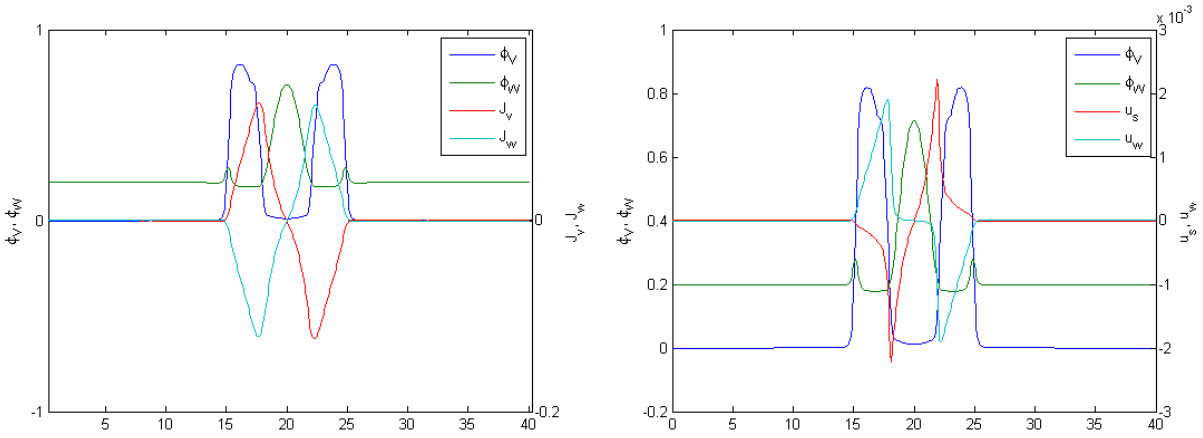

(a) Flux comparison

(b) velocity comparison

(c) pressure

Figure 3.3: Flux and velocity comparisons for the stable tumor spheroid at $t = 200$

$M_V = 200.0$	$\alpha_{VW} = 0.5$	$\phi_W^H = 0.2$	$\phi_D = 0.10$	$\alpha_V = 50.0$
$M_W = 100.0$	$\alpha_{WH} = 0.5$	$\phi_W^V = 0.2$	$C_0 = 0.10$	$\alpha_W = 50.0$
$\gamma = -0.1$	$\alpha_{WDH} = 100.0$	$k_w = 1.0$	$\lambda_l = 0.2$	$\alpha_D = 50.0$
$\epsilon = 0.05$	$\alpha_{VWDH} = 50.0$	$k_l = 1.0$	$\lambda_N = 5.0$	$\alpha_H = 50.0$
	$\alpha_{vitro} = 0.0$	$\nu_{PO} = 0.5$		
	$\kappa = 0.035$			

Table 3.1: basecase parameters

This is consistent with experimental observations. As we will show in section 4.3 increasing the necrosis rate does decrease the level of viable cells inside the hypoxic region. We can also observe a quiescent region is seen within the tumor. As the nutrient level get close the viability level we see a gradual increase in the level of dead cells as the viable cell necrose. This effect can be better seen in two dimension. In figure (3.4) the dark red edge of the viable cells is the proliferating rim and the lighter ring inside is the quiescent region. In the dead cell figure we see the highest dead cell fraction is at the quiescent region and necrotic core interface. The ring of dead cells outside this interface overlaps with the quiescent region for the viable cells. The quiescent zone can also be seen in figure (3.4e). The highest growth rate is seen at the boundary of the proliferating rim and the growth rate decreases further inside the tumor. These results are consistent with previous models of tumor growth [51, 9, 57].

In figure (3.1g) we can see the tumor density outside the bulk of the tumor is very small but nonzero. The reflects the fact that the adhesive force is not strong enough to hold all the proliferating cells together and a very small amount escapes into the host domain. This behavior is consistent with steady spherical solutions of the Cahn-Hillard equation where the velocity and source terms are neglected [33]. This behavior is also consistent with the behavior in the constant water model [71]

3.3 Non-symmetric Initial Condition

We now explore the evolution of a non-symmetric initial tumor. The initial tumor in figure (A.10a) is a combination of a 2, 3, and 4 mode with a radius of three to create a non-symmetric initial condition. In particular, the contour of an n-mode of radius 3 is given by the set $\{(r, \theta)|r = 3+0.5\sin(n\theta)\}$ (i.e. the modes are rose curves with the respective number of petals). Figure (A.10) shows that the initial perturbations on the tumor boundary are quickly smoothed out as the tumor grows and becomes more circular. The growth sequence

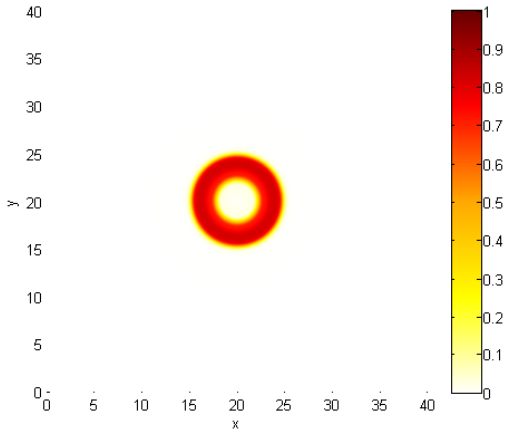

(a) viable cells ϕ_V

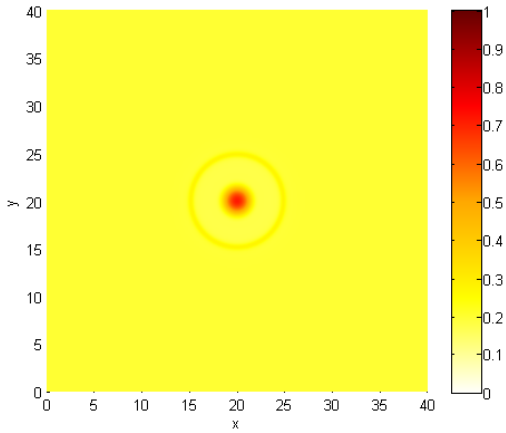

(b) water ϕ_W

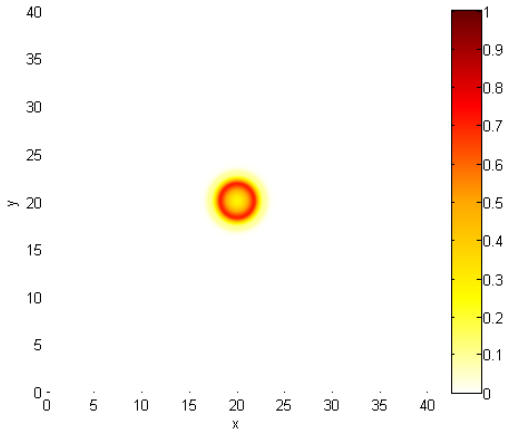

(c) dead cells ϕ_D

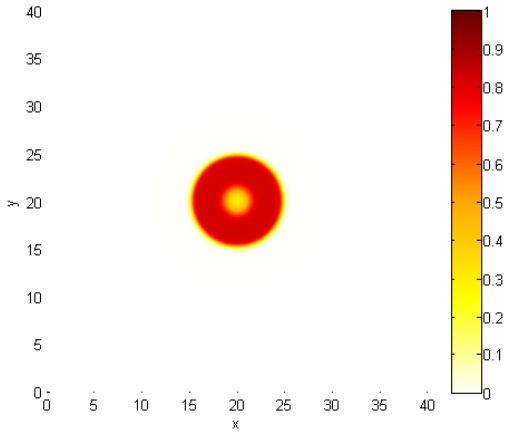

(d) tumor cells ϕ_T

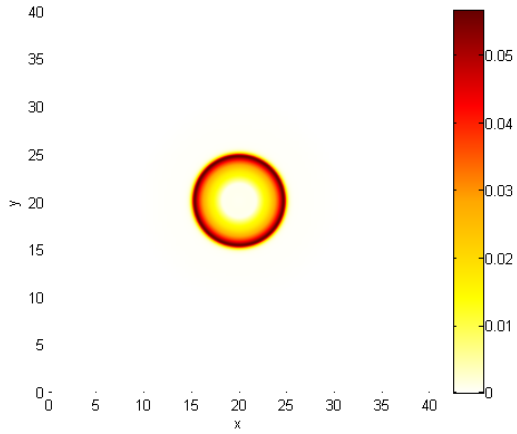

(e) proliferation rate of the tumor

Figure 3.4: The stable tumor spheroid at $t = 200$. In figure (a) the quiescent region can be seen as the lighter ring inside the viable cells and the proliferating rim.

of the viable cells is seen in figure (A.1) and we can see that once the tumor becomes elliptic then the growth rate become faster and the tumor elongates by growing at the two end caps of the ellipse. Interestingly, this is the only place where the tumor is growing (figure (3.5)). As the tumor develops we see that perpendicular to the growing axis there is a bulb that stays dormant in the quiescent region. This bulb is the quiescent region that developed in the initial necrotic core in earlier times, see figure (A.5b).

As the tumor elongates and expands this quiescent region does not grow and is left behind as the tumor evolves. Further, the growing caps expand and leave a quiescent trail of cells in their wake (figure (3.7e)). Indeed, the only part of the tumor that is evolving is the end caps. We can also observe there is a necrotic region behind the advancing tumor end caps. At approximately $t \approx 280$ we see the elongated necrotic core begins to collapse between the advancing core behind the growing ends and original necrotic core. As the tumor grows, the elongated the dead cells in the necrotic core are lysed to water and the water is fluxed out of the system. However, the cells in the quiescent region are not growing fast enough to balance the inward flux and the core pinches shut. The initial necrotic core does not close as its more circular shape is more conducive to maintaining a necrotic core since there are more viable cells in a curved region than a straight section and the proliferation rate is higher (figure (3.5)). Thus the curved section will produce enough dead cells to maintain the initial necrotic core. The elongation of the tumor is typical behavior in the preliminary stage of malignant cancer development. The non-symmetric simulation presented here has a similar morphology to the two cancer types presented in figure (3.6).

Looking at the water fraction and dead cell fractions in figures (A.2) and (A.3) we see the initial liquid necrotic core is formed by $t = 40$. By $t = 120$ most of the liquid has fluxed out of the center as the tumor begins to elongate. As the tumor grows we can see the decrease in the water fraction and an increase dead cells in the wake of the proliferating rim and the water peaks at the tumor-host interface are also present in this non-symmetric case. In figure

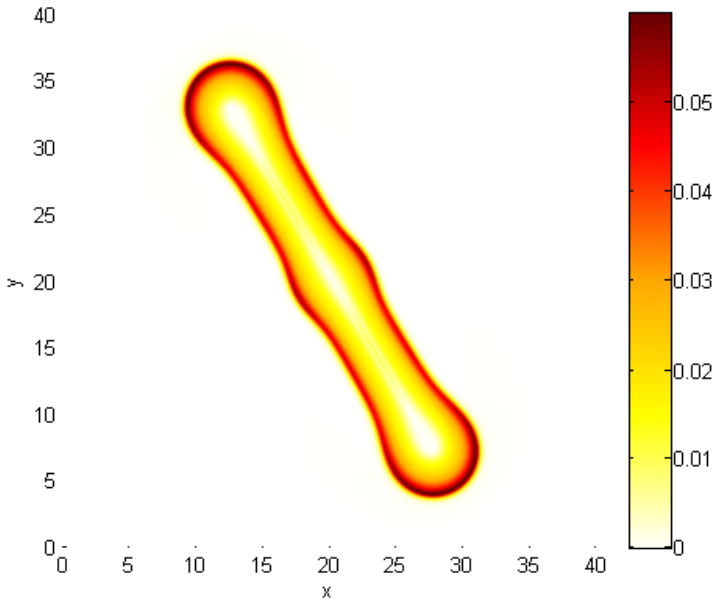

Figure 3.5: proliferation rate of the tumor

(3.7b) we see the conversion of the viable cells to dead cells to water as the tumor progresses. In the elongated portion of the tumor we can see the the remnants of the dead cells that did not undergo lysis and leave a trail behind the progressing tumor. We can also see the corresponding decrease of the water fraction in the advancing necrotic core as the osmotic pressure drives the water out of the tumor to create this slight water fraction difference.

We can also observe the different pressure gradients at the different stages of the tumor progression in figure (A.4). We can see that the pressure is negative where the tumor is moving inward and positive where the tumor is expanding. Initially, the tumor will shrink inward as the center has a negative pressure and the proliferating rim will grow outward where the pressure is positive. From time $t = 40$ to $t = 120$ we can observe the positive pressure where the tumor will expand and a negative pressure in the center indicating the formation of a necrotic core and the water fluxing out of the system. As the tumor progresses the positive pressure is greatest where the tumor is advancing and the decrease in the pressure where the water is fluxed out of the straight section of the tumor and the viable cells pinch

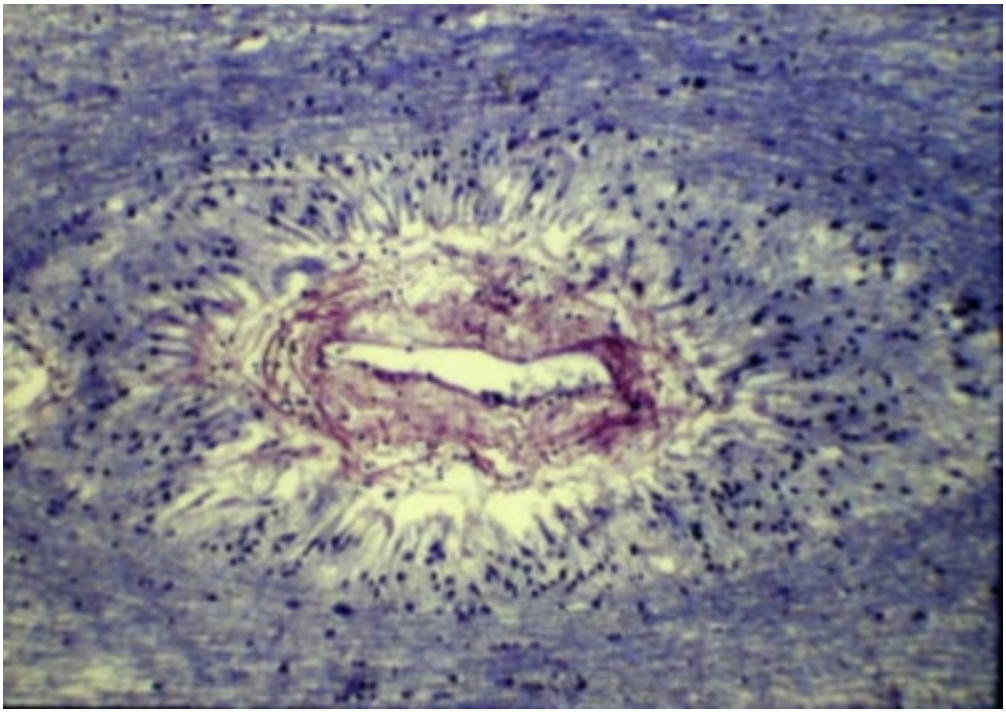

(a) Histological section showing elongated dark-staining gliomatosis cerebri cells in a preivascular state [45]

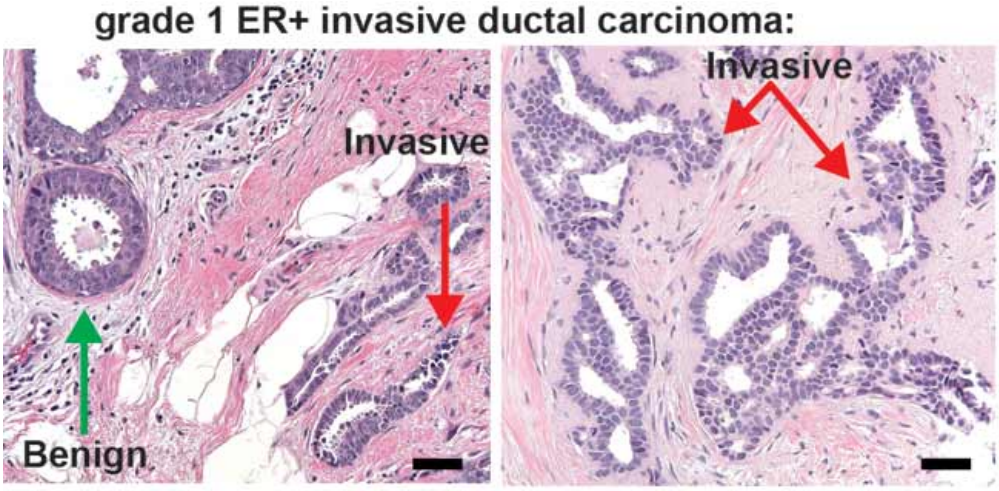

(b) Mammary epithelial tissue structures undergo characteristic changes as tumors progress from benign to invasive. [54]

Figure 3.6: Two in-vivo tumors that have developed morphologies similar to the non-symmetric simulations.

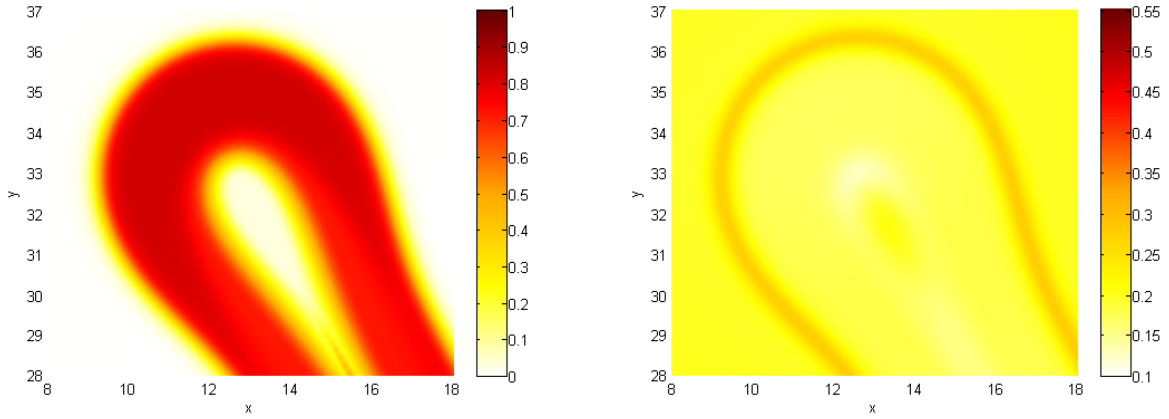

(a) viable cells ϕ_V

(b) water ϕ_W

(c) dead cells ϕ_D

(d) pressure p

(e) proliferation rate of the end cap

Figure 3.7: A closeup of a proliferating end of the non-symmetric tumor at $t = 400$

together. Thus, the pressure of the system can gives us an indication of how the tumor will develop.

We now consider the evolution of the non-symmetric initial tumor with an combination of a 2, 3, and 4 mode with a smaller radius of $\sqrt{3}$ to see how the tumor development is influenced by the size of the non-symmetric tumor. In figure (A.5) we can see that the tumor appears to be circular between $t = 80$ to $t = 160$ and then the tumor begins to grow like the case with $r = 3$. We also saw that the simulation with the larger radius also evolved to a circular shape before it began to grow in an oblong shape (figure (A.10)). In figure (A.9) we see the non-symmetric initial conditions with radii $r = 3$ and $r = \sqrt{3}$ and the overlaid contour of the circular initial with an equivalent volume. The radii of these corresponding circular initial conditions are $r = 4.0472$ and $r = 2.3368$ for the non-symmetric cases $r = 3$ and $r = \sqrt{3}$ respectively. The evolutions of the non-symmetric initial conditions are then overlaid with the contours of the steady state of the circular initial condition. In figure (A.9c) at $t = 40$ the non-symmetric tumor is close to the circular steady state but it is slightly more oblong. This difference in the proliferating rim creates the instability that elongates the tumor. In figure (A.9a) a close up of the equivalent situation is shown at $t = 200$ with the steady state of the circular tumor with the smaller initial radius. This tumor is closer to the steady state than the larger initial condition but, it is slightly oblong along the same axis of growth. The inhomogeneity in the proliferating rim is much smaller and it takes a longer time for the instability to develop. Once the tumor begins to elongate the growth rate is the same as the larger initial condition. This behavior can also be seen in the following figure (3.8). Note that the circular initial conditions both converge to the same steady state and after the tumor leaves the steady state regime they develop at same rate, although at different times.

Looking at the graph of the total tumor volume (figure 3.9) we see growth of the tumor is primarily due to the growth of the viable cells. Between $t = 25$ and $t = 100$ the initial growth rate is slowed when the tumor morphology is similar to the steady state for the

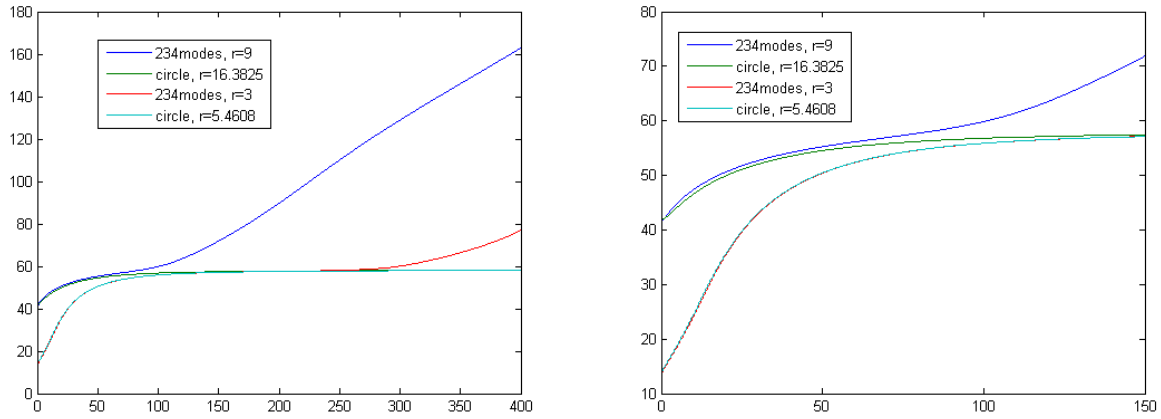

(a) Total tumor volume

(b) Close up of the total tumor volume

Figure 3.8: Total tumor volume for the 234-mode and circular initial conditions with different radii.

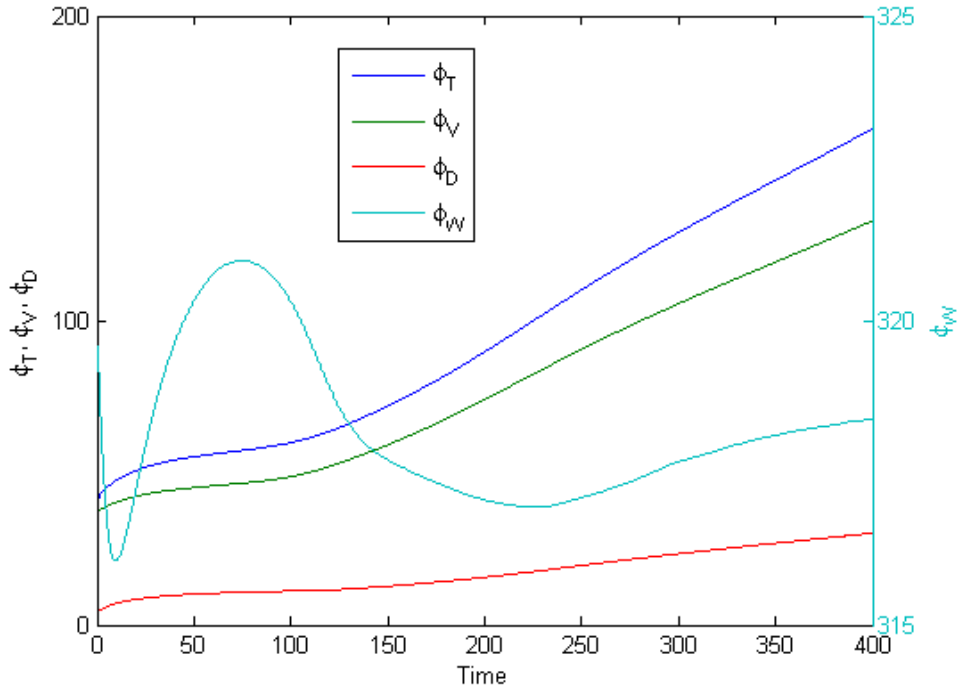

Figure 3.9: Total volume for the different cell species for the non-symmetric initial condition with $r = 3$ that develops an invasive morphology

symmetric tumor. Once the proliferating rim instability is large enough to destabilize the tumor we see the linear growth rate caused by the steady advancement of the the tumor end caps beginning at time $t = 100$. The volume of the dead cells also follow this same behavior. Once the tumor begins to elongate the dead cells are produced in the wake of the advancing viable cells. However, the dead cells are slower to accumulate since only ten percent of the dead cells produced will remain after lysis as opposed to the viable cell levels that remain at 70% in the quiescent behind the advancing front. The total volume of the water fraction exhibits the more interesting non-monotonic behavior. Initially the water is uptaken by the viable cells, but the tumor quickly develops a hypoxic region so the viable cells begin to die and the lysed cells begin to increase the water volume. As the tumor begins to elongate at $t \approx 80$ the water is fluxed out of the center of the tumor and the water level begins to fall. The longer the tumor grows the smaller the initial necrotic core becomes and the less water is present to flux out of the center. This slows the decrease in the water level in the tumor between $t \approx 120$ and $t \approx 240$. Beginning at time $t \approx 240$ we see the separation between the initial necrotic core and the core formed behind the advancing end caps (A.1g). As the tumor continues to grow the dead cells are lysed where the viable cells begin to pinch together and the overall water level begins to rise.

3.4 Numerical Method

To solve the equations an adaptive finite difference nonlinear multigrid method is used. The method know as BSAM (Block-Structured Adaptive Multigrid Solver) was developed by Wise et.al. [69, 70]. This solver, based on the multigrid algorithm the system solves the system with near optimal complexity. In this approach, this fourth order system is written as a system of second order equations and an implicit second order Crank-Nicholson algorithm is used for the time discretization. This allows us to avoid a high order time step constraint

that would result from an explicit method. This method is known to be stable with $\Delta t \approx h$. The spatial derivatives are discretized with a second order central difference scheme. The nonlinear equations at implicit time levels are solved with a nonlinear multigrid method. The advection terms are treated with an unwinding WENO scheme developed by Jiang and Shu in 1996 [36].

Block structured refinement is used to increase local resolution where the gradient of the volume fractions is large. The volume fraction for the viable cells has a steep gradient at the tumor-host and the necrotic core interface. Thus, the simulations will have finer resolution at these critical interfaces. The composite mesh consists of a hierarchy of levels. Each refinement of the mesh is half the length of the parent mesh and each child mesh sits on top of the courser parent mesh. The equations are sloved on a computational domain of $[0, 40]^2$ with time step $\Delta t = .005$. The coarsest mesh level uses 64×64 grid points and there are three levels of mesh refinement each doubling the number of grid points. The finest grid has an effective resolution of 512×512 grid points, see figure (3.10). Due to the mesh adaptivity, the highest resolution of the image is obtained at a fraction of the cost of using the finest mesh grid uniformly over the entire domain.

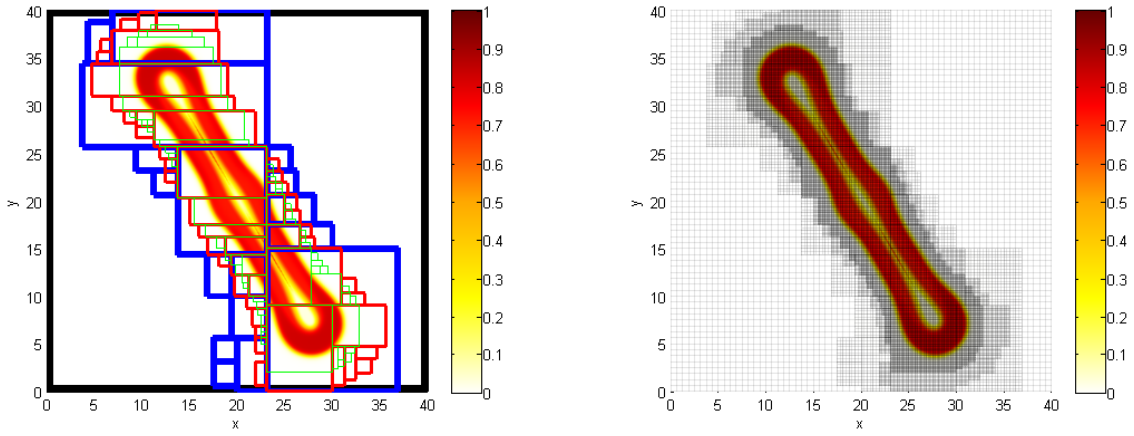

(a) The three levels of the mesh are presented here. The coarsest grid is black and the levels areshown. The first level of the graph is seen away refined in blue, red, and, green levels respectivelywhere green is the finest mesh.

(b) The three levels of the mesh refinement are presentedfrom the tumor where the grid is sparsest and we can see that the densest grid overlays the tumor.

Figure 3.10: The three levels of mesh refinement are presented on the viable cells for non-symmetric case at $t = 400$

Chapter 4

Parameter Studies for Spherically Symmetric Tumors

4.1 Introduction

We now consider how the parameters can affect spherically symmetric in-vivo tumor growth in two dimensions. It is well known that a compact solid tumor will grow to a diffusion-limited size that is stable. To produce morphological instabilities, substrate gradients, necrosis, and inhomogeneous proliferation allow the tumor further growth by exposing more surface area of the proliferating rim to the nutrients and growth factors [71]. We will examine which parameters are capable of destabilizing the stable tumor and how sensitive the radius of the steady state tumor is to a given parameter change. This chapter is divided into three sections. We consider the cases of parameters that are physical vs model-based and sensitive vs nonsensitive. Appropriately, there are no model-based parameters that are sensitive.

The first section discusses the parameters that can destabilize the tumor spheroid and have a significant impact on the radius of the steady state. The seven parameters in this category

	Parameter	Meaning	Figures
Sensitive Physical Parameter	λ_l	lysis rate	B.1,B.2
	κ	diffusion rate	B.3,B.4
	M_V	viable cell mobility	B.5, B.6, B.8
	ϕ_W^H	water level in host	B.9,B.10,B.11,B.12
	ϕ_W^V	water level in viable cells	B.13,B.14, B.15
	C_0	hypoxia level	B.18,B.19
	ν_{PO}	nutrient production	B.20,B.21
Nonsensitive Physical Parameters	M_W	water mobility	B.22,B.23
	γ	adhesion force	B.24,B.25, B.26
	λ_n	necrosis rate	B.27,B.28
Nonsensitive Model Parameters	ϵ	interface thickness	B.29,B.30
	α_{VW}	water level in viable cell control	B.31,B.32
	α_{WH}	water level in host control	B.33,B.34
	α_{vitro}		B.11,B.12
	α_{WDH}		
	α_{VWDH}		
	α_V,α_W,α_D,α_H		

Table 4.1: Parameters for spherically symmetric tumor growth, definitions and figures

are λ_l, κ, M_V, $\bar{\phi}_W^H$, $\bar{\phi}_W^V$, $\bar{C}_0$, and ν_{PO}. We will show that the lysis rate λ_l, the diffusion rate κ, and the water level in the viable cells $\bar{\phi}_W^V$ have ranges that produce an unstable tumor. The other parameters, the hypoxia level $\bar{C}_0$, the nutrient production rate ν_{PO}, and the water level in the host $\bar{\phi}_W^H$ can significantly impact the final size of the steady state tumor, but they produce stable tumors in their parameter regimes. The parameter mobility rate of the viable cells can produce tumor branching if the value is set too low since small values of this parameter are capable of producing inhomogeneous thickness in the proliferating rim. It is important to note that κ, $\bar{\phi}_W^H$, $\bar{\phi}_W^V$ are new parameters not seen in previous models.

The second section concerns the physical parameters that do not significantly impact the stable tumor radius and produce stable tumors above a certain threshold. The water mobility parameter M_W can destabilize the tumor if the values are too low, but in higher ranges the tumor will be stable. The destabilization that occurs if M_W is set too low is due to the decrease in the diffusion parameter in the previous section. The necrosis rate, λ_n, produces

stable tumors if it is above a certain threshold and the tumor radius is not significantly affected. For small values of λ_n we see that although the tumor radius is affected, the viable cell fraction becomes too high in the necrotic core. The last parameter γ that measures the adhesion forces and does not affect the stable tumor radius in the considered range. This is consistent with previous mixture models.

In the third section the model based parameters that are necessary to tune the behavior of the system and to provide a computational framework are analyses. These parameters are given by α_{VW}, α_{WH}, ϵ, α_{vitro}, α_{VWDH}, α_{WDH}, α_V, α_W, α_D, and α_H. The α_{VW} and α_{WH} parameters are used to enforce the water levels in the respective species. The ϵ parameter is a manifestation of the diffuse interface method that we use to numerically solve the system. It is shown that for a large enough α_{VW} and α_{WH} parameters the stable tumor radius will not be affected and ϵ does not significantly affect the tumor radius. The α_{vitro} parameter enforces a phase separation between the host and water fractions when we are modeling the in-vitro case ($\phi_W^H = 1.0$). The α_{WDH} parameter prevents unphysical build up of host in the necrotic core of the tumor and the α_{VWHD} parameter prevents the unphysical generation of a phase in an interfacial region. The α_V, α_W, α_D, and α_H parameters prevent the volume fractions from becoming negative. Only the first three parameter are studied in this section as the other parameters are only necessary to prevent unphysical phase generation and varying them does not influence the development of the tumor.

4.2 Sensitive Physical Parameters

The lysis parameter, λ_l, controls how fast the dead cells degrade and release their intracellular fluid. In figure (B.1) we can see that the lower the lysis rate is the larger the radius of the tumor will be at time 200. We can also observe the lower the lysis rate the higher the percentage of dead cells at the necrotic core interface as the slower lysis rate allows a greater

buildup of dead cells before they are converted to water after they necrose. For $\lambda_l = 0.05$ we see a dip in the water fraction at the necrotic core interface in figure (B.1e). This dip occurs as the viable cell uptake the water and the dead cells are not dying fast enough to replace this water. Indeed, this dip in the water fraction is only seen for $\lambda_l < 0.2$. Interestingly, the larger the lysis rate the smaller the water fraction inside the necrotic core. As we can see in figure (B.2) for high λ_l the dead cells are lysed rapidly and the water is fluxed out to balance the tumor. For smaller lysis rates the dead cells accumulate and the buildup of the water fraction from the degradation of the dead cells is greater than rate of water diffusion from the necrotic core. We can see in figure (B.2a) the tumor stabilizes slowly for $\lambda_l = 0.1$ and is unstable for $\lambda = 0.05$. In figure (B.2c) we examine the total tumor volumes for intermediate lysis rates between 1.0 and 0.05 out to $t = 500$. We see the rate the tumor stabilizes and how fast the tumor continues to grows after the formation of the necrotic core will influence the choice of the lysis parameter. We can see that the different lysis levels form a continuum of growth rates and it is not always clear how to determine what constitutes a stable tumor.

Additionally, For $\lambda_l = 1.0$ we a smaller steady state tumor that converges to its steady state by $t = 20$. This is consistent with the behavior in the constant water model [71]. However, for larger lysis values the tumor has a higher percentage of viable cells in the necrotic core. For $\lambda_l = 1.0$ the dead cells are converted to water fast enough to maintain a viable cell fraction of $\approx 12\%$ within the necrotic core. In the constant water fraction model the water fraction does not influence the growth rate of the viable cells so the necrotic core contains no viable cells in that model.

The κ parameter is the rate water diffuses from out of necrotic core. We can see in figure (B.3) that the larger the parameter the smaller the radius of the tumor. This is due to the higher the diffusion rate the greater the flux of water out of the center of the tumor and the more the viable cells flux inwards to stabilizes the tumor. If the diffusion rate is too low then the water released from the dead cell degradation will accumulate in the necrotic core faster

than it is fluxed out and the tumor will not stabilize. In figure (B.4a) for $\kappa = 0.005$ we see precisely this behavior for an unstable tumor. We also note that the smaller the parameter the slower the tumor stabilizes. This behavior is similar to the lysis rate above. How fast the tumor continues to grows after the formation of the necrotic core will influence the choice of the diffusion parameter. Further, we can see that the diffusion parameter influences the amount of liquid and dead cells in the necrotic core. For higher diffusion rates the lower the water level in the core and the higher the dead cell fraction. For high diffusion levels we can also see the water fraction in the viable cells dip as it approaches the necrotic core as the diffusion fluxes the water out.

This diffusion parameter can also be increased to stabilize unstable models. The in vitro case ($\bar{\phi}_W^H = 1.0$) is unstable for the base case parameters but we can make the tumor stable by increasing the parameter κ to 0.10 (see figure (B.12)). This can be interpreted as the osmotic pressure gradient working against the diffusion gradient. This demonstrates the principle value of this parameter. The water diffusion term is necessary to produce stable tumors and as the diffusion rate goes to zero we see the unbounded growth of the tumor.

The viable cell mobility, M_V, is a measure of how fast the viable cells can move around the tumor to minimize the energy. The tumor stabilizes by balancing the flux between water out of the tumor and the cells in the proliferating rim fluxing back toward the center. In figure (B.5) we see the greater the cell mobility the smaller the radius of the tumor and the higher the dead cell fraction in the necrotic core. As the dead cells lyse and the water is fluxed out of the core the higher viable cell mobility fluxes the cells towards the center of the tumor faster which increases the fraction of viable cells in the hypoxic region. For small M_V the viable cells do not replace the dead cells fast enough and all the dead cells are converted to water which raises the water level in the center of the tumor. In effect, the higher the viable cell mobility the more the water is forced out of the center of the tumor. In figure (B.8b) we see the increase in water is from the lysis of the dead cells after time $t \approx 20$.

In figure (B.5d) we see that for a high enough viable cell mobility the radius of the steady state does not decrease by a significant amount. Doubling the viable cell mobility rate from the base case results in a radius decrease of $\approx 4\%$. Thus, for a high enough viable cell mobility this parameter does not significantly impact the steady state tumor radius. However, we do see a new morphology for small viable cell mobilities. For $M_V = 25$ the tumor becomes unstable and we see the tumor is no longer circular. The tumor evolution to a square shape is shown in more detail in figure (B.6). The tumor is circular at time $t = 150$ and there is a gradual progression to a square shape as the viable cells begin to accumulate at the corners. We interpret this as the viable cells do not have the mobility to move around the tumor fast enough to maintain the circular shape. Figure (B.7) show the morphology for the $M_V = 25$ case carried out to time $t = 500$. After time 200 we see that the tumor continues to grow where the viable cells are the thickest and by time $t = 300$ we see the viable cells have coalesced at the corners of the square. These buds continue to grow until they also develop necrotic cores. As the buds continue to grow they begin to thin at head of the cap as the viable cells are not moving fast enough to maintain a viable cell rim of uniform thickness. This thinning at the head of the tumor eventually splits the bud into two new buds at time $t = 500$. Here we can see that the new buds have already grown enough to develop additional necrotic cores and this process will repeat itself. Thus, if the viable cell mobility parameter is set too low then the tumor will be unstable and will develop an irregular morphology due to an inhomogeneous proliferating rim. These different parameter regimes will have profound effects on the tumor growth in the non-symmetric case.

The parameter $\bar{\phi}_W^H$ is the fraction of water present with the host fraction. Differing tissues have different densities and different water levels so this parameter is necessary to model these different tissue types. Further, the in-vitro case can be considered by setting $\bar{\phi}_W^H = 1.0$. We consider the in-vivo cases first. In figure (B.9) we notice that the larger the outside water fraction the larger the tumor radius and the higher the water level in the necrotic core. This is due to the water flux depending on the amount of water present. For a higher water level

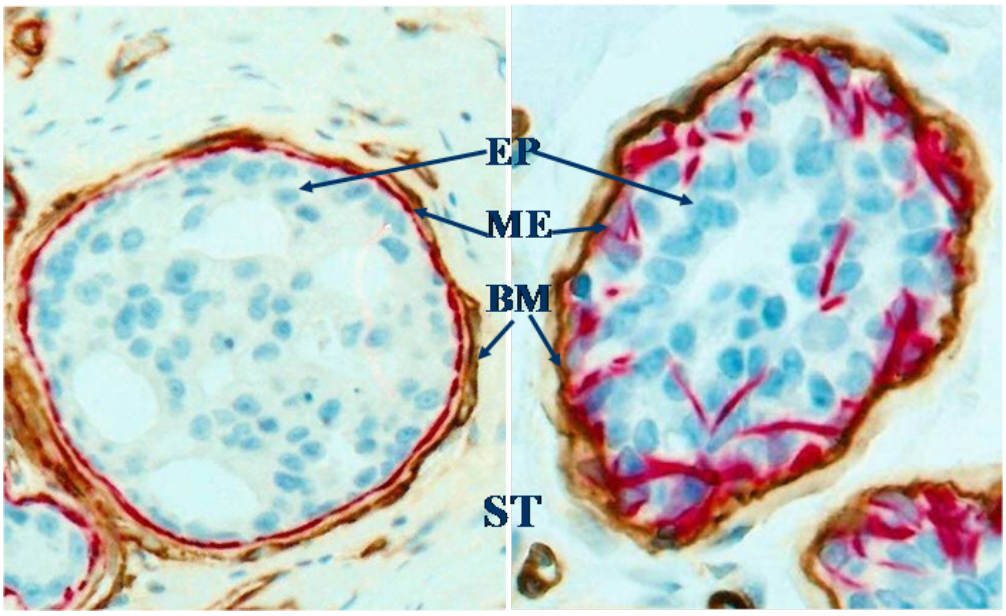

Figure 4.1: Structural relations among epithelium (EP), myoepithelium (ME), basement membrane (BM) and stroma (ST). Human breast sections were double immunostained for smooth muscle actin (red) and collagen IV (brown). 500X [20]

outside the tumor the greater the water flux into the proliferating viable cells and hence a higher water level in the necrotic core. Also note that as the water level increases and the host fraction decreases, the greater the host buildup at the tumor-host interface (figure (B.9e)). This buildup of host around the expanding tumor is seen in certain experimental cases. For example, in figure (4.1) we the buildup of breast tissue at the tumor-host interface.

However, this buildup of host may not be realistic for all cell types being studied. It is possible to adjust the α_{WH} parameter to lessen the buildup of the host at the tumor-host interface. In figure (B.9f) we see that increasing the parameter from 0.25 to 2.5 results in a 60% decrease in the peak height. However, increasing this parameter produces a 16% increase in the tumor radius. In figure (B.10) we can see that the lower water fraction produce a lower tumor growth rate and consequently the necrotic core is developed at a later time. The figure also shows that the higher the water fraction outside the tumor the larger the stabilized tumor. However, we can note that varying $\bar{\phi}_W^H$ does not change the stability of

the tumor.

In the in vitro case we still see the buildup of host tissue at the tumor-host interface. However, in this instance there should be no host present. To remedy this situation we include the energy term,

$$\frac{\alpha_{vitro}}{2}\phi_W^2\phi_H^2$$

with $\alpha_{vitro} = 100$. This term has the effect of separating the host and water species, but the water is present in the entire domain so this has the effect of eliminating the buildup of the host species. In figure (B.11d) we see the difference with and without the extra term in the energy. It is important to note that the host fraction is not entirely gone with the extra energy term. The maximum value of the host fraction with the extra energy term is $\approx 10^{-3}$. It is not possible to simply increase the α_{WH} parameter to eliminate the host buildup as in the in-vivo case. For in-vivo case ($\bar{\phi}_W^H < 1.0$) the energy term $\alpha_{WH}\bar{\phi}_H^2(\phi_W - \bar{\phi}_W^H)^2$ is a double well potential but, in the in vitro case this term becomes a single well potential $\alpha_{WH}\bar{\phi}_H^2(\phi_W - \bar{\phi}_W^H)^2 = \alpha_{WH}\bar{\phi}_H^4$ since outside the tumor we have $\phi_H + \phi_W = 1$. Therefore, any deviation of the host from 0.0 does not induce the same energy penalty as a deviation in the in-vivo case. However, in figure (B.12) we can see that for the base case diffusion parameter the tumor is unstable with the new energy term. This in vitro case can be made to be stable by increasing the diffusion parameter κ from 0.035 to 0.10. The increase produces a stable tumor with a similar volume, initial growth rate, and morphology as the simulation without the in-vitro energy term. Thus, with this energy modification we are able to produce stable tumor spheroids in the in vitro case.

The parameter $\bar{\phi}_W^V$ is the water fraction level in viable cells. In figure (B.13a) we see that $\bar{\phi}_W^V = 0.5$ has distinctly different behavior than the lower water levels. As $\bar{\phi}_W^V$ increases the viable cells levels decrease, but for smaller viable cell levels the tumor grows to a larger

radius since the source term for the viable cells is maximized for $\phi_V = \phi_W = 0.5$ and lower levels of viable cells uptake less nutrients. We can see the differences in the viable cell water concentration in figure (B.13b). We can note that the water concentration is less what is prescribed by the $\bar{\phi}_W^V$ parameter. As the parameter increases the percent difference can be see in figure (B.13e). The higher the prescribed water level in the viable cells is above the water level in the host the less that state is preferred by the energy for the system. We can also see in figure (B.15) the higher the $\bar{\phi}_W^V$ parameter the faster the initial growth rate and the larger the final tumor volume. The trend holds except for in the $\bar{\phi}_W^V = 0.4$ and $\phi_W^V = 0.5$ cases. For $\bar{\phi}_W^V = 0.4$ the growth rate in the same as the $\bar{\phi}_W^V = 0.3$ case but it is not sustained as long as there are fewer viable cells after the necrotic core is formed. However, the larger source term for the viable cells allows the 0.4 case to eventually surpass the volume of the 0.3 case.

In the $\bar{\phi}_W^V = 0.5$ case we see the volume grows initially at the same rate as $\bar{\phi}_W^V = 0.4$, but once the tumor reaches its peak volume at ≈ 45 the tumor begins to shrink. As the tumor develops we see the tail of viable cell fraction begins to grow further out into the host as seen in figure (B.14b). The higher the viable cell water parameter is set the longer the viable cell tail becomes (figure (B.14a)). We note that the nutrient production in the system is only active when $\phi_T < 0.01$. and for the $\bar{\phi}_W^V = 0.5$ case the tails begin to branch from the bulk of the viable cells for $\phi_T > 0.02$ due to the higher water level. This higher branching site inhibits the nutrient production and greatly reduces the nutrient concentration at the proliferating rim (see figure (B.14c)). As the nutrient level decreases and the tumor mitosis rate slows. The viable cells necrose and are cleared out of the necrotic core faster than viable cells can proliferation. Thus, the tumor collapses back to a steady state. This regression of the tumor is unphysical and an adjustment to the model can be made to produce more physically realistic results.

All of the parameters here produce stable tumors. The main reason for the aberrant behavior

in the $\bar{\phi}_W^V = 5.0$ case is the level of shedded cells inhibit the nutrient production. To prevent this steady state collapse in this case we change the tumor fraction necessary to cease nutrient production from 0.01 to 0.03. Thus, we take the production function to be,

$$\tilde{Q}(\phi_T) = \begin{cases} 1.0 & \text{if } \phi_T < 0.03 \\ 0 & \text{if } \phi_T \geq 0.03. \end{cases}$$

Figure (B.16) shows how this new nutrient production term impacts the tumor. We see similar behavior to $M_V = 25$ case as the proliferation rate is now greater than the viable cell mobility. For the base case parameter $M_V = 100$ we see buds forming on the corners of the square as in the $M_V = 25$ case. Increasing the viable cell mobility rate to 200 we no longer see a square but we can see an elongation process forming as the viable cell rim becomes thinner on the left side of the tumor. Increasing M_V again to 300 produces a spherical tumor as the viable cells can move fast enough to form a homogeneous rim and stabilize the tumor. Increasing M_V to 400 also shows a stable spherical tumor with a slight decrease in the radius that is consistent with higher levels of the viable cell mobility parameter. In figure (B.17) we see that the initial growth rate for $\bar{\phi}_W^V = 0.5$ case is greater that the $\bar{\phi}_W^V = 0.4$ case regardless of the change in viable cell mobility rates. Note the tumor stabilizes for the $M_V = 300$ mobility and for the $M_V = 100$ case we see a sharp increase in the growth rate of the tumor as the corners of the tumor begin to bud. We also note that for $M_V = 300$ the tails of the viable cells are still present and the water level inside the viable cells has not increased. Indeed, increasing the lower bound of the nutrient production term produces a more reasonable morphology that is consistent with the other viable cell water levels once the mobility of the viable cell is increased to balance the increased proliferation rate.

The parameter $\bar{C}_0$ sets the hypoxia level, below which, the cells begin to necrose. In figures (B.18) we can see that a decrease in $\bar{C}_0$ creates a tumor with a larger radius and a thicker proliferating rim. We can also see the the increase in the tumor radius is mainly due to the

increase thickness in the viable cells. Indeed, this is the only parameter that does influence the width of the proliferating rim. Figure (B.19) shows the lower the $\bar{C}_0$ value the longer the tumor is in its growth state and the later the formation of the necrotic core. This is because it takes a longer time to uptake the nutrients to the viable level and a lower level of nutrient can support more viable cells. Further, the lower the viability level the more cells are dying in the necrotic core which will raise the water level in the core. We can also see that the higher the viability level the faster the tumor stabilizes. Doubling the necrosis level of the base case value of $\bar{C}_0 = 0.10$ results in a $\approx 38\%$ increase in the stable tumor radius and halving the base case value results in a $\approx 25\%$ decrease in the tumor radius (figure (B.18e)). However, all of these cases result in a stable tumor. As long as the necrosis level is nonzero the resulting tumor will be stable.

The parameter ν_{PO} controls the rate that the surrounding vasculature replaces the nutrients that are uptaken by the tumor. In figure (B.20) we see that the smaller the nutrient production rate and the smaller the stable tumor radius. For slower nutrient production rates the slower growth rate. This results in more dead cells in the center of the tumor and a lower water level in necrotic core. Alternatively, the higher the nutrient production rate the faster the tumor grows and we see a correspondingly higher water level in the necrotic core. However, the radius graph in figure (B.20d) shows the radius of the steady state tumor increases at a slower rate as the production rate increases. Thus, greater the production rates will not lead to a stable tumor of an arbitrary radius.

This behavior can be seen in the average nutrient concentration in the host (see figure (B.20e)). Initially there is a drop in the level of nutrients in the host as the tumor expands and the nutrient concentration levels out once the tumor begins to stabilize. Note that the nutrient concentration does not return to the initial concentration as the steady state is dynamic and the viable cells are continually uptaking nutrients. Also observe that the higher the production rate the higher the average nutrient concentration in the host

tissue. For $\nu_{PO} = 2.0$ the average nutrient concentration is already $\approx 99\%$ and higher values will asymptotically approach 1.0. Hence increasing the production rate past 2.0 will not substantially change the nutrient concentration near the host.

We can see in figure (B.21) that the smaller the nutrient production rate the slower the initial tumor growth since the effective nutrient levels will be lower near the tumor as the uptaken nutrients are replaced at a slower rate. The slower growth rate produces less dead cells and uptakes less water. We can also see that all of these nutrient production rates produce a stable steady state. This parameter is measurable and one which can be easily controlled in the in-vivo and in-vitro environments to control the steady state tumor radius.

4.3 Nonsensitive Physical Parameters

The first parameter we look at in this section is M_W, the mobility of the water fraction. This variable measures how fast the water fraction can move within the system to minimize the energy. In figure (B.22) we can see that a larger water mobility results in a lower water fraction in the necrotic core because the higher the water mobility is the faster the water can flux out of the necrotic core of the tumor. In figure (B.22b) it is observed that the smaller the water flux the greater the buildup of water in the necrotic core and larger the core is (figure B.22c). Although the dead cell volumes don't vary significantly while varying M_W the buildup of water does change the morphology of the dead cells. This change in the radius of the core is what causes the decrease of the tumor radius as the water mobility increases. If the water mobility is low enough then the water will not be able to flux out of the necrotic core fast enough to prevent the buildup of water in the core and the tumor will not stabilize. Indeed, for $M_W = 50$ the tumor is no longer stable. In figure (B.22d) we can observe that for a high enough water mobility the radius does not change significantly which is why we term this parameter nonsensitive. Doubling the initial water mobility to 400 the radius is

only decreased by 2%.

In figure (B.23b) we can observe how the different water mobilities impact the tumor development. The initial dip in the water volumes is due to the water being uptaken by the proliferating cells and to balance this decrease, the water fluxes into the tumor. As the water mobility decreases the initial growth rate of tumor decreases and the more water is uptaken by the proliferating rim. Once the cells begin die in the hypoxic region and begin to undergo lysis the water level increases in the necrotic core. The higher mobility the faster this water in the center can flux out of the tumor. For $M_W = 50.0$ the flux is too slow to prevent the buildup of water in the core as the intracellular fluid is released by lysing. If this water mobility rate is set too low then the tumor will be unstable as this rate lowers the water diffusion parameter into the unstable regime. Thus, the volume fractions are insensitive to changes in M_W once the parameter is set high enough.

The γ parameter measures the adhesion force between the cells and controls the stiffness of the tumor boundary. The larger values represent a stiffer boundary interface and the stiffer the interface the less susceptible the morphology is to morphological instability. Thus, for the symmetric case presented here there should be no significant distinction between the different adhesion parameters [71]. This is exactly what we see in the figures (B.24) and (B.25). This behavior is consistent with the constant water model. However, the effect of the γ parameter is evident in the pressure and velocity terms (figure (B.26)). This adhesion parameter scales the pressure and velocities inside the tumor. In figure (B.24d) we see increasing this parameter produce a more slightly more compact tumor. For positive γ the velocities now move with the fluxes and make the tumor more compact. For negative γ, the adhesion force is negative and this was chosen in the base case model to counteract the adhesion introduced by the Cahn-Hillard equation. At any rate changing the gamma parameter will have less than 1% difference in the stable tumor radius.

The parameter λ_n controls the rate that the viable cells necrose when they are in the hypoxic

region (where the nutrients are below the level needed for viability). The main effect of the necrosis rate is on the cell distribution in the necrotic core. We divide the analysis into two cases, $\lambda_n > 1.0$ and $\lambda_n < 1.0$, as this value is the nondimensionalized mitosis rate. For $\lambda_n > 1.0$ the higher the rate the higher the water level in the core as a greater number of dead cells are lysed to water before it is fluxed out of the center. The higher necrosis rate also decreases the number of viable cells in the necrotic core. In the base case with $\lambda_n = 5.0$ the core is approximately 1% viable cells. At five times this rate there are no viable cells in the core and at 1/5 the rate the viable cells in the core is approximately 10%.

For $\lambda_n < 1.0$ the steady state tumor will stabilize at larger radii as the necrosis rate decreases but, the level of viable cells will rise in the core of the tumor as well. In figure (B.27e) the viable cell fraction increases to over half the total species in the core. Note these small necrosis rates do produce stable tumors (see figure (B.28c)). However, the viable cell level in the necrotic core is not characteristic of typical tumor spheroid cell distributions that we model here. It is also interesting to note the behavior of the radius size. In figure (B.27d) we can see that the necrosis rate $\lambda_n = 10.0$ gives the largest radius size in the regime that produces viable cell fractions in the necrotic core. For larger necrosis rates the viable cells die and are lysed out of core at a faster rate and this produces the slight decrease in the stable radius size. For smaller necrosis rates the viable cells die at a slower rate and the viable cells flux into the center to raise the viable cell fraction. The viable cell inward flux produces the decrease in the stable tumor radius. However, if the necrosis rate is too low then the viable cells will grow in the center of the tumor and expand the radius of the tumor. In any case, for λ_n large enough there is no significant impact on the radius of the steady state radius. Increasing the base value of $\lambda_n = 5.0$ to $\lambda_n = 25.0$ decreases the radius by $\approx 1\%$. Thus, $\lambda_n > 1.0$ is considered an insensitive parameter.

4.4 Nonsensitive Model Parameters

The model parameters are ϵ, α_{VW}, α_{WH}, α_{vitro}, α_{VWDH}, and α_{WDH}. The ϵ parameter is a consequence of the diffuse interface model. In classical models the interface between two species is treated as an infinitely thin dividing surface. The equations are then solved in the separate domains and the boundary conditions are applied to the interface that is tracked explicitly. In diffuse-interface models the interface is represented by continuous variations of the volume fraction. The variations give rise to an interface region of nonzero thickness that smoothly connect the bulk volumes on either side of the interface. The equations are solved over the entire domain and no interface tracking is required. The parameters α_{VW} and α_{WH} are necessary to maintain reasonable water levels in the host and water fractions as well will see below. The α_{vitro} parameter enforces a phase separation between the host and water fractions when we are modeling the in-vitro case ($\phi_W^H = 1.0$). The α_{WDH} parameter prevents unphysical build up of host in the necrotic core of the tumor and the α_{VWHD} parameter prevents the unphysical generation of a phase in an interfacial region. These last three parameter are not studied in this section as they are only necessary to prevent unphysical phase generation and varying them does not influence the development of the tumor.

The ϵ parameter controls the interface thickness. The smaller the ϵ value the thinner the interface thickness. In figure (B.29a) the viable cell fraction is steeper for the smaller ϵ. This increase in steepness corresponds to a decrease in the tumor-host interface (figure B.29e). Notice that the viable-dead interface thickness does not change for different ϵ as the gradient terms in the energy only include the host, viable cell, and water (B.29d). Additionally, the larger the ϵ the more shedding can be seen from the tumor (B.29b). This behavior is consistent with the constant water model in [71]. We can also see that the water peaks at the tumor-host interface are thinner for smaller epsilons. This is a direct consequence of the different interface thicknesses.

In figures (B.30a) and (B.29f) we see that ϵ does alter the volume and the radius of the stable tumor. As noted above the smaller the ϵ the thinner the interface tumor-host thickness, and in particular, the steeper the proliferating rim of the tumor. The more viable cells there are at the boundary of the proliferating rim the faster the tumor growth. For $\epsilon = 0.1$ the growth is slower than the $\epsilon = 0.05$ case and so the accumulation of dead cells will be slower. In figure (B.29c) we can see that the system can flux out this slower accumulation of water and remains with a lower water level inside the necrotic core. If figure (B.29a) we can see that the radial differences between the different epsilons is mainly due to the steepness of the tumor boundary. In each of these cases the tumor remains stable at the steady state. Thus, the interface thickness and the shedding of the cells can be controlled with the epsilon parameter in the range $[0.025, 0.1]$ without affecting the stability of the tumor or a significant difference in tumor volume or spheroid radius.

The α_{VW} parameter controls the level of the water fraction in the viable cells. Increasing the parameter holds the water level at the prescribed level of $\bar{\phi}_W^V$, and consequently, the viable cells are held at $1.0 - \bar{\phi}_W^V$. In this case we use the base case value of $\phi_W^V = 0.2$. Decreasing the parameter allows the water fraction to decrease as it is uptaken by the viable cells (figure (B.31b)) and increasing the parameter we can see that the water fraction is held closer to the $\bar{\phi}_W^V$ value. Thus, the radius of the tumor increases as the parameter increases since the increase in the water fraction allows the tumor to grow faster. Also, decreasing the parameter decreases the radius since the decrease in of the water fraction in viable region slows the growth of the tumor as water is needed to proliferate. This parameter also affects the level of the water peaks at the tumor-host interface. For higher values of α_{VW} the shallower the depression in the tumor-host interface and the less water is necessary to fill the void.

We can also see that the larger the water fraction in the viable cells the more dead cells are produced which increases the water fraction in the necrotic core as the cells are lysed. In figure (B.32) we can see the smaller parameter grows the slowest and the later the necrotic

core forms. However, this parameter does not significantly impact the radius of the stead state tumor if the value is set high enough. Increasing α_{VW} by a factor of ten increases the radius by approximately 4%. The purpose of this model parameter is to maintain a reasonable water fraction inside the viable cells. As we can see in figure (B.31b) if the value is too low then all the water will be uptaken by the viable cells and the tumor will not evolve once the proliferating rim contains no water. The parameter range presented here produces a stable steady state that does not create a significant difference in the tumor volume. For non-symmetric tumors parameter values in the low range will have a meaningful impact on the morphology.

The α_{WH} parameter controls the level of the water fraction in the host. As with the α_{VW} parameter the higher the parameter the more the water level is held at the prescribed level (figure (B.33b)). We can see for $\alpha_{WH} = 0.025$ the water fraction decreases as we move from the boundary to the tumor interface. For larger values we do not see this dip in the water level at the tumor boundary. There is also a change in the water peak heights as the parameter is changes. The higher the α_{WH} parameter the smaller the water peak at the tumor-host interface. In figure (B.33d) we see the change in the parameter produces a greater tumor-host overlap which lessens the depression at the interface and less water is needed to fill this gap. As the water level decreases at the tumor interface this in turn raises the host fraction at the tumor interface (figure (B.33f)). For $\alpha_{WH} = 0.025$ we can see a pronounced increase in the host fraction at the tumor-host interface. On the other hand, increasing this parameter will prevent the buildup of the host fraction at the interface. This was demonstrated in the in-vivo case for $\bar{\phi}_W^H = 0.9$ (figure (B.9f)). The buildup of the host decreased by 60% using $\alpha_{WH} = 2.5$. In figure (B.34) we can see that this dip in the water level outside the tumor is greatest as the tumor is expanding and the water level takes much longer to recover. We can also see that the α_{WH} parameter does not have a significant effect on the tumor radius. Increasing the parameter by a factor of ten decreases the radius by $\approx 1.7\%$. This model parameter maintains a reasonable water level outside of the tumor and

	Parameter	Initial Value	Variations
Sensitive Physical Parameters	λ_l	0.2	$0.05, 0.1, 0.5, 1.0$
	κ	0.035	$0.005, 0.015, 0.025, 0.045$
	M_V	100	$25, 50, 200$
	ϕ_W^H	0.2	$0.4, 0.6, 0.8, 1.0$
	ϕ_W^V	0.20	$0.1, 0.3, 0.4, 0.5$
	C_0	0.10	$0.05, 0.20$
	ν_{PO}	0.5	$0.1, 0.25, 1.0, 2.0$
Nonsensitive Physical Parameters	M_W	200	$50, 100, 400$
	γ	-0.1	$-0.5, 0.0, 0.1, 0.5$
	λ_n	5.0	$0.1, 0.5, 1.0, 25.0$
Nonsensitive Model Parameters	ϵ	0.05	$0.025, 0.1$
	α_{VW}	0.25	$0.025, 2.5$
	α_{WH}	0.25	$0.025, 2.5$
	α_{vitro}	0.0	100.0
	α_{WDH}	100.0	
	α_{VWDH}	50.0	
	α_V,α_W,α_D,α_H	50.0	

Table 4.2: Parameters for spherically symmetric tumor growth, base case values and variation ranges

the parameter range presented here produce a stable steady state that do not produce a significant change in the tumor volume.

4.5 Conclusion

In this chapter we performed a one-at-a-time parameter study on the non-constant water fraction model with a symmetric initial condition. This model is capable of producing a wide range of different stable tumor variations. All seven of the sensitive physical parameters are capable of changing the radius of the stable tumor and adjusting the water level and dead cell ratio in the necrotic core. The width of the proliferation rim can be controlled with the $\bar{C}_0$ parameter. We also saw parameter regimes that destabilize the tumor for λ_l, κ, and M_V.

The κ parameter provides the mechanism necessary to stabilized the tumor. As this param-

eter decreases the tumor becomes larger and larger until it is unstable as the water cannot flux out of the necrotic core faster than the water is released by the dead cell degradation. For the unstable λ_l and κ cases the necrotic core becomes mostly liquid and the accumulation of the water fraction expands the proliferating rim. The κ parameter can be adjusted to flux the water out of the core to create a stable tumor.

We also see affirmation that the additional terms we added to the system energy are indeed necessary to the model. Setting the parameters α_{VW} and α_{WH} at reasonable levels holds the water fractions at the prescribed levels in their respective species. If the α_{VW} parameter is set too low then the water fraction is uptaken by the viable cells and the development of the tumor is inhibited. Further the water fraction is not maintain in the viable cells. If α_{WH} is set too low then the prescribed water level is not maintained in the host region while the host fraction builds up at the tumor-host interface.

Further, the $\bar{\phi}_W^H, \bar{\phi}_W^V$ parameters demonstrate the motivation for developing this model. In different components of the tumor there should be different concentrations of water. For instance, as have seen, the water fraction should be larger in the necrotic core than in the viable cells. In addition, different tumor and host species may maintain different water levels. This is especially important for considering secondary tumors that have metastasized from different tissues as indicated earlier [54]. The simulations above demonstrate that all of these different cases can now be explored. In particular, the in-vitro case can be simulated in conjunction with the in-vivo case.

It is also worth noting that seven of the parameters (α_{VW}, α_{WH}, λ_n, M_W, M_V, κ, and γ) are nonsensitive as long as they are set large enough. Therefore, the model can tolerate a higher degree of uncertainty in the measurements of these parameters, if they are measurable at all. The five parameters ($\bar{\phi}_W^H$, $\bar{\phi}_W^V$, $\bar{C}_0$, ν_{PO}, λ_l) are measurable and ν_{PO} is a controllable the parameter. This model also gives a way to measure low viable cell mobility rates by comparing the degree of tumor branching between the in-vivo and in-silico morphologies.

We can adjust the $\bar{\phi}_W^H$, $\bar{\phi}_W^V$ parameters in the in-vivo case by suspending the initial tumor seed in gels of various densities including the in-vitro case ($\bar{\phi}_W^H = 1.0$) where the initial tumor is placed in a nutrient rich bath. This gives us a clear path to model calibration and validation which will help further refine the model for practical applications.

Chapter 5

Parameter Studies for Non-Symmetric Tumors

5.1 Introduction

In this chapter we consider how the parameters can affect the development of a tumor with a non-symmetric initial shape in two dimensions. The initial non-symmetric initial condition viable cell distribution provides the instabilities necessary to destabilize the tumor and produce the elongation seen in the base case in section 3.3. We will examine which parameter choices influence the development and growth rate of the tumor. In particular, which parameter regimes produce stable tumor spheroids and which parameters can influence the morphology of the unstable tumor will be studied. The parameters are divided into four categories, physical vs model parameters and sensitive vs nonsensitive parameters. The four sections in this chapters discuss the parameters in each of these categories.

The first section considers the parameters that measure the physical properties of the system and can significantly impact the growth and morphology of the tumor. The seven parameters

in this category are λ_l, κ, M_V, $\bar{\phi}_W^H$, $\bar{\phi}_W^V$, $\bar{C}_0$, and ν_{PO}. Note that these are also the parameters physical and sensitive parameters for symmetric case. The lysis and diffusion rates are capable of influencing the growth rates of the tumor and the parameter regimes that produce unstable tumors in the symmetric case produce large tumors with liquid necrotic cores. The ν_{PO} parameter can increase the growth rate of the tumor for large values and if the value is too low the tumor will converge to a stable spheroid. Similarly, for low values of C_0 the tumor will grow larger and for high values the tumor will be collapse to a steady state. The ϕ_W^V parameter can also influence the tumor growth rate and, as in the symmetric case, increasing the water fraction level in the viable cells increases the growth of the tumor until $\phi_W^V = 0.5$ when the shedding of the viable cells inhibits the nutrient production. Adjusting $\bar{C}_0$ we see a new morphology emerge. The ϕ_W^H parameter also influences the growth rate of the tumor for the in-vivo cases. In the in-vitro case we see it is possible to produce stable tumor spheroids by increasing the diffusion rate and for smaller diffusion rates it is possible to produce tumor fragmentation. The parameter that has the greatest effect on the morphology on the tumor is the mobility of the viable cells, M_V. Lower values of this parameter encourages more branching of the tumor. The low viable cell mobility rate exaggerates the initial inhomogeneity of the proliferating rim while higher levels of this parameter produce stable tumor spheroids.

The second section discusses the physical parameters that do not significantly affect the growth or morphology of the tumor. These parameters are M_W, λ_n, and γ. The water mobility given by M_W can increase the size of the central necrotic core of the tumor if the value is too low since this would also decrease the diffusion parameter. The necrosis rate does not influence the growth of the tumor if the rate is set high enough. For lower rates, the development of the tumor is slowed but the viable cells begin to make up a larger fraction of the necrotic core. The last parameter γ measures the adhesion forces between the cells and does not have a noticeable effect on tumor volume or development. Note that these are also the physical and nonsensitive parameters for symmetric case.

The third section considers the model parameters that significantly impact the tumor development. For the symmetric case, there are no parameters that fall into this category. However, we will see that the model parameter ϵ can influence the growth of the tumor with a non-symmetric initial condition. This parameter measures the thickness of the tumor-host interface and is a consequence of the diffuse interface method that is used to solve the system. A thinner tumor-host interface implies that the tumor interface is steeper and the steeper the interface the more viable cells are at the boundary of the proliferating rim. This increases the growth rate at the tumor boundary and amplifies the initial non-symmetry of the viable rim. Setting $\epsilon = 0.025$ produces a morphology similar to the $M_V = 50$ case and for $\epsilon = 0.1$ the growth rate is low enough that the tumor stabilizes. Thus, this parameter is capable of altering the morphology and growth rate of the tumor.

The fourth section considers the model based parameters that do not have a significant influence on the tumor progression. The parameters in this category are α_{VW} α_{WH}, α_{vitro}, α_{VWDH}, α_{WDH}, α_V, α_W, α_D, and α_H. These parameters are necessary to tune the behavior of the system and enforce the water levels in the respective species. The α_{WH} parameter controls the water level in the host and does not affect the growth or morphology of the tumor in the range presented here. Further, this parameter can be used to control the amount of buildup in host fraction at the tumor-host interface. The α_{VW} controls the water level in the viable cells and this parameter does not affect the tumor if the level is set high enough. For low values, the the water fraction is decreased and the growth of the tumor is impeded. These parameters are also nonsensitive in the symmetric case although one has to be more vigilant of the α_{VW} value to ensure biophysical tumor development. As in the symmetric case, the α_{vitro} parameter enforces a phase separation between the host and water fractions when we are modeling the in-vitro case ($\phi_W^H = 1.0$). The α_{WDH} parameter prevents unphysical build up of host in the necrotic core of the tumor and the α_{VWHD} parameter prevents the unphysical generation of a phase in an interfacial region. The α_V, α_W, α_D, and α_H parameters prevent the volume fractions from becoming negative. Only the

first two parameter are studied in this section as the other parameters are only necessary to prevent unphysical phase generation and varying them does not influence the development of the tumor.

5.2 Sensitive Physical Parameters

The first parameter we consider is λ_l, the lysis parameter. This parameter controls the rate the dead cells degrade and their water content is released back into the system. In figure (C.1) we can see that the higher the lysis rate the smaller and more compact the elongated tumor. For lower lysis rates the tumor is larger with wider necrotic cores and for $\lambda_l = 0.05$ the tumor no longer has the characteristic shape of the elongated tumor in the base case. Instead the tumor is near circular and contains one large necrotic core as the water accumulates. In the $\lambda_l = 1.0$ case, the central necrotic core is barely discernible, the viable cell end caps are narrowed, and the necrotic cores behind the advancing end caps contain approximately 10% viable cells. Similar to the symmetric case, the higher lysis rate increases the water level in the necrotic core faster and creates a larger flux of water from the center. This allows more viable cells to flux into the center of the tumor. Decreasing the lysis rate increases the width of the end caps and increases the diameter of the central necrotic core as more dead cells can buildup before being lysed. The increasing end cap widths and central necrotic core size can be see in figure (C.3). For $\lambda_l = 0.1$ we can see the raised water level in the central necrotic core compared to the $\lambda_l = 0.2$ case and for $\lambda_l = 0.05$ we see the same behavior in the water fraction as in the symmetric case (figure B.1). We also observe the lower the lysis rate the higher the percentage of dead cells at the necrotic core interface as a slower lysis rate results in less dead cells being converted to water after they initially die.

Further, there is an associated dip in the water fraction at the necrotic core interface for $\lambda_l = 0.05$ (figure (C.1j)). This dip occurs as the viable cell uptake the water fraction and the

	Parameter	Meaning	Figures
Sensitive	λ_l	lysis rate	C.1,C.2,C.3, C.4, C.5
Physical	κ	diffusion rate	C.6,C.7,C.8, C.9,C.10
Parameters	M_V	viable cell mobility	C.11,C.12,C.13, C.14,C.15,C.16
	ϕ_W^H	water level in host	C.17,C.18,C.19, C.20,C.21,C.22, C.23,C.24,C.25, C.26,C.27,C.28, C.29
	ϕ_W^V	water level in viable cells	C.30,C.31,C.32, C.33,C.34,C.35, C.36,C.37,C.38
	C_0	hypoxia level	C.39,C.40,C.41
	ν_{PO}	nutrient production	C.42,C.43,C.44, C.45
Nonsensitive	M_W	water mobility	C.46,C.47,C.48, C.49
Physical	γ	adhesion force	C.50,C.51,C.52, C.53
Parameters	λ_n	necrosis rate	C.54,C.55,C.56, C.57
Sensitive	ϵ	interface thickness	C.58,C.59,C.60, C.61,C.62
Model			
Parameters			
Nonsensitive	α_{VW}	water level in viable cell control	C.63,C.64,C.65
Model	α_{WH}	water level in host control	C.66,C.67,C.68
Parameters	α_{vitro}		C.24,C.25,C.26, C.27,C.28,C.29
	α_{WDH}		
	α_{VWDH}		
	α_V,α_W,α_D,α_H		

Table 5.1: Parameters for non-symmetric tumor growth, definitions and figures

dead cells are not dying fast enough to replace the water. In figure (C.2e) we can see that the large necrotic core in this case is mainly due to an increase in the liquid fraction. For smaller lysis rates the dead cells begin to accumulate and the lysis rate is not high enough to convert the dead cells to water and flux the water out of the system. To see how varying the lysis parameter between $\lambda_l = 0.05$ and $\lambda_l = 0.1$ results in the compact shape we can examine figure (C.4). Between 0.1 and 0.08 the length of the tumor is not greatly effected and the change occurs in the width of the central necrotic core. For $\lambda_l = 0.07$ the tumor begins to shorten as the pinched ends between the cores begin to widen. In the range 0.06 and 0.05 the tumor length no longer decreases, but the central core grows larger. The central core is not able to stabilize and thus the viable cells to not close together in the wake of the proliferating end caps. These cases correspond to the unstable cases for the symmetric case (figure B.2). In figure (C.5) we see that for $\lambda_l > 0.2$ the volume progressions are similar and they are attracted to the steady state for similar times. For $\lambda_l = 0.1$ the total volume is slowed by the proximity to the steady state for a longer time, but the overall volume is always larger than the base case. For $\lambda_l = 0.05$ the tumor is no longer attracted to a steady state as the tumor is not stable in the symmetric case for this lysis rate. In figure (C.5) we see the growth rate in this case is approximately constant. The lysis rates that are larger than the base case value of 0.2 initially increase the water volume as the dead cells are lysed. The water is then fluxed out of the tumor and the gradual increase in the water volume results from the lysing of the newly created dead cells as the tumor expands. For $\lambda_l = 0.1$ the slower buildup of the water volume is evident as the release of the water is slower. The $\lambda_l = 0.05$ case shows the continual increase of the water volume as the liquid core builds.

The parameter, κ, is the rate the water will diffuse from lower concentrations of nutrients to higher concentrations. In figure (C.6) we see that as the diffusion rate decreases the morphology of the tumor is not significantly affected until $\kappa = 0.015$ when we can see a substantial increase in the size of the central necrotic core and the necrotic cores behind the proliferating end caps. For $\kappa = 0.005$ we see the tumor no longer has the characteristic shape

of the base case tumor. In this case the symmetric tumor is also unstable for the diffusion parameter $\kappa = 0.005$ and so the non-symmetric tumor is not able to from an central necrotic core before it expands. Instead the tumor expands from its initial configuration into the oval shape seen here. We can also see for higher κ values the water level inside the tumor is lower as the greater diffusion rate fluxes the water out of the center of the tumor. For $\kappa = 0.025$ we see the water begin to buildup in the necrotic cores and for $\kappa = 0.005$ we see the center of the tumor is almost entirely liquid as the diffusion rate is too low to flux out the accumulated water. In figure (C.7) we see the higher the diffusion rate the higher the dead cell fraction in the necrotic cores. This is consistent with the behavior in the symmetric case. For the $\kappa = 0.005$ case we see the low levels of dead cells in the center and an increase of the dead cell level near the growing ends of the tumor. We can see how the different diffusion rates impact the overall tumor development in figure (C.8). The larger the diffusion rate the shorter the tumor and the narrower the central necrotic core. The higher diffusion rates produced tumor of smaller radii in the symmetric case and thus the smaller the central necrotic core when the tumor first progresses. If the diffusion rate is too low then we see the oval shape produced by the $\kappa = 0.005$ case that results from the unstable central core.

Figure (C.9) shows the contours of the intermediate diffusion rates. As the parameter decreases the tumor decreases in length as the width of the central necrotic core expands. For $\kappa = 0.009$ we see the viable cells no longer neck down as the central necrotic core increases. Figure (C.10) shows thats the total volume progression for the diffusion parameters between $0.025 \leq \kappa \leq 0.045$ does not significantly change. For $\kappa = 0.015$ we see that although the initial growth rate is larger in this case it takes longer to escape the steady state regime. When $\kappa = 0.005$ we see the tumor exhibits linear continuous growth. However, this parameter does not influence the proliferation rate of the viable cells. The reason for the apparent change in the growth rates is the buildup of water in the necrotic cores. We see the total water volume progression is similar for the three highest values of κ and the difference in water fraction levels in the necrotic core is the reason for the difference in the tumor volumes.

For $\kappa = 0.015$ we can see a much larger accumulation of water in the central necrotic core before it begins to diffuse outward. Once the tumor begins to elongate the necrotic cores formed behind the advancing end caps have increased water levels. For $\kappa = 0.005$ we see the continual buildup of water in the core pushes the proliferating rim outward and increases the volume of the tumor. Therefore we can see that this diffusion parameter influences the final size and shape of the tumor and controls the water level inside the tumor.

The M_V parameter measures how fast the viable cells can move to minimize the energy of the system. Figure (C.11) shows the impact this parameter has. Doubling the base case parameter we see the tumor has converged to its stable circular shape. Using half the base case value of 100 we see the tumor is no longer growing symmetrically. Note that this shape is similar to the morphology for the $\epsilon = 0.025$ case (figure (C.58c)). If the parameter is decreased by half again then we can see the tumor has now developed six different branches. The water fraction for this case shows the tumor grown has five necrotic cores with liquid centers. In figure (C.12) we see there are in fact ten necrotic cores present for the lowest viable cell mobility. The contours in figure (C.13) shows just how different all of these morphologies are.

The evolution for the $M_V = 25$ case is shown in figure (C.14). By time $t = 50$ we see that viable cells are not able move around the necrotic core fast enough to maintain a proliferating rim around the entire core as in the base case. By time $t = 100$ the viable cell have grown and the places where the viable cells were thickest remain. Since the viable cells are too slow to even out around the tumor we now see two gaps in the proliferating rim. As the tumor evolves we see the three end caps growing in size and by time $t = 200$ the left and bottom branches have separated into two new buds and the right branch has developed a necrotic core. By time $t = 300$ the right branch has separated into two new buds. As the necrotic core develops behind an advancing end cap the tumor begins to thin in the center of the rim as the viable cells are not moving fast enough to maintain a viable cell rim of

uniform thickness. This creates the initial splitting of the cap of the tumor. Once the bud is split the sides begin to grow and form new buds. The new buds form necrotic cores as they advance and the process begins again. The figure for $t = 300$ shows the remnants of the central necrotic core that produced the three buds and the necrotic cores that formed the next series of buds.

However, there is a large difference between the $M_V = 50$ and the $M_V = 25$ case. The intermediate cases are considered in figure (C.15). The smaller the mobility rate the more budding we see and the more elongated the end caps are. For $M_V = 30$ the mobility is high enough where we do not see a third branch form on the right side of the tumor and for $M_V = 45$ we do not see any branching on the advancing end caps at time $t = 300$. In figure (C.16) we see the stabilization of the $M_V = 200$ case and for the $M_V = 50$ case we see the tumor volume escapes the steady state regime faster than the base case. For the $M_V = 25$ case there is no steady state attraction and the tumor grows nonlinearly. The dividing end caps that develop as the tumor grows for this case expose more proliferating cells to the nutrients and produce this accelerated growth rate. In figure (C.16b) the water volume for the $M_V = 200$ case shows the water uptake during the initial phase and the water is produced as the dead cell lyse. The perturbations present in the water volume remind us that this steady state is a dynamic one. For $M_V = 50$ we see a faster increase in the water volume as the faster growing tumor produces more dead cells that increase the water level. For the $M_V = 25$ case a much more erratic pattern emerges. This is the result of the increase uptake of the water fraction when the end caps bud and an increase in the water volume where the necrotic cells begin to lyse.

The parameter $\bar{\phi}_W^H$ is the amount of water in the host fraction. We first consider the in vivo case with $\bar{\phi}_W^H < 1.0$. We can see in figure (C.17) that the greatest increase in tumor length occurs after increasing the host-water fraction from 0.2 to 0.4. Further increases in the parameter result in a larger central necrotic core and wider advancing necrotic cores.

We also see higher water levels in the necrotic cores as the host-water fraction increases. This increase in growth is due to the greater flux of water into the cell as the rate of flux depends on the water level. If the host-water fraction impacts the tumor growth rate then the tumors should be more elongated for higher $\bar{\phi}_W^H$ values. However, in figure (C.19)) we see the tumor are all roughly the same length for $\bar{\phi}_W^H > 0.2$. This discrepancy can be answered by examining the total volume plots in figure (C.20). We see the initial growth rates and the growth rates after escaping the steady state regime are greater for larger water-host fractions. What varies between parameter choices is the time spent near the steady state regime. The tumor with $\bar{\phi}_W^H = 0.4$ water level has the shortest delay before elongating while $\bar{\phi}_W^H = 0.8$ level produces the longest delay. At time $t = 150$ the volume of the tumor with $\bar{\phi}_W^H = 0.8$ level is below the volume of the tumor with parameters $\bar{\phi}_W^H = 0.4$ and $\bar{\phi}_W^H = 0.6$ despite its larger growth rate. At time $t = 300$ the $\bar{\phi}_W^H = 0.8$ volume level has caught up to $\bar{\phi}_W^H = 0.6$ tumor volume. Larger domains with longer runs will produce tumors with more disparate sizes.

Varying the $\bar{\phi}_W^H$ parameter in the in vivo case produces significantly varied tumor progressions, most notably in the growth rates of the tumor and developmental delays in the steady state regime. Nevertheless, the difference in growth rates is not enough to produce a different morphology. Figure (C.18) shows the decrease in the host fraction for different values of the parameter and, as in the symmetric case, we see the buildup of the host around the tumor as the host fraction decreases. Figure (C.17h) shows the corresponding decrease in the water fraction around the proliferating rim of the tumor where the host builds up. Similar to the symmetric case, the α_{WH} parameter can be increased to reduce this encapsulation behavior of the host. Figure (C.21) shows that increasing the parameter α_{WH} from 0.25 to 2.5 eliminates the buildup of host around the tumor and the water fraction no longer decreases at the tumor-host interface. However, we do see a change in the size of the tumor. Figure (C.22) shows that the tumor is shorter in length but the necrotic core is wider. Looking at the volume plot in figure (C.23) we see that the initial growth rate is the same for both

parameters but it takes longer for the higher parameter to enter the steady state regime and longer to leave it. During this time the tumor with the $\alpha_{WH} = 2.5$ parameter is forming the central necrotic core and the longer the tumor is in the steady state regime the larger central core will be as seen in figure (C.22). When the tumor with the larger parameter leaves the steady state regime the tumors grow at the same rate. This is the same behavior seen in the α_{WH} parameter variation (figure (C.68)) only the increased growth rate produces a more exaggerated effect on the central necrotic core formation. Thus, we see it is possible to model tumors surrounded by different water fraction levels in the host region in the in-vivo case. Further, the encapsulation behavior of the host fraction as the tumor develops can be controlled by adjusting the model parameters.

For the in-vitro case we add the term,

$$\frac{\alpha_{vitro}}{2}\phi_W^2\phi_H^2$$

to the energy and set $\alpha_{vitro} = 100.0$. As in the symmetric case, this term has the effect of eliminating the host fraction in the entire domain and avoiding the buildup of the host tissue at the tumor-host interface. In figure (C.24) we two cases for the development for the in-vitro case. For high enough diffusion rates ($\kappa = 0.1$ and $\kappa = 0.075$) the tumor stabilizes to spheroid and the higher the diffusion rate the smaller the radius of the tumor. For the $\kappa = 0.05$ and $\kappa = 0.035$ cases we see the tumor progress in a similar fashion to the in-vivo case where the tumor elongates and the growth is determined by two advancing end caps. However, unlike the in-vivo case we see the quiescent region of the viable cells buckles inward to the necrotic core. We can also see there is a dip in the water fraction where the viable cells are buckling. This decrease in the water fraction is due to the buildup of the dead cells as seen in figure (C.25). The difference in in-vitro tumor progression for different diffusion rates can also be seen in figure (C.26).

One of the assumptions of the model is that there is a minimum level of dead cells needed to initiate lysis. Therefore if a region of the domain was ever contained in necrotic core then the minimal level of dead cells needed for lysis will remain. Once the viable cells begin to buckle inward the dead cells left in the necrotic core become exposed. The dead cell fractions for the $\kappa = 0.05$ and $\kappa = 0.035$ cases show how large the necrotic core was before the viable cells entered the quiescent zone. Figure (C.29) show the evolution for the $\kappa = 0.035$ case for longer times. As the quiescent viable cell region begins to buckle we see the rim begins to thin and decrease in density. By time $t = 480$ the viable cells have merged in the middle of tumor. The water fraction shows that necrotic core developed by time $t = 380$ does not decrease as the tumor's elongated portion collapses toward the center. As we will see below for the $\bar{\phi}_W^V = 0.5$ case, the necrotic core remnants inhibit the nutrient production/delivery near the viable cells (figure (C.28)). Hence the further the viable cells bend into the necrotic core of the tumor and the less nutrient they receive. Eventually as the viable cells enter the hypoxic region, the viable cells necrose, and the tumor will split as seen in $t = 480$. The tumor progression in this case is characteristic of tumor fragmentation and metastasis. In figure (C.27) we see the stabilization for the higher diffusion rates and for the lower rates we see the decrease in the water fraction beginning at $t = 380$. Therefore, depending on the diffusion parameter, we can produce compact tumors or locally invasive behavior.

The parameter $\bar{\phi}_W^V$ determines amount of water present in the viable cell region. In figure (C.30) we can see that this parameter has a profound effect on the development of the tumor. In the $\bar{\phi}_W^V = 0.1$ case we see that the proliferation rate is low enough that the tumor is not able to escape the steady state regime. Higher parameter values greatly increases the length of the tumor and the width of the advancing necrotic cores. However, we see that increasing the parameter to $\bar{\phi}_W^V = 0.5$ produces a shorter and thinner tumor. As seen the the symmetric case, this is due to the increase in shedding caused by increasing the water fraction level in the viable cells. Figure (C.30) shows the amount of viable cell shedding produced by different $\bar{\phi}_W^V$ parameters. We note that the greater the prescribed water fraction level, the

further the cells spread from the bulk of the tumor and the larger the viable cell fraction we see outside the tumor.

Setting $\bar{\phi}_W^V = 0.5$ sheds enough viable cells to inhibit the nutrient production. Although the $\bar{\phi}_W^V = 0.4$ parameter also sheds a considerable amount of viable cells, figure (C.32) shows that in this case the nutrient production is relatively unaffected. Figure (C.33) shows the difference in the size and morphology of the tumors for the different parameter choices. Note that the larger the $\bar{\phi}_W^V$ parameter the larger and wider viable cell end cap. This is consistent with an increase in the proliferation rate. For the $\bar{\phi}_W^V = 0.5$ case the lower nutrient concentration in the bulk of the tumor decreases in the growth rate and produces a smaller central necrotic core and a shorter and thinner elongated tumor. Also note that the $\bar{\phi}_W^V = 0.5$ case does not grow along the same path as the tumors in the other cases. Indeed, the lower portion of the tumor curves to the left and the upper portion curves to the right as the tumor evolves. This deviation is an edge effect produced by the shedding of the viable cells. This is also the effect that elongates the advancing end caps towards the boundary in the $\bar{\phi}_W^V = 0.4$ case. Figure (C.30) shows the range of the shedded cells that extend beyond the computational grid for these two cases. Figure (C.31) shows the differences in the viable cell water fraction for different choices of $\bar{\phi}_W^V$. Similar to the symmetric case, the viable cell water level in not precisely what is prescribed by the parameter. The difference between the prescribed water level and the level maintained in the model is the same as the levels attained in the symmetric case (B.13e).

The total volume in figure (C.34) shows the difference in the growth rates for different parameter choices. We see the $\bar{\phi}_W^V = 0.1$ case collapses to the steady state case immediately. Next, the larger the $\bar{\phi}_W^V$ parameter, the larger the initial growth rate, the less time is spent in the steady state regime, and the greater the growth rate once the tumor begins to elongate. We can also see the curious behavior of the volumes for the $\bar{\phi}_W^V = 0.5$ case. At approximately $t = 110$ we see the dead cell and viable cell volumes begin to oscillate and although the

total volume of the tumor also oscillates, the amplitude of these variations is less than the individual cell species. These oscillations can also be observed in the water volume for this case. Figure (C.34c) show a closeup of these oscillations for the volumes that are appropriately vertically shifted so they overlap. In this close up we can observe that the viable cell peaks and the dead cell peaks are inverted and water peaks are located at nodes of the viable cell and dead cell oscillations. The oscillations here are due to the growth and death cycles in the elongated portion of the tumor. At a local minimum for the viable cell volume the viable cells grow as the dead cells undergo lysis. The dead cells begin to lyse and the water is fluxed out center of the tumor. This causes the viable cells flux into the hypoxic region and the necrosis rate overtakes the growth rate of the viable cells. Thus, total volume of the viable cells decreases as the volume of the dead cells increases. The steady overall increase of the tumor volume is due to the advancing end caps. Note the offset peaks of the water fraction volume and the decrease in amplitude is due to the competing actions of the uptake by the viable cells and addition of water to the system from lysis. Although this growth and death cycle is shared by all tumor systems it is more exaggerated here due to the slower growth rate and the unstable shape of the tumor.

The main issue with the $\bar{\phi}_W^V = 0.5$ case is impact of the shedding cells on the nutrient production. To alleviate this we can change the tumor fraction necessary to prevent the nutrient production. We increase the production threshold from 0.01 to 0.03 and set,

$$Q(\phi_T) = \begin{cases} 1.0 & \text{if } \phi_T < 0.03 \\ 0 & \text{if } \phi_T \geq 0.03. \end{cases}$$

With this new function we can see the morphology of the tumor for the $\bar{\phi}_W^V = 0.5$ case in figure (C.35). We see that the increase in the threshold level allows the nutrients to reach the proliferating rim of the tumor and the increase in the growth rate is enough to destabilize the tumor from the typical elongations in the base case. The evolution of this tumor in figure

(C.36) is consistent with the behavior seen when the viable cell mobility, M_V, is decreased to 25. The non-symmetry of the initial condition and the increased growth rate produce the instability necessary to produce this morphology. At time $t = 60$ we can see that the viable cells are proliferating faster than they can migrate around the necrotic core. As the tumor continue to evolve a new gap in the proliferating rim appears. At time $t = 120$ the sides of the proliferating end caps are growing faster than the center and by time $t = 150$ four new buds are formed as the original end caps split. Figure (C.37) shows the tumor contours for the other values of $\bar{\phi}_W^V$ at time $t = 150$. We see that the $\bar{\phi}_W^V = 0.4$ case has a similar morphology as the $\bar{\phi}_W^V = 0.5$ case except the slower growth rate has delayed the development and the other two cases do not have a proliferation rate high enough to change the elongated morphology. Figure (C.38) shows a more ordered volume progression with the higher water levels correspond to larger growth rates and overall volume of the tumor.

The $\bar{C}_0$ parameter is the level of nutrients necessary to maintain cell viability. That is, the concentration of nutrients necessary for the viable cells to thrive, below which, the cells begin to necrose. In figure (C.39) we see that decreasing the hypoxia level increases the length and width of the tumor. A smaller $\bar{C}_0$ level allows the tumor to remain the growth phase for a longer period of time before the necrotic core develops. The lower hypoxia level also allow a proliferating rim along the length of the tumor which increases the over all width of the tumor. For $\bar{C}_0 = 0.20$ we see that the tumor was unable to develop. The higher hypoxia level puts the initial viable cells in the quiescence zone and the tumor cannot progress. Also note that in this case the tumor is not circular at $t = 400$ as the viable cells are arrested in the quiescence zone. The decrease in the viable cell fraction also decreases the viable cell mobility and the cells are unable to move into a circular morphology by $t = 400$. In figure (C.40) we see the necrotic cores for the base case and $\bar{C}_0 = 0.05$ are roughly the same size and the increase in the tumor volume is due to the increase in the width of the viable cell rim. This behavior is consistent with the symmetric case.

In figure (C.41) the total volume of the $\bar{C}_0 = 0.05$ case is still slowed by the attraction to the steady state, but in this case the steady state is the symmetric tumor with $\bar{C}_0 = 0.05$ which has a larger volume. The total volume for the $\bar{C}_0 = 0.20$ actually decreases from the initial volume as the initial tumor is already under the hypoxia level. We can also see that the total water volume increases as the dead cells lyse. For the $\bar{C}_0 = 0.05$ case we can see the total water volume decreases as the greater growth rate uptakes more water. The greater growth rate produces more dead cells and the released water increases the water volume to a greater level than the base case. We can see that this parameter has a significant influence on the morphology of the tumor. Decreasing the $\bar{C}_0$ parameter produces thicker tumors and wider proliferating end caps. Increasing the $\bar{C}_0$ parameter shrinks the tumor and can prevent the progression entirely if the hypoxia level is too high to support proliferating cells.

The parameter ν_{PO} is the rate that the surrounding vasculature replenishes the nutrients that are uptaken by the viable cells. Figure (C.42) shows that increasing this parameter results in an increase in tumor length and viable cap width and for larger parameters there is no pinching together of the elongated portion of the viable cells. Decreasing the parameter slows the growth of the tumor and if the parameter is too low the tumor does not grow fast enough to escape the steady state. Further, we can see the larger the ν_{PO} parameter the larger the necrotic cores behind the advancing end caps and the greater the water concentrations in the cores as more dead cells are lysed for larger growth rates. Figure (C.43) shows that for $\nu_{PO} = 2.0$ the necrotic cores are large enough to have a decrease in the dead cell fraction in the center as they lyse and raise the water level. Additionally, the contours in figure (C.44) show that the the larger the production rate the larger the central necrotic core and the larger the proliferating end caps are. We can also see the increase in the tumor length begins to slow as the ν_{PO} parameter increases. This is similar to the behavior seen in the symmetric case where the increase in the radius slows as ν_{PO} is increased. That is, the radius vs ν_{PO} plot is concave down (B.20d). This behavior is also seen in figure (C.45), the volume change is greater when ν_{PO} is doubled from 0.25 to 0.5 than when ν_{PO} is doubled from 1.0 to 2.0.

The total volume growth is larger for greater production rates, but the tumors all leave the steady state regime at approximately the same time. For $\nu_{PO} = 0.25$ we see a much slower growth rate and the volume escapes the steady state regime at a much later time. For $\nu_{PO} = 0.1$ the tumor grows too slowly to escape the steady state regime and the total water volume shows an initial increase as the cells die and are lysed, then once the water is fluxed out of the system the tumor remains at this steady state. For the other parameter variations we see the same water volume progression as the base case except it is more exaggerated by the increased growth rate. Thus, this parameter does not significantly alter the morphology of the tumor if the rate is high enough. However, it does have a evident influence on the volume and size of the tumor and if the parameter is set too low then the tumor will not develop and will tend to a symmetric steady state.

5.3 Nonsensitive Physical Parameters

The first parameter we consider in this section is M_W, the mobility of the water fraction. This parameter measures how fast the water can move in the system to minimize the energy. In figure (C.46) we see that the higher the water mobility the faster it is fluxed out of the center of the tumor. For $M_W = 100$ we can see the higher water levels in the central core and in the core behind the advancing end caps. For $M_W = 50$ the water level in the necrotic core much higher and the water level is lower in the viable cell region. The decrease in the water mobility slows the water movement enough that it will not flux into the viable cell region fast enough to maintain the water level. The slower mobility rate also decreases the diffusion rate out of the necrotic sections of the tumor which accounts for the water fraction buildup in these areas. Also note that the higher the mobility rate the higher the dead cell fractions in the necrotic core (figure (C.47)). This is consistent with the symmetric case. For high mobility rates the water is fluxed out of the core and allows more dead cells to

accumulate in the necrotic core. For lower mobility rates the water is not evacuated from the cores fast enough to provide room for the dead cells to buildup and consequently the cores grow wider as the tumor progresses.

In figure (C.48) we see that the lower the water mobility rate the less elongated the tumor is but the wider the necrotic cores are. We saw above that the lower mobility rate results in a smaller water fraction in the viable cells and thus the growth is impeded. The buildup of water and dead cells in the necrotic cores accounts for the wider cores. The contours and the figure (C.49) show that for high enough M_W there is not a significant difference in the tumor volume or progression. However, as in the symmetric case, if the value is too low then we see a significant delay in the tumor progression and overall volume. In the water volume graph we can see the delayed and exaggerated water movement. For the case $M_W = 50$ we see a large dip in the initial growth phase as the viable cells uptake the water and recovery as the dead cells begin to lyse and the slow decline as the water is fluxed out of the center of the tumor. Therefore, for larger enough values of M_W there is not a significant change in the morphology of the tumor or its volume. Hence, this parameter is classified as non-sensitive.

The γ parameter measures the adhesion force between the cells and controls the stiffness of the tumor boundary. In figure (C.50) there is no immediate difference between the variations. In figure (C.51) we see the pressure has been scaled by γ as in the symmetric case. In figure (C.52) we see the effect of parameter. The larger the γ value the more compact the tumor is and the smaller the γ value the more elongated the tumor and in figure (C.53) we see the smaller the γ the faster the tumor escapes the well of the steady state regime. Once the tumors begin to grow past the steady state they all progress at the same rate. The same behavior is also present in the volume of the water fraction. Therefore, the γ parameter influences how long it takes the for the tumor to grow beyond the steady state volume. However, it is evident that the morphology of the tumor is not affected and although the progression of the tumor is changed the difference is not significant despite its effect on the

sign and magnitude of the pressure.

The parameter λ_n is the rate the viable cells necrose once they are in the hypoxic region. In figure (C.54) we see that all the variations have a similar morphologies. For the higher necrosis rate the main difference is the length of the tumor. The higher necrosis rate kills the viable cells faster which lyses the dead cells and fluxes the water out of the necrotic core faster than the base case which results in slightly narrower tumor. For slower rates there are slivers of viable cells that extend down the length of the tumor to the central necrotic core. We can also observe that the quiescent cells do not pinch together as the dead cells no longer die fast enough to produce this collapse in the elongated portion of the tumor. We can also see that the viable cell levels in the necrotic portion of the tumor are larger for smaller necrosis rates. This is consistent with the behavior in the symmetric case. The increase in the viable cell fraction also increases the width of the growing end caps. This is can be seen in figure (C.55) where the slower the necrosis rate produces a lower dead cell fraction in the necrotic region.

Figure (C.56) shows the same differences in tumor length that were observed for the radii for the symmetric case (B.27d). The longest tumor is seen for $\lambda_n = 5.0$ and the other values decrease the tumor length. For larger necrosis rates the viable cells die and are lysed out of the core at a faster rate. This produces the slight decrease in the tumor length and a narrower advancing necrotic core. For smaller necrosis rates the viable cells die at a slower rate and the viable cells flux into the center to raise the viable cell fraction. The viable cell inward flux produces the decrease in the tumor length and the increase in the width of the necrotic core. However, if the necrosis rate is too low then the viable cells will grow in the center of the tumor and expand the radius of the necrotic cores. This also slows the progress of the tumor. Figure (C.57) shows similar growth of the tumor and the water volume for different necrosis rates. We can observe that the higher the necrosis rate the sooner the dead cells are converted to water and the largest value does flux the water out of the necrotic

core faster that the base case. For lower values it takes longer for lysis to initiate and the eventual buildup of water in the central necrotic core is slower to flux out of the center. However, we can see that there is no significant difference in the progression of the tumor or the morphology for the different necrosis rates $\lambda_n > 1.0$.

5.4 Sensitive Model Parameters

In this section we consider the only sensitive model parameter, ϵ. This parameter controls the interface thickness and the smaller the parameter the thinner the interface thickness. In figure (C.58) we can see in the viable cell and host species, that the smaller the ϵ the more rapid the transition between species. Additionally, as was seen in the symmetric case, the epsilon parameter controls the amount of viable cells that shed into the host region. Figure (C.61) shows the minimal shedding present in the $\epsilon = 0.025$ case and the more diffuse shedding found in the $\epsilon = 0.1$ case. As mentioned in Chapter 3 this behavior is consistent with steady spherical solutions of the Cahn-Hillard equation where the velocity and source terms are neglected [33].

Further, in the water fraction we can see that the larger the parameter the wider the water peaks at the interface (figure (C.58)). This is consistent with the behavior seen in the symmetric case. However, in the symmetric case this parameter was nonsensitive. For the symmetric case the difference in the radii and the tumor volumes for different ϵ was due to the steepness of the viable cells. In the non-symmetric case this change in steepness is what causes the radically different tumor morphologies. The steeper the tumor is the viable cells will be in the boundary of the proliferating rim and the more gradual in interface transition is the lower the proliferation rate in the viable rim. In figure (C.62) we see for $\epsilon = 0.1$ the tumor does not grow fast enough to escape the steady state and stabilizes to the circular shape we see in the symmetric case. For the $\epsilon = 0.025$ case the growth rate is large enough

to escape the steady state regime in roughly half the time as the base case and the initial non-symmetry of the viable cells becomes more pronounced as the tumor progresses.

In figure (C.59) we see the evolution of the tumor for $\epsilon = 0.025$. In addition to growing faster than the base case we see the tumor curving to the left as it develops. Figure (C.60) shows the viable cell development for early times. We can see that the largest divot in the initial condition, found on the left side of the tumor, remains as the tumor evolves and smaller perturbations are smoothed out. By time $t = 100$ this divot is more pronounced and the remaining proliferating cells are angled to the left. As the tumor progresses this deviation to the left becomes more pronounced.

In figure (C.62) we can see the increase of the water volume for the $\epsilon = 0.1$ case as the tumor quickly converges to the steady state. For $\epsilon = 0.025$ the water volume has a greater dip as the increased growth rate uptakes water more rapidly. At $t = 300$ the water fraction begins to decrease as the viable cell end caps elongate and more water is absorbed. In the symmetric case the ϵ parameter does not greatly influence the steady state of the tumor. The differences in the radius and volume occur due to the steepness of the proliferating rim. In the symmetric case there is no viable cell inhomogeneity to cause instability. In the non-symmetric case the steepness of the tumor produces noticeable different behavior. The steepness of the tumor corresponds to the growth rate in the proliferating rim which can enhance any non-uniformity in the viable rim.

5.5 Nonsensitive Model Parameters

The first nonsensitive model parameter we consider is α_{VW} which enforces the prescribed water level in the viable cells. Similar to the symmetric case, increasing the parameter holds the water level at $\bar{\phi}_W^V = 0.2$. If α_{VW} is set too low the water is allowed decrease as

it is uptaken by the viable cells. As in the symmetric case, increasing the parameter to $\alpha_{VW} = 2.5$ does not increase the growth of the tumor by a significant amount. However, decreasing the parameter to $\alpha_{VW} = 0.025$ does cause a significant delay in the evolution of the tumor (see figure (C.64)). In the symmetric case the tumor does not grow as large as the non-symmetric case and therefore the decrease in the water fraction does not cause as much of a delay. In figure (C.63) we see the smaller the parameter the greater the viable cell fraction in the end caps and the lower the corresponding water fraction. We can also see the smaller the parameter the larger the water peaks are in the tumor-host interface. This behavior is consistent with the symmetric case.

In figure (C.65) we can see that if α_{VW} is greater than the base case value of 0.25 then the evolution of the tumor and water volume are similar. If the parameter is smaller than the base case parameter we can see a noticeable slower increase in the total tumor volume and the water volume does not rebound as the tumor progresses since the water is being uptaken by the tumor faster than the lysing dead cells can replace it. It is also worth noting that although this parameter impacts the rate of the tumor development it does not alter the morphology of the tumor. Thus, if the α_{VW} parameter is set high enough, the tumor progression is not significantly altered by variations in this parameter.

The next model parameter we consider is α_{WH}. This parameter enforces the prescribed water level in the host. As in the symmetric case, the lower the parameter the more the water fraction will drop in the host around the proliferating rim of the viable cells. For larger values we see less of a decrease in the water fraction around the tumor. There is also a change in the water peak heights for different parameter choices. The smaller the chosen value the higher the water peaks at the tumor-host interface. Additionally, the decrease in the water level in the host causes an increase in the host fraction around the tumor (figure (C.66)). Depending on the stiffness of the host we see that this host buildup at the tumor-host interface can be controlled with this parameter. In figure (C.67) we see the interesting phenomenon that the

base case parameter produces a slightly longer tumor. In the volume plot for the symmetric case (B.34) we can see the base case parameter produces the largest tumor volume while the tumor is in the initial growth stage. When the growth rate begins to slow as the tumor stabilizes, the smaller parameter produces a larger volume. This same behavior can be seen in the non-symmetric case (figure (C.68)). During the initial stage of growth when the tumor development is close to circular, the smaller parameter value produces the largest tumor. After the tumor elongates, the base case tumor volume overtakes the volume of the smaller parameter. We can also see that the dip in the total amount of water in the system is much greater for the smaller parameter and it take longer to recover. For the parameter α_{WH} we see that there is no significant change in the tumor volume in the range presented here. We also see that the development of the tumor is not affected by this parameter.

5.6 Conclusion

In this chapter we performed a one-at-a-time parameter study on the non-constant water fraction model with a non-symmetric initial condition. All seven of the sensitive physical parameters can influence the growth rate and the size of the tumor. In the non-symmetric case we now see the model parameter ϵ is capable of affecting the growth and morphology of the tumor. Additionally, the parameters ϕ_W^H, M_V are two physical parameters that are also capable of changing the morphology of the developing tumor. Therefore, the model able to capture a wide range of tumor behavior by considering a range of parameters.

The capacity of the model to produce different morphologies is particularly important. The $\bar{\phi}_W^V$, $\bar{C}_0$, ν_{PO} parameters are capable of producing stable tumors for certain parameter regimes. Thus, tumors in stable parameter regime are not sensitive to the initial shape of the tumor. In the in-vitro case we are also able to produce stable tumor spheroids with high enough water diffusion rates. Most of the stable tumors in seen in the symmetric case

	Parameter	Initial Value	Variations
Sensitive Physical Parameters	λ_l	0.2	$0.05, 0.1, 0.5, 1.0$
	κ	0.035	$0.005, 0.015, 0.025, 0.045$
	M_V	100	$25, 50, 200$
	ϕ_W^H	0.2	$0.4, 0.6, 0.8, 1.0$
	ϕ_W^V	0.2	$0.1, 0.3, 0.4, 0.5$
	C_0	0.10	$0.05, 0.20$
	ν_{PO}	0.5	$0.1, 0.25, 1.0, 2.0$
Nonsensitive Physical Parameters	M_W	200	$50, 100, 400$
	γ	-0.1	$-0.5, 0.0, 0.1, 0.5$
	λ_n	5.0	$0.1, 0.5, 1.0, 25.0$
Sensitive Model Parameters	ϵ	0.05	$0.025, 0.1$
Nonsensitive Model Parameters	α_{VW}	0.25	$0.025, 2.5$
	α_{WH}	0.25	$0.025, 2.5$
	α_{vitro}	0.0	100.0
	α_{WDH}	100.0	
	α_{VWDH}	50.0	
	α_V,α_W,α_D,α_H	50.0	

Table 5.2: Parameters for non-symmetric tumor growth, base case values and variation ranges

produce unstable tumors for non-symmetric initial conditions due to morphological instabilities. Therefore, outside of the parameter regimes that produce stable compact tumors for the non-symmetric case it could be difficult to produce stable tumor spheroids. The in-vitro simulations also showed that for low water diffusion levels the tumors undergo elongation and fragmentation. This is an important step for tumor invasion and metastasis that has clinical significance. Hence this model could be a valuable tool in predicting the factors involved in tumor fragmentation.

We also see further confirmation that the additional terms we added to the energy of the system are necessary. The value of 0.25 that are chosen for the α_{VW} and α_{WH} parameters is enough to keep the water fractions at the prescribed level for their respective species. If the α_{VW} is set too low the tumor growth becomes greatly impeded and the water level in the viable cells is not maintained. Similarly, if α_{WH} is set too low the water fraction decreases around the tumor-host interface and the host builds up and encapsulates the tumor. Hence, the new model parameters provide a way to maintain the water level in the host and viable cells. It is not necessary to maintain the water level inside the necrotic core since the water released by cell lysis balances out the water diffusion from high concentrations of nutrients to low concentrations.

Chapter 6

Cancer Stem Cells

6.1 Introduction

In this section we extend the model given in [23] to incorporate cancer stem cells and their progeny. In previous chapters we did not distinguish between types of viable cells. However, the viable cells are known to be composed of different cell types that are related by a set of progenitor-progeny relationships such that progressive changes in cell character occur. This progenitor-progeny relationship, know as the cell lineage, begins with the self-perpetuating stem cells and ends with the terminally differentiated cells that either divides slowly compared to its lifespan or don't divide at all. It has been demonstrated that the growth and division of the stem cells are controlled by feedback signals [7]. In particular, the control of the cell population involves feedback loops that determine mitosis and self-renewal rates [72, 38]. Therefore, to provide a more realistic description of the viable cells we need to account for this heterogeneity of the viable cells and incorporate the cell lineage into the non-constant water fraction model.

6.2 Model Extension

The general model developed in chapter one will now be adapted to the lineage model. The cell lineage is composed of cancer stem cells (SC), committed progenitor cells (CP), terminal cells (TC). The local volume fractions of the cells species including host (H) and water (W) are,

$$\phi_W, \phi_D, \phi_{SC}, \phi_{CP}, \phi_{TC}, \phi_H.$$

We will simplify the model and consider only two types of viable tumor cells, terminal cells and non-terminal cells. The non-terminal cells contain the stem cells and committed progenitor cells and for simplicity we refer to the non-terminal cells as stem cells even though the CP cells will dominate the non-terminal cell compartment. Therefore, the mitosis rate of this combined population is taken to be the mitosis rate of the CP cells. That is, the stem cell species will have a mitosis rate on the order of one day and the terminal cells divide at a much slower rate. Note that we now have, $\phi_V = \phi_{SC} + \phi_{TC}$. The same energy considered in chapter one will be restated here,

$$E = \int_\Omega f(\phi_W, \phi_D, \phi_V) + \frac{\epsilon^2}{2}\left(|\nabla\phi_W|^2 + |\nabla\phi_T|^2 + |\nabla(\phi_W + \phi_D + \phi_V)|^2\right) dx$$

where,

$$\begin{aligned} f(\phi_W, \phi_D, \phi_V) =& \frac{1}{4}\phi_T^2\phi_H^2 + \frac{\alpha_{HW}}{2}\phi_H^2(\phi_W - \bar{\phi}_W^H)^2 + \frac{\alpha_{VW}}{2}\phi_V^2(\phi_W - \bar{\phi}_W^V)^2 \\ &+ \frac{\alpha_{Vitro}}{2}\phi_W^2\phi_H^2 + \frac{\kappa}{2}(C_0 - 1.0)^2\phi_W^2 + \frac{\alpha_{WDH}}{2}\phi_W^2\phi_D^2\phi_H^2 \\ &+ \frac{\alpha_{VWDH}}{2}\phi_V^2\phi_W^2\phi_D^2\phi_H^2 + \frac{\alpha_V}{2}\phi_V^2\mathcal{H}(-\phi_V) + \frac{\alpha_W}{2}\phi_W^2\mathcal{H}(-\phi_W) \\ &+ \frac{\alpha_D}{2}\phi_D^2\mathcal{H}(-\phi_D) + \frac{\alpha_H}{2}\phi_H^2\mathcal{H}(-\phi_H). \end{aligned} \tag{6.1}$$

6.2.1 Generalized Diffusion Term

From equation (2.14) have

$$\mathbf{J}_i = -M_i \nabla \left(\frac{\delta E}{\delta \phi_i} - \frac{\delta E}{\delta \phi_4} \right), 0 \leq i \leq 3$$

and $\mathbf{J}_4 = -\sum_{i=0}^{3} \mathbf{J}_i$, where $M_i > 0$ is the motility. Specializing to the cell lineage case ($\phi_0 = \phi_W$, $\phi_1 = \phi_D$, $\phi_2 = \phi_{SC}$, $\phi_3 = \phi_{TC}$, $\phi_4 = \phi_H$) and taking the motilities $M_i = -\bar{M}_i \phi_i$ for $0 \leq i \leq 3$ where $\bar{M}_i$ is constant. Thus, we see

$$\mathbf{J}_i = -\bar{M}_i \phi_i \nabla \frac{\delta E}{\delta \phi_i}$$

where we have used that the energy does not depend on ϕ_4. Further,

$$\begin{aligned}
\frac{\delta E}{\delta \phi_0} &= \frac{\delta E}{\delta \phi_W} = \frac{\partial f(\phi_W, \phi_D, \phi_V)}{\partial \phi_W} - \epsilon^2 \nabla^2 \phi_V - 2\epsilon^2 \nabla^2 \phi_W - \epsilon^2 \nabla^2 \phi_D \\
\frac{\delta E}{\delta \phi_1} &= \frac{\delta E}{\delta \phi_D} = \frac{\partial f(\phi_W, \phi_D, \phi_V)}{\partial \phi_D} - 2\epsilon^2 \nabla^2 \phi_V - \epsilon^2 \nabla^2 \phi_W - 2\epsilon^2 \nabla^2 \phi_D \\
\frac{\delta E}{\delta \phi_2} &= \frac{\delta E}{\delta \phi_V} = \frac{\partial f(\phi_W, \phi_D, \phi_V)}{\partial \phi_V} - 2\epsilon^2 \nabla^2 \phi_V - \epsilon^2 \nabla^2 \phi_W - 2\epsilon^2 \nabla^2 \phi_D \\
\frac{\delta E}{\delta \phi_3} &= \frac{\delta E}{\delta \phi_V} = \frac{\partial f(\phi_W, \phi_D, \phi_V)}{\partial \phi_V} - 2\epsilon^2 \nabla^2 \phi_V - \epsilon^2 \nabla^2 \phi_W - 2\epsilon^2 \nabla^2 \phi_D.
\end{aligned}$$

Hence, the flux term for the components is given by,

$$\begin{aligned}
\mathbf{J}_W &= -M_W\phi_W\nabla\nu \\
\mathbf{J}_D &= -M_D\phi_D\nabla\delta \\
\mathbf{J}_{CS} &= -M_{SC}\phi_{SC}\nabla\mu \\
\mathbf{J}_{TC} &= -M_{TC}\phi_{TC}\nabla\mu \\
\nu &= \frac{\delta E}{\delta\phi_W} = \frac{\partial f}{\partial\phi_W}(\phi_W,\phi_D,\phi_V) - \epsilon^2\nabla^2\phi_V - 2\epsilon^2\nabla^2\phi_W - \epsilon^2\nabla^2\phi_D \\
\delta &= \frac{\delta E}{\delta\phi_D} = \frac{\partial f}{\partial\phi_D}(\phi_W,\phi_D,\phi_V) - 2\epsilon^2\nabla^2\phi_V - \epsilon^2\nabla^2\phi_W - 2\epsilon^2\nabla^2\phi_D \\
\mu &= \frac{\delta E}{\delta\phi_V} = \frac{\partial f}{\partial\phi_V}(\phi_W,\phi_D,\phi_V) - 2\epsilon^2\nabla^2\phi_V - \epsilon^2\nabla^2\phi_W - 2\epsilon^2\nabla^2\phi_D
\end{aligned}$$

We assume that both species of the viable cells move with the same rate and let $M_{SC} = M_{TC} = M_V$. This gives $\mathbf{J}_V = \mathbf{J}_{SC} + \mathbf{J}_{TC} = -M_V\phi_V\nabla\mu$, the same generalized diffusion term seen in chapter one. Thus, the flux is again a fourth order nonlinear advection-diffusion of Cahn-Hilliard type [10]. The flux is for the host component is

$$\mathbf{J}_H = -\sum_{i=0}^{2}\mathbf{J}_i = M_W\phi_W\nabla\nu + M_D\phi_D\nabla\delta + M_V\phi_V\nabla\mu.$$

6.2.2 Advection

From (2.13) we know the resulting generalized Darcy laws for the velocity of components are given by

$$\begin{aligned}
\mathbf{u}_0 &= -k_0\phi_0\nabla p \\
\mathbf{u}_1 &= -k_1\phi_1\nabla\left(p + \frac{\delta E}{\delta\phi_1} - \frac{\delta E}{\delta\phi_0}\right) \\
\mathbf{u}_j &= -k\left(\phi_s\nabla p - \phi_s\nabla\frac{\delta E}{\delta\phi_0} + \sum_{j=2}^{N}\phi_j\nabla\frac{\delta E}{\delta\phi_j}\right) - k_j\phi_j\nabla\left(p + \frac{\delta E}{\delta\phi_j} - \frac{\delta E}{\delta\phi_0}\right), j \geq 2.
\end{aligned} \tag{6.2}$$

For the lineage model ($\phi_0 = \phi_W$, $\phi_1 = \phi_D$, $\phi_2 = \phi_{SC}$, $\phi_3 = \phi_{TC}$, $\phi_4 = \phi_H$) we have

$$\mathbf{u}_0 = -\, k_0\phi_0\nabla p \tag{6.3}$$

$$\mathbf{u}_1 = -\, k_1\phi_1\nabla\left(p + \delta - \nu\right) \tag{6.4}$$

$$\mathbf{u}_2 = -\, k_s\left(\phi_s\nabla p - \phi_s\nabla\nu + \phi_V\nabla\mu\right) - k_2\phi_V\nabla\left(p + \mu - \nu\right) \tag{6.5}$$

$$\mathbf{u}_3 = -\, k_s\left(\phi_s\nabla p - \phi_s\nabla\nu + \phi_V\nabla\mu\right) - k_3\phi_V\nabla\left(p + \mu - \nu\right) \tag{6.6}$$

$$\mathbf{u}_4 = -\, k_s\left(\phi_s\nabla p - \phi_s\nabla\nu + \phi_V\nabla\mu\right) - k_4\phi_H\nabla\left(p - \nu\right). \tag{6.7}$$

Here we again use that the energy does not depend on ϕ_H. The coefficients k, k_j are motilities that reflect the response of the water and cells to the pressure gradients. As a further simplifying assumption we take $k_j = 0$ for $j \geq 1$ which is consistent with assuming the host and tumor cells are tightly packed and that they march together. Thus each tumor and host component has the velocity

$$\mathbf{u}_s = -k_s\left(\phi_s\nabla p - \phi_s\nabla\nu + \phi_V\nabla\mu\right). \tag{6.8}$$

Note that $k > 0$ may depend on ϕ_i for $0 \leq i \leq 4$ and other variables. This constitutive law for velocity assumes the tumor can be treated as a viscous, inertialess fluid and models this flow through a porous medium.

Now we write the continuity equation for the ϕ_i for $0 \leq i \leq 4$

$$\frac{\partial\phi_i}{\partial t} + \nabla\cdot\left(\mathbf{u}_i\phi_i\right) = -\nabla\cdot\mathbf{J}_i + S_i$$

where ρ is absorbed into the motility constant for $\mathbf{J}$ and the source term. Assuming the source term for the host tissue is 0 (i.e., $S_H = 0$), the continuity equations for $0 \leq i \leq 4$ can

be summed to yield

$$0 + \nabla \cdot (\phi_s \mathbf{u}_s + \phi_D \mathbf{u}_1 + \phi_W \mathbf{u}_0) = -\nabla \cdot \sum_{i=0}^{3} \mathbf{J}_i + \sum_{i=0}^{3} S_i.$$

Thus by equations (2.4) and (2.5),

$$\nabla \cdot (\phi_s \mathbf{u}_s + \phi_D \mathbf{u}_1 + \phi_W \mathbf{u}_0) = 0.$$

This equation with (6.8). (6.3). and (6.4) can be used to solve for the pressure (a linear elliptic equation for p). This closes the system and it remains to account for the source terms.

6.2.3 Source/Mass-Exchange

Assume that the fraction of SC that self-renew is P_0 and the SC, and TC mitosis rates are linearly proportional to the level of oxygen, glucose, and other survival promoting factors that are modeled as a single concentration C_0. Also note that the differentiation rates of SC is given by $(1 - P_0)$. Death of the cells may occur by apoptosis or necrosis if the nutrient levels are too low to support cell viability. The source terms are given by,

$$\begin{aligned} S_H =& 0 \\ S_{SC} =& \lambda_{MSC}(2P_0 - 1)\phi_{SC}\phi_W C_0 - \lambda_{ASC}\phi_{SC} - \lambda_{NSC}\mathcal{H}(\bar{C}_0 - C_0)\phi_{SC} \\ S_{TC} =& 2\lambda_{MSC}(1 - P_0)\phi_W\phi_{SC}C_0 + \lambda_{MTC}\phi_{TC}\phi_W C_0 - \lambda_{ATC}\phi_{TC} \\ & - \lambda_{HTC}\mathcal{H}(\bar{C}_0 - C_0)\phi_{TC} \end{aligned} \tag{6.9}$$

where $\lambda_M, \lambda_A, \lambda_H$ denote mitosis, apoptosis, and necrosis rates and $\bar{C}_0$ is the minimum level of oxygen, glucose, and growth promoting factors required for cell viability. The source term

for the dead cells is,

$$\begin{aligned} S_D =& \lambda_{ASC}\phi_{SC} + \lambda_{ATC}\phi_{TC} + \lambda_{NSC}\mathcal{H}(\bar{C}_0 - C_0)\phi_{SC} \\ &+ \lambda_{NTC}\mathcal{H}(\bar{C}_0 - C_0)\phi_{TC} - \lambda_L\phi_D\mathcal{H}(\bar{\phi}_D - \phi_D) \end{aligned}$$

where λ_L is the lysis rate. Note that the source terms for the viable cells and the water fraction are given by,

$$\begin{aligned} S_V =& S_{SC} + S_{TC} = \lambda_{MSC}\phi_{SC}\phi_W C_0 + \lambda_{MTC}\phi_{TC}\phi_W C_0 - \lambda_{ASC}\phi_{SC} - \lambda_{ATC}\phi_{TC} \\ &- \lambda_{NSC}\mathcal{H}(\bar{C}_0 - C_0)\phi_{SC} - \lambda_{NTC}\mathcal{H}(\bar{C}_0 - C_0)\phi_{TC} \\ S_W =& - \lambda_{MSC}\phi_{SC}\phi_W C_0 - \lambda_{MTC}\phi_{TC}\phi_W C_0 + \lambda_L\phi_D\mathcal{H}(\bar{\phi}_D - \phi_D). \end{aligned}$$

Now everything in the source terms above is a parameter or dependent variable except for P_0, and C_0. We consider C_0 first. Denote oxygen, glucose, and other growth promoting factors as O. Assume the uptake of O is negligible in the host domain compared to the uptake by the tumor cells. On the time scale of cell proliferation the diffusion of O is rapid and the time derivatives and advection terms can be neglected. Therefore the concentration of O is given by,

$$\begin{aligned} 0 =& \nabla \cdot (D_0 \nabla C_0) - (\nu_{UOSC}\phi_{SC} + \nu_{UOTC}\phi_{TC})C_0 \\ &+ \nu_{PO}(\bar{C}_{AO} - C_0)Q(\phi_T). \end{aligned}$$

Here D_0 is the diffusion coefficient, ν_{UOSC}, ν_{UOTC} are the uptake rates of oxygen by SC and TC respectively. ν_{PO} is the rate that O is supplied to the microenvironment. $\bar{C}_{AO}$ is the concentration of O in the blood (in vivo) or in the medium (in vitro) far from the tumor. The function $Q(\phi_T) \approx 1 - \phi_T$ approximates the characteristic function of the host domain and thus models the source of O as being external to the tumor (i.e., the tumor is avascular).

More specifically the function Q can be taken to be,

$$Q(\phi_T) = \begin{cases} 1 & \text{if } \phi_T < 0.01 \\ 0 & \text{if } \phi_T \geq 0.01 \end{cases}$$

The uptake of O in the host domain is assumed to be negligible compared to the uptake in the viable tumor domain. Thus, the PDE for C_0 is given the Dirichlet boundary condition $C_0 = \bar{C}_{AO}$ on Σ_∞.

Next we consider P_0. Following [41], we assume that the proliferation and differentiation of the tumor cells in lineages are regulated by factors in the tumor microenvironment that feedback on the self-renewal fractions and mitosis rates. TCs produce soluble differentiation promoters denoted as T that reduce the self-renewal fractions and mitosis rates of SCs. Examples of possible promoters are TGF-β superfamily members [48]. There is also a self-renewal promoter W, which increases the self-renewal fraction of SC and an inhibitor of W denoted WI. Examples of possible Ws are Wnts, with the inhibitors Dkk and SFRPs [5]. Other examples of W include Notch, Shh, and FGF. Define the self-renewal fraction of SC to be [23],

$$P_0 = P_{Min} + (P_{Max} - P_{Min})\Big(\frac{\xi C_W}{1 + \xi C_W}\Big)\Big(\frac{1}{1 + \Psi C_T}\Big). \tag{6.10}$$

Here, P_{Max} is the maximal level of self-renewal of SC. P_{min} is the minimum level of self-renewal of the SC cells. The functions C_W, and C_T are the concentrations of the self-renewal promoter W and the differentiation promoter T respectively. The parameters ξ and Ψ quantify the feedback response of the SC to the regulating proteins.

The the mitosis rate λ_{MSC} may also depend on the differentiation and self-renewal promoters in a relation similar to (6.10) although this is not modeled here. As in the case for O we assume that T diffuses more rapidly than W or WI and the time derivative can be neglected.

Thus, C_T satisfies,

$$0 = \nabla \cdot (D_T \nabla C_T) - (\nu_{UT}\phi_{SC} + \nu_{DT})C_T + \nu_{PT}\phi_{TC} \tag{6.11}$$

where D_T is the diffusion coefficient, ν_{DT} and ν_{PT} are the rates of natural decay, and the rate of production by the TC respectively and ν_{UT} is the uptake rate by SC. These reaction diffusion equations have the Dirichlet boundary condition $C_T = 0$ on Σ_∞ to mimic the intravasation of C_T into the underlying vascular network.

To model the self-renewal promoter W and its inhibitor WI we use the Gierer-Meinhardt-Turing system of reaction-diffusion equations [1]. Assume that W is the activator and WI is the inhibitor. Wnt and Wnt producing cells tend to be co-localized in space [67] and we assume that W diffuses only over a short range while WI is assumed to diffuse over a longer range, which is consistent with biological data for Wnt and its inhibitors. Also, since Wnt and Dkk are produced by SCs [67, 37] we assume that this is also the case for W and WI and that their production rates depend on the levels of oxygen, glucose and O available. Thus,

$$\begin{aligned} \frac{\partial C_W}{\partial t} &= \nabla \cdot (D_W \nabla C_W) + f(C_W, C_{WI}) \\ \frac{\partial C_{WI}}{\partial t} &= \nabla \cdot (D_{WI} \nabla C_{WI}) + g(C_W, C_{WI}) \end{aligned} \tag{6.12}$$

here C_{WI} is the concentration of WI and

$$\begin{aligned} f(C_W, C_{WI}) &= \nu_{PW} \frac{C_W^2}{C_{WI}} C_0 \phi_{SC} - \nu_{DW} C_W + u_0 C_0 \phi_V \\ g(C_W, C_{WI}) &= \nu_{PWI} C_W^2 C_0 \phi_{SC} - \nu_{DWI} C_{WI}. \end{aligned}$$

Here D_W and D_{WI} are the diffusion coefficients, $\nu_{PW}, \nu_{DW}, \nu_{PWI}, \nu_{DWI}$ are the production are decay rates of W and WI. The parameter u_0 is the low-level source of W from all the viable tumor cells. This is the assumption that W is mainly produced by SC but the

TC may also produce a small amount of this factor. Finally this system of PDE has the Neumann boundary condition $\omega_\infty \cdot \nabla C_W = \omega_\infty \cdot \nabla C_{WI} = 0$ on Σ_∞. Other choices of boundary conditions are also possible but the choice has little affect on the tumor progression while the tumor is sufficiently far from the domain boundary. Also, other model equations besides the Gierer-Meinhard system could also be used, but the equation should be able to form patterns.

As before, we assume that neither cell species undergo apoptosis. The viable cells will die by necrosis before they undergo apoptosis as evasion of apoptosis is a hallmark of cancer characteristics. We also assume that $\mathbf{u}_1 = 0$ and $M_D = 0$ (i.e., the dead cell have no mobility or velocity). Thus, the movement of the dead cells is dominated by necrosis and dead cell degradation.

Following the nondimensionalization in section 2.4 we nondimensionalize the system equations using the oxygen diffusion length scale and the mitosis rate of the CP cells as the time scale. These can be estimated as $l \approx 200\mu m$ and $\tau \approx 1$ day. The oxygen concentration is measured against the concentration in the blood or in the medium in the vitro case. The nondimensionalized equations are presented below.

$$
\begin{aligned}
\partial_t \phi_V =& M_V \nabla \cdot (\phi_V \nabla \mu) + S_V - \nabla \cdot (\phi_V \mathbf{u}_s) \\
\partial_t \phi_W =& M_W \nabla \cdot (\phi_W \nabla \nu) + S_W - \nabla \cdot (\phi_W \mathbf{u}_w) \\
\partial_t \phi_D =& S_D \\
\partial_t \phi_{SC} =& M_V \nabla \cdot (\phi_{SC} \nabla \mu) + S_{SC} - \nabla \cdot (\phi_{SC} \mathbf{u}_s) \\
\mu =& \alpha_{VW} \phi_V (\phi_W - \bar{\phi}_W^V)^2 - \alpha_{HW} (\phi_W - \bar{\phi}_W^H)^2 \phi_H - \frac{1}{2} \phi_T^2 \phi_H + \frac{1}{2} \phi_T \phi_H^2 \\
& - \alpha_{Vitro} \phi_W^2 \phi_H - \alpha_{WDH} \phi_W^2 \phi_D^2 \phi_H + \alpha_{VWDH} \phi_V \phi_W^2 \phi_D^2 \phi_H^2 \\
& - \alpha_{VWDH} \phi_V^2 \phi_W^2 \phi_D^2 \phi_H + \alpha_V \phi_V \mathcal{H}(-\phi_V) - \alpha_H \phi_H \mathcal{H}(-\phi_H) \\
& - 2\epsilon^2 \Delta \phi_V - \epsilon^2 \Delta \phi_W - 2\epsilon^2 \Delta \phi_D \\
\nu =& \alpha_{VW} (\phi_W - \bar{\phi}_W^V) \phi_V^2 + \alpha_{HW} (\phi_W - \bar{\phi}_W^H) \phi_H^2 - \alpha_{HW} (\phi_W - \bar{\phi}_W^H)^2 \phi_H \\
& + \alpha_{Vitro} \phi_W \phi_H^2 - \alpha_{Vitro} \phi_W^2 \phi_H - \frac{1}{2} \phi_T^2 \phi_H - \kappa (C_0 - 1)^2 \phi_W \\
& + \alpha_{WDH} \phi_W \phi_D^2 \phi_H^2 - \alpha_{WDH} \phi_W^2 \phi_D^2 \phi_H + \alpha_{VWDH} \phi_V^2 \phi_W \phi_D^2 \phi_H^2 \\
& - \alpha_{VWDH} \phi_V^2 \phi_W^2 \phi_D^2 \phi_H + \alpha_W \phi_W \mathcal{H}(-\phi_W) - \alpha_H \phi_H \mathcal{H}(-\phi_H) \\
& - 2\epsilon^2 \Delta \phi_D - \epsilon^2 \Delta \phi_W - 2\epsilon^2 \Delta \phi_V \\
\mathbf{u}_s =& - k_s (\phi_s \nabla p + \frac{\gamma}{\epsilon} \phi_V \nabla \mu - \frac{\gamma}{\epsilon} \phi_s \nabla \nu) \\
\mathbf{u}_w =& - k_w \phi_W \nabla p \\
0 =& \nabla \cdot ((k_s \phi_s^2 + k_w \phi_W^2) \nabla p) + k_s \frac{\gamma}{\epsilon} \nabla \cdot (\phi_s \phi_V \nabla \mu - \phi_s^2 \nabla \nu) \\
S_V =& \phi_V \phi_W C_0 + \lambda_{MTC} \phi_{TC} \phi_W C_0 - \lambda_{NSC} \phi_{SC} \mathcal{H}(\bar{C}_0 - C_0) \\
& - \lambda_{NTC} \phi_{TC} \mathcal{H}(\bar{C}_0 - C_0) \\
S_W =& - \phi_V \phi_W C_0 - \lambda_{MTC} \phi_{TC} \phi_W C_0 + \lambda_l \phi_D \mathcal{H}(\bar{\phi}_D - \phi_D) \\
S_D =& \lambda_{NSC} \phi_{SC} \mathcal{H}(\bar{C}_0 - C_0) + \lambda_{NTC} \phi_{TC} \mathcal{H}(\bar{C}_0 - C_0) - \lambda_l \phi_D \mathcal{H}(\bar{\phi}_D - \phi_D) \\
S_{SC} =& (2P_0 - 1) \phi_{SC} \phi_W C_0 - \lambda_{NSC} \phi_{SC} \mathcal{H}(\bar{C}_0 - C_0)
\end{aligned}
$$

$$
\begin{aligned}
0 =& \nabla^2 C_0 - C_0(\phi_{SC} + \nu_{UOTC}\phi_{TC}) + \nu_{PO}(1 - C_0)Q(\phi_T) \\
0 =& \nabla^2 C_T - C_T(\nu_{UT}\phi_{SC} + \nu_{DT}) + \nu_{PT}\phi_{TC} \\
P_0 =& P_{Min} + (P_{Max} - P_{Min}) \left(\frac{\xi C_W}{1 + \xi C_W} \right) \left(\frac{1}{1 + \Phi C_T} \right) \\
\partial_t C_W =& D_W \nabla^2 C_W + Rf(C_W, C_{WI}) \\
\partial_t C_{WI} =& D_{WI} \nabla^2 C_{WI} + Rg(C_W, C_{WI}) \\
f(C_W, C_{WI}) =& \frac{C_W^2}{C_{WI}} C_0 \phi_{SC} - C_W + u_0 C_0 \phi_V \\
g(C_W, C_{WI}) =& C_W^2 C_0 \phi_{SC} - \nu_{DWI} C_{WI}.
\end{aligned}
$$

6.3 Base Case

Now we investigate the progression of a two dimensional tumor. The non dimensional parameters for the simulation are given in table 6.1. The parameters are chosen from experimentation and parameter studies. The mobility of the viable cells is chosen to be $M_V = 10.0$ to encourage tumor branching. The parameters for the self-renewal and feedback responses are obtained from numerical experiments that require that W and WI form co-localized patterns. In figure 6.1 the simulations of this model are shown at time $t = 200$ and in figures, (D.1), (D.2), (D.3), (D.4), and (D.5) the evolution of the tumor species are shown. The initial circular tumor develops a morphological instability as stem cell clusters begin to appear at the viable cell boundary. This prediction of the stem cell arrangement was confirmed in a recent study [68]. As the tumor begins to expand the stems cells become more localized in discrete clusters. By time $t = 40$ a necrotic core has developed and as the tumor continues to expand additional stem clusters begin to appear between the original

formations. The tumor expands in this manner until $t = 140$ where we begin to see buds beginning to form at the corners of the the viable cell fraction. At time $t = 180$ we see the stem cell clusters at the buds start to split into two new discrete groups. By $t = 200$ we see that five buds are growing larger and developing their own necrotic cores. We also notice the terminal cells are localized next to the stem cells and the concentration of terminal cells is largest near the stem cell clusters.

The heterogeneous distribution of the stem and terminal cells is due to the Gierer-Meinhardt-Turning equations (6.12) that lead to pattern formation of W which influences the self-renewal fraction of SCs. In figure (6.1g) and (6.1h) the concentrations of W and WI are shown at time $t = 200$ against the contour of the tumor. As expected the system forms patterns that have isolated regions of high concentration that are co-localized. The regions form near the boundary of the tumor because the production of W and WI depend on the nutrient concentration and the nutrient concentration is the greatest at the boundary. Far outside the tumor the concentration is uniform at 1 and the interior of the tumor has a concentration near zero due to the rapid uptake. These prediction of the co-localized of W and WI near the boundary have also been observed in in-vitro tumors [66, 42].

In the regions where W is large the self-renewal fraction P_0 is also large. Thus, near the boundary of the tumor the self-renewal fraction of the stem cells is higher than the interior of the tumor as seen in figure (6.1g). Therefore the stem cells near the boundary of the tumor have a higher mitosis rate than the stem cells near the interior. Hence, more stem cells are produced near the tumor boundary compared to the interior. This is the mechanism that produces the instability of the tumor and the eventual bud formation. The negative feedback factor T also reinforces this behavior of the stem cell clusters. In figure (6.1f) the stem cell clusters are in the region of lowest C_T concentration inside the tumor. Thus, the gradient of the concentration of T furthers the development of the stem cells and the growth of the tumor.

Figure (6.2a) shows that initially the tumor begins to grow as the stem cells uptake water and nutrients. After time $t = 30$ we see a slow down in the growth rate when the necrotic core develops and only the proliferating rim of the cells contribute to the growth. Additionally, the stem cells begin to differentiate to the slower growing terminal cells. The growth rate of the stem cells increases as the buds begin to form at the corners of the viable cells. We see a delayed increase in the growth rate of the terminal cells and dead cells as the buds begin to form necrotic cores. We see an initial dip in the water fraction volume as the stem cells expand and uptake water and then a gradual increase as the necrotic expands. Then we see another decrease as the buds form and uptake water.

We began the tumor simulation from an initial circular distribution of stem cells and water with 80%, 20% respectively. After time $t = 40$ viable cell fraction maintains approximately 70% stem cells and approximately 30% terminal cells (figure 6.2b). These percentages can be altered by adjusting the ξ and Φ parameters. The steady-state values for the concentration of W and WI are obtained by setting $f = g = 0$ with $C_0 = 1$ and letting ϕ_{SC} and ϕ_{TC} equal the initial percentages. Thus we see,

$$C_W(x, 0) = (1.2 + 0.1(\text{rand} - 0.5))\phi_T \tag{6.13}$$

$$C_{WI}(x, 0) = 1.21\phi_T. \tag{6.14}$$

The concentrations are multiplied by ϕ_T to confine the initial conditions to the initial tumor. Here *rand* is a random number that differs at each point in the computational grid and is uniformly distributed in the unit interval. Lastly, there is no initial condition for C_T and C_0 since they satisfy quasi-steady diffusion equations.

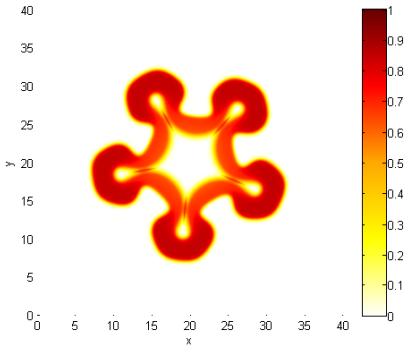

(a) viable cells ϕ_V

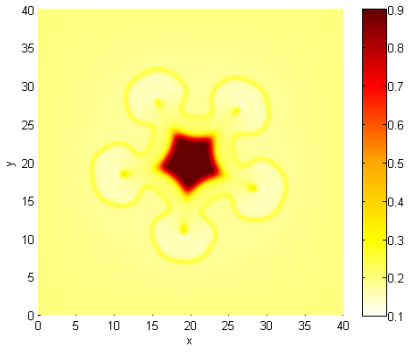

(b) water ϕ_W

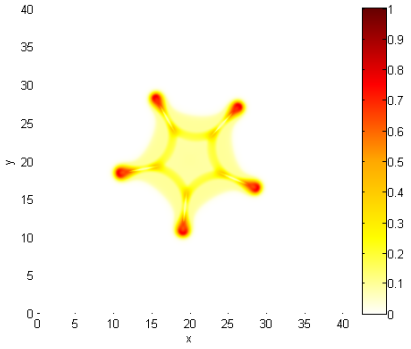

(c) dead cells ϕ_D

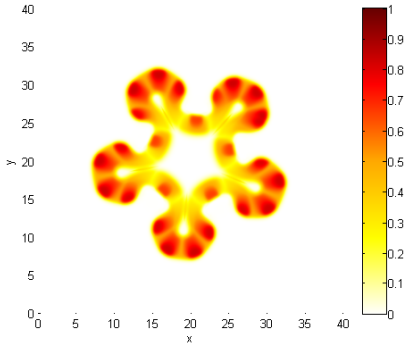

(d) stem cells ϕ_{SC}

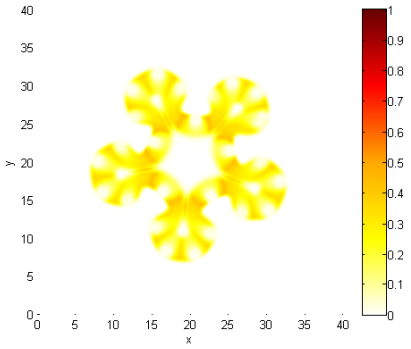

(e) terminal cells ϕ_{TC}

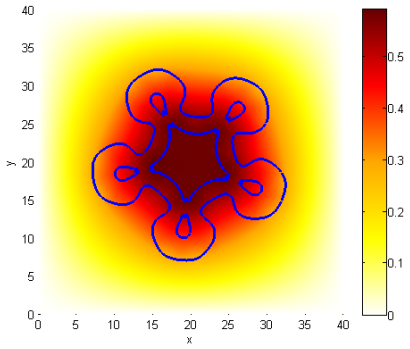

(f) TGF-β1 concentration C_T

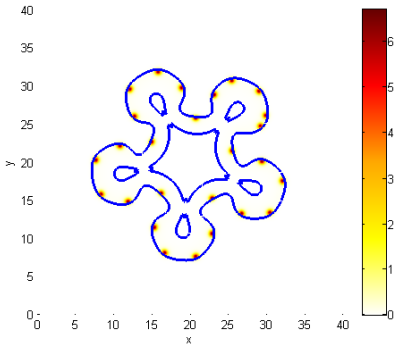

(g) wnt concentration C_W

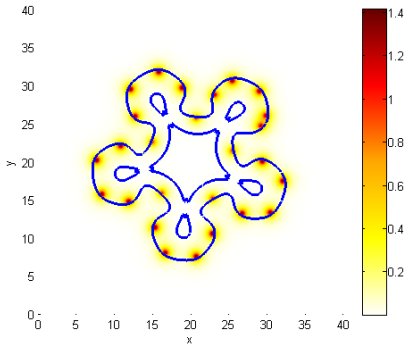

(h) Dkk concentration C_{WI}

Figure 6.1: Species for the non-constant water model with stem cells at time $t = 200$. The contours are given for $\phi_V = 0.5$

Table 6.1: Non-Dimensional Parameters

P_0	Source Terms	W and WI	T	Oxygen	other
$\xi = 50.0$	$\lambda_{MTC} = 0.1$	$\nu_{DWI} = 1.0$	$\nu_{UT} = 0.1$	$\nu_{UOTC} = 1.0$	$\gamma = -0.1$
$\Psi = 0.01$	$\lambda_L = 0.2$	$D_{WI} = 25.0$	$\nu_{DT} = 0.0$	$\nu_{UOSC} = 1.0$	$\epsilon = 0.05$
$P_{Max} = 1.0$	$\lambda_{NCS} = 5.0$	$D_W = 1.0$	$\nu_{PT} = 5.0$	$\nu_{PO} = 0.5$	$M_V = 10.0$
$P_{Min} = 0.2$	$\lambda_{NTC} = 5.0$	$R = 50.0$		$D_0 = 1.0$	$M_W = 200.0$
	$C_0 = 0.10$	$u_0 = 0.2$			$\alpha_{VW} = 0.25$
	$\bar{\phi}_D = 0.10$				$\alpha_{WH} = 0.25$
					$\kappa = 0.035$

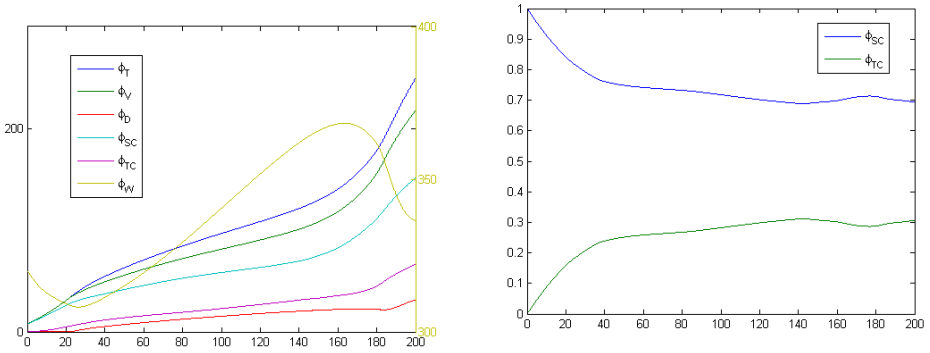

(a) Total volume of cell species

(b) stem cell and terminal cell percentage of the viable cells

Figure 6.2: Total volume of the species with stem cells included and the stem cell and terminal cell percentages of the viable cells

6.4 Parameter Variations

In this section we present parameter variations for three of the variables that influence the growth and morphology of the tumor. In particular, we consider the Φ and ξ parameters that influence the differentiation rate of the stem cells and the M_V parameter that was shown to encourage branching for low values.

The Φ parameter controls how sensitive the stem cell differentiation rate is to the differentiation promoter T produced by the terminal cells. In other words, Φ is the sensitivity of the differentiation rate to negative feedback. Figure (D.6) shows that parameter has a range between 0.1 and 1.0 that drastically alters the morphology of the tumor. Increasing

Φ by an order of magnitude from 0.01 to 0.1 does not significantly affect the morphology of the tumor at $t = 200$. Figure (D.10) shows that although the $\Phi = 0.01$ does produce more stem cells the difference is minimal. For $\Phi = 0.01$ the stem cell fraction of the viable cells stabilizes at 70% and for $\Phi = 0.1$ the fraction of stem cells stabilizes at 65%.

The parameter range between 0.1 to 1.0 produces the greatest difference in the tumor growth and morphology. For $\Phi = 0.5$, the tumor still exhibits the same budding behavior as seen in figure (D.6), however, in this case, each bud only contains one stem cell cluster. In figure (D.10a) we see the fewer stem cell clusters in the buds results in a slower stem cell growth rate. Additionally, figure (D.10b) shows the increase in the terminal cell fraction whcih accounts for 70% of the viable cells at this point in the tumors progression. Increasing the parameter to $\Phi = 1.0$, we no longer see any branching of the tumor although there is a slight pentagon shape for the viable cells. This suggests that the localization of the stem cells still impacts the tumor shape despite of their decreased level. Indeed the stem cell fraction has now decreased to 10%. In figure (D.10) we can see that after the initial growth rate of the tumor we see a decrease in the volume as the stem cells differentiate to terminal cells and the slower increase in then number of the terminal cells cannot out pace cell death in the necrotic core and the tumor collapses back to its steady state.

Increasing the parameter Φ once again from 1.0 to 10.0 yields a smaller tumor that is almost entirely terminal cells. The stem cells are hardly discernible in the figure at about 1%. Note that for this high negative feedback rate we see the tumor stabilizes at approximately $t = 40$ with a radius of 3.7. Thus, compared to the model without the cell lineages, this stable tumor has a much smaller radius and a smaller necrotic core. As the tumor in this case is mainly composed of terminal cells, the slower mitosis rate of the viable cells results in a smaller compact tumor.

The parameter ξ measures the sensitivity of the stem cell differentiation factor to the self-renewal promoter W produced by the stem cells positive feedback. Here we see the counter-

intuitive behavior that increasing the positive feedback on the growth parameter decreases the volume of the tumor. Indeed figure (D.11) shows that during the initial growth phase the higher parameter value produces a slightly larger tumor. Then a sharp increase in the growth rate is observed when the viable cells begin to bud and produce new branches. The lower the parameter value the sooner the tumor begin this second growth phase. Although, if ξ is taken to be too small, most of the stem cells will differentiate and the tumor will stabilize as in the $\Phi = 10.0$ case. We can see that the higher this self-renewal parameter the greater the percentage of the viable are stem cells. For $\xi = 100$ the tumor is approximately 82% stem cells and for $\xi = 25$ the tumor is approximately 55% stem cells. These stem cell percentage give an indication why increasing this parameter delays the tumor branching. Figure (D.8) shows that the smaller the parameter the more localized the stem cell cluster are. The budding of the tumor occurs because stem cell clusters at the boundary have a greater proliferation rate than the surrounding viable cells. If the stem cell density is too high, as in the $\xi = 100$ case, the budding process will take longer as the surrounding cells have a similar growth rate. For the $\xi = 100$ case we do see some early buds and the increase growth rate of the viable rim has produced a larger necrotic core than the smaller parameters. In the $\xi = 25$ case we see the stem cell clusters are much more localized. The initial necrotic core is smaller that the other case due to the earlier branching and the buds have already formed a necrotic core.

As mentioned in previous chapters the M_V parameter determines how fast the viable cells are able to more around the proliferating rim of the tumor. In figure (D.9) we see that increasing the mobility parameter produces a rounder shape. For $M_V = 25$ we no longer see any branching of the tumor at the corners of the pentagon. For $M_V = 50$ the tumor becomes rounder and the pentagon shape that occurs for smaller mobility rates is no longer present. Figure (D.12) we see the parameter M_V does not significantly alter the stem cell percentage of the viable cells. The minor variations occur because the higher mobility rates decrease the spacing between the stem cell clusters. The figure also shows that tumors are

stable for the higher mobility rates despite the non circular morphologies.

6.5 Conclusion

We see above that the model above is capable of producing a detailed morphology of a hierarchically organized tumor that develops necrotic regions. The differing mitosis rates of the cells species in tandem with the localized stem cell clusters generate morphological instabilities that produce the budding and branching as the tumor develops. In addition, it is also possible to produce stable tumor spheroids by increasing the viable cell mobility rate or the differentiation promoter feedback gain. This is consistent with the results obtained from the in constant water fraction model [23]. However, in the extension presented here the tumors also contain a liquid necrotic core.

We also performed selected parameter studies that have clinical significance concerning the tumor development. In particular, increasing the feedback gain of the stem cell differentiation to the T factor shrinks and stabilizes the tumor size and morphology, respectively. Thus, either increasing the stem cell sensitivity or producing more of this factor will reduce the size of the tumor and decrease it invasive potential. Therapies targeting this negative feedback pathway are currently underway [12, 14]. Further, increasing the sensitivity of the stem cells to W factor delays the invasiveness of the tumor. The higher the sensitivity to W, or the more W there is in the system, the greater the delay until the tumor forms buds and invades the host tissue. Cancer treatments targeting this signaling pathway are also being investigated [56, 63].

Chapter 7

Conclusion

In this thesis we have developed a general mixture model that incorporates a non-constant water fraction. A novel energy for the system was created that allows for different water fractions to be considered in the host and viable cell regions. Further, this energy provides a way to flux the water out of the necrotic region and produce stable tumor spheroids. This feature of the model will be critical to performing model validation where the model predictions can be compared with tumor spheroids grown experimentally in-vitro. Also, with a non-symmetric initial condition we were able to produce an invasive tumor that displayed behaviors characteristic of a malignant cancer in the preliminary stage of development.

We also performed one-at-a-time parameter variations under the symmetric and non-symmetric initial conditions. The parameters that can influence the size of the stable tumor and the growth rate were identified as they are important for experimental purposes. Additionally, the parameter regimes that can destabilize the tumor in both size and shape were explored and parameters that had little effect of the tumor progression were identified. Thus, we were able to capture a wide range of tumor behavior by exploring different parameter regimes. We also showed that the additional model-based terms that were added to the energy were

necessary to capture the physically realistic tumor behavior. In particular, we are now able to model and control to a certain degree the effects of different water fraction levels in the host and the tumor.

Finally, the non-constant water fraction model was extended to the include cancer stem cells and their progeny. The model is capable of producing a detailed invasive morphology of a tumor that also develops a largely liquid necrotic core. It is also capable of forming stable tumors with heterogeneous cell distributions. A parameter study of the positive and negative feedback gains for the stem cells show how the morphology of the tumor is dependent on the sensitivity to these parameters and possible avenues for therapy are seen.

Future directions for this work can proceed in two basic directions. The first way is to incorporate additional biophysical processes. Tissue elasticity, angiogenesis, viscolastic effects, and ECM degradation are not considered and could improve the predictive power of the model. It is well known that tumor growth produces stress on the surrounding host tissue and recent studies have shown the importance of growth induced tissue stress in tumor development [19, 17]. Thus, the stress produced by the tumor on its surrounding environment needs to be incorporated into the model to capture the physiological affect the tumor has on its microenvironment. The second direction this work can proceed is to validate the model with in-vitro experiments. The stable tumor spheroids predicted by this model can be compared against tumor spheroids developed in in-vitro cultures to help refine the model and increase its predictive power. Additionally, this model can also be extended to include therapy. An extension of this type was done for the cell lineage model in [23]. However, with the non-constant water fraction model considered here we have a more realistic viable cell and liquid distributions that will result in more accurate therapy levels and agent uptake mechanisms. Thus, this model can provide a more accurate way to model drug uptake by the tumor and the tumor response. Ultimately, the model should help advance the development of precision medicine.

Bibliography

[1] H. M. A. Gierer. A theory of biological pattern formation. *Biological Cybernetics*, 12(1):30–39, December 1972.

[2] M. L. Agata Nyga, Umber Cheema. 3d tumor models: Novel in vitro approaches to cancer studies. *Journal of Cell Communication and Signalling*, 5(3):239–248, August 2011.

[3] P. L. Ambrosi, D. On the closure of mass balance models for tumor growth. *Math. Models Methods Appl. Sci*, 12.

[4] M. D. Araujo, R. A mixture theory for the genesis of residual stresses in growing tissues i: a general formulation. *SIAM Journal of Applied Mathematics*, 65.

[5] S. P. H. M. Bailey, J.M. Cancer metastasis facilitated by developmental pathways: Sonic hedgehog, notch, and bone morphogenic proteins. *J. Cell Biochem*, 102(4):829–839, 2007.

[6] D. J. Bonnet, D. Human acute myeloid leukemia is organized as a hierarchy that originates from a primitive hematopoietic cell. *Nat. Medicine*, 3(7):730–737, 1997.

[7] W. Bullough. Mitotic and functional homeostasis: A speculative review. *Cancer Res.*, 25(10):1683–1727, 1965.

[8] P. L. Byrne, H. Modelling solid tumour growth using the theory of mixtures. *Math. Med. Biol*, 20.

[9] P. L. Byrne H. Modeling solid tumor growth using the theory of mixtures. *Math Medical Biology*.

[10] J. W. Cahn and J. E. Hilliard. Free energy of a nonuniform system. i. interfacial free energy. *J. Chem. Phys*, 28(258):1436–1437, 1958.

[11] S. Chandrasekaran and M. R. King. Gather round: In vitro tumor spheroids as improved models of in vivo tumors. *Journal of Bioengineering and Biomedical Science*, 2(4).

[12] R. C. J. C. S. F. E. R. A. d. G. Cindy Neuzilleta, Annemila Tijeras-Raballandb. Targeting the tgfβ pathway for cancer therapy. *Pharmacology and Therapeutics*, 147.

[13] A. Collins. Prospective identification of tumorigenic prostate cancer stem cells. *Cancer Res.*, 65(23):10946–10951, 2005.

[14] M. J. S. P. Fabregat I, Fernando J. Tgf-beta signaling in cancer treatment. *Current Pharmaceutical Design*, 20(17):2934–3947, 2014.

[15] Z. X. S. C.-H. T. B. G. R. C. V. Frieboes, H. An integrated computational/experimental model of tumor invasion. *Cancer Res.*, 66.

[16] S. Y. O. M.-K. K. K. M. O. H. M. Y. K. Y. Fukuda, K. Tumor initiating potential of side population cells in human gastric cancer. *Int.J.Oncol.*, 34(5):1201–1207, 2009.

[17] Y. C. Fung. What are the residual stresses doing in out blood vessels? *Ann. Biomed. Engineering*, 19.

[18] K. M. Furth, J. The transmission of leukemia of mice with a single cell. *American Journal of Cancer*, 31.

[19] H. L.-R. M. G. Helmlinger, P.A. Netti and R. Jain. Solid stress inhibits the growth of multicellular tumor spheroids. *Nature Biotechnology*, 15.

[20] Y. gao Man. Tumor cell budding from focally disrupted tumor capsules: a common pathway for all breast cancer subtype derived invasion? *Journal Cancer*, 1.

[21] W. H.-H. B.-C. K. J. K. E. M. M. J. J. L. A. C. A. Gokoffski, K.K. Activin and gdf11 collaborate in feedback control of neuro epithelial stem cell proliferation and fate. *Development*, 138(19):4131–4142, 2011.

[22] S. B. Goldacre RJ. On the access of blood-borne dyes to various tumor regions. *British Journal of Cancer*, 16.

[23] A.-J. H. Youssefpour, X.Li. Multispecies model of cell lineages and feedback control in solid tumors. *Journal of Theoretical Biology*, 304.

[24] D. Hanahan and R. A. Weinberg. Hallmarks of cancer: the next generation. *Cell*, 144(5):646–674, March 2011.

[25] R. A. Hanahan, Douglas; Weinberg. The hallmarks of cancer: The next generation. *Cell*, 144(5):646–674, January 2011.

[26] B. N. Harald Garcke and B. Stinner. A diffuse interface model for alloys with multiple components and phases. *SIAM Applied Math*, 64(3):775–799, 2004.

[27] B. N. Harald Garcke and B. Stinner. Multicomponent alloy solidification: Phase-field modeling and simulations. *Physical Review*, E(71):041609, 2005",

[28] B. N. Harald Garcke and B. Stoth. On anisotropic order parameter models for multi-phase systems and their sharp interface limits. *Physica D*, 115.

[29] B. N. Harald Garcke and B. Stoth. A multiphase field concept: Numerical simulations of moving phase boundaries and multiple junctions. *SIAM Applied Math*, 60(1):295–315, 1999.

[30] N. I. L. J.-M.-S. M. G. D. B.-F. M. K. H. Hemmati, D.D. Cancerous stem cells can arise from pediatric brain tumors. *Proc. Nat. Acad. Sci.*, 100(25):15178–15183, 2003.

[31] B. N.-M. S. R. P. G. S. I. Steinbach, F. Pezzolla. A field concept for mulitphase systems. *Physica D*, 94.

[32] N. C. Institute. Defining cancer.

[33] L. T. J. Lowengrub. Quasi-incomptressible cahn-hillard fluids and topological transitions. *The Royal Society*, A(454):2617–2654, 1998",

[34] F. J. Y.-L. C. X. L. P. M. S. M. W. V. C. J S Lowengrub, H B Frieboes. Nonlinear modeling of cancer: bridging the gap between cells and tumors. *Nonlinearity*, 23.

[35] R. K. Jain. Transport of molecules in the tumor interstitium: A review. *Cancer Research*, 47.

[36] S. C.-W. Jiang, G.-S. Efficient implementation of weighted eno schemes. *Journal of Computational Physics*, 126.

[37] N. K. T.-M. V. Y.-W. Q. T. J. R. Joseph J. Pinzone, Brett M. Hall and J. John D. Shaughnessy. The role of dickkopf-1 in bone development, homeostasis, and disease. *Blood*, 113(3):517–525, January 2009.

[38] M. G. Y. M. S. E. I.-C. Z. P. Kirouac, D.C. Cellcell interaction networks regulate blood stem and progenitor cell fate. *Molecular Systems Biology*, 5(293).

[39] B. W. Klaus, A. Wnt signaling and its impact on development and cancer. *Nat. Rev. Cancer*, 8(5):387–398, 2008.

[40] M. Lancaster. Dishing up mini-organs. *Science*, 342.

[41] G. K. W. F. N. Q. C.-A. Lander, A.D. Cell lineages and the logic of proliferative control. *PLoS Biology*, 7(1):387–398, 2009.

[42] S. A. O. S. D. O. R.-J. K. R.-D. N. P. D. H. E. G. C. Lee, N. A potential role for dkk-1 in the pathogenesis of osteosarcoma predicts novel diagnostic and treatment strategies. *Br.J.Cancer*, 97(11):1552–1559, 2007.

[43] C. C.-S. G. K. W.-F. L. A.-C. A. N. Q. Lo, W.-C. Feedback regulation in multistage cell lineages. *Mathematical Biosci. English*, 6(1):59–82, 2009.

[44] D. B. Louis-Bastien Weiswald and V. Dangles-Marie. Spherical cancer models in tumor biology. *Elsevier*, 17(1):1–15, 2015.

[45] B. R. M. Dharan. Fatal gliomatosis cerebri in a pregnant woman. *Internet Journal of Gynecology and Obstetrics*, 3(1).

[46] P. C. M. Soltani. Numerical modeling of fluid flow in solid tumors. *PLoS ONE*, 6(6).

[47] P. C. McArthur, B. Residual stress generation and necrosis formation in multicell tumor spheroids. *Math Bio*, 49.

[48] T. P. Meulmeester, E. The dynamic roles of tgf-b in cancer. *Journal of Pathology*, 223(2):205–218, 2011.

[49] C. A. A. Z. S. S. R. P.-A. B. A. T. Michele Zanoni, Filippo Piccinini. 3d tumor spheroid models for in vitro therapeutic screening: a systematic approach to enhance the biological relevance of data obtained3d tumor spheroid models for in vitro therapeutic screening: a systematic approach to enhance the biological relevance of data obtained. *Scientific Reports*, 6(19103).

[50] E. S. N. Mikala Egeblad and Z. Werb. Tumors as organs: complex tissues that interface with the entire organism. *Dev Cell*, 18(6):884–901, June 2010.

[51] C. M.J. Tindall. Modeling the cell cycle and cell movement in multicellular tumor spheroids. *Bulletin of Mathematical Biology*.

[52] W. H. Organization. The top 10 causes of death fact sheet n310.

[53] W. H. Organization. *World Cancer Report*. World Health Organization.

[54] C. B. d. C. J.-W. S.-C. S. V. K. H. A. D. J. M. Ovijit Chaudhuri, Sandeep T. Koshy. Extracellular matrix stiffness and composition jointly regulate the induction of malignant phenotypes in mammary epithelium. *Nature Materials*, 13.

[55] L. T. B. Y. B. R. S.-R. K. J. Paolo, A. Netti. Macro and microscopic fluid transport in living tissues: Application to solid tumors. *AIChE Journal*, 43(3):818–834, March 1997.

[56] P. Polakis. Wnt signaling in cancer. *Cold Spring harbor Perspectives in Biology*, 4(5).

[57] L. S. M. R. P. Araujo. A history of the study of solid tumour growth: The contribution of mathematical modeling. *Bulletin of Mathematical Biology*.

[58] J. RK. Normalization of tumor vasculature: An emerging concept in antiangiogenic therapy. *Science*, 307.

[59] N. P. M. L. B. Y. J. R. Roose, T. Solid stress generated by spheroid growth using a linear poroelastic model. *Microvasc. Res.*, 66.

[60] W. B. Rowlinson, J. *Molecular theory of capillarity*. Clarendon Press, Oxford, 1982.

[61] S. S. P. D. V. R.-e. a. Sands H, Jones PL. Correlation of vascular permeability and blood ow with monoclonal antibody uptake by human clouser and renal cell xenografts. *Cancer Research*, 48.

[62] T. Sato and H. Clevers. Growing self-organizing mini-guts from a single intestinal stem cell: Mechanism and applications. *Science*, 340.

[63] N. R. T Zhan and M. Boutros. Wnt signaling in cancer. *Oncogene*, 4(5):1–13, September 2016.

[64] L. V. Tijana Borovski, Felipe De Sousa E Melo and J. P. Medema. Cancer stem cell niche: the place to be. *Cancer Res*, 71(3):634–639, February 2011.

[65] e. Toshiro Sato, Johan H. van Es. Paneth cells constitute the niche for lgr5 stemcells in intestinal crypts. *Nature*, 469.

[66] M. F. H. M. C. K. J. J.-B. T. T. J. T. M. M. C. R. H. S. M. K. K. R. D. S. G. M. J. Vermeulen, L. Wnt activity defines colon cancer stem cells and is regulated by the microenvironment. *Nature*, 12(5):468–476, 2010.

[67] v. d. H. M. C. K. d. J. J. B. T. T. J. T. M. M. C. R. H. S. M. K. K. R. D. S. G. M. J. Vermeulen L, De Sousa E Melo F. Wnt activity defines colon cancer stem cells and is regulated by the microenvironment. *Nature Cell Biology*, 12(5):468–476, May 2010.

[68] K. K. L. C. D. L. M. J. E. M. S. J. S. E. M. W. P. F. Vlashi, E. Invivo imaging, tracking, and targeting of cancer stem cells. *JNCIJ.Natl.CancerInst*, 101(5):350–359, 2009.

[69] K. J. L. J. Wise, S. Solving the regularized, strongly anisotropic chanhilliard equation by an adaptive nonlinear multigrid method. *Journal of Computational Physics*, 226.

[70] L. J. C. V. Wise, S.M. An adaptive multigrid algorithm for simulating solid tumor growth using mixture models. *Math. Computational Model*, 53(1-2):1–20, 2011.

[71] L. J. F. H. C. V. Wise, S.M. Three-dimensional multispecies nonlinear tumor growthi model and numerical method. *Journal of Theoretical Biology*, 253(3):524–543, 2008.

[72] I. S. M. R. J. S. L. K. J. J. C. A. Wu, H.H. Autoregulation of neurogenesis by gdf11. *Neuron*, 37.

[73] D. S. R. W. Y.R. Kim, M.D. Savellano and A. B. Jr. Measurement of tumor interstitial volume fraction: Method and implication for drug delivery. *Magnetic Resonance in Medicine*, 52.

Appendix A

Non-Symmetric Tumor Evolution for the Base Case Slides

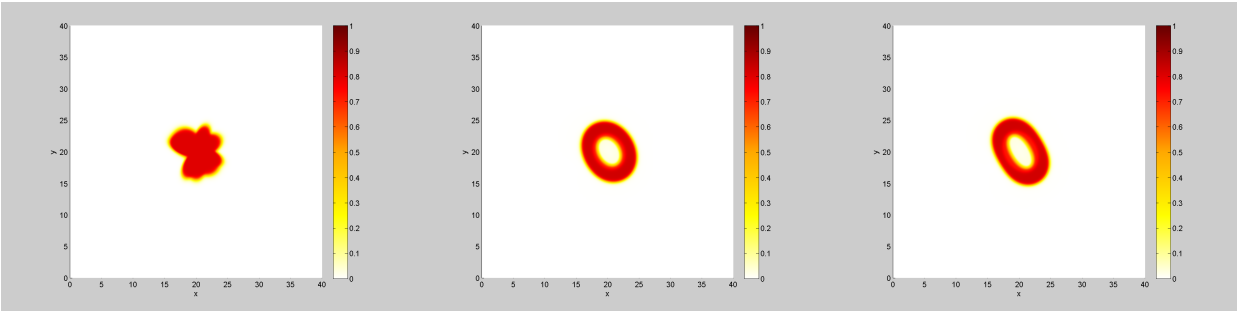

(a) $t = 0$ (b) $t = 40$ (c) $t = 80$

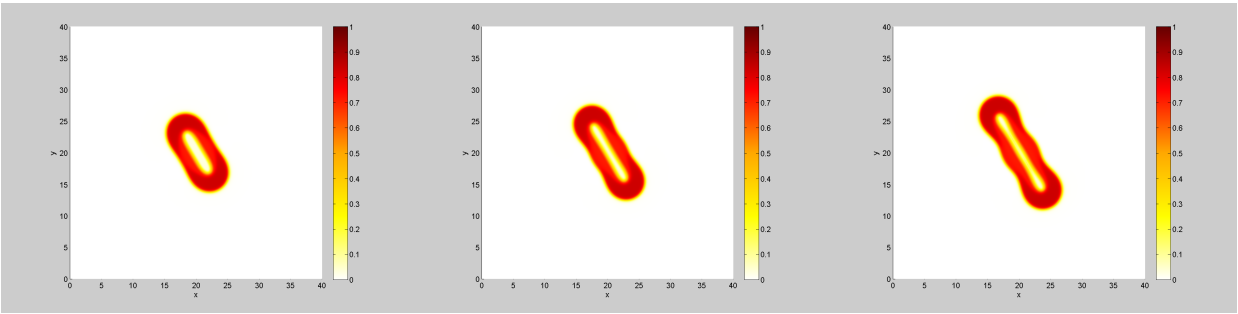

(d) $t = 120$ (e) $t = 160$ (f) $t = 200$

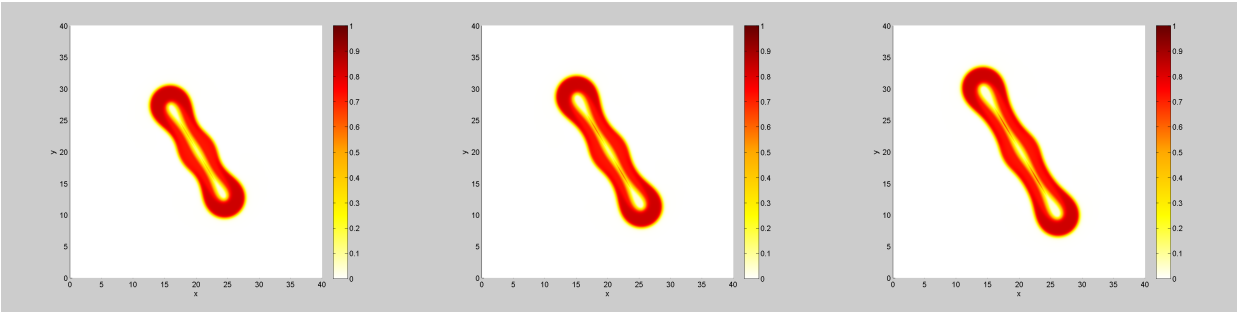

(g) $t = 240$ (h) $t = 280$ (i) $t = 320$

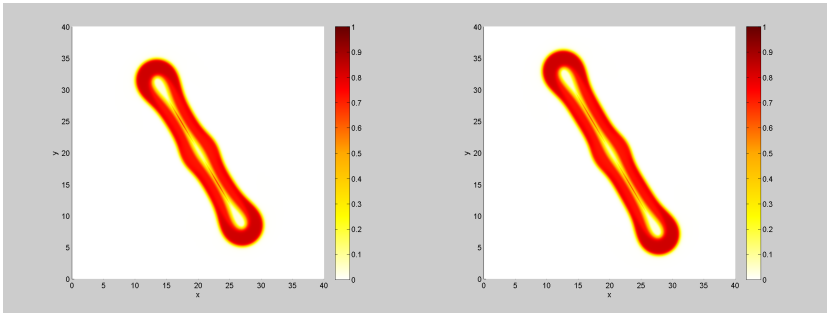

(j) $t = 360$ (k) $t = 400$

Figure A.1: viable cells ϕ_V $r = 3$

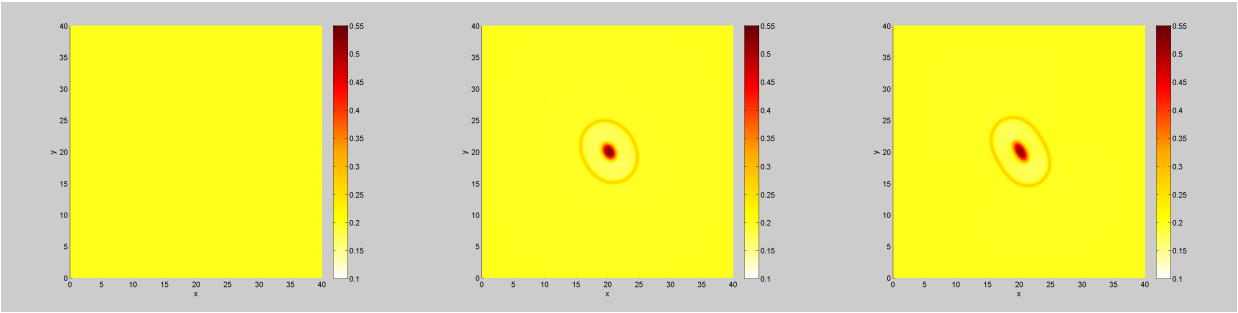

(a) $t = 0$ (b) $t = 40$ (c) $t = 80$

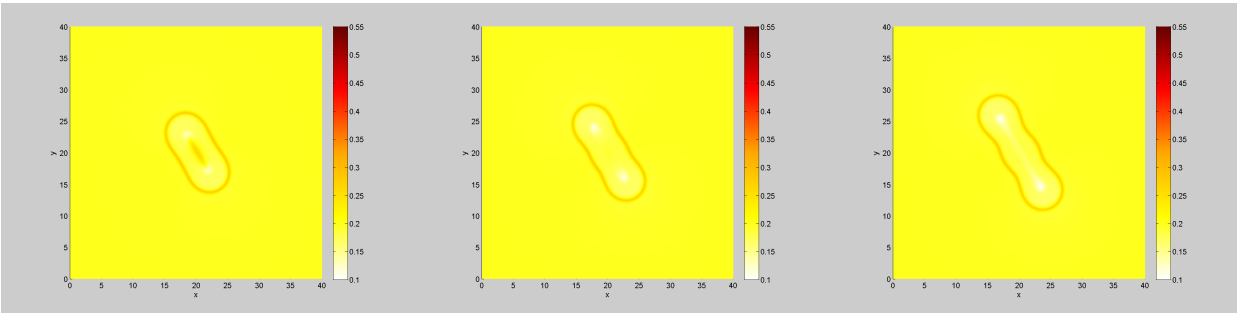

(d) $t = 120$ (e) $t = 160$ (f) $t = 200$

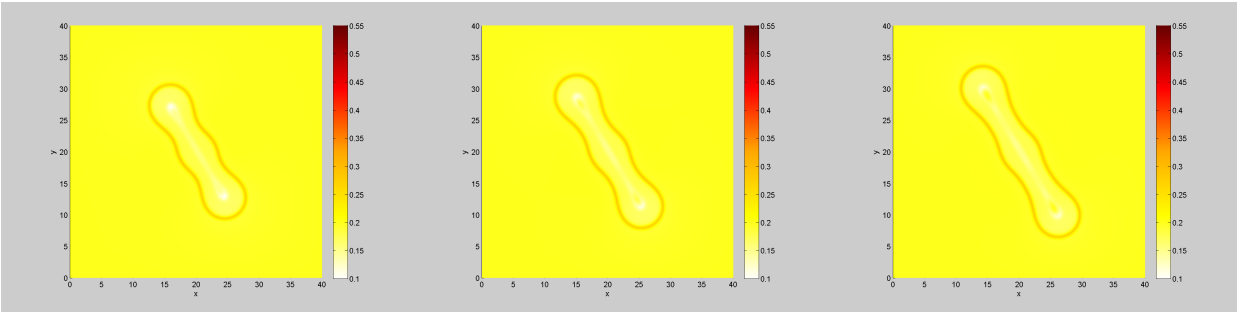

(g) $t = 240$ (h) $t = 280$ (i) $t = 320$

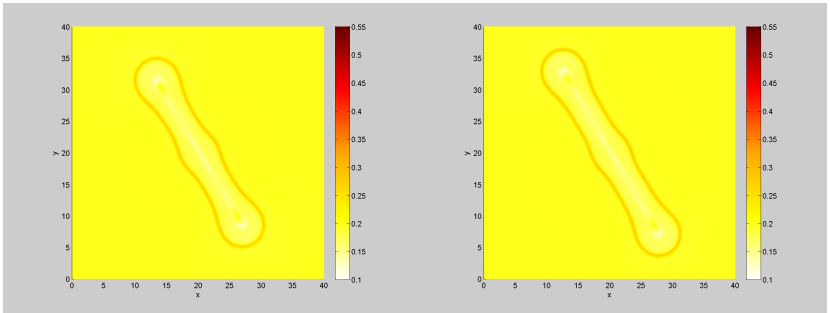

(j) $t = 360$ (k) $t = 400$

Figure A.2: water ϕ_W, $r = 3$

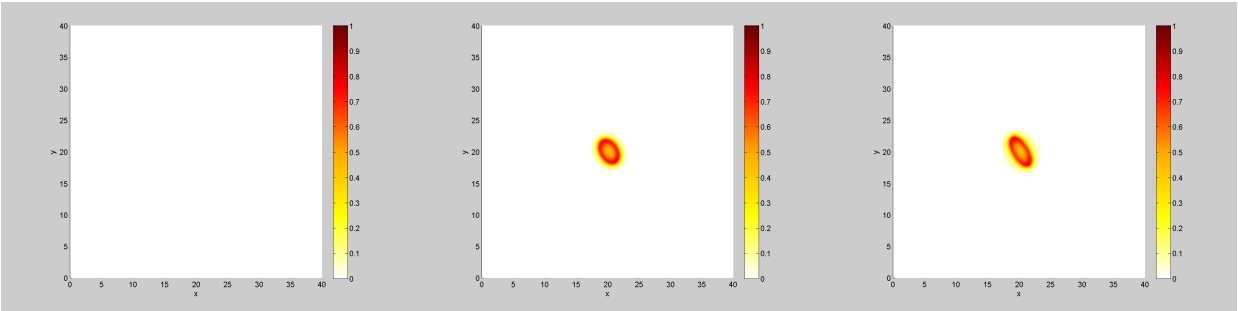

(a) $t = 0$ (b) $t = 40$ (c) $t = 80$

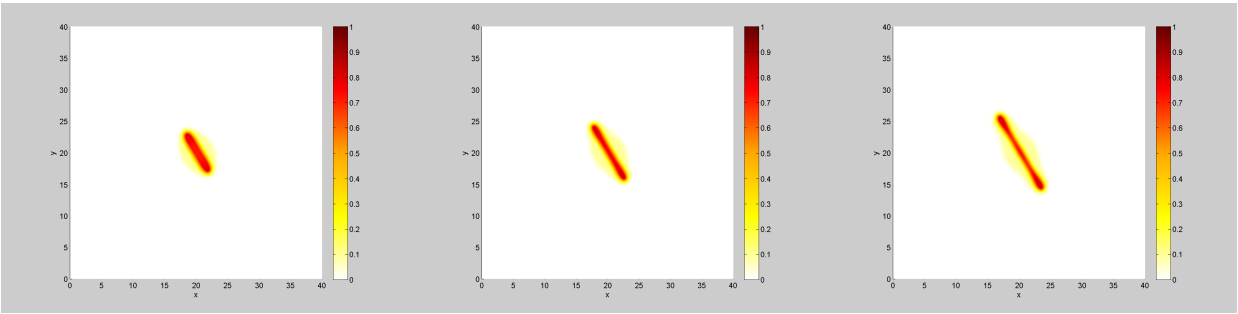

(d) $t = 120$ (e) $t = 160$ (f) $t = 200$

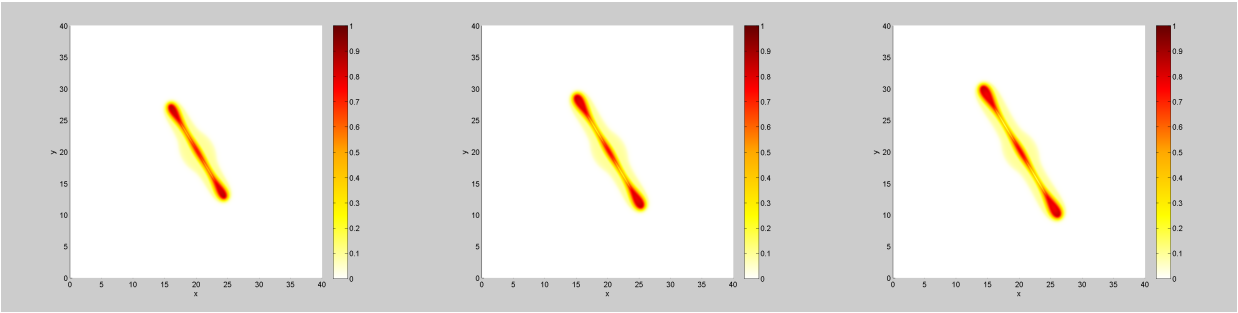

(g) $t = 240$ (h) $t = 280$ (i) $t = 320$

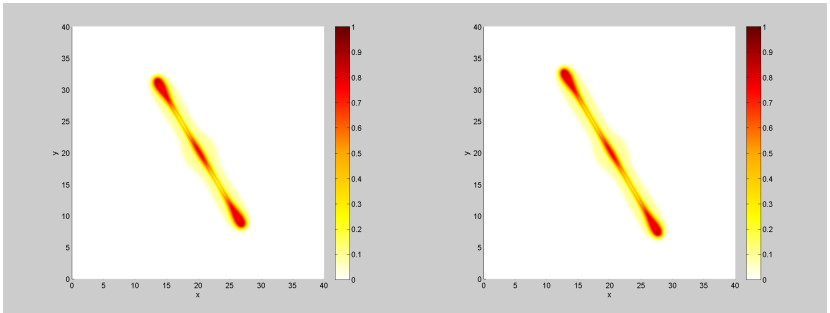

(j) $t = 360$ (k) $t = 400$

Figure A.3: dead cells ϕ_D, $r = 3$

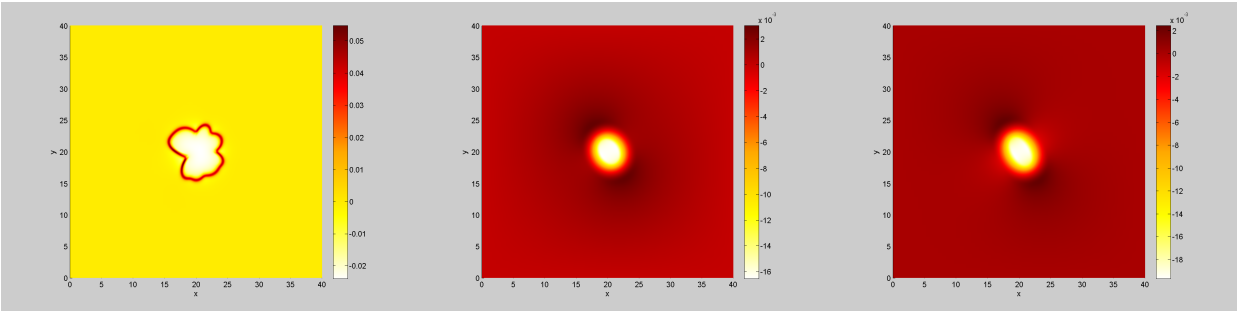

(a) $t = 0$ (b) $t = 40$ (c) $t = 80$

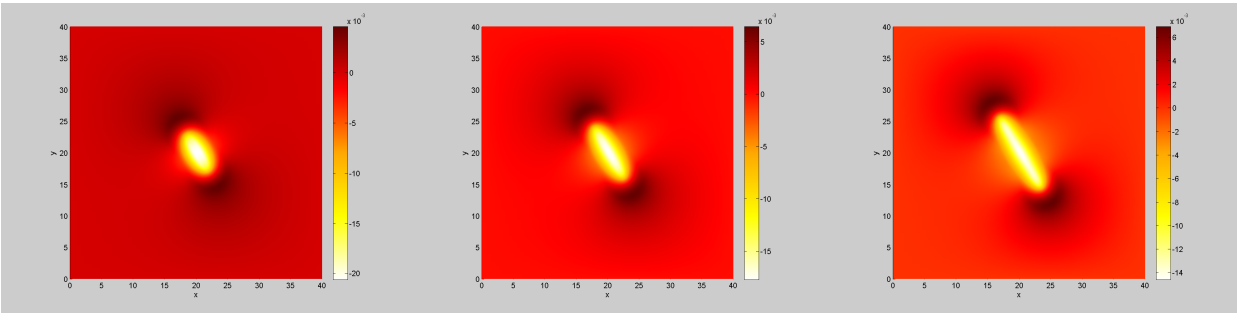

(d) $t = 120$ (e) $t = 160$ (f) $t = 200$

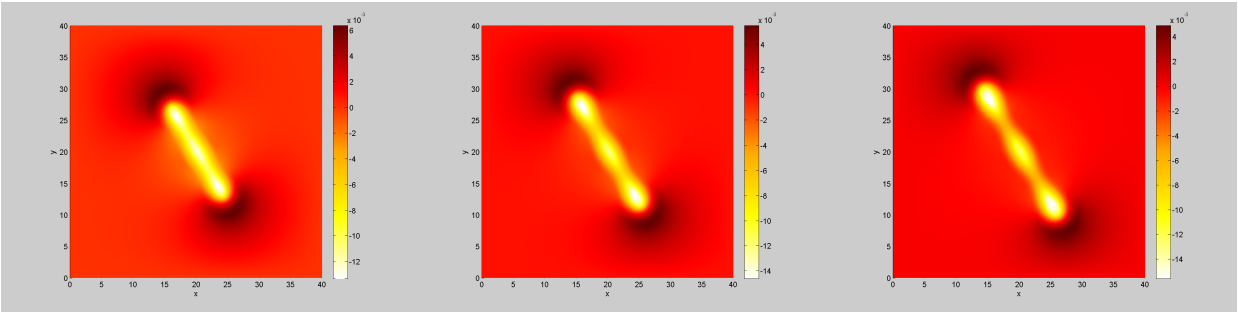

(g) $t = 240$ (h) $t = 280$ (i) $t = 320$

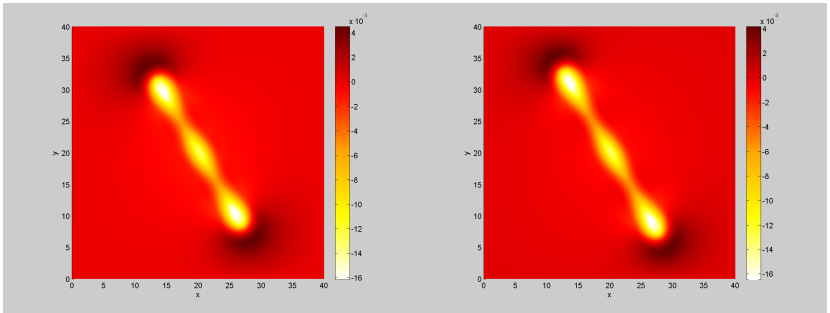

(j) $t = 360$ (k) $t = 400$

Figure A.4: pressure p, $r = 3$

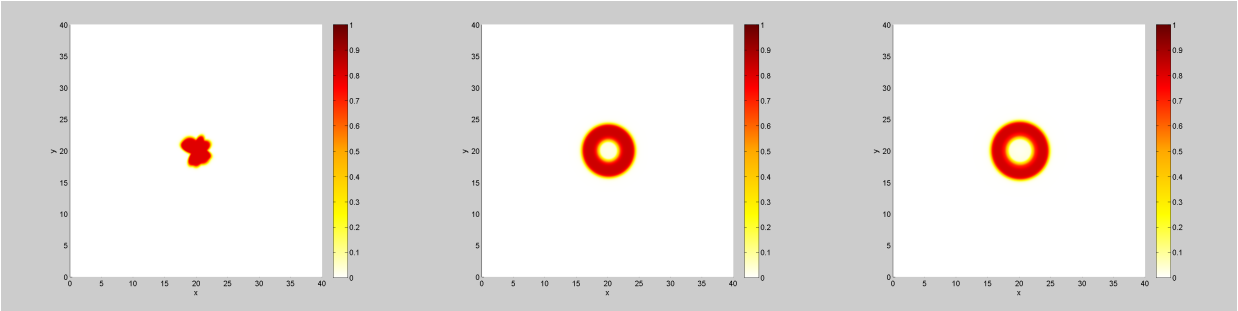

(a) $t = 0$ (b) $t = 40$ (c) $t = 80$

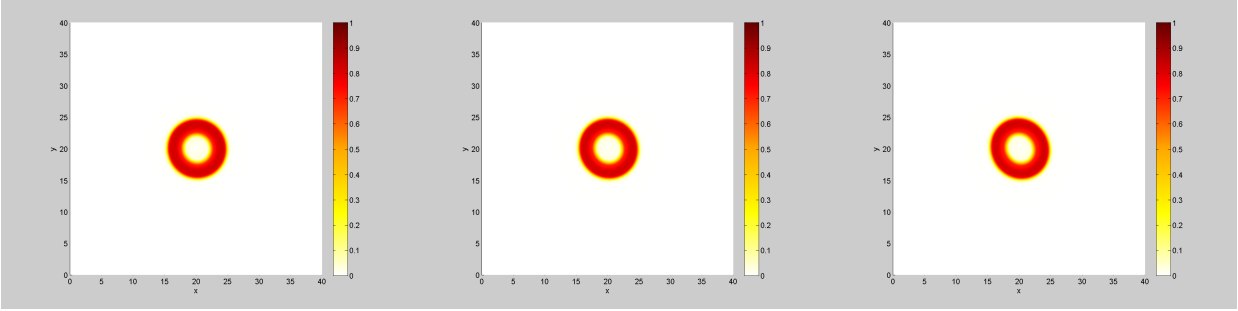

(d) $t = 120$ (e) $t = 160$ (f) $t = 200$

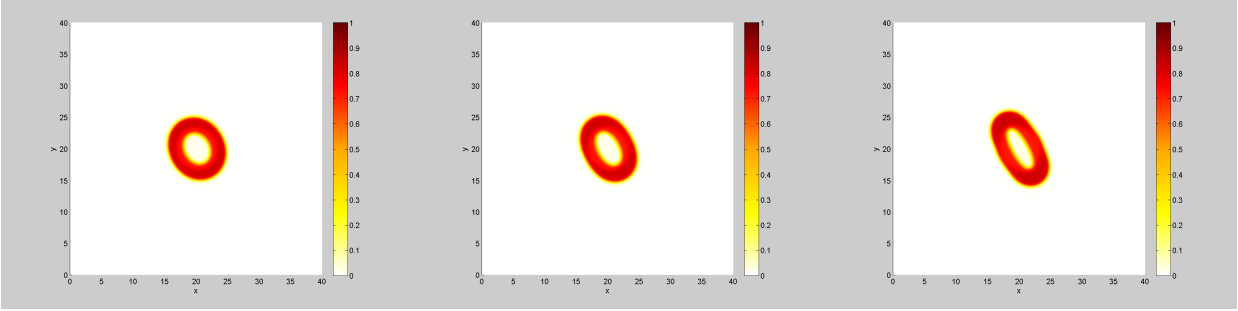

(g) $t = 240$ (h) $t = 280$ (i) $t = 320$

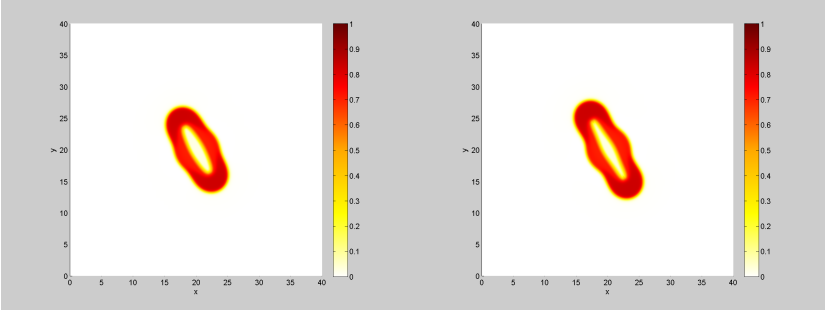

(j) $t = 360$ (k) $t = 400$

Figure A.5: viable cells ϕ_V, $r = \sqrt{3}$

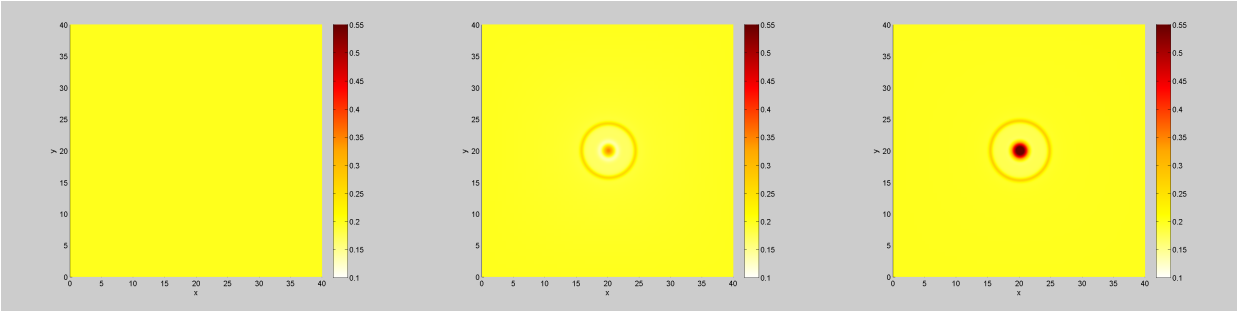

(a) $t = 0$ (b) $t = 40$ (c) $t = 80$

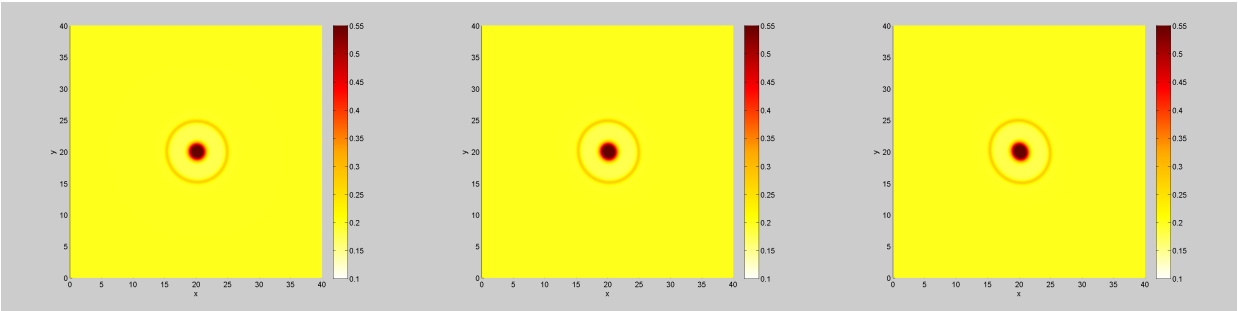

(d) $t = 120$ (e) $t = 160$ (f) $t = 200$

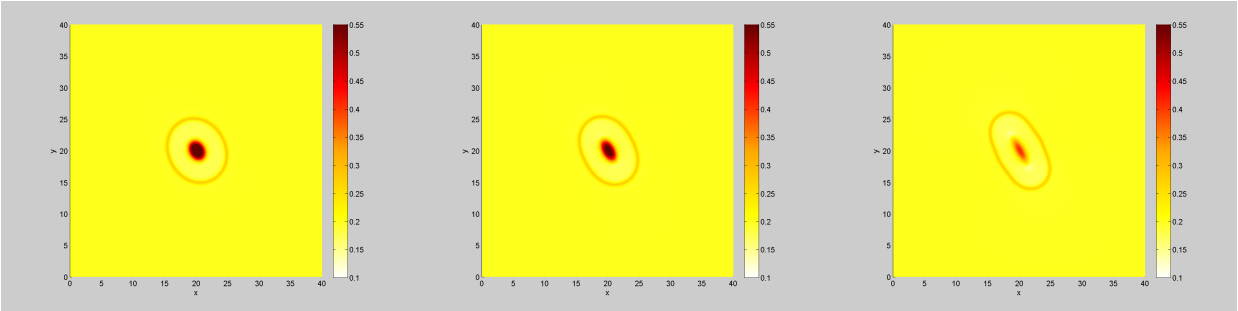

(g) $t = 240$ (h) $t = 280$ (i) $t = 320$

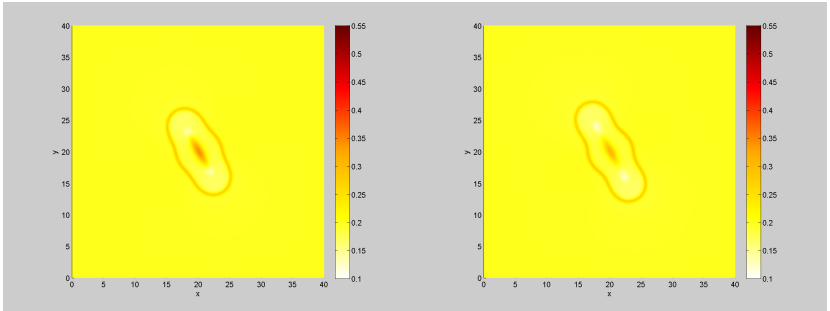

(j) $t = 360$ (k) $t = 400$

Figure A.6: water ϕ_W, $r = \sqrt{3}$

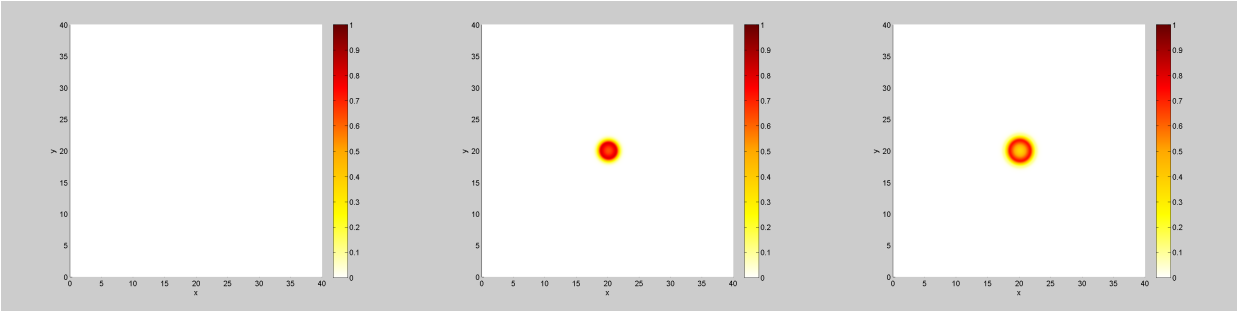

(a) $t = 0$ (b) $t = 40$ (c) $t = 80$

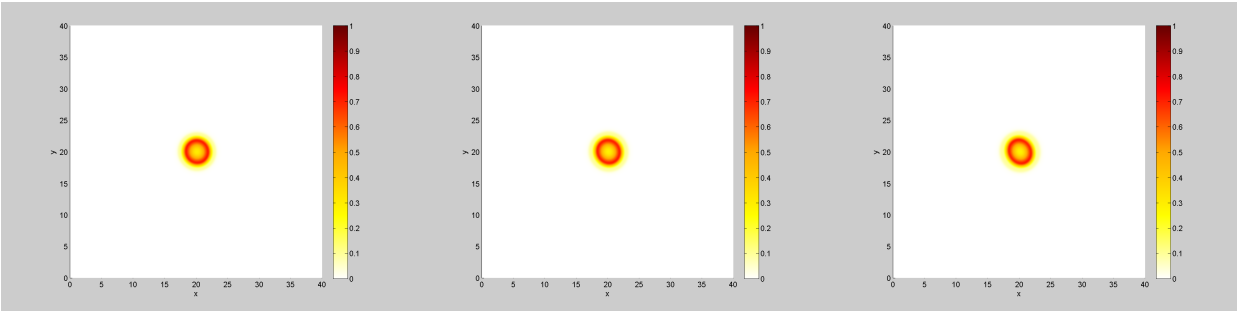

(d) $t = 120$ (e) $t = 160$ (f) $t = 200$

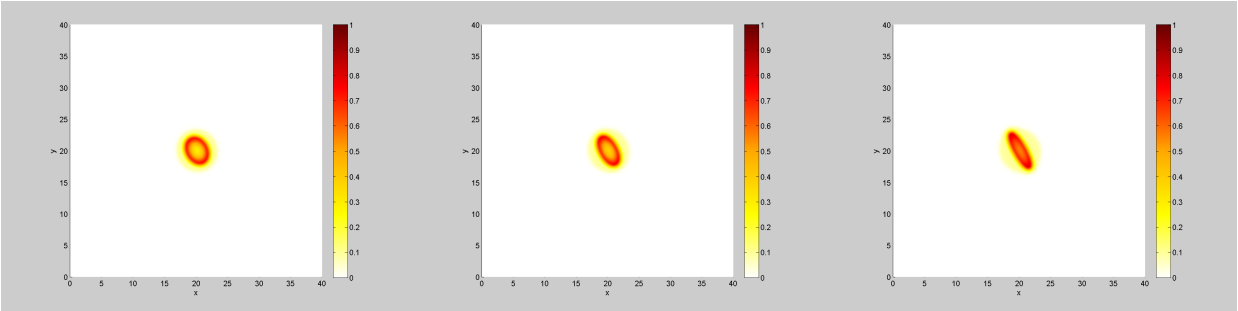

(g) $t = 240$ (h) $t = 280$ (i) $t = 320$

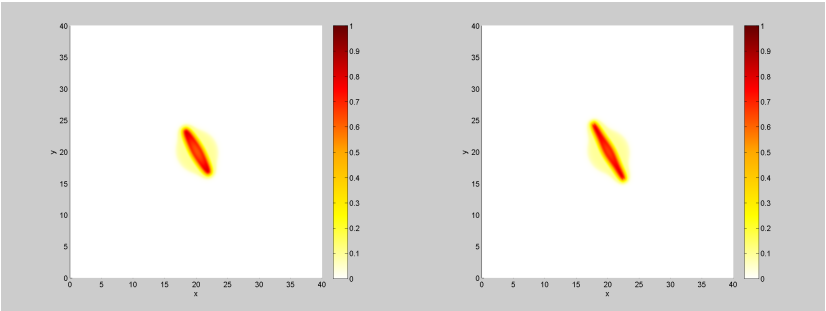

(j) $t = 360$ (k) $t = 400$

Figure A.7: dead cells ϕ_D, $r = \sqrt{3}$

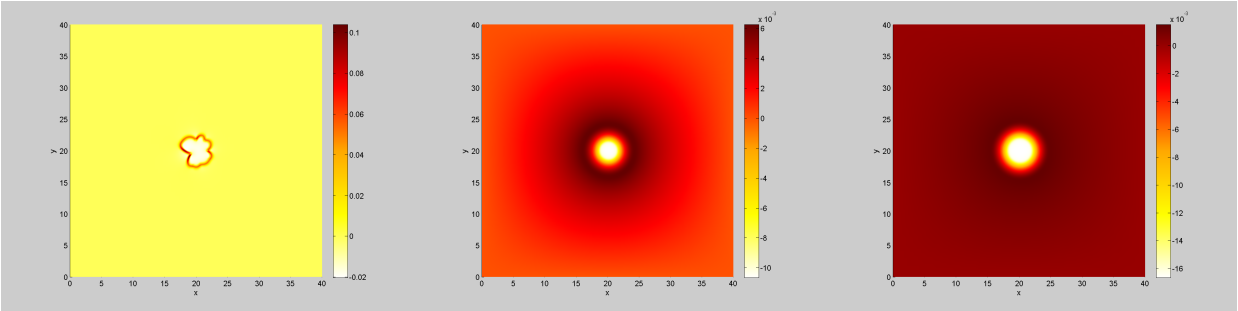

(a) $t = 0$ (b) $t = 40$ (c) $t = 80$

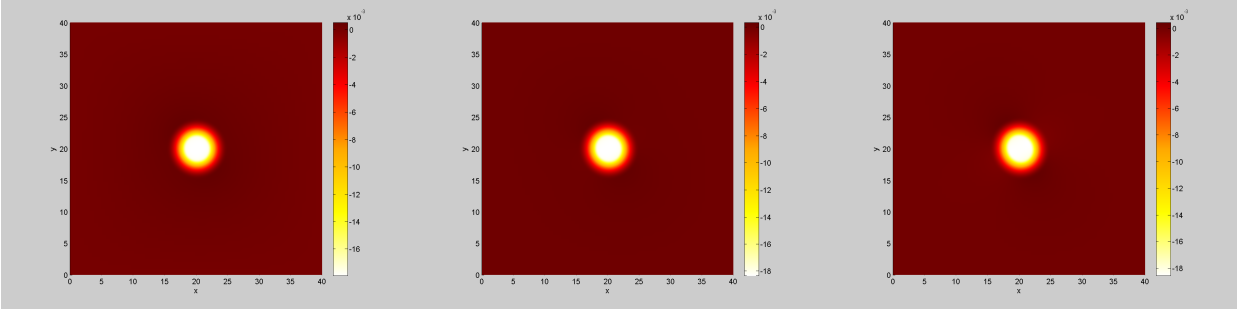

(d) $t = 120$ (e) $t = 160$ (f) $t = 200$

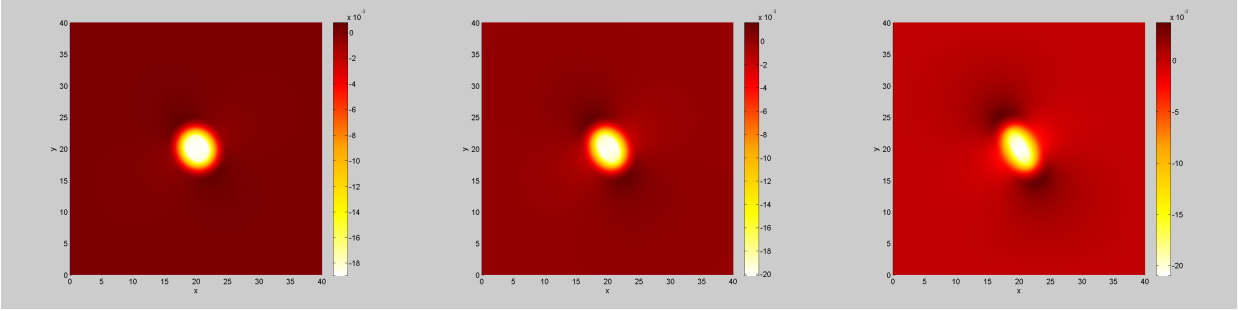

(g) $t = 240$ (h) $t = 280$ (i) $t = 320$

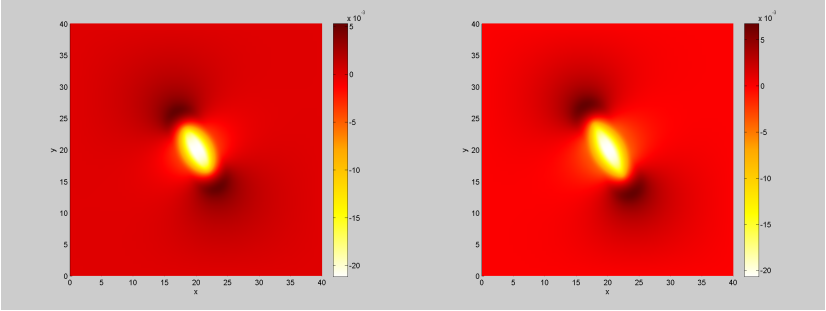

(j) $t = 360$ (k) $t = 400$

Figure A.8: pressure p, $r = \sqrt{3}$

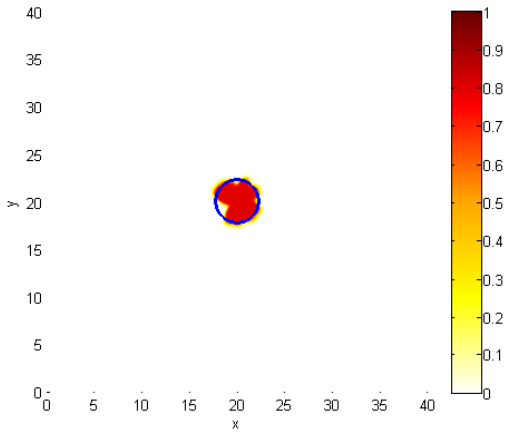

(a) $t = 0$, $r = 2.3368$

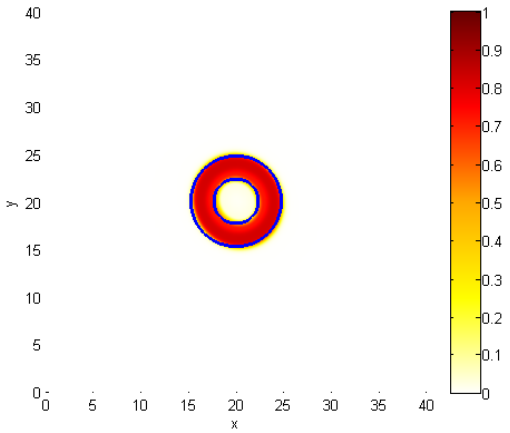

(b) $t = 200$, $r = 2.3368$

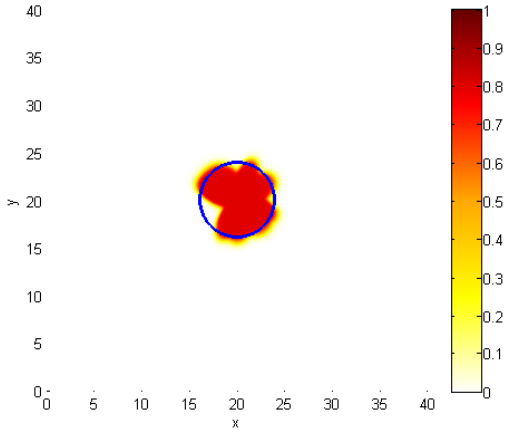

(c) $t = 0$, $r = 4.0472$

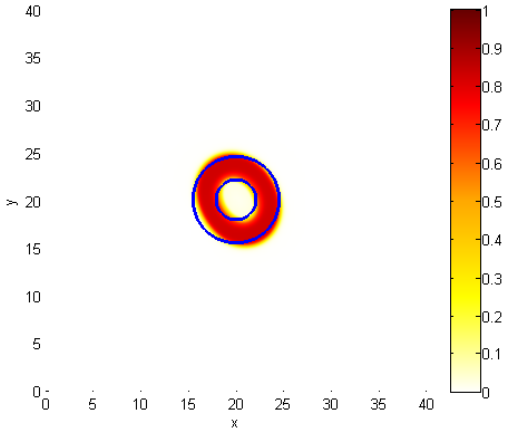

(d) $t = 40$, $r = 4.0472$

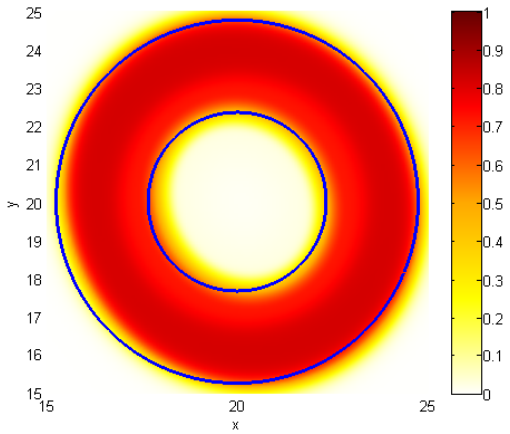

(e) $t = 200$, $r = 2.3368$ (closeup)

Figure A.9: In figures (a) and (b) Two non-symmetric initial conditions with different radii are shown against the contours ($\phi_V = 0.5$) for circular initial condition with the same volume. In figures (c) and (d) the evolution of the non-symmetric initial conditions are show against the contours of the evolved symmetric tumors with the same volumes.

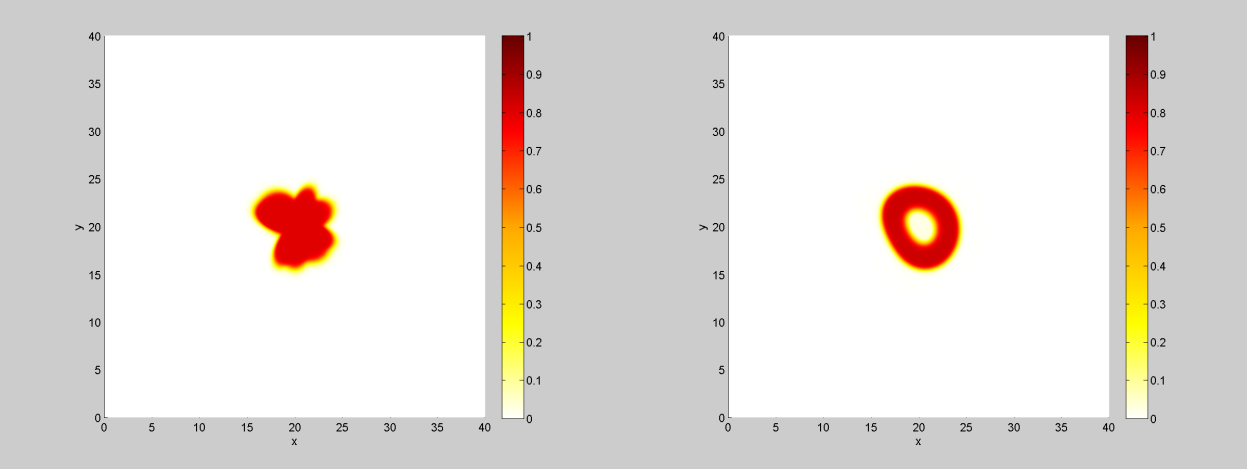

(a) $t = 0$ (b) $t = 10$

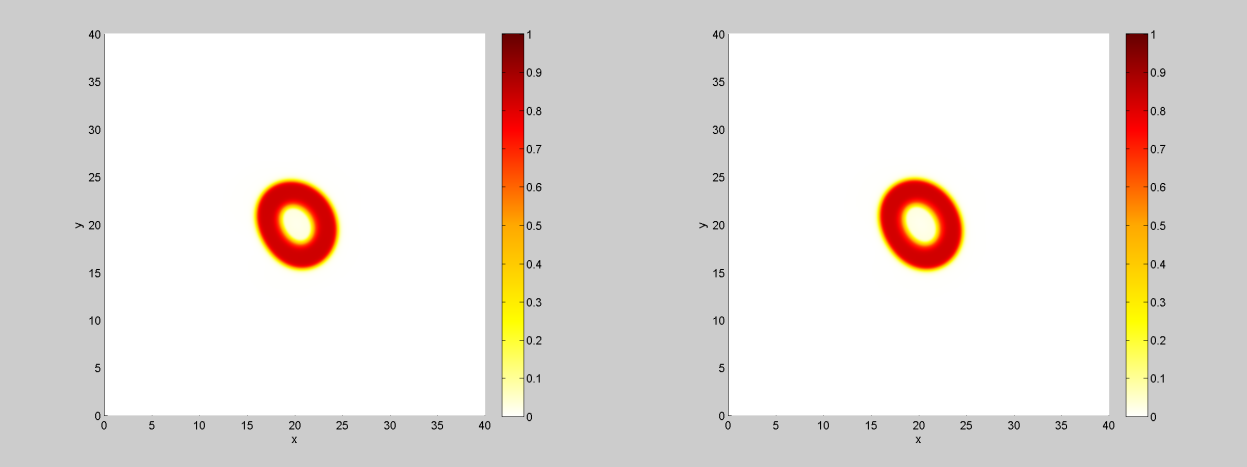

(c) $t = 20$ (d) $t = 30$

Figure A.10: The early time evolution for the non-symmetric initial condition with $r = 3$.

Appendix B

Symmetric Tumor Parameter Study Slides

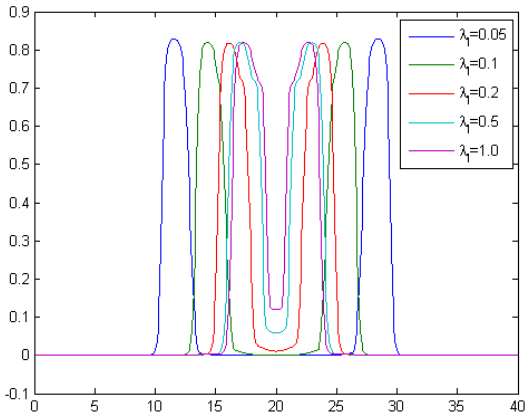

(a) viable cells ϕ_V

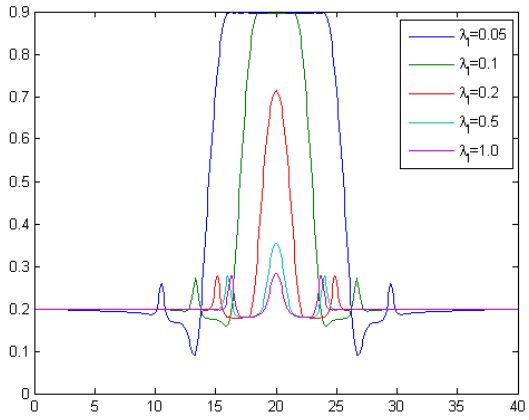

(b) water ϕ_W

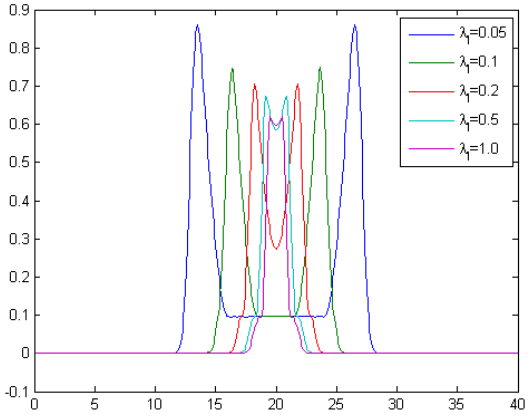

(c) dead cells ϕ_D

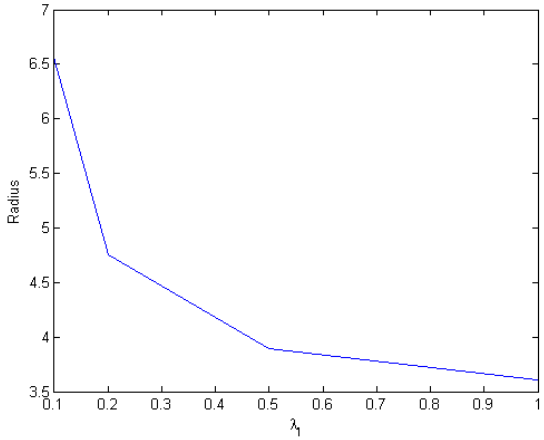

(d) size of the radius

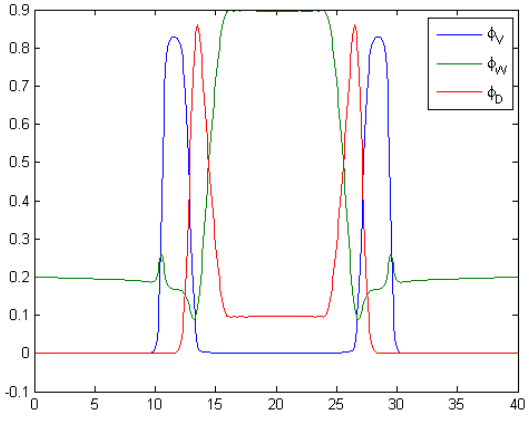

(e) Tumor for $\lambda_l = 0.05$

Figure B.1: cell types of λ_l variations at $t = 200$

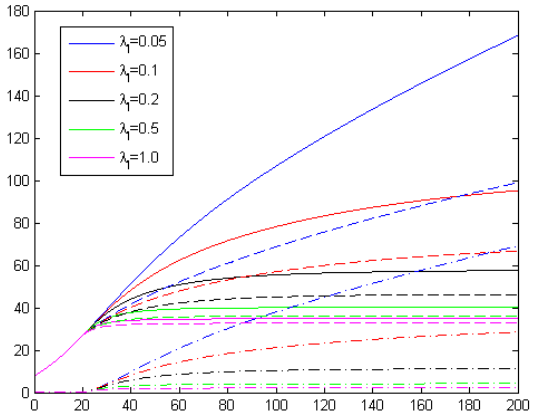

(a) ϕ_V (dashed line), ϕ_D (dash dot line), and ϕ_T (solid line)

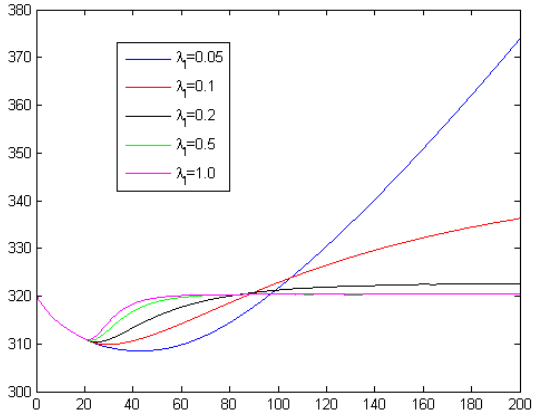

(b) water ϕ_W

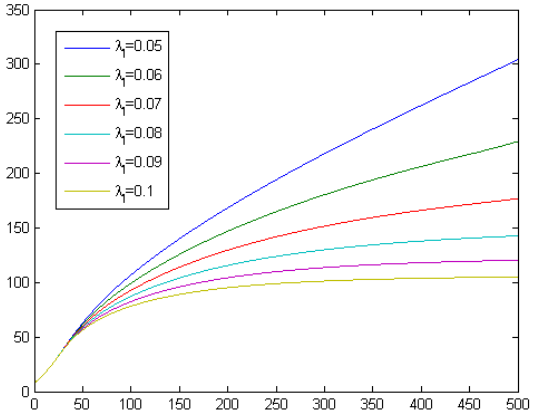

(c) total tumor volumes

Figure B.2: Total volume of λ_l variations

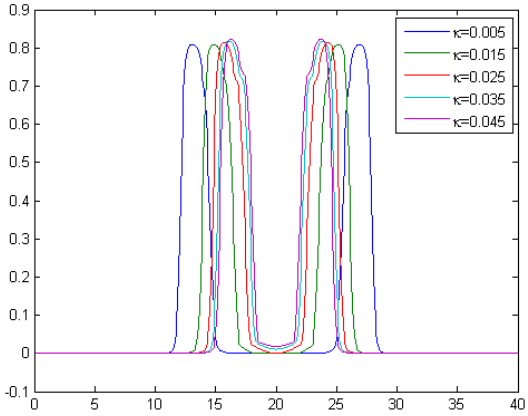

(a) viable cells ϕ_V

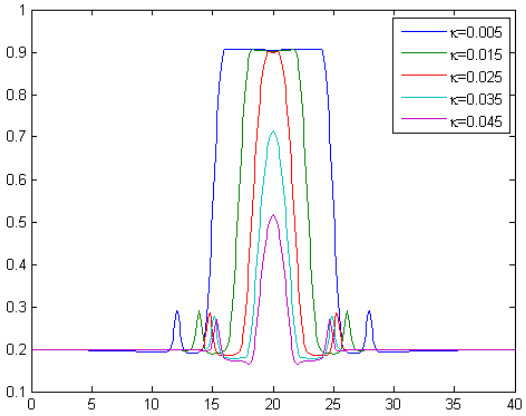

(b) water ϕ_W

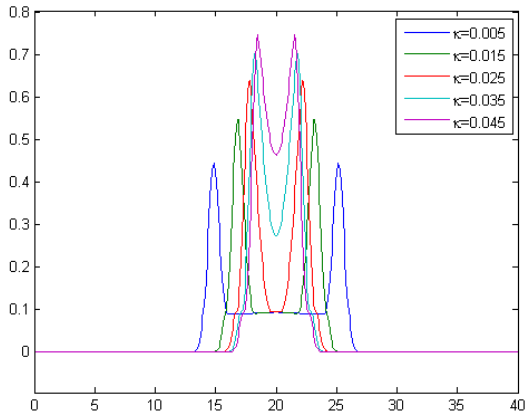

(c) dead cells ϕ_D

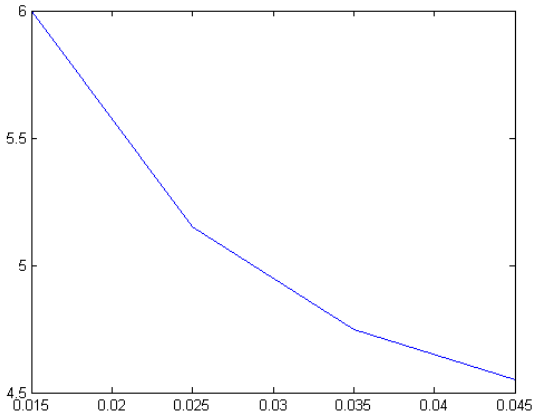

(d) size of the radius

Figure B.3: cell types of κ variations at $t = 200$

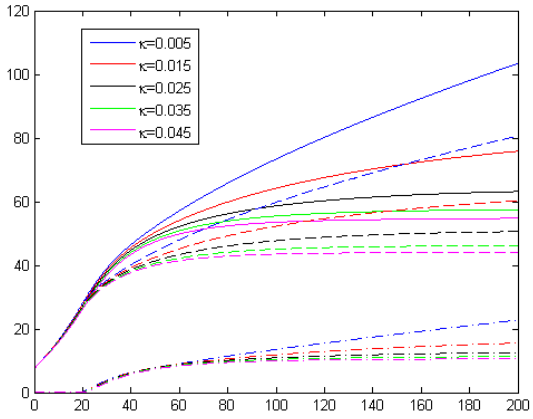

(a) ϕ_V (dashed line), ϕ_D (dash dot line), and ϕ_T (solid line)

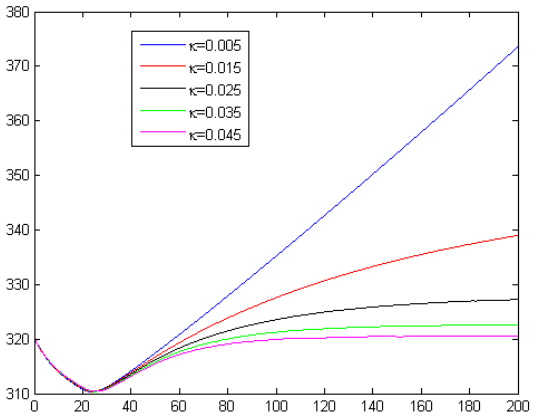

(b) water ϕ_W

Figure B.4: Total volume of κ variations

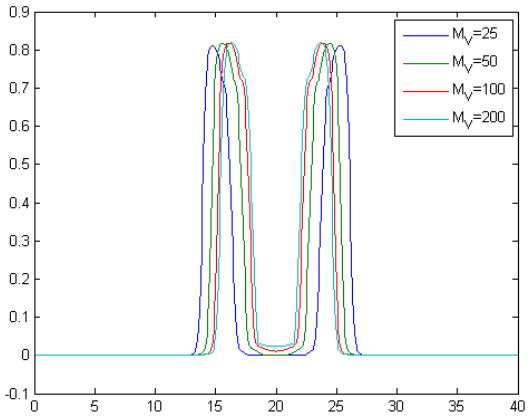

(a) viable cells ϕ_V

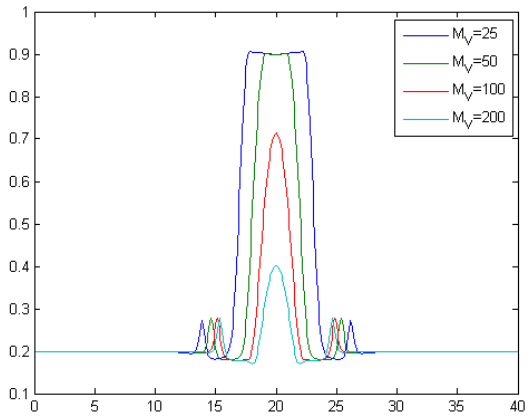

(b) water ϕ_W

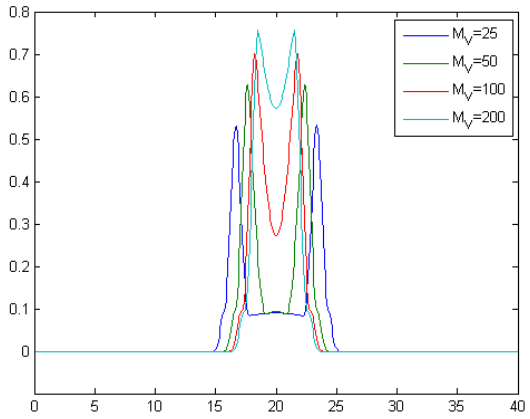

(c) dead cells ϕ_D

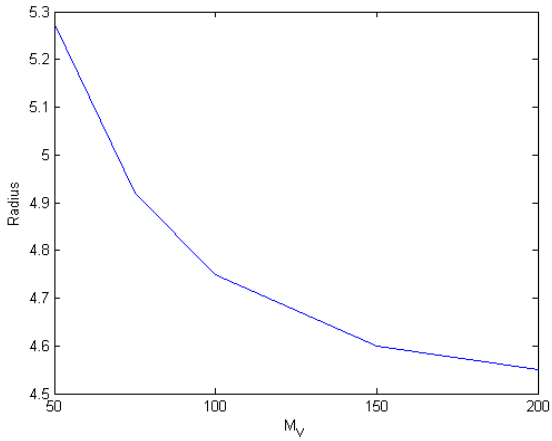

(d) size of the radius

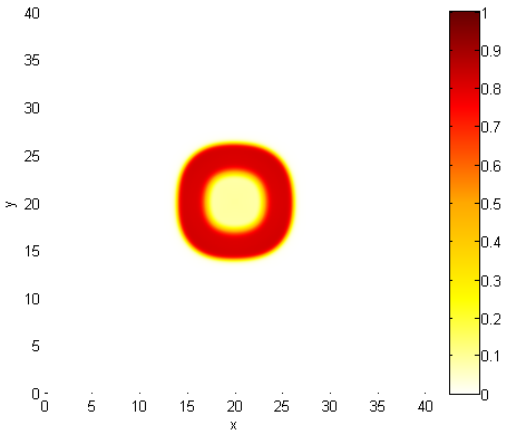

(e) morphology of the tumor for $M_V = 25$

Figure B.5: cell types of M_V variations at $t = 200$

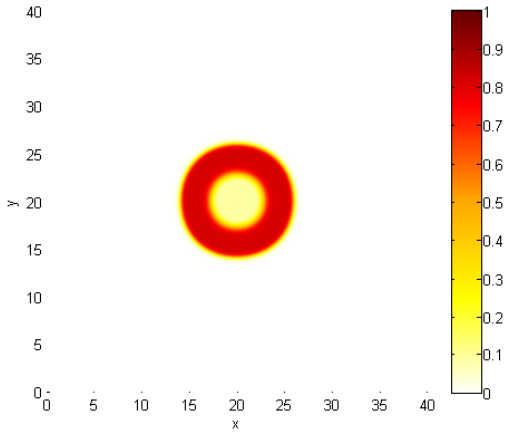

(a) $t = 150$

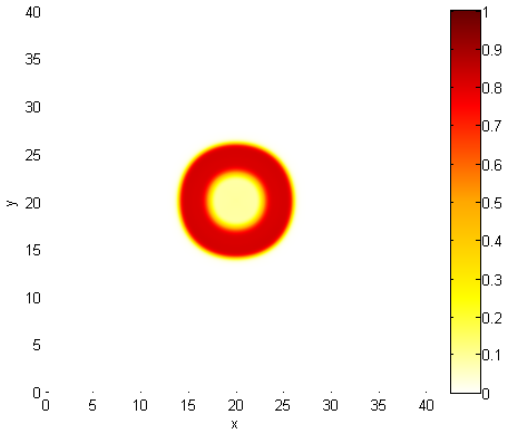

(b) $t = 160$

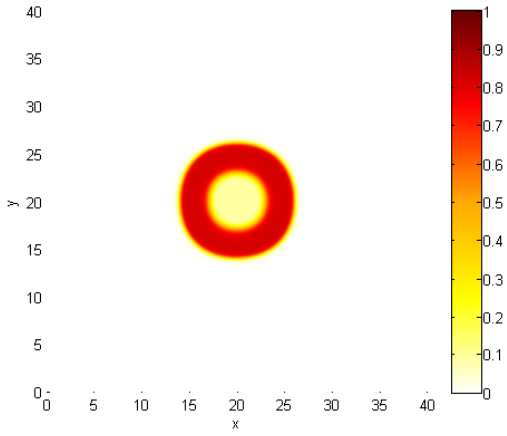

(c) $t = 170$

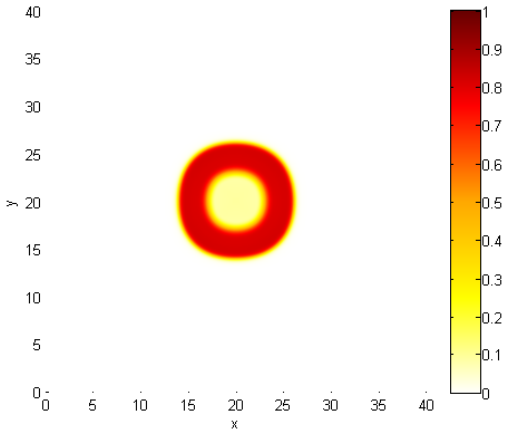

(d) $t = 180$

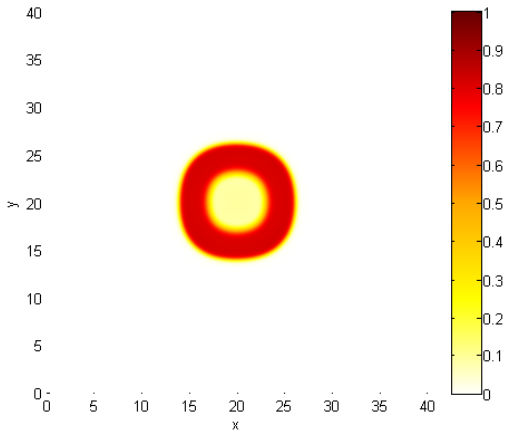

(e) $t = 190$

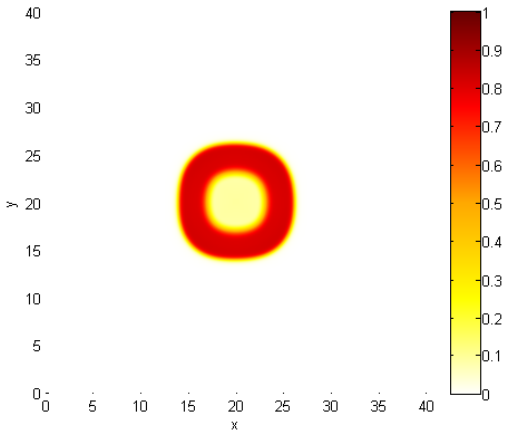

(f) $t = 200$

Figure B.6: tumor evolution for $M_V = 25$

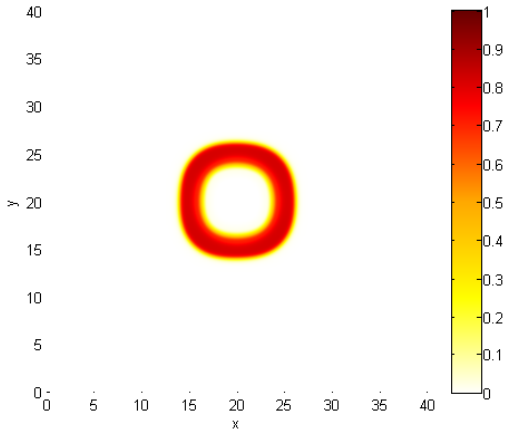

(a) $t = 200$

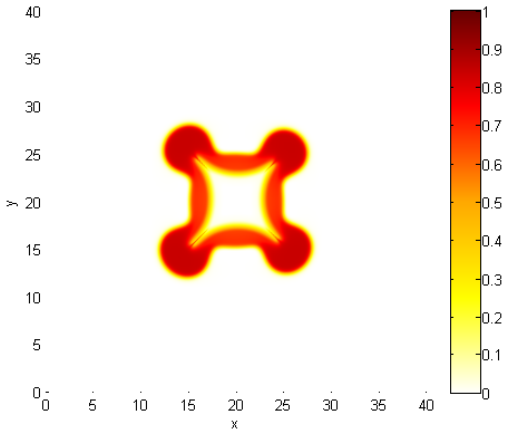

(b) $t = 300$

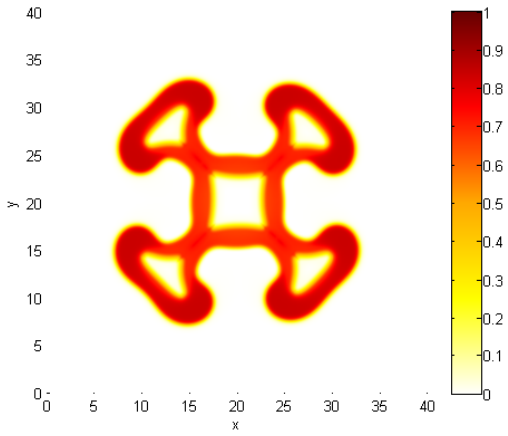

(c) $t = 400$

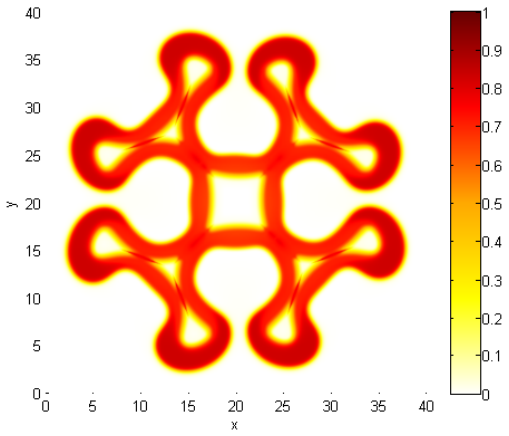

(d) $t = 500$

Figure B.7: viable cell evolution for $M_V = 25$

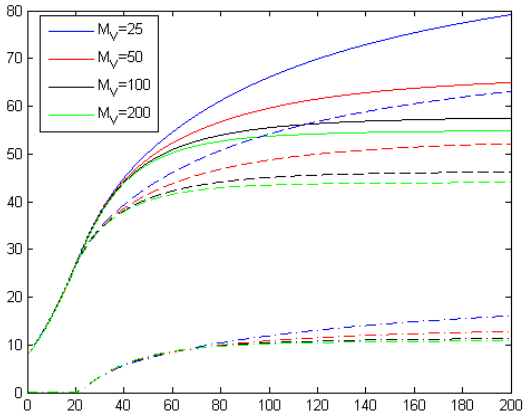

(a) ϕ_V (dashed line), ϕ_D (dash dot line), and ϕ_T (solid line)

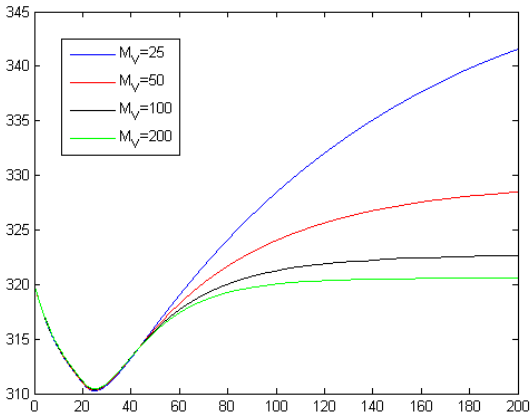

(b) water ϕ_W

Figure B.8: Total volume of M_V variations

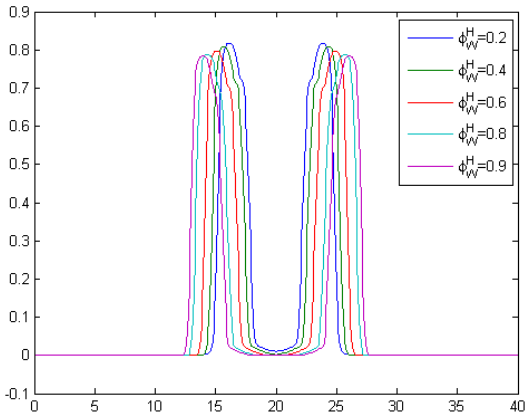

(a) viable cells ϕ_V

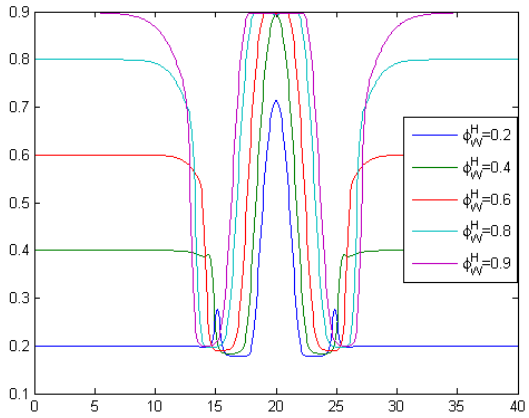

(b) water ϕ_W

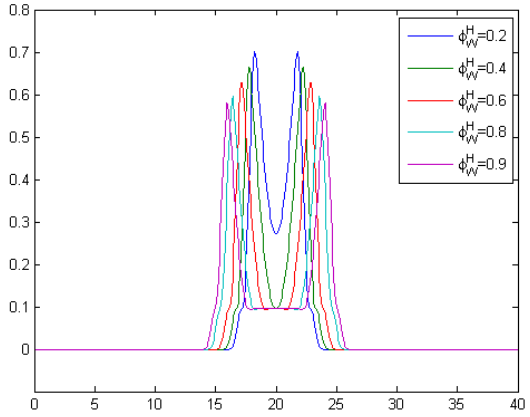

(c) dead cells ϕ_D

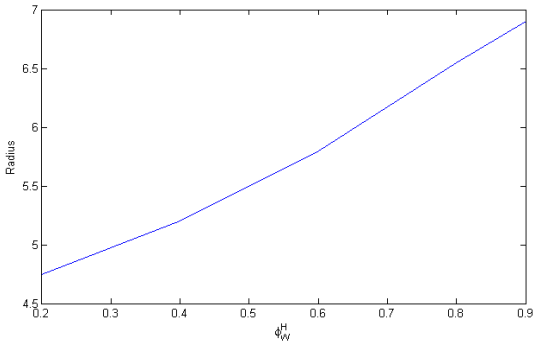

(d) size of the radius

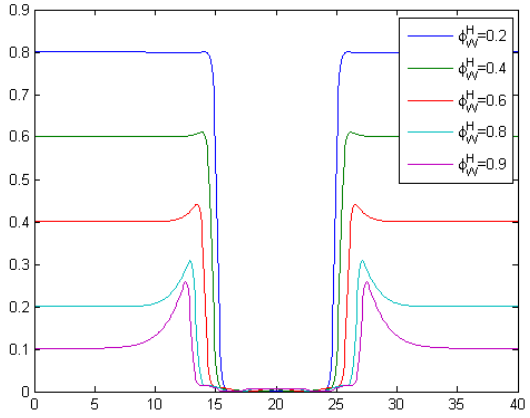

(e) host ϕ_H

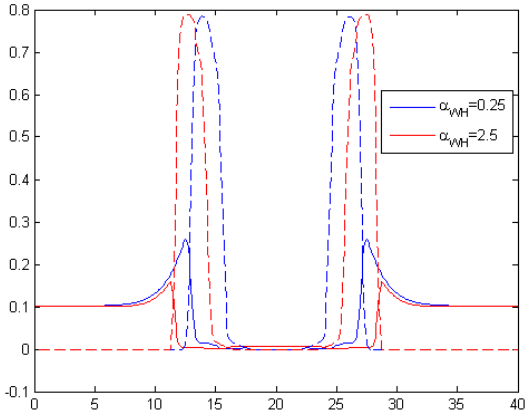

(f) ϕ_H (solid line), ϕ_V (dash line)

Figure B.9: cell types of ϕ_W^H variations at $t = 200$

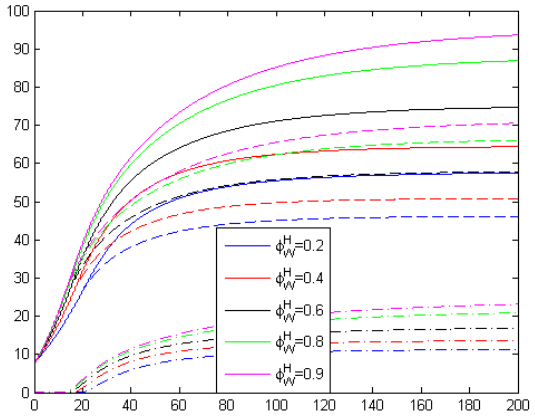

(a) ϕ_V (dashed line), ϕ_D (dash dot line), and ϕ_T (solid line)

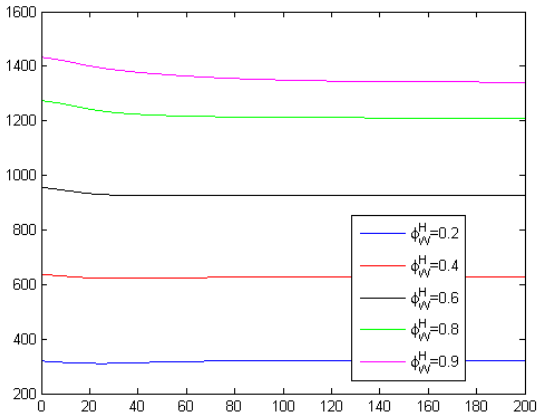

(b) water ϕ_W

Figure B.10: Total volume of ϕ_W^H variations

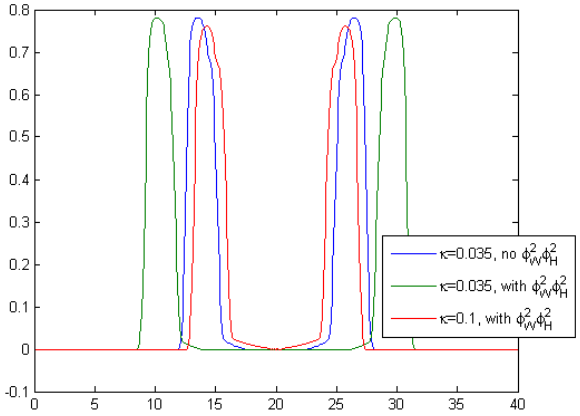

(a) viable cells ϕ_V

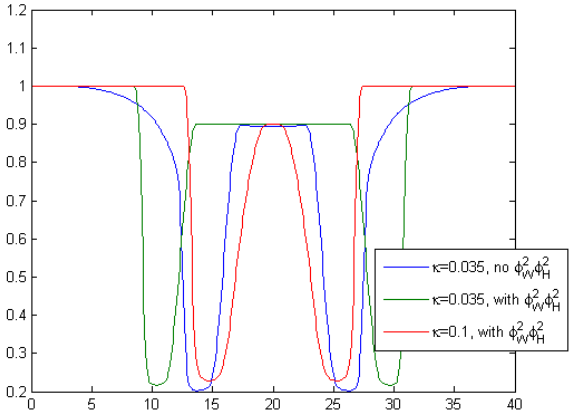

(b) water ϕ_W

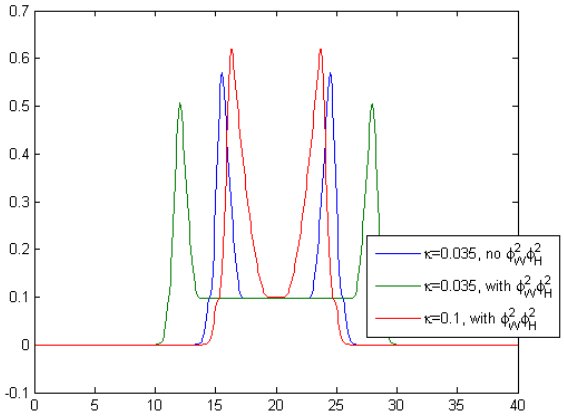

(c) dead cells ϕ_D

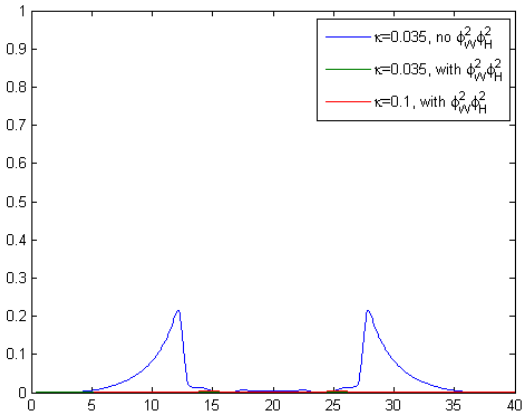

(d) host ϕ_H

Figure B.11: cell types of $\bar{\phi}_W^H = 1.0$ variations at $t = 200$

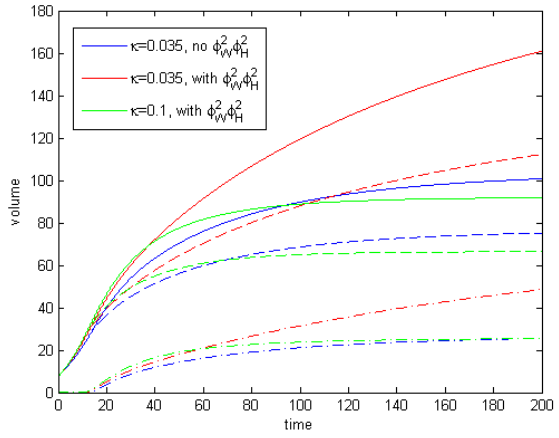

(a) ϕ_V (dashed line), ϕ_D (dash dot line), and ϕ_T (solid line)

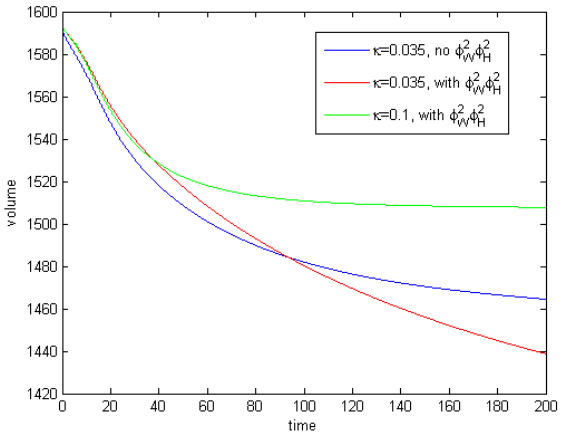

(b) water ϕ_W

Figure B.12: Total volume of $\bar{\phi}_W^H = 1.0$ variations

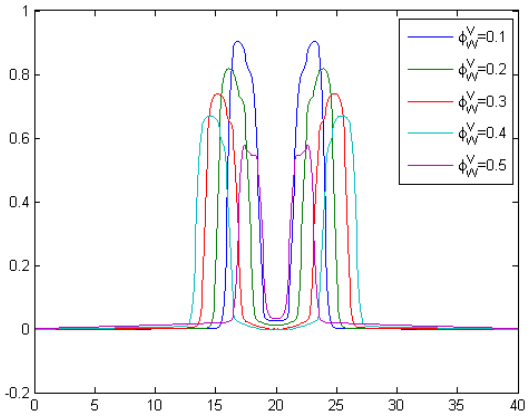

(a) viable cells ϕ_V

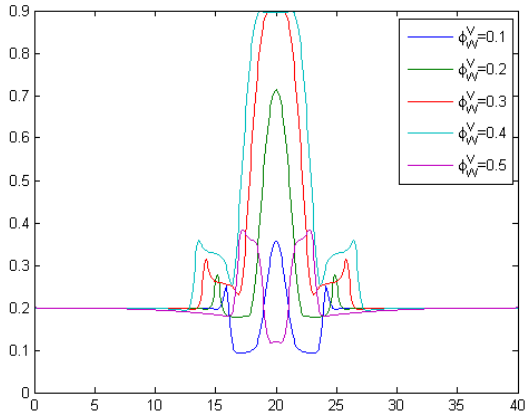

(b) water ϕ_W

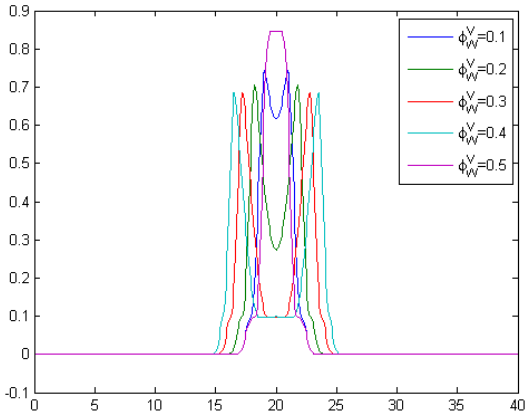

(c) dead cells ϕ_D

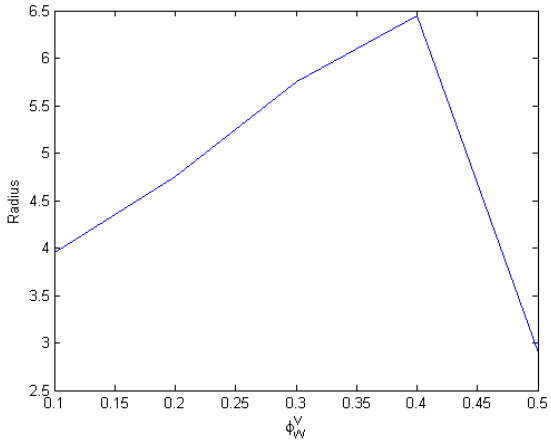

(d) size of the radius

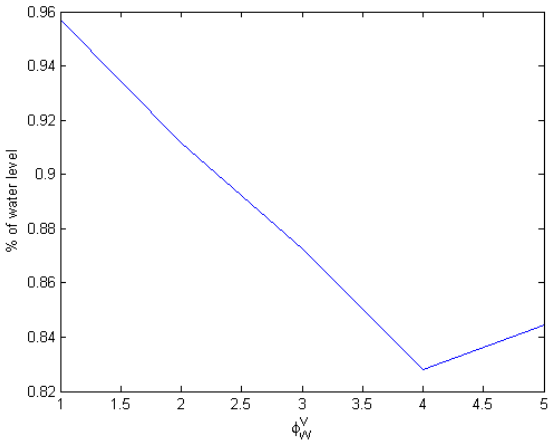

(e) percentage of the prescribed water level to the attained water level

Figure B.13: cell types of ϕ_W^V variations at $t = 200$

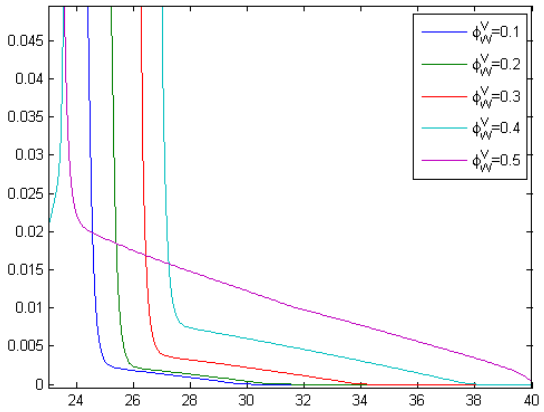

(a) ϕ_V close up

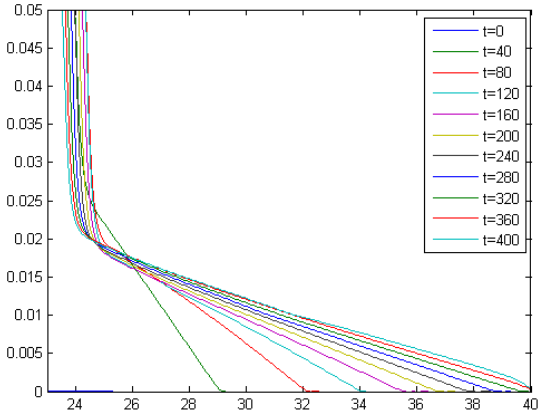

(b) evolution of ϕ_V for $\bar{\phi}_W^V = 5.0$ close up

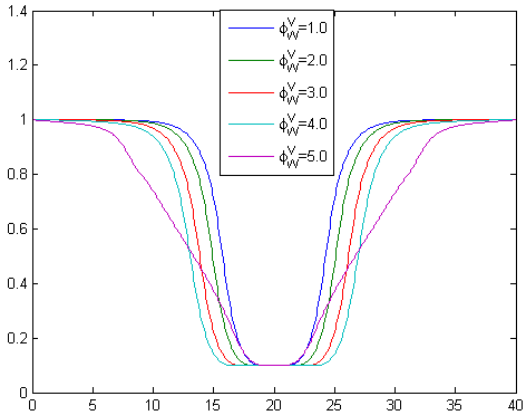

(c) nutrient n

Figure B.14: ϕ_W^V variations

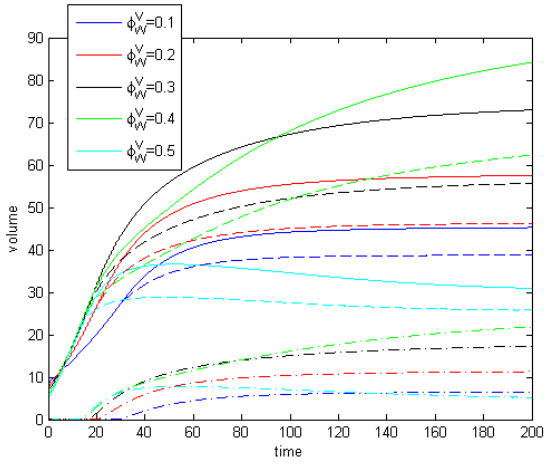

(a) ϕ_V (dashed line), ϕ_D (dash dot line), and ϕ_T (solid line)

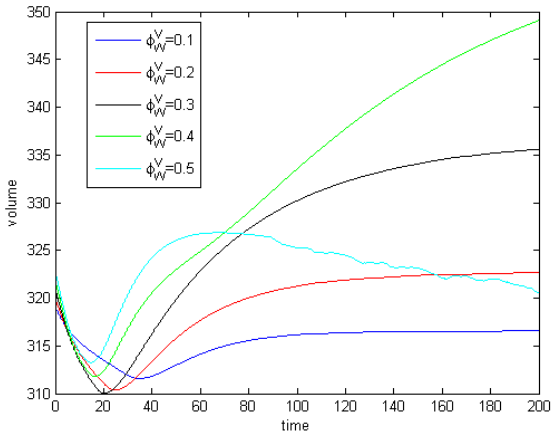

(b) water ϕ_W

Figure B.15: Total volume of ϕ_W^V variations

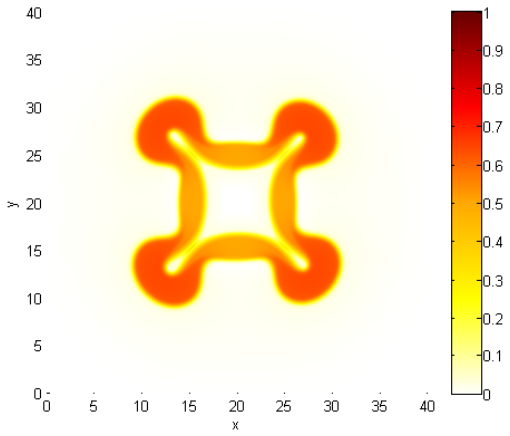

(a) $M_V = 100$

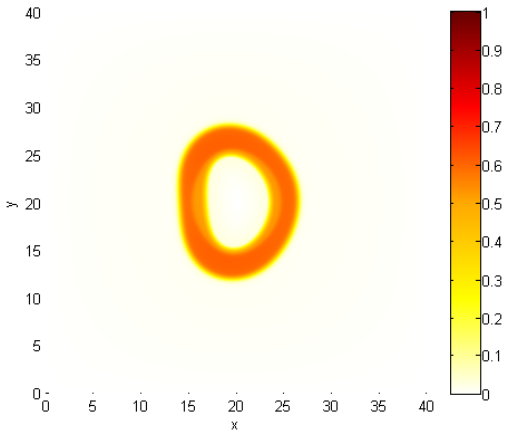

(b) $M_V = 200$

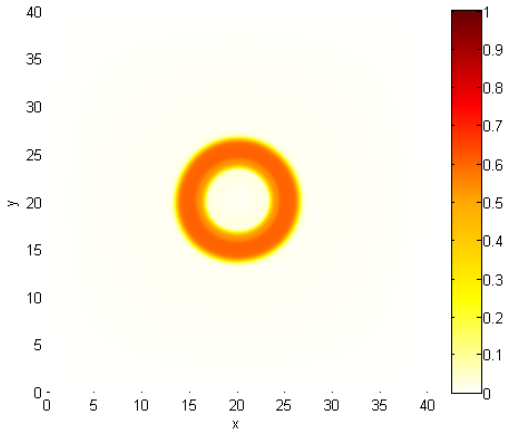

(c) $M_V = 300$

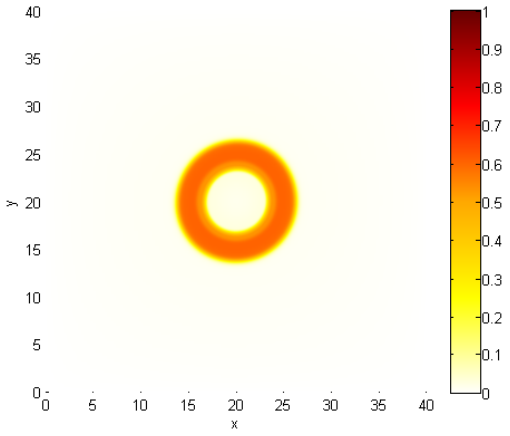

(d) $M_V = 400$

Figure B.16: viable cells for $\phi_W^V = 5.0$ with $\tilde{Q}(\phi_T)$ at $t = 200$

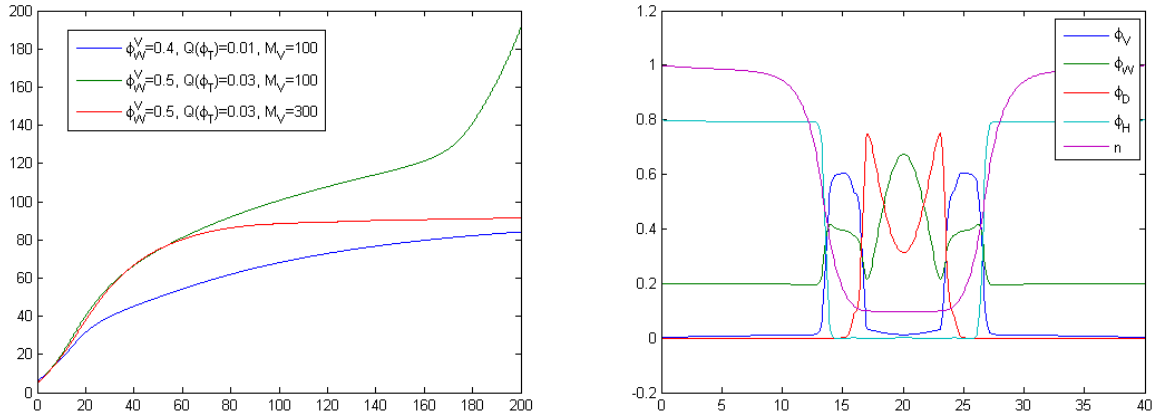

(a) Total tumor volume for $\bar{\phi}_W^V = 0.4$, $\bar{\phi}_W^V = 0.5$ with $\tilde{Q}(\phi_T)$ and different M_V

(b) One dimensional cross section of $\bar{\phi}_W^V = 0.5$ with $\tilde{Q}(\phi_T)$ and $M_V = 300$

Figure B.17: Tumor volume and morphology for new nutrient production

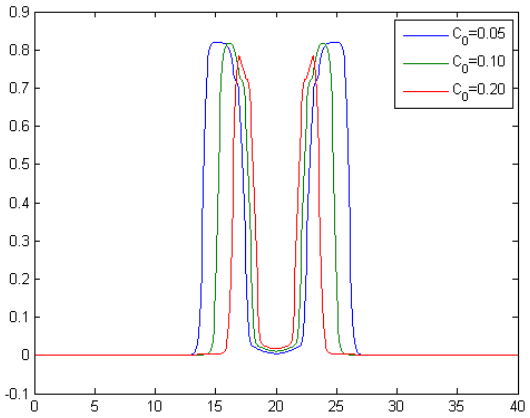

(a) viable cells ϕ_V

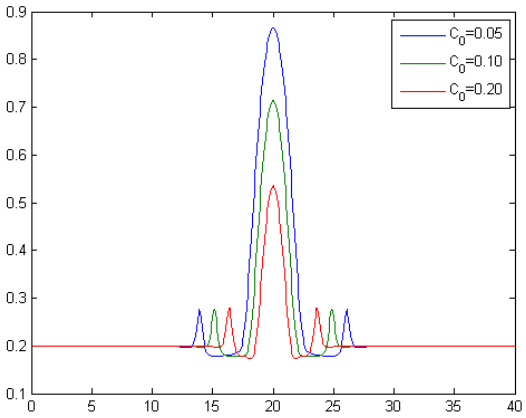

(b) water ϕ_W

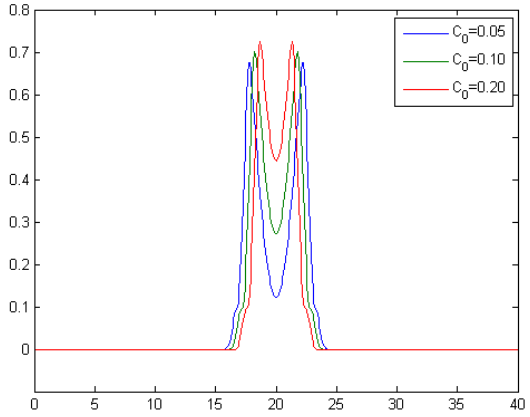

(c) dead cells ϕ_D

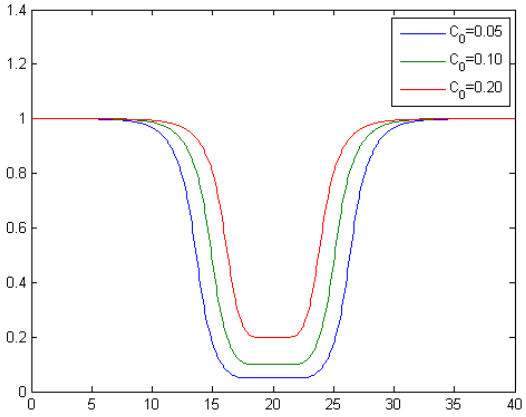

(d) nutrient levels

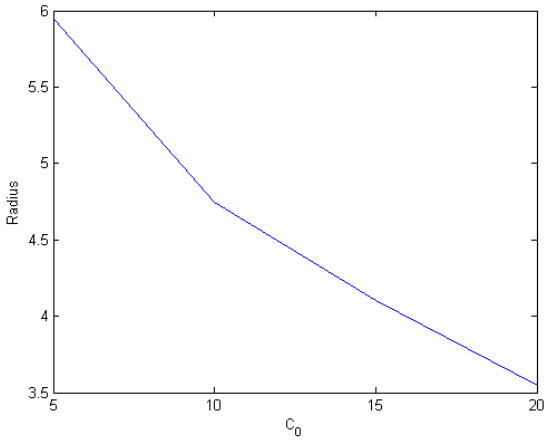

(e) size of the radius

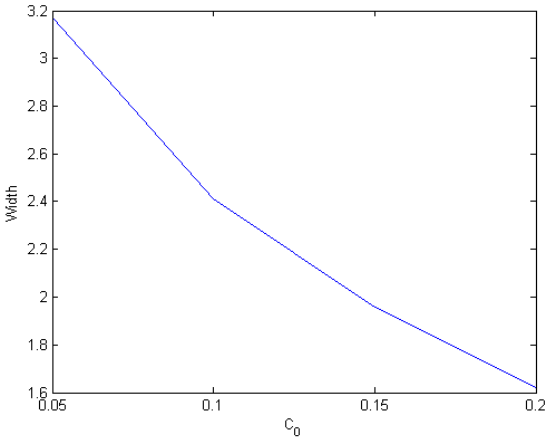

(f) width of the viable cell region

Figure B.18: cell types of $\bar{C}_0$ variations at $t = 200$

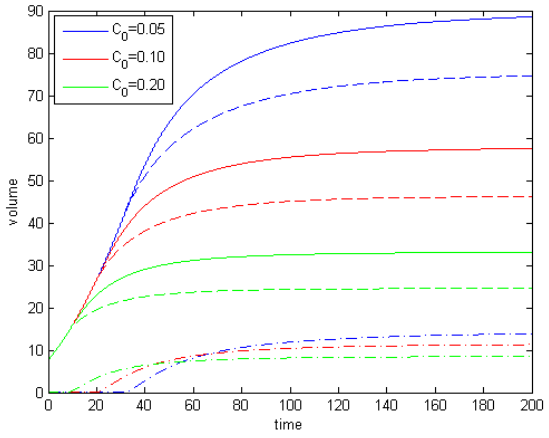

(a) ϕ_V (dashed line), ϕ_D (dash dot line), and ϕ_T (solid line)

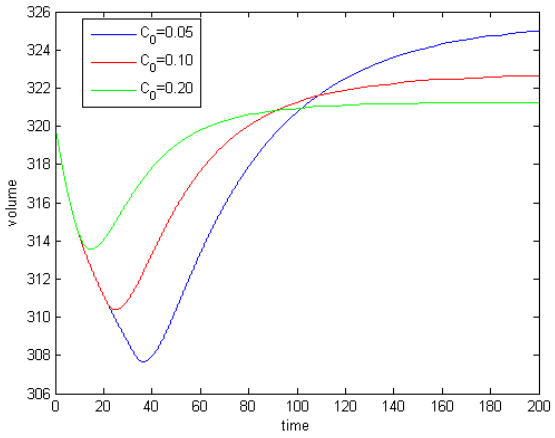

(b) water ϕ_W

Figure B.19: Total volume of $\bar{C}_0$ variations

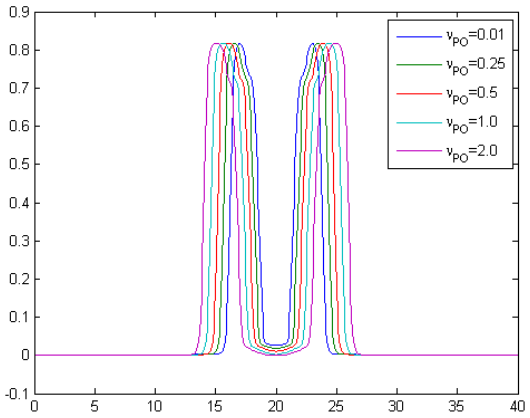

(a) viable cells ϕ_V

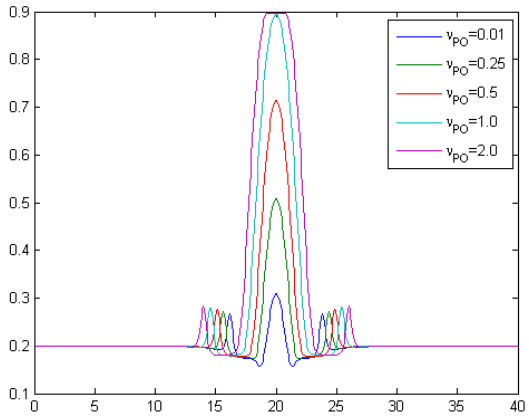

(b) water ϕ_W

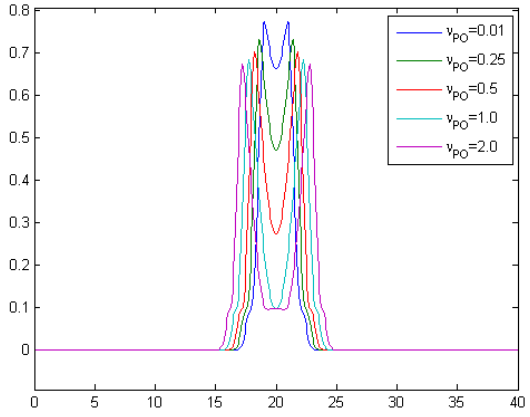

(c) dead cells ϕ_D

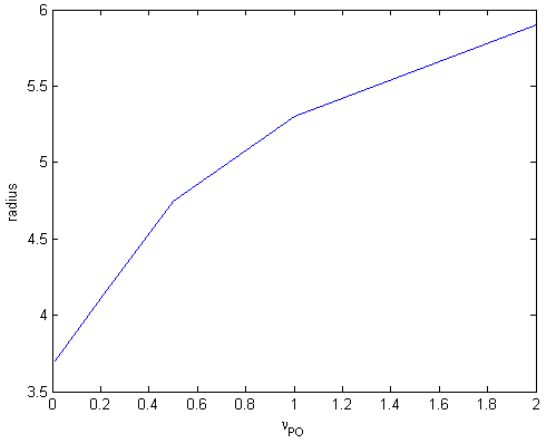

(d) size of the radius

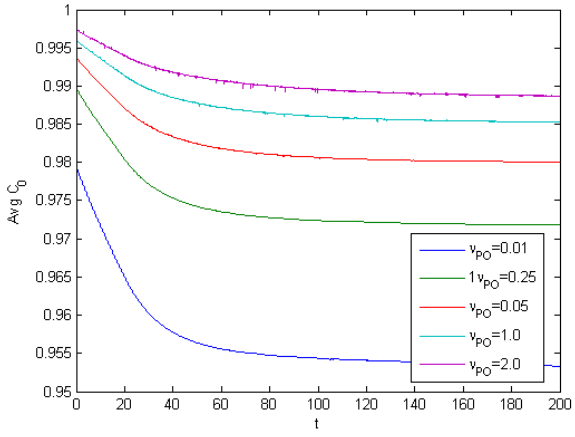

(e) average nutrient concentration

Figure B.20: cell types of ν_{PO} variations at $t = 200$

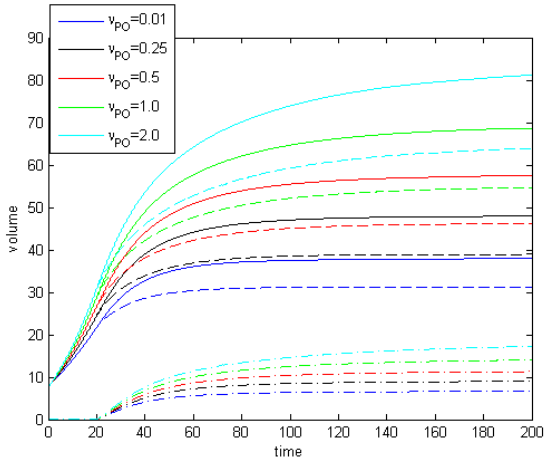

(a) ϕ_V (dashed line), ϕ_D (dash dot line), and ϕ_T (solid line)

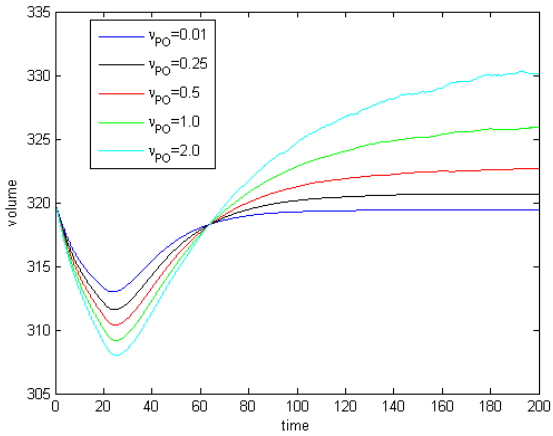

(b) water ϕ_W

Figure B.21: Total volume of ν_{PO} variations

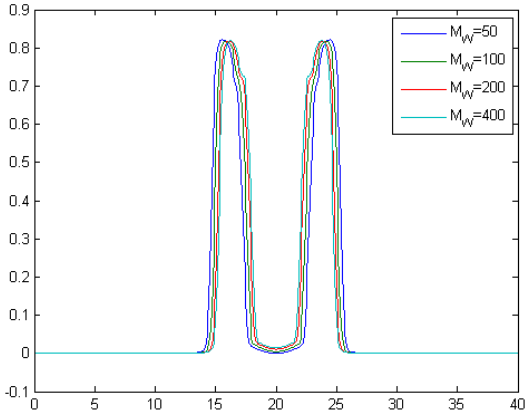

(a) viable cells ϕ_V

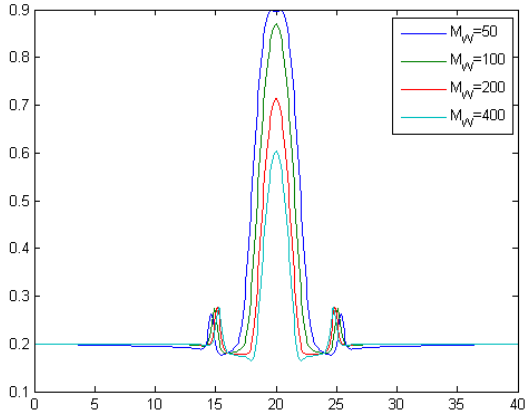

(b) water ϕ_W

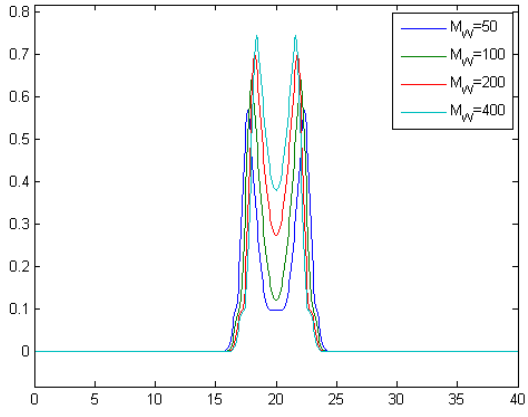

(c) dead cells ϕ_D

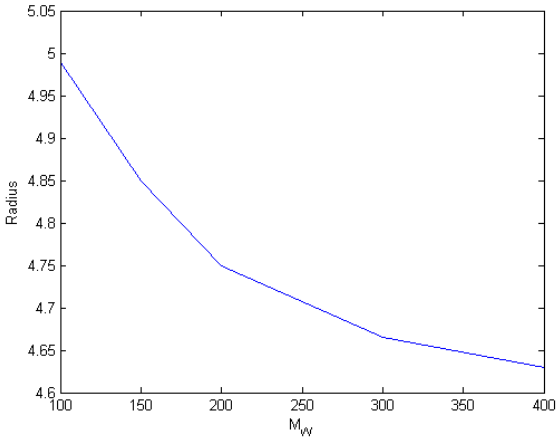

(d) size of the radius

Figure B.22: cell types of M_W variations at $t = 200$

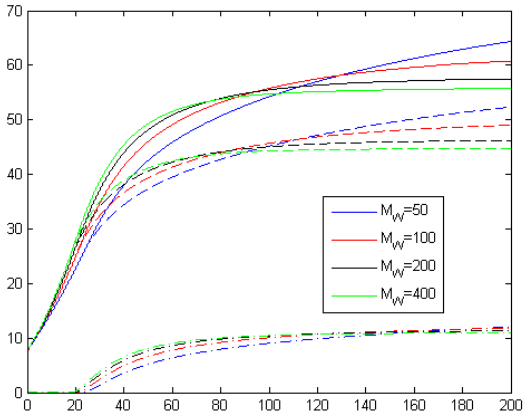

(a) ϕ_V (dashed line), ϕ_D (dash dot line), and ϕ_T (solid line)

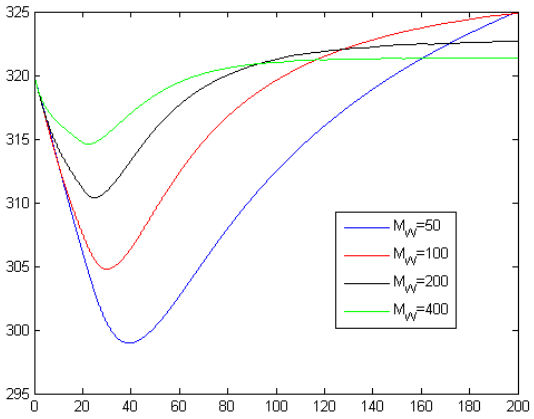

(b) water ϕ_W

Figure B.23: Total volume of M_W variations

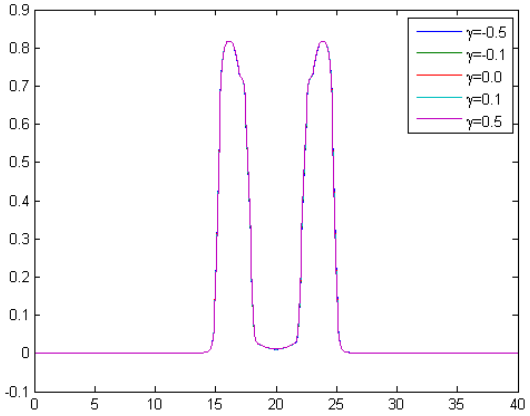

(a) viable cells ϕ_V

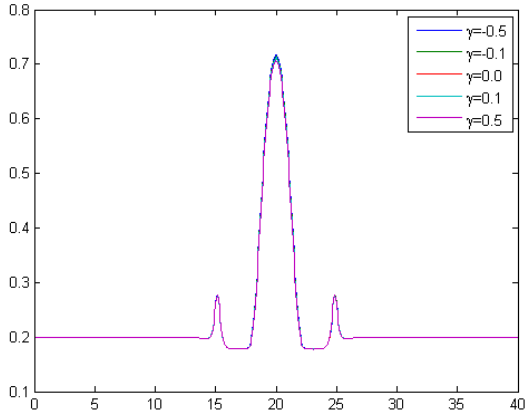

(b) water ϕ_W

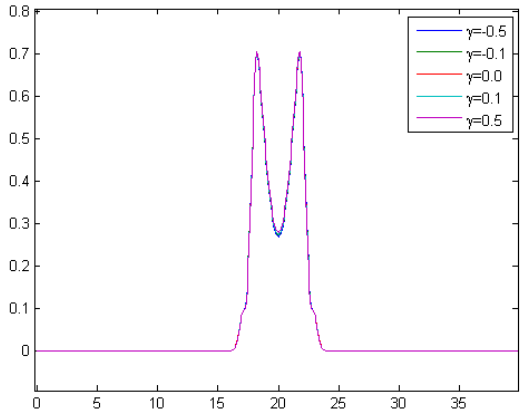

(c) dead cells ϕ_D

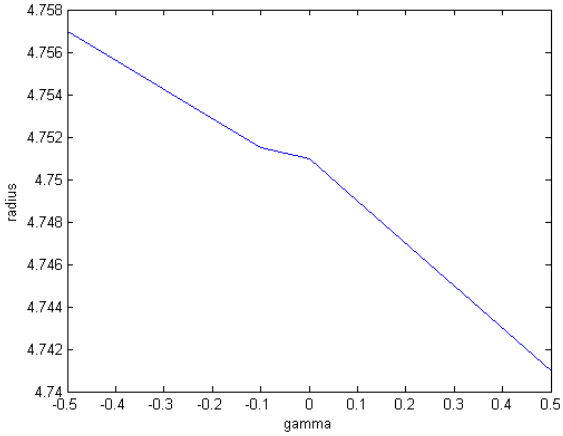

(d) size of the radius

Figure B.24: cell types of γ variations at $t = 200$

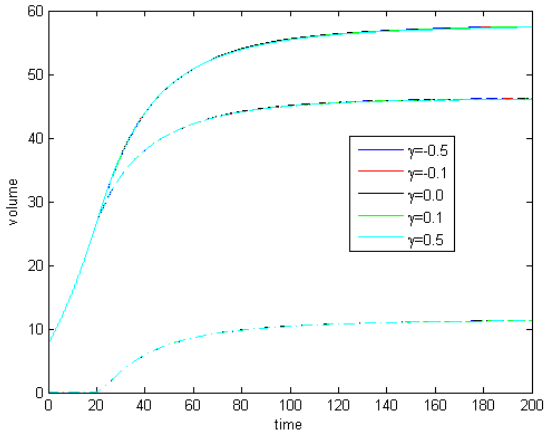

(a) ϕ_V (dashed line), ϕ_D (dash dot line), and ϕ_T (solid line)

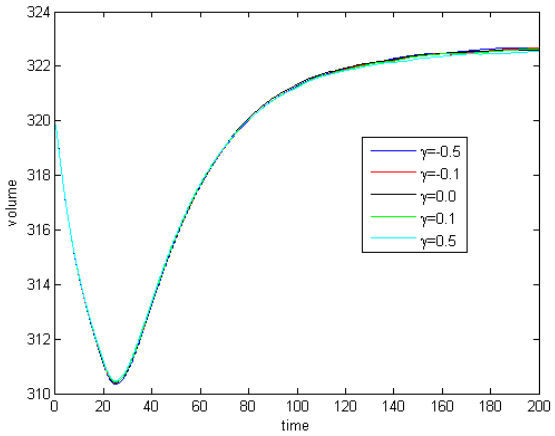

(b) water ϕ_W

Figure B.25: Total volume of γ variations

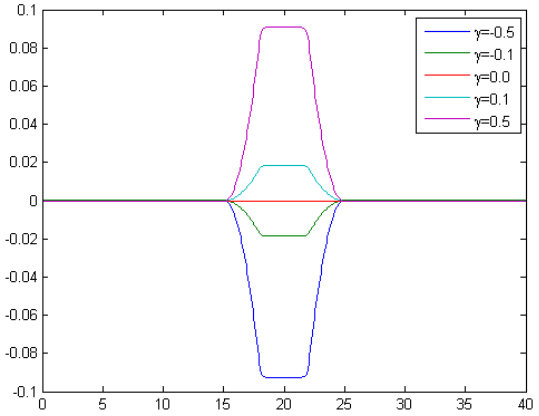

(a) pressure

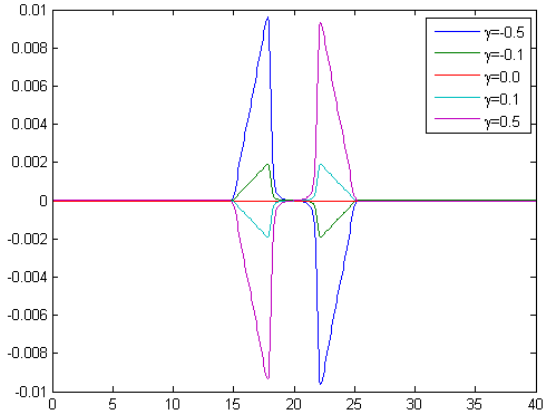

(b) water velocity $\mathbf{u}_w$

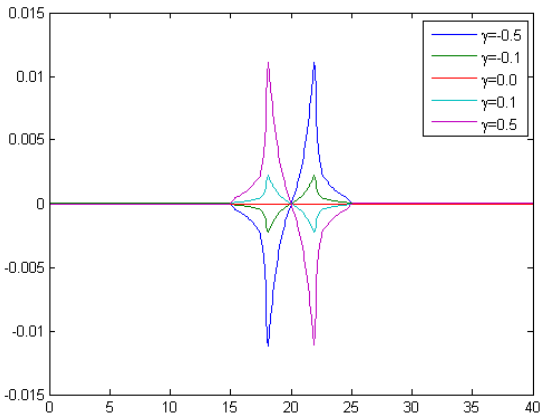

(c) viable cell and host velocity $\mathbf{u}_s$

Figure B.26: pressure and velocities for γ variations at $t = 200$

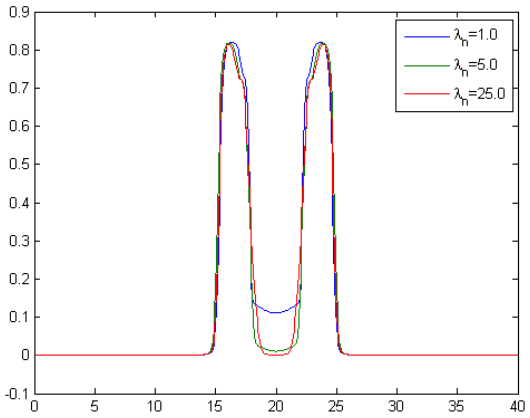

(a) viable cells ϕ_V

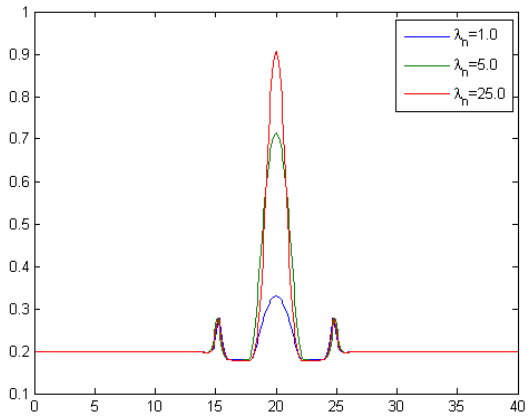

(b) water ϕ_W

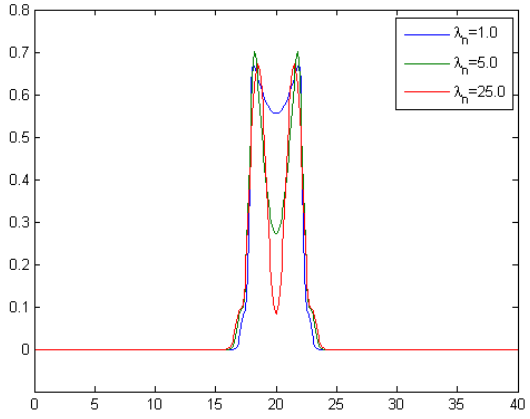

(c) dead cells ϕ_D

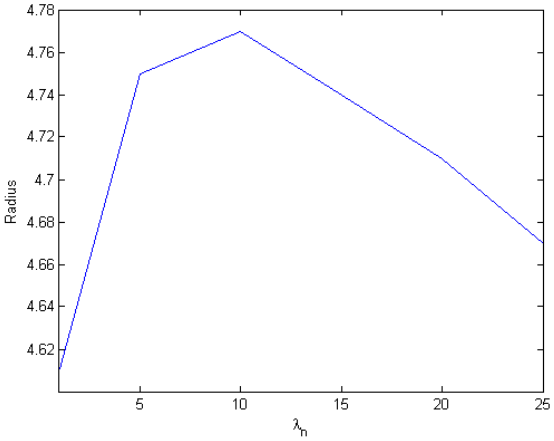

(d) size of the radius

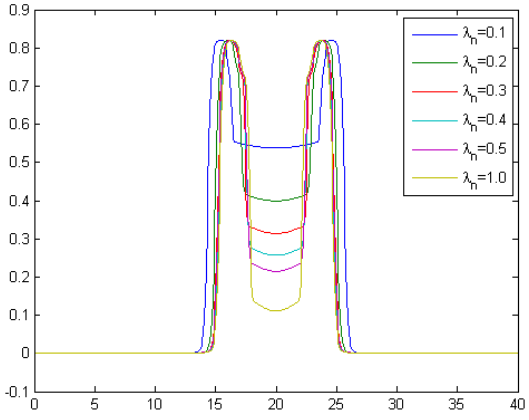

(e) viable cells for small λ_n

Figure B.27: cell types of λ_n variations at $t = 200$

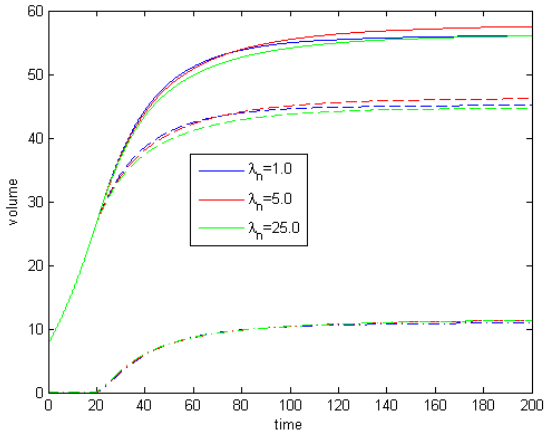

(a) ϕ_V (dashed line), ϕ_D (dash dot line), and ϕ_T (solid line)

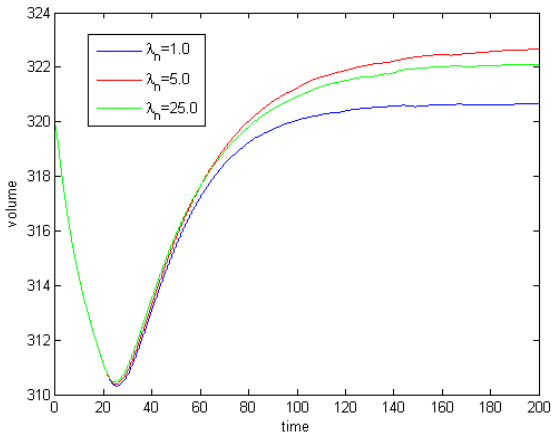

(b) water ϕ_W

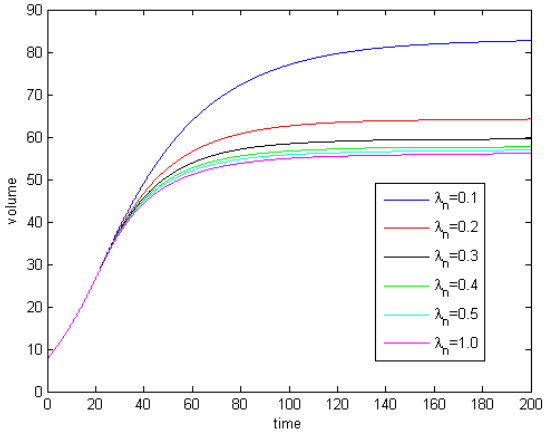

(c) Total tumor volume

Figure B.28: Total volume of λ_n variations

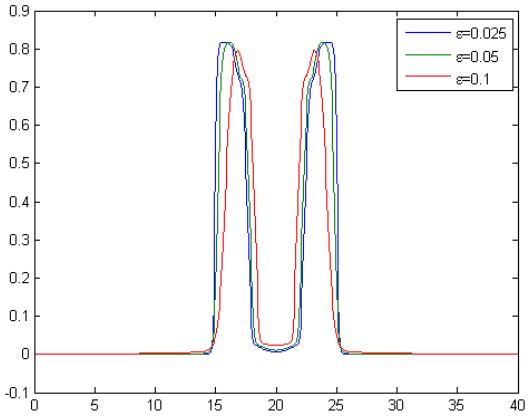

(a) viable cells ϕ_V

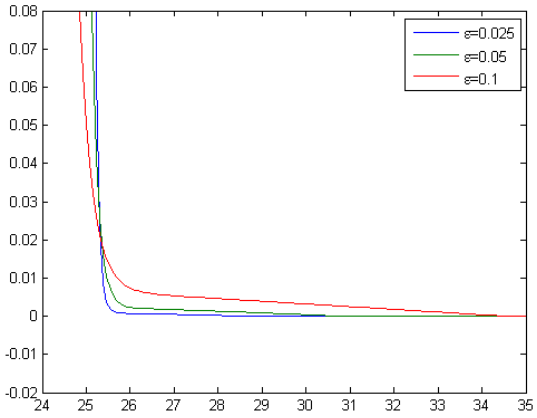

(b) viable cells ϕ_V close-up

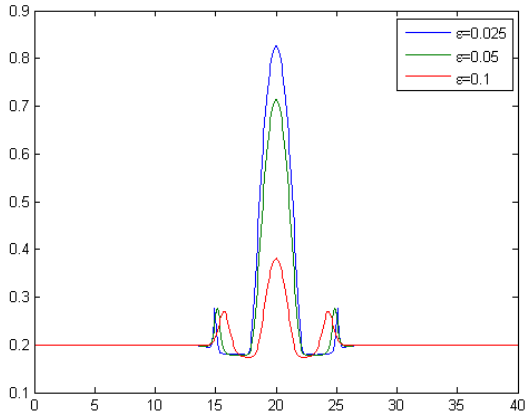

(c) water ϕ_W

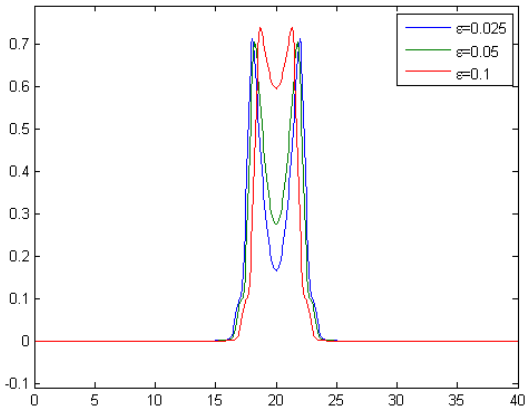

(d) dead cells ϕ_D

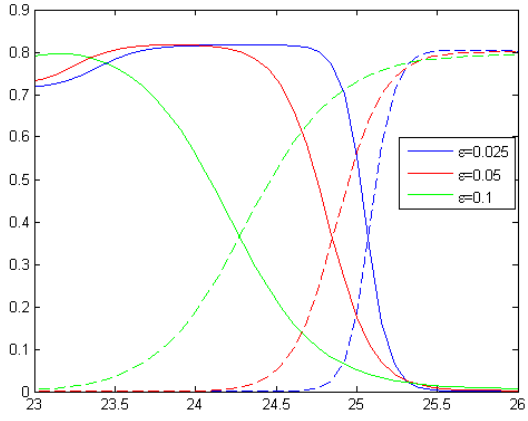

(e) close up of tumor-host interface,
viable cells (solid line), host cells (dashed line)

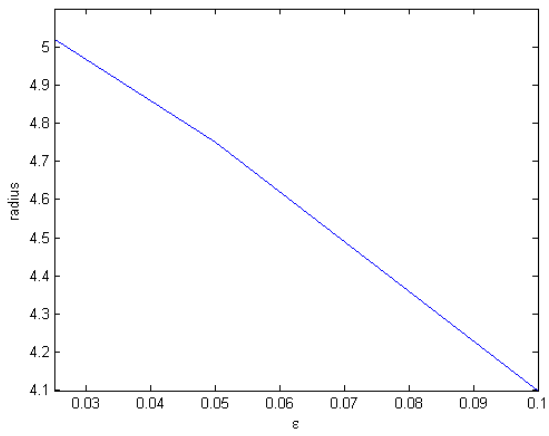

(f) size of the radius

Figure B.29: cell types of ϵ variations at $t = 200$

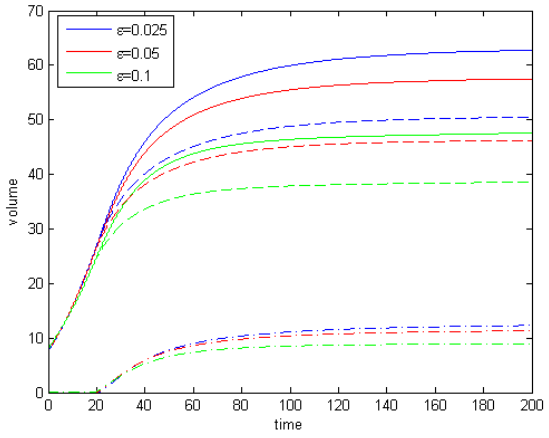

(a) ϕ_V (dashed line), ϕ_D (dash dot line), and ϕ_T (solid line)

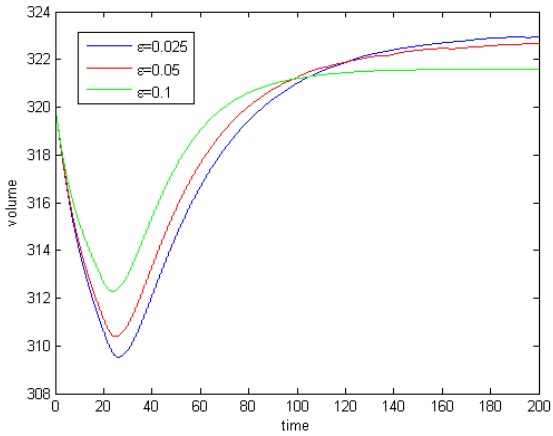

(b) water ϕ_W

Figure B.30: Total volume of ϵ variations

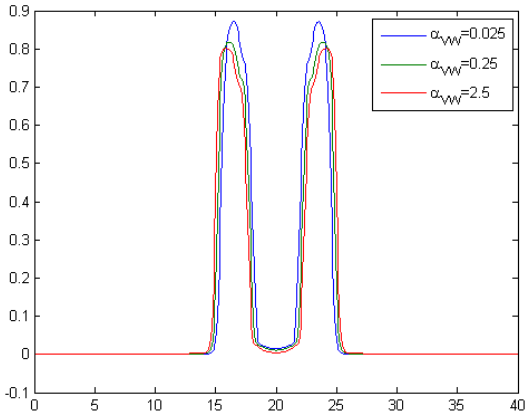

(a) viable cells ϕ_V

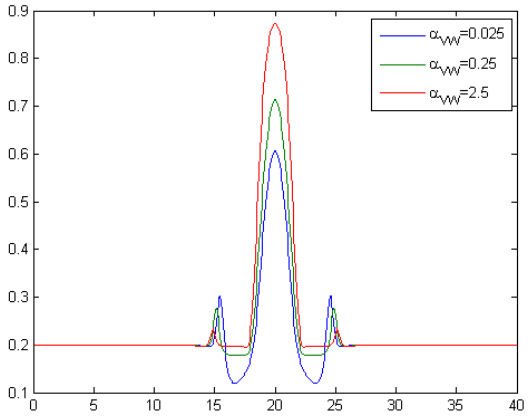

(b) water ϕ_W

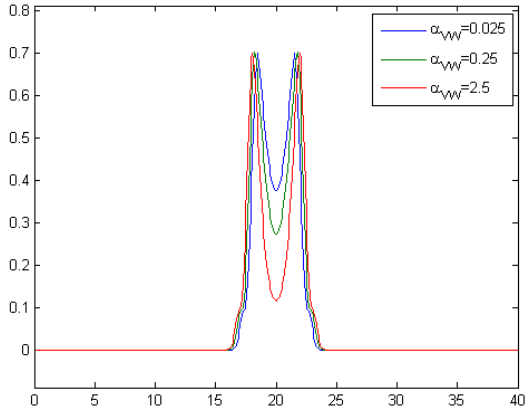

(c) dead cells ϕ_D

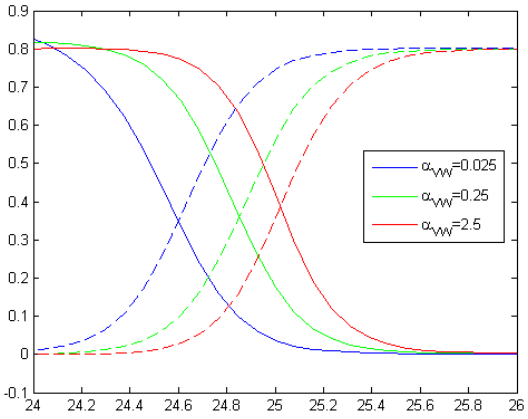

(d) Tumor-Host interface, ϕ_T (solid lines), ϕ_H (dashed lines)

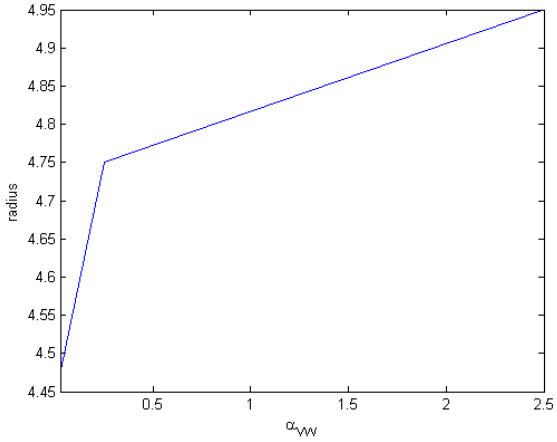

(e) size of the radius

Figure B.31: cell types of α_{VW} variations at $t = 200$

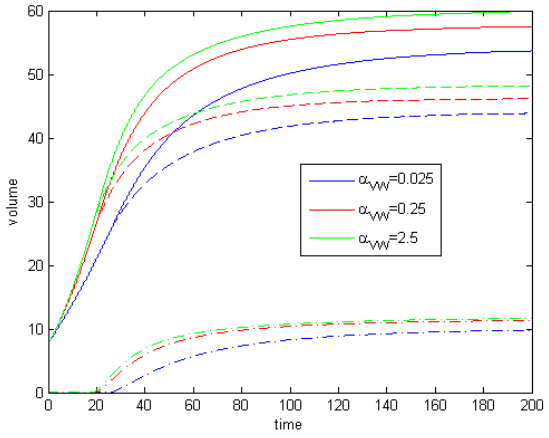

(a) ϕ_V (dashed line), ϕ_D (dash dot line), and ϕ_T (solid line)

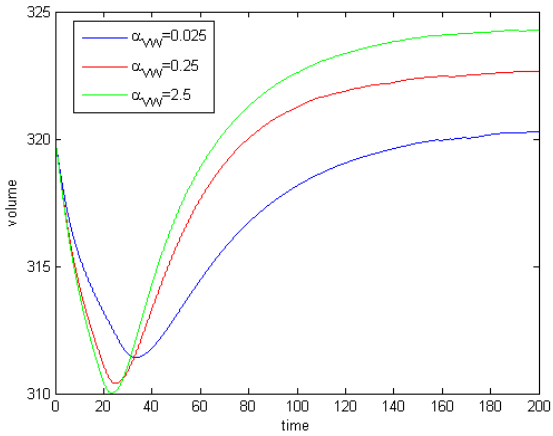

(b) water ϕ_W

Figure B.32: Total volume of α_{VW} variations

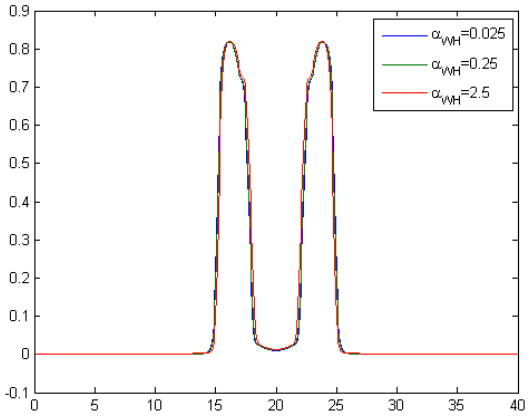

(a) viable cells ϕ_V

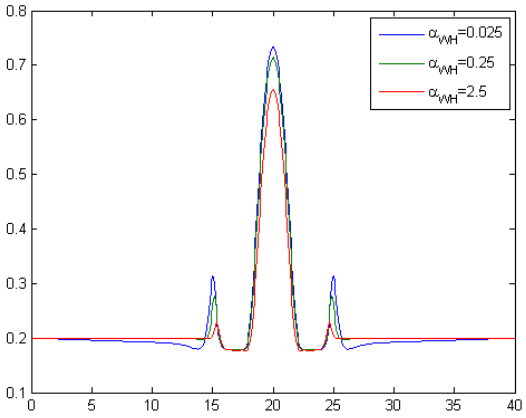

(b) water ϕ_W

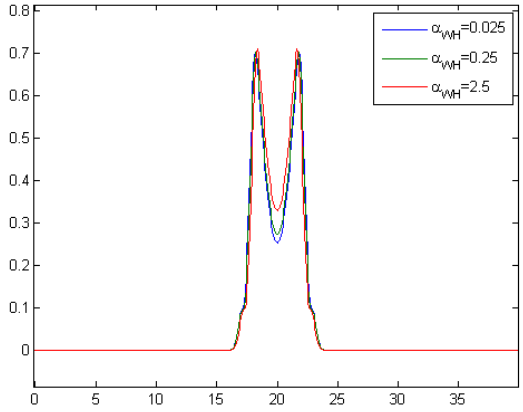

(c) dead cells ϕ_D

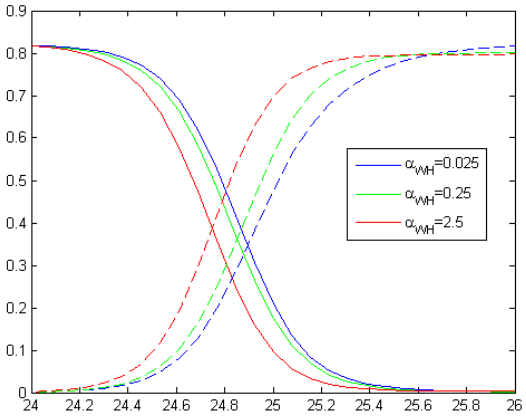

(d) Tumor-Host interface, ϕ_T (solid lines), ϕ_H (dashed lines)

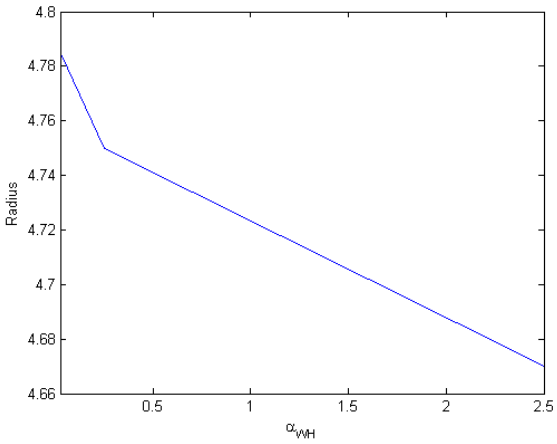

(e) size of the radius

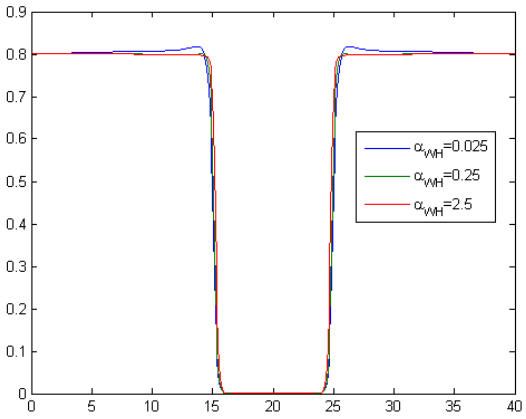

(f) host cells ϕ_H

Figure B.33: cell types of α_{WH} variations at $t = 200$

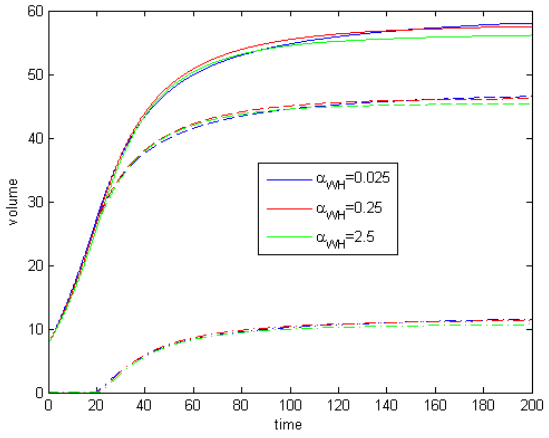

(a) ϕ_V (dashed line), ϕ_D (dash dot line), and ϕ_T (solid line)

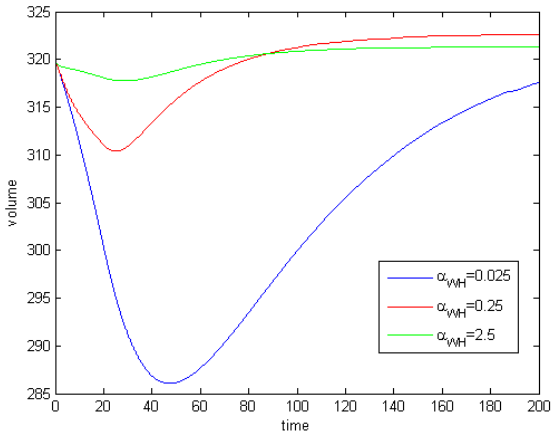

(b) water ϕ_W

Figure B.34: Total volume of α_{WH} variations

Appendix C

Non-Symmetric Tumor Parameter Study Slides

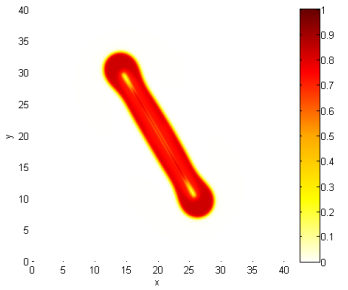

(a) viable cells ϕ_V, $\lambda_l = 1.0$

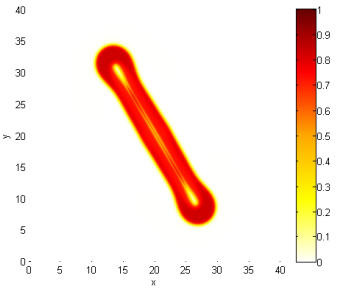

(b) viable cells ϕ_V, $\lambda_l = 0.5$

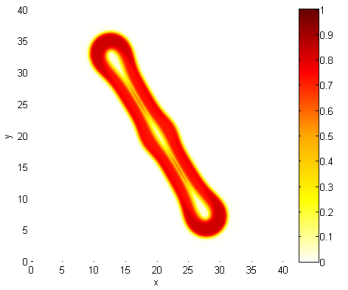

(c) viable cells ϕ_V, $\lambda_l = 0.2$

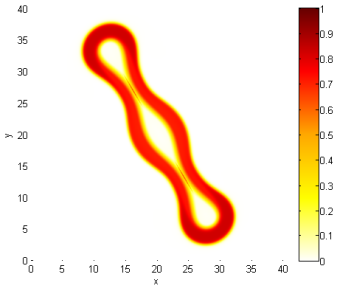

(d) viable cells ϕ_V, $\lambda_l = 0.1$

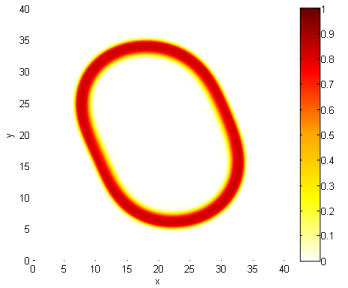

(e) viable cells ϕ_V, $\lambda_l = 0.05$

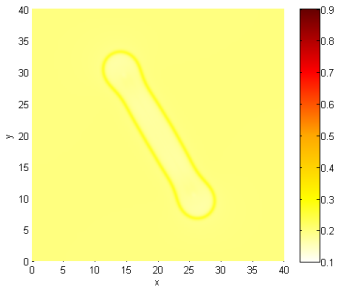

(f) water ϕ_W, $\lambda_l = 1.0$

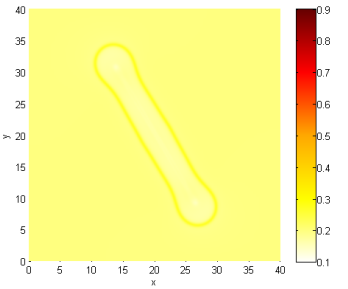

(g) water ϕ_W, $\lambda_l = 0.5$

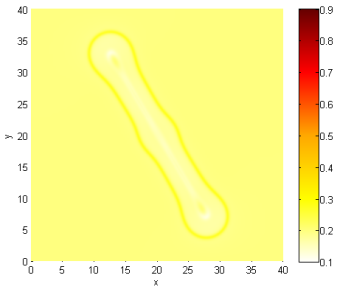

(h) water ϕ_W, $\lambda_l = 0.2$

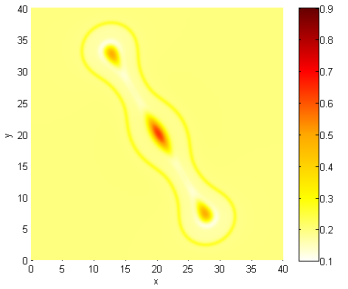

(i) water ϕ_W, $\lambda_l = 0.1$

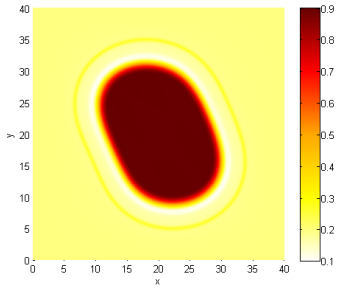

(j) water ϕ_W, $\lambda_l = 0.05$

Figure C.1: water and viable cells of λ_l variations at $t = 400$

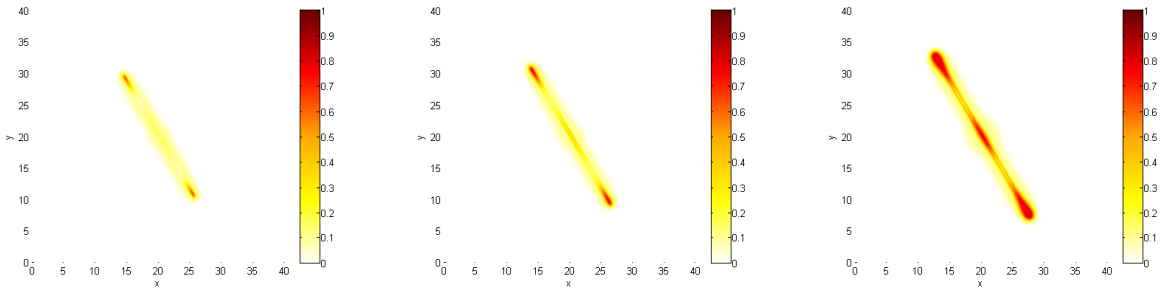

(a) dead cells ϕ_D, $\lambda_l = 1.0$ (b) dead cells ϕ_D, $\lambda_l = 0.5$ (c) dead cells ϕ_D, $\lambda_l = 0.2$

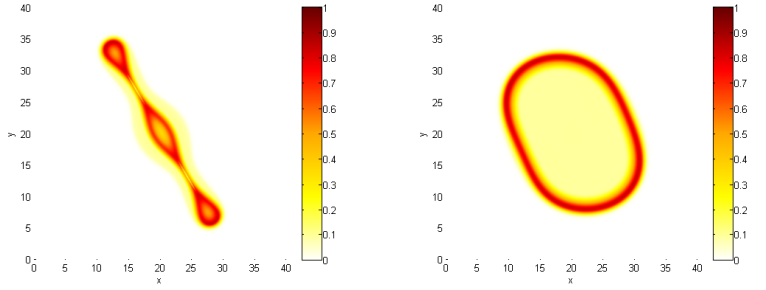

(d) dead cells ϕ_D, $\lambda_l = 0.1$ (e) dead cells ϕ_D, $\lambda_l = 0.05$

Figure C.2: dead cells of λ_l variations at $t = 400$

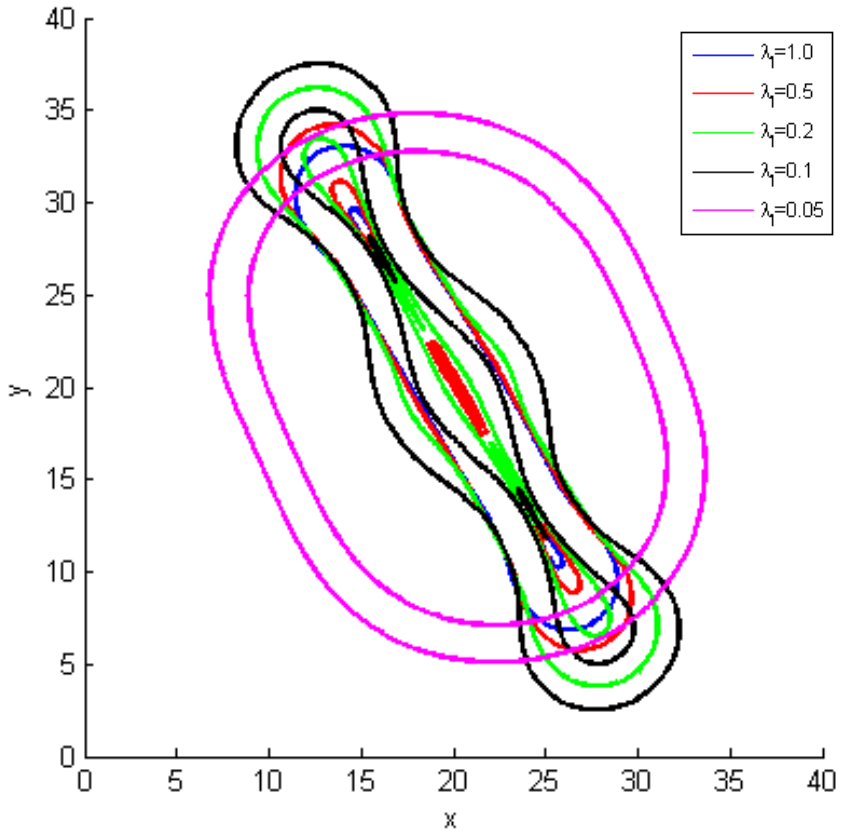

Figure C.3: Contours of the viable cells at $\phi_V = 0.5$ for λ_l variations at $t = 400$

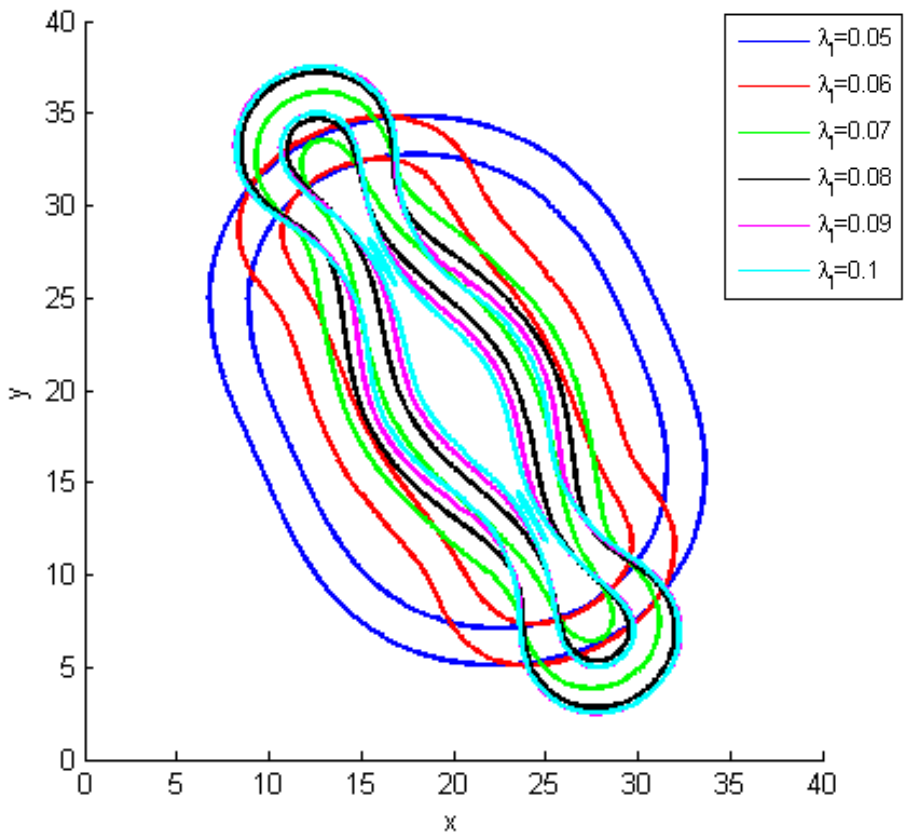

Figure C.4: Contours of the viable cells at $\phi_V = 0.5$ for λ_l variations at $t = 400$

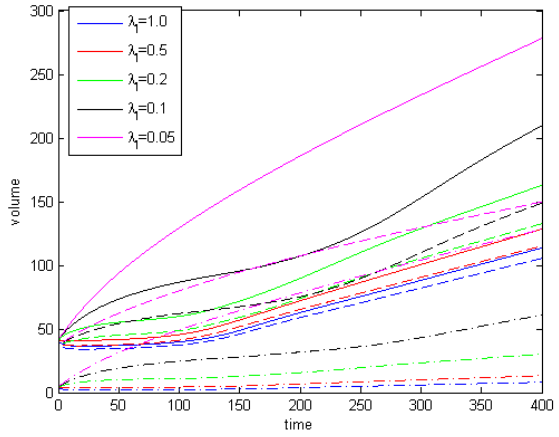

(a) ϕ_V (dashed line), ϕ_D (dash dot line), and ϕ_T (solid line)

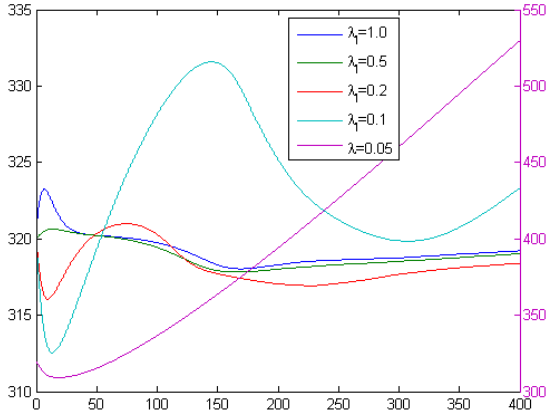

(b) water ϕ_W

Figure C.5: Total volume of λ_l variations

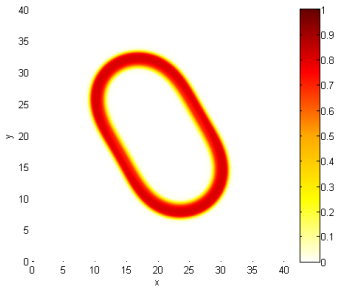

(a) viable cells ϕ_V, $\kappa = 0.005$

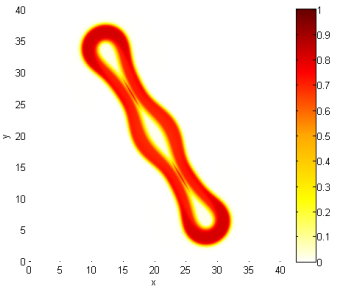

(b) viable cells ϕ_V, $\kappa = 0.015$

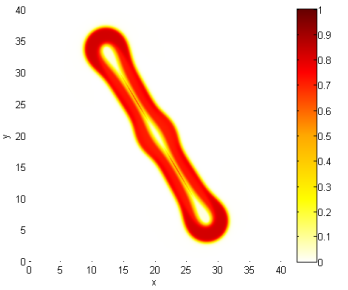

(c) viable cells ϕ_V, $\kappa = 0.025$

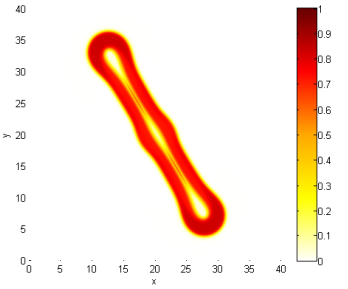

(d) viable cells ϕ_V, $\kappa = 0.035$

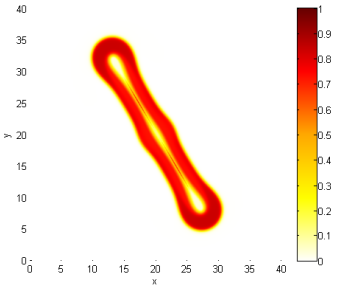

(e) viable cells ϕ_V, $\kappa = 0.045$

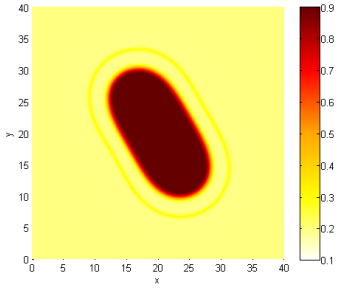

(f) water ϕ_W, $\kappa = 0.005$

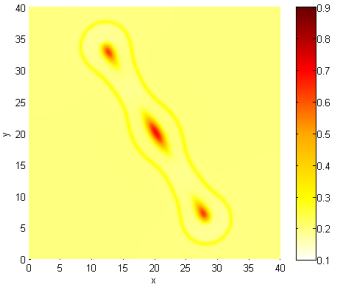

(g) water ϕ_W, $\kappa = 0.015$

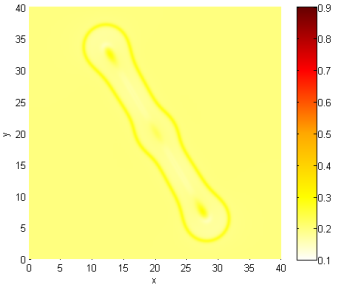

(h) water ϕ_W, $\kappa = 0.025$

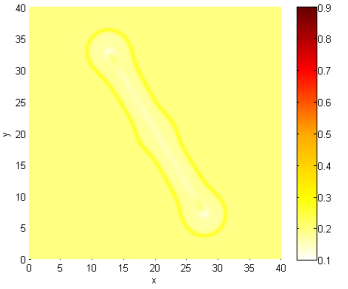

(i) water ϕ_W, $\kappa = 0.035$

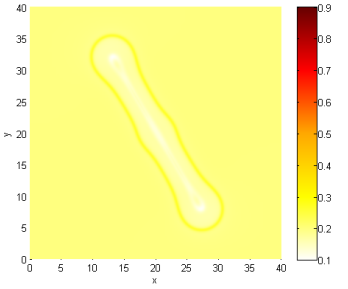

(j) water ϕ_W, $\kappa = 0.045$

Figure C.6: water and viable cells of κ variations at $t = 400$

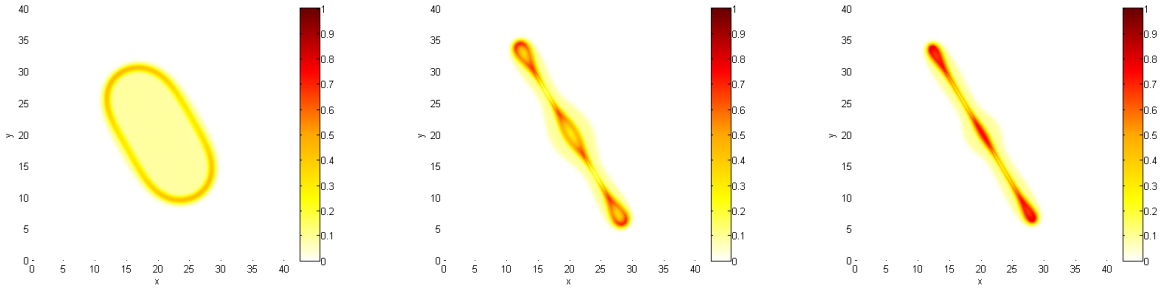

(a) dead cells ϕ_D, $\kappa = 0.005$ (b) dead cells ϕ_D, $\kappa = 0.015$ (c) dead cells ϕ_D, $\kappa = 0.025$

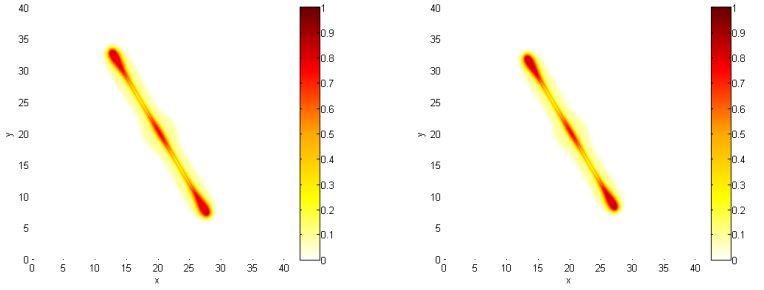

(d) dead cells ϕ_D, $\kappa = 0.035$ (e) dead cells ϕ_D, $\kappa = 0.045$

Figure C.7: dead cells of κ variations at $t = 400$

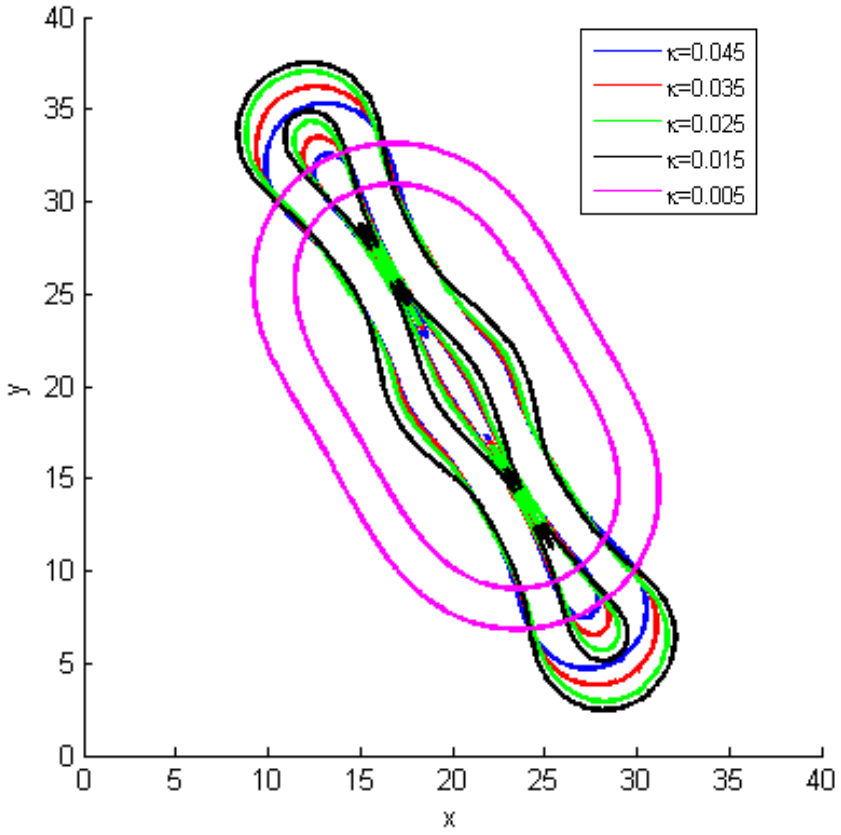

Figure C.8: Contours of the viable cells at $\phi_V = 0.5$ for κ variations at $t = 400$

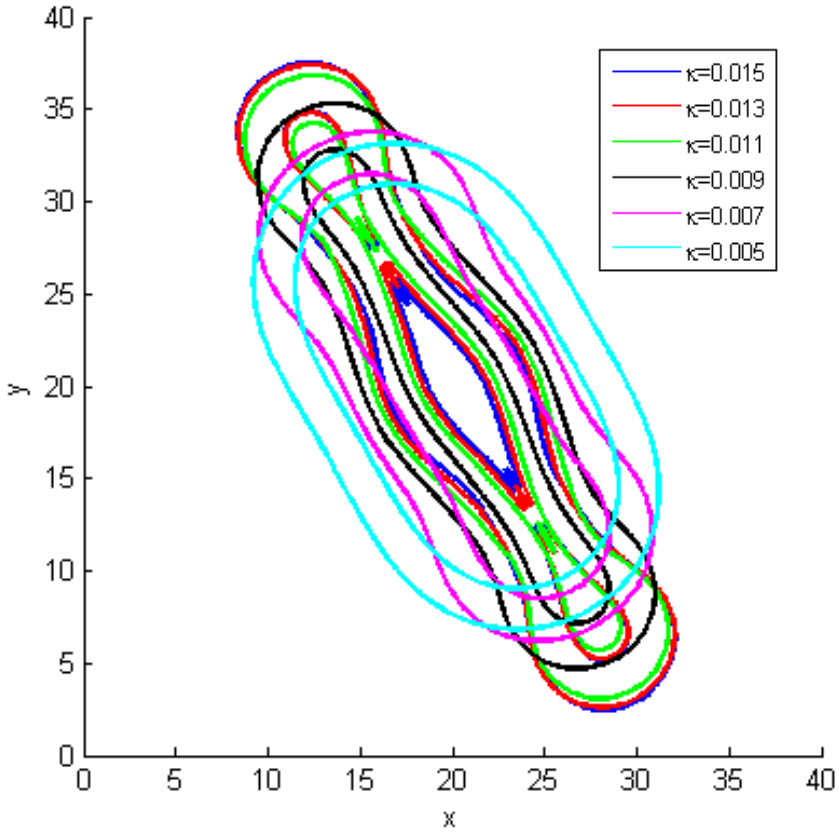

Figure C.9: Contours of the viable cells at $\phi_V = 0.5$ for κ variations at $t = 400$

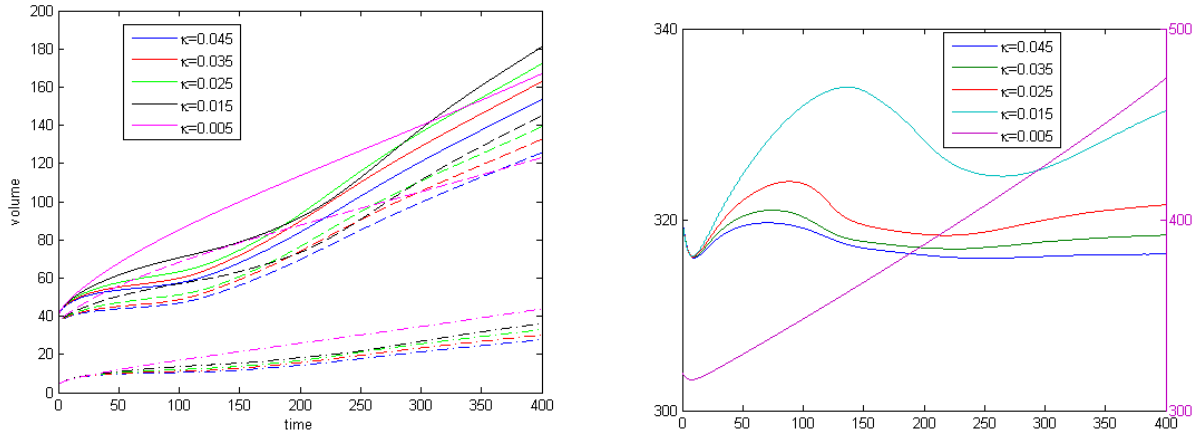

(a) ϕ_V (dashed line), ϕ_D (dash dot line), and ϕ_T (solid line)

(b) water ϕ_W

Figure C.10: Total volume of κ variations

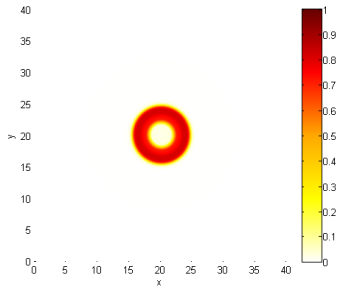

(a) viable cells ϕ_V, $M_V = 200$

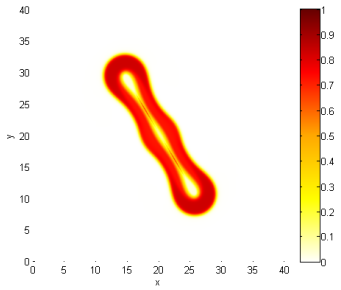

(b) viable cells ϕ_V, $M_V = 100$

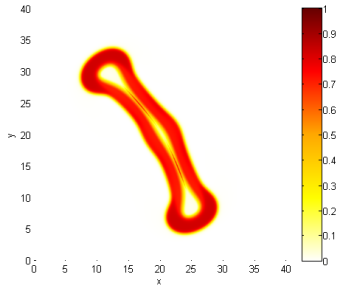

(c) viable cells ϕ_V, $M_V = 50$

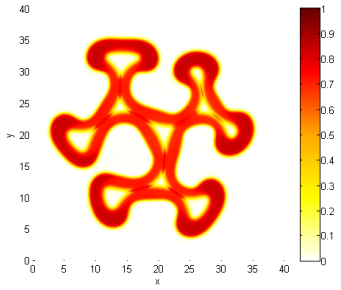

(d) viable cells ϕ_V, $M_V = 25$

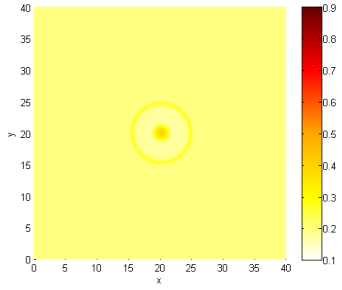

(e) water ϕ_W, $M_V = 200$

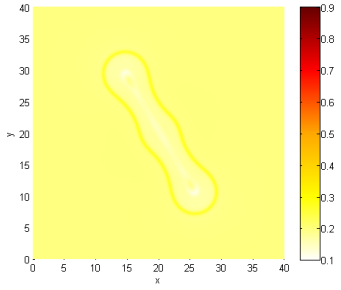

(f) water ϕ_W, $M_V = 100$

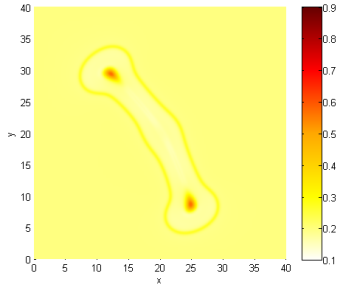

(g) water ϕ_W, $M_V = 50$

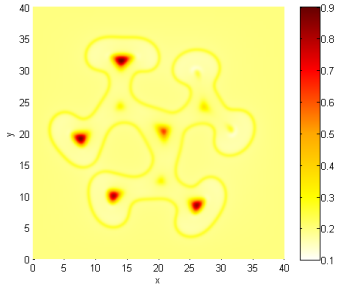

(h) water ϕ_W, $M_V = 25$

Figure C.11: water and viable cells of M_V variations at $t = 300$

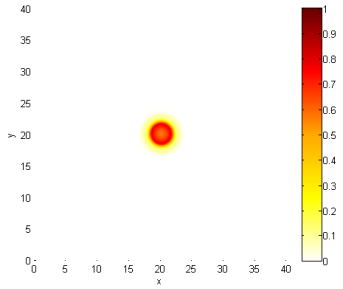

(a) dead cells ϕ_D, $M_V = 200$

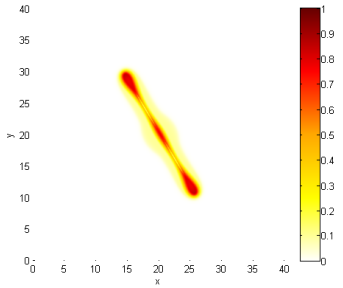

(b) dead cells ϕ_D, $M_V = 100$

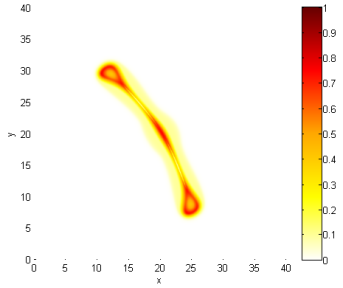

(c) dead cells ϕ_D, $M_V = 50$

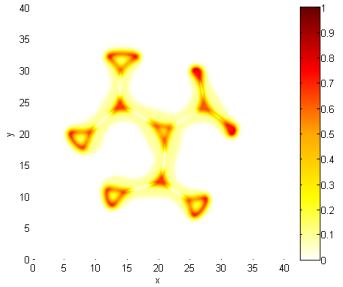

(d) dead cells ϕ_D, $M_V = 25$

Figure C.12: dead cells of M_V variations at $t = 300$

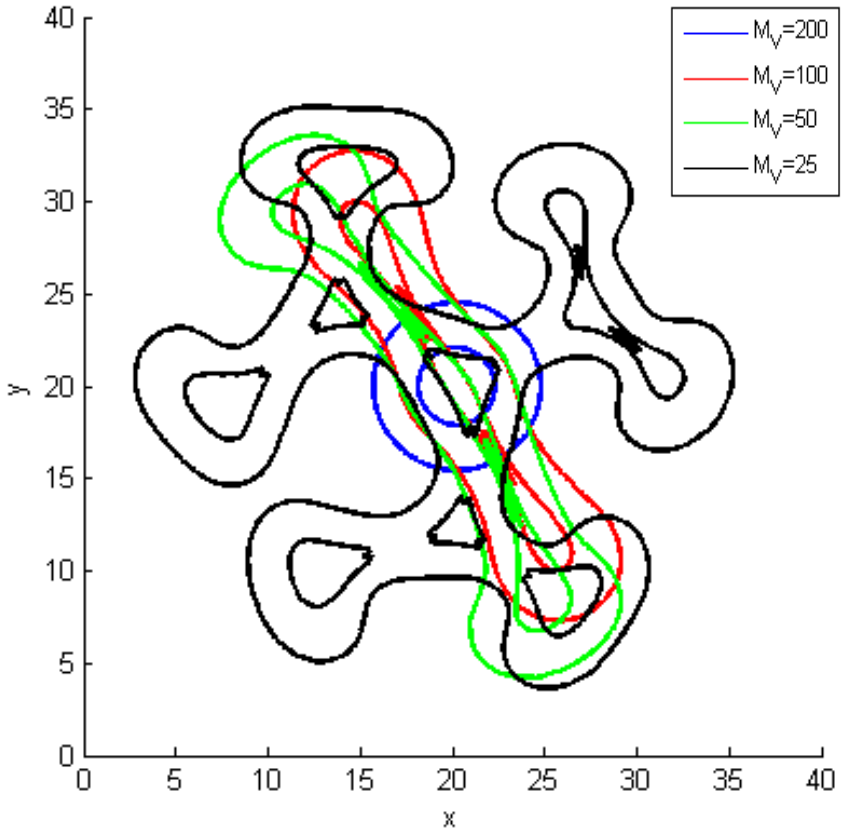

Figure C.13: Contours of the viable cells at $\phi_V = 0.5$ for M_V variations at $t = 300$

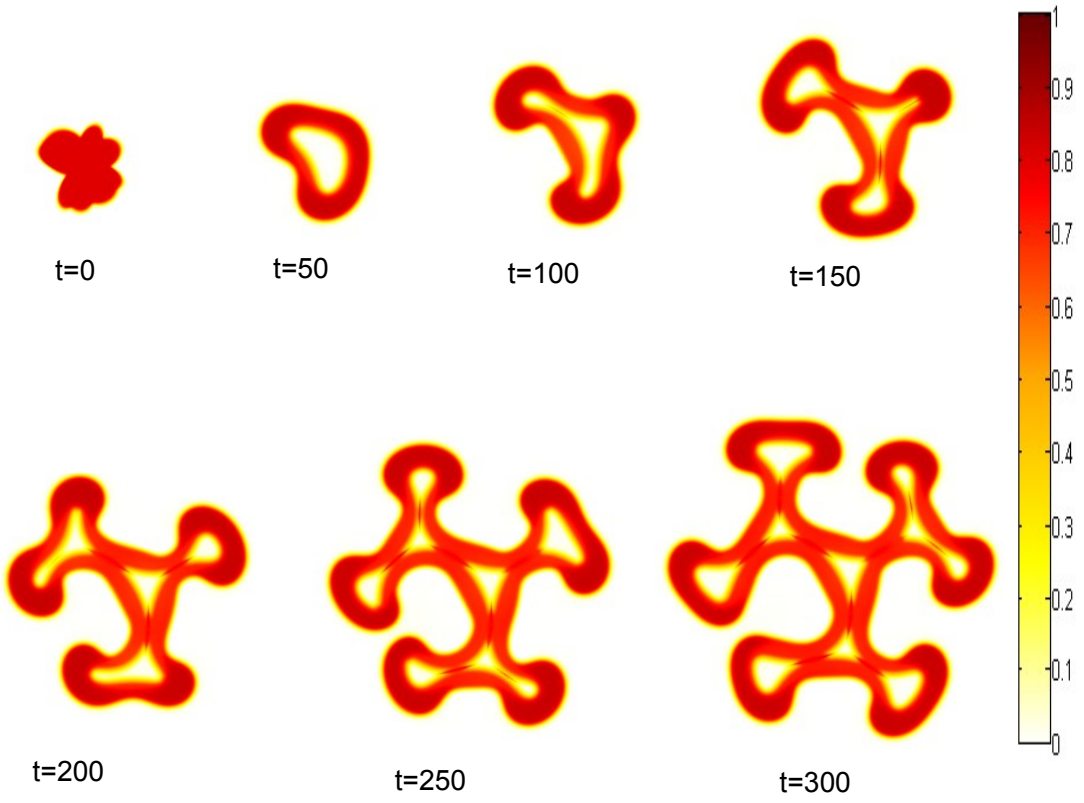

Figure C.14: The evolution of the viable cells for $M_V = 25$

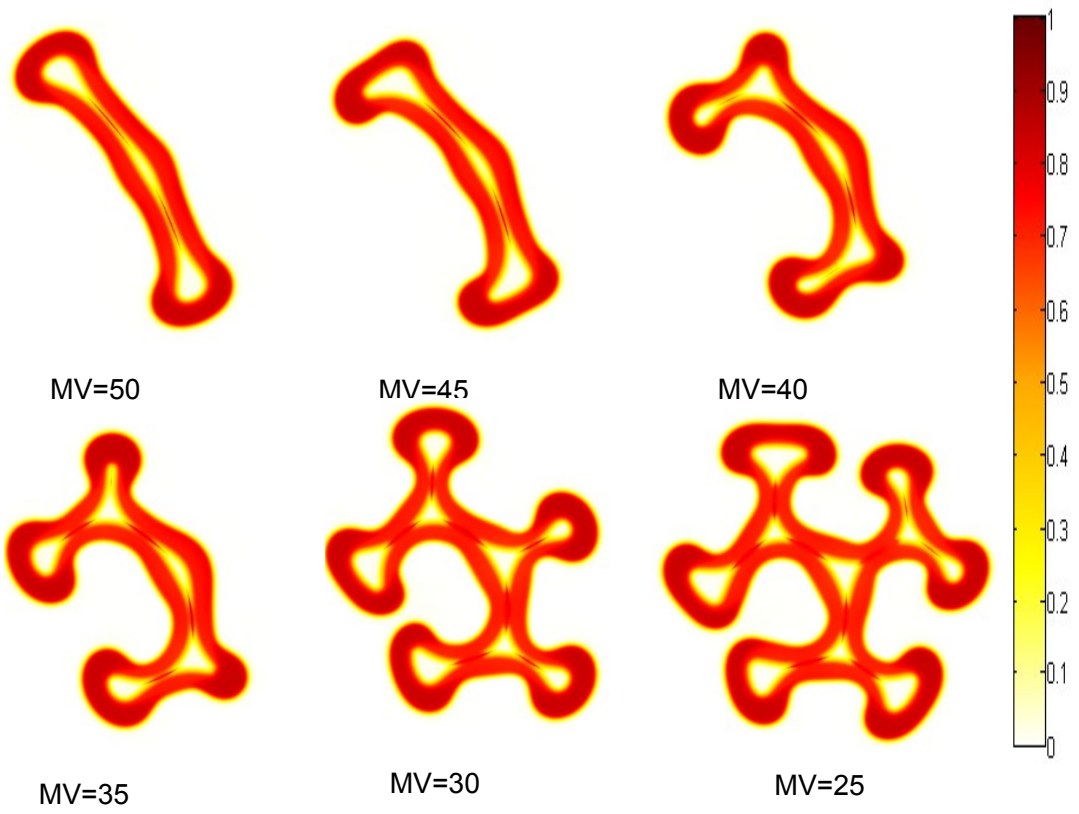

Figure C.15: Comparison of the viable cells for M_V between 25 and 50 at $t = 300$

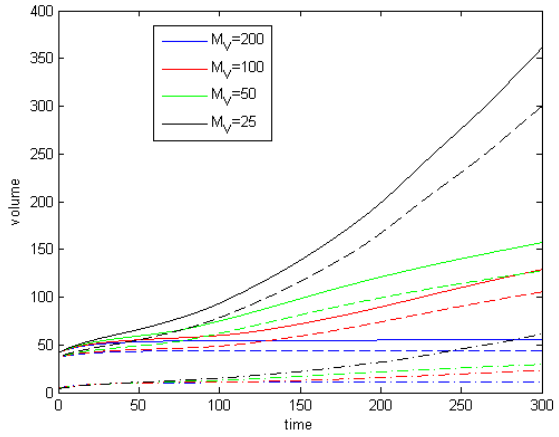

(a) ϕ_V (dashed line), ϕ_D (dash dot line), and ϕ_T (solid line)

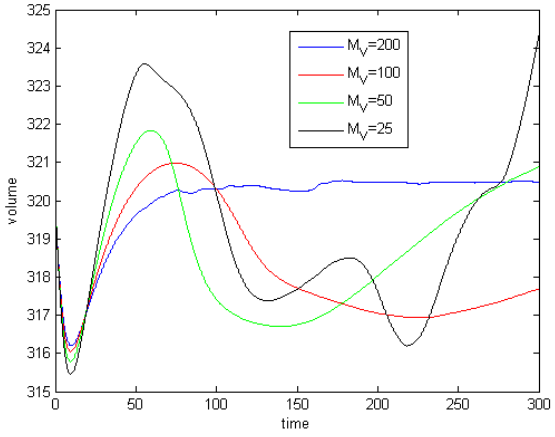

(b) water ϕ_W

Figure C.16: Total volume of M_V variations

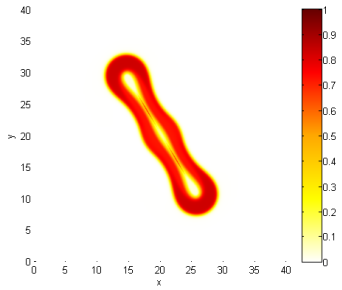

(a) viable cells ϕ_V, $\bar{\phi}_W^H = 0.2$

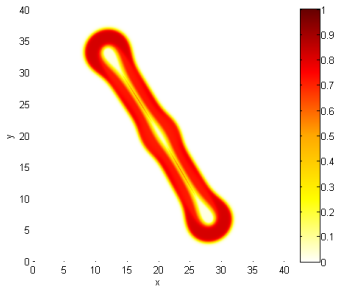

(b) viable cells ϕ_V, $\bar{\phi}_W^H = 0.4$

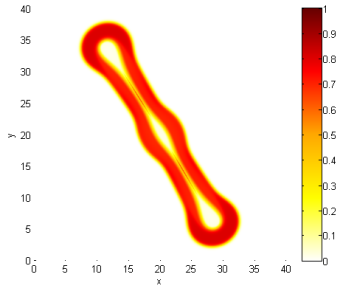

(c) viable cells ϕ_V, $\bar{\phi}_W^H = 0.6$

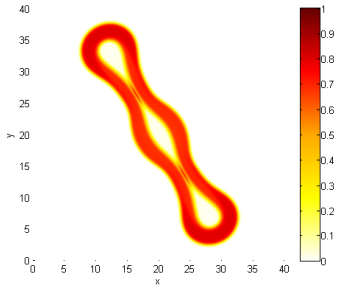

(d) viable cells ϕ_V, $\bar{\phi}_W^H = 0.8$

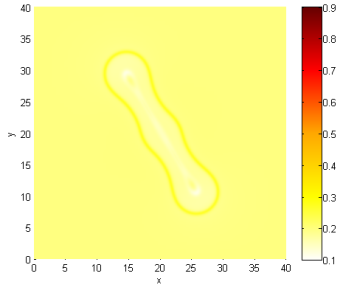

(e) water ϕ_W, $\bar{\phi}_W^H = 0.2$

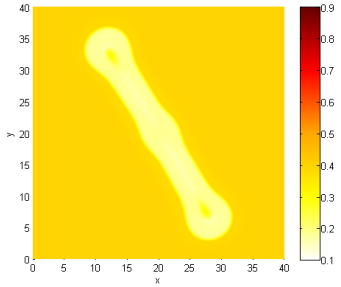

(f) water ϕ_W, $\bar{\phi}_W^H = 0.4$

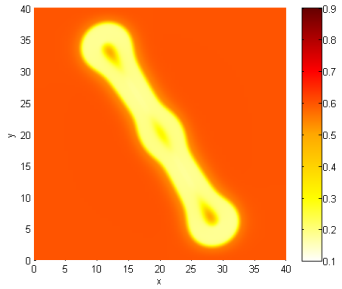

(g) water ϕ_W, $\bar{\phi}_W^H = 0.6$

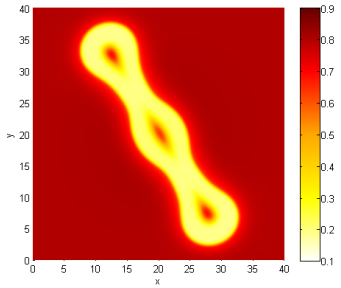

(h) water ϕ_W, $\bar{\phi}_W^H = 0.8$

Figure C.17: water and viable cells of $\bar{\phi}_W^H$ variations at $t = 300$

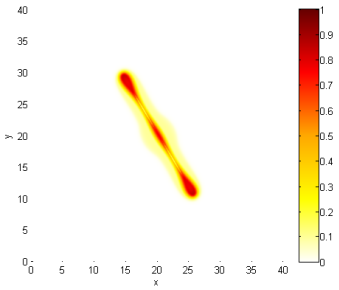

(a) dead cells ϕ_D, $\bar{\phi}_W^H = 0.2$

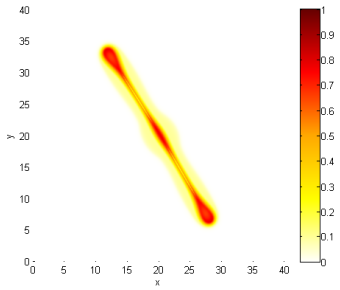

(b) dead cells ϕ_D, $\bar{\phi}_W^H = 0.4$

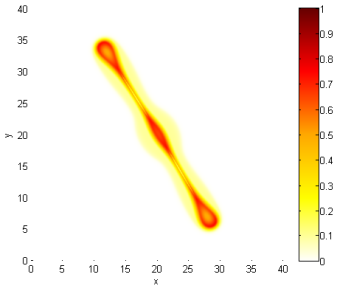

(c) dead cells ϕ_D, $\bar{\phi}_W^H = 0.6$

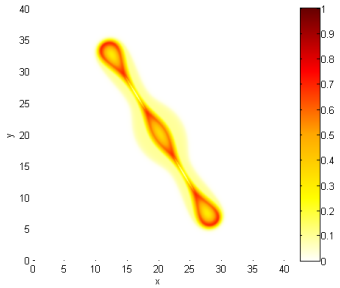

(d) dead cells ϕ_D, $\bar{\phi}_W^H = 0.8$

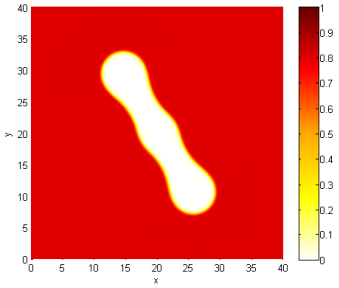

(e) host ϕ_H, $\bar{\phi}_W^H = 0.2$

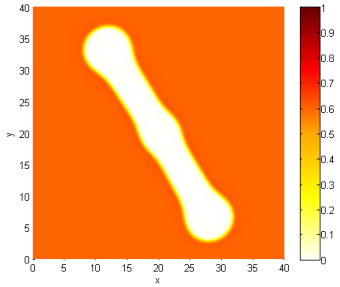

(f) host ϕ_H, $\bar{\phi}_W^H = 0.4$

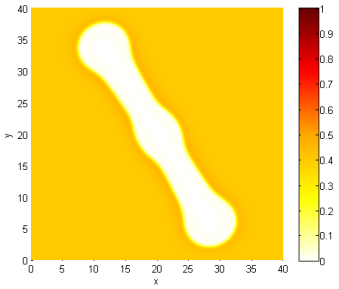

(g) host ϕ_H, $\bar{\phi}_W^H = 0.6$

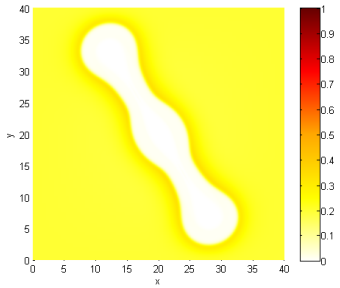

(h) host ϕ_H, $\bar{\phi}_W^H = 0.8$

Figure C.18: dead cells and host of $\bar{\phi}_W^H$ variations at $t = 300$

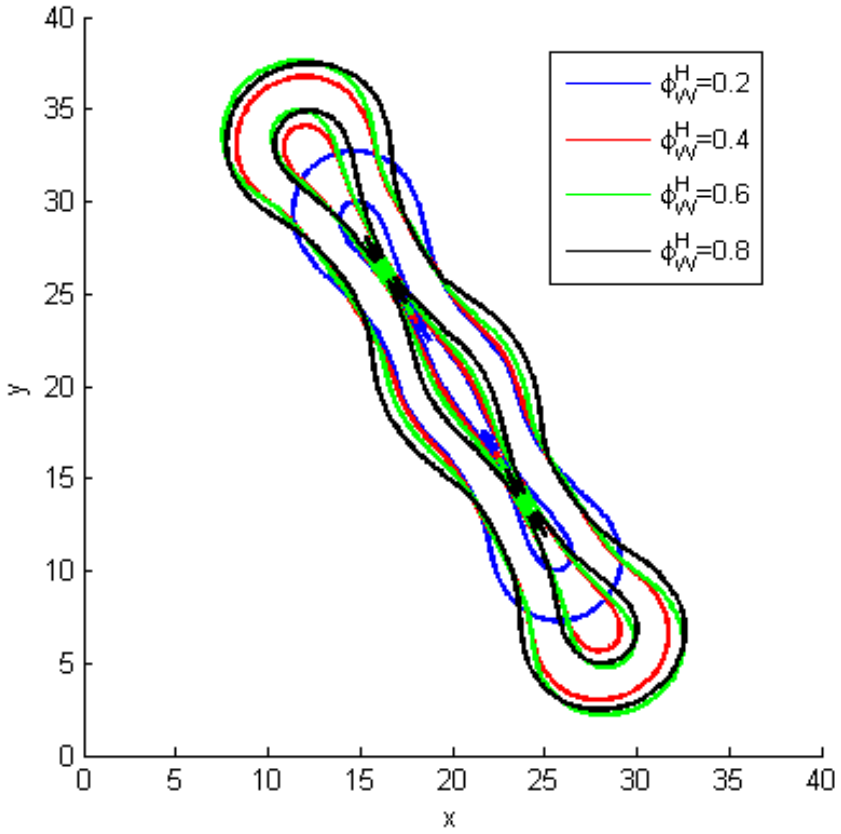

Figure C.19: Contours of the viable cells at $\phi_V = 0.5$ for $\bar{\phi}_W^H$ variations

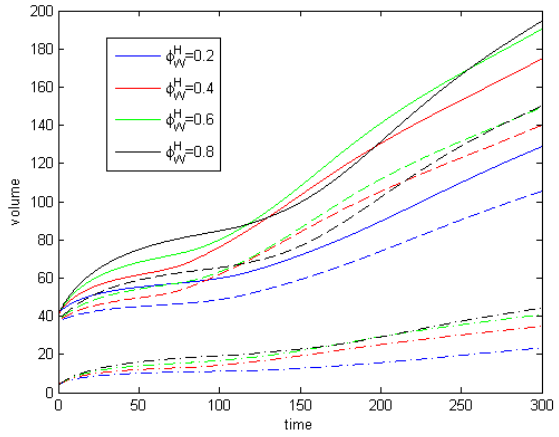

(a) ϕ_V (dashed line), ϕ_D (dash dot line), and ϕ_T (solid line)

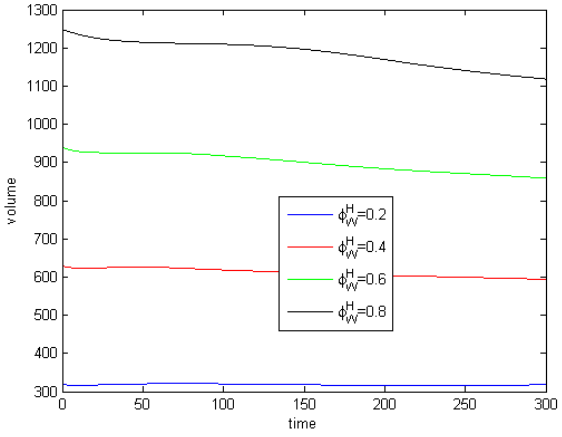

(b) water ϕ_W

Figure C.20: Total volume of $\bar{\phi}_W^H$ variations

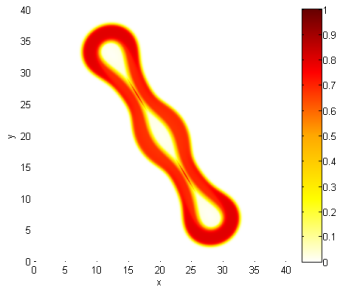

(a) viable cells ϕ_V, $\alpha_{WH} = 0.25$

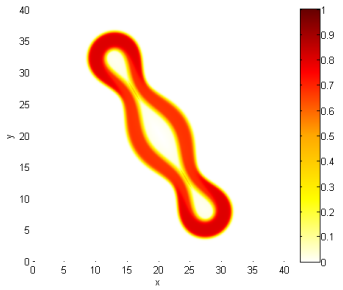

(b) viable cells ϕ_V, $\alpha_{WH} = 2.5$

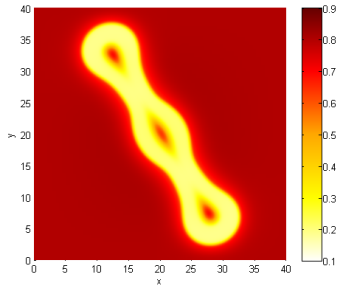

(c) water ϕ_W, $\alpha_{WH} = 0.25$

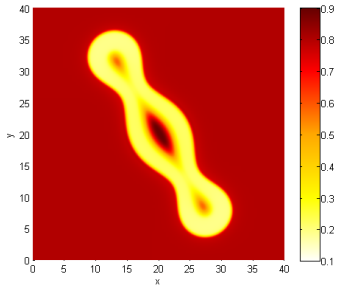

(d) water ϕ_W, $\alpha_{WH} = 2.5$

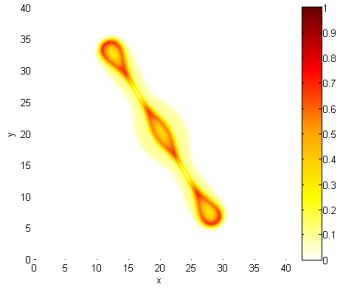

(e) dead cells ϕ_D, $\alpha_{WH} = 0.25$

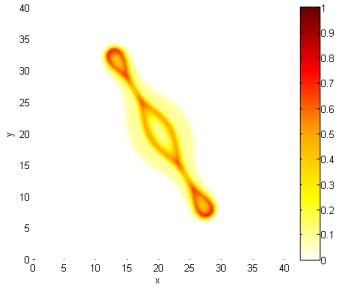

(f) dead cells ϕ_D, $\alpha_{WH} = 2.5$

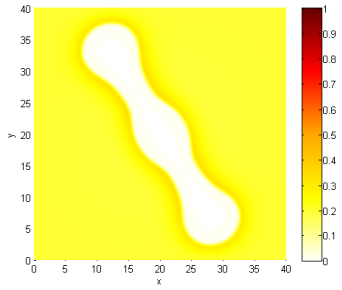

(g) host ϕ_H, $\alpha_{WH} = 0.25$

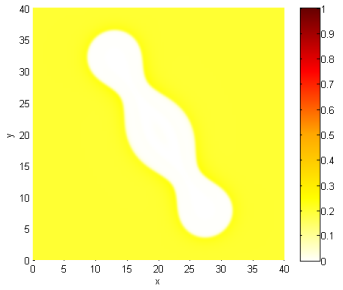

(h) host ϕ_H, $\alpha_{WH} = 2.5$

Figure C.21: species of the $\bar{\phi}_W^H = 0.8$ case with $\alpha_{WH} = 0.25$ and $\alpha_{WH} = 2.5$ at $t = 300$

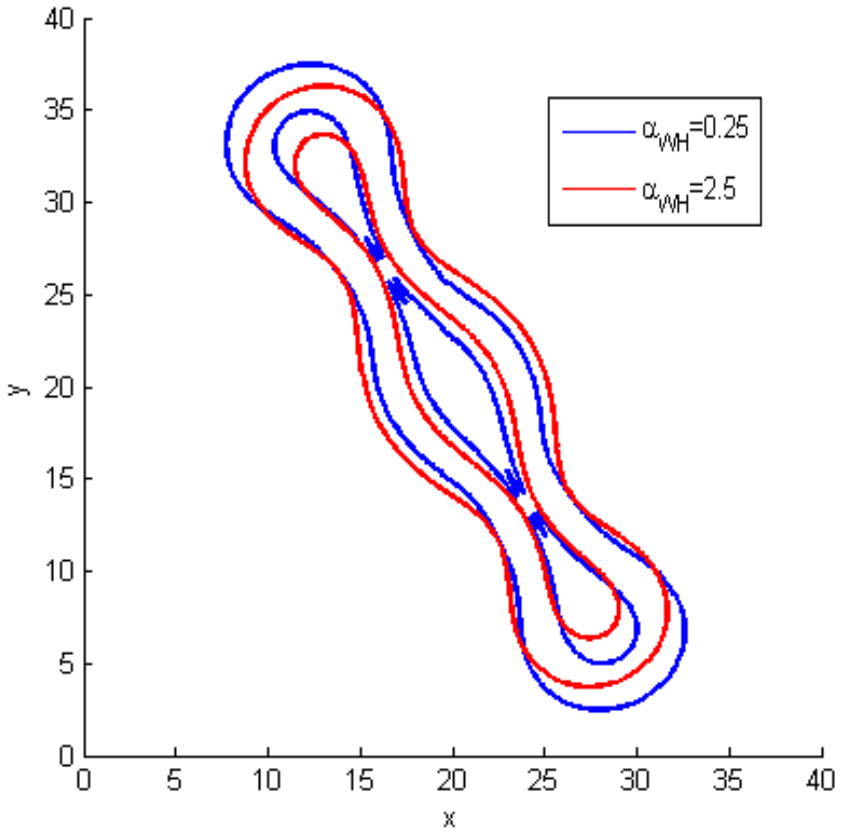

Figure C.22: Contours of the viable cells at $\phi_V = 0.5$ for $\bar{\phi}_W^H = 0.8$ with $\alpha_{WH} = 0.25$ and $\alpha_{WH} = 2.5$ at $t = 300$

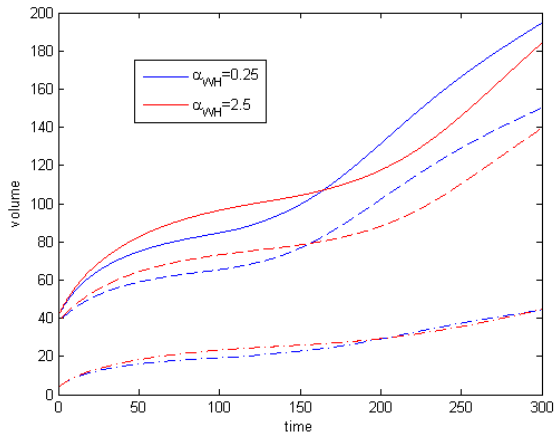

(a) ϕ_V (dashed line), ϕ_D (dash dot line), and ϕ_T (solid line)

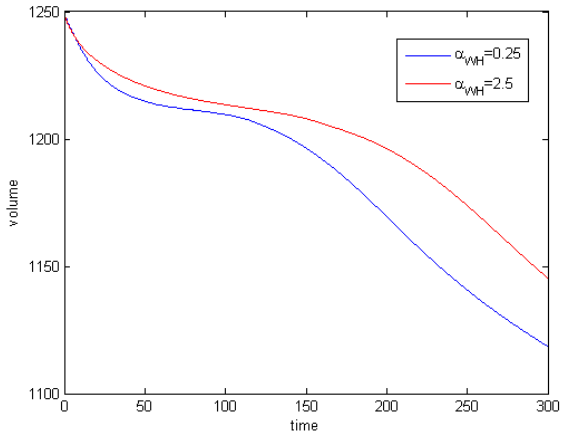

(b) water ϕ_W

Figure C.23: Total volume of $\bar{\phi}_W^H = 0.8$ with $\alpha_{WH} = 0.25$ and $\alpha_{WH} = 2.5$

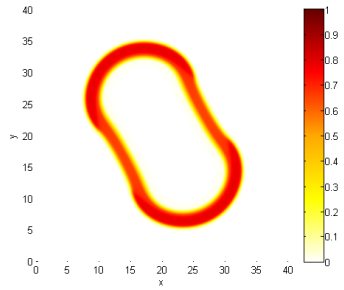

(a) viable cells ϕ_V, $\kappa = 0.035$

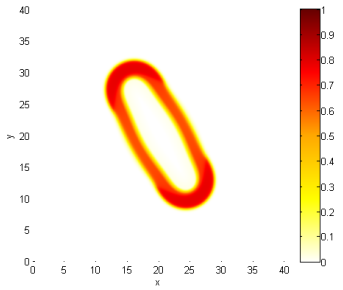

(b) viable cells ϕ_V, $\kappa = 0.05$

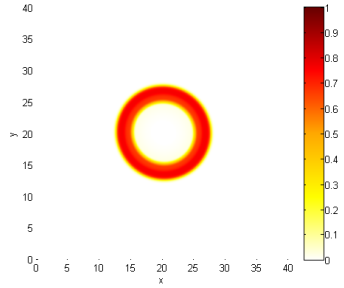

(c) viable cells ϕ_V, $\kappa = 0.075$

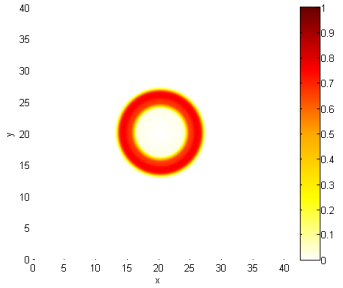

(d) viable cells ϕ_V, $\kappa = 0.1$

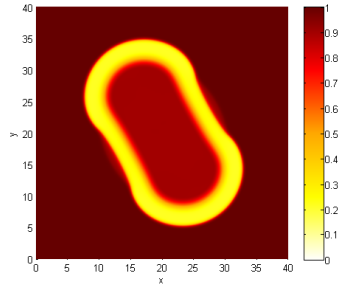

(e) water ϕ_W, $\kappa = 0.035$

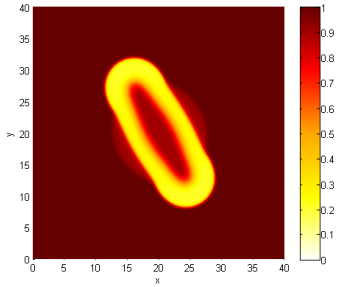

(f) water ϕ_W, $\kappa = 0.05$

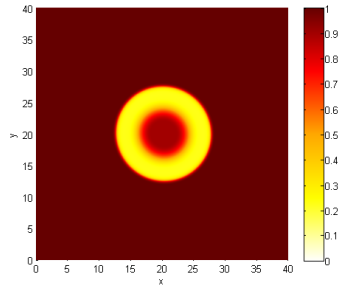

(g) water ϕ_W, $\kappa = 0.075$

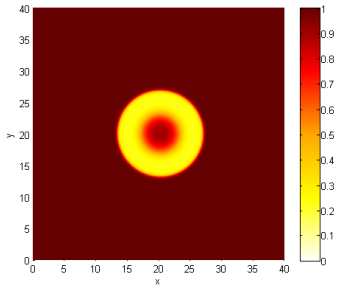

(h) water ϕ_W, $\kappa = 0.1$

Figure C.24: viable cells and water for the in vitro case ($\bar{\phi}_W^H = 1.0$) with κ variations at $t = 400$

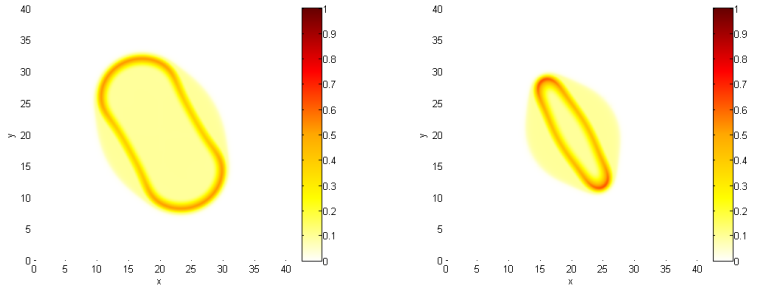

(a) dead cells ϕ_D, $\kappa = 0.035$ (b) dead cells ϕ_D, $\kappa = 0.05$

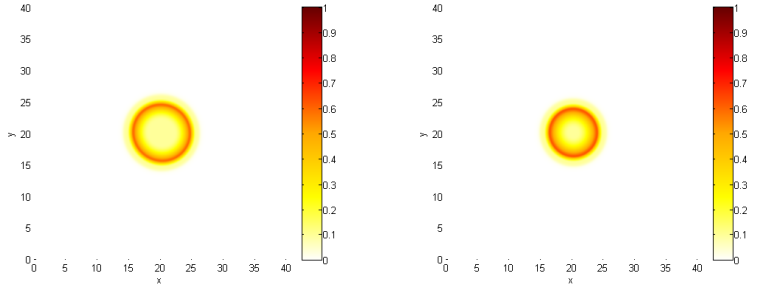

(c) dead cells ϕ_D, $\kappa = 0.075$ (d) dead cells ϕ_D, $\kappa = 0.1$

Figure C.25: dead cells for the in vitro case ($\bar{\phi}_W^H = 1.0$) with κ variations at $t = 400$

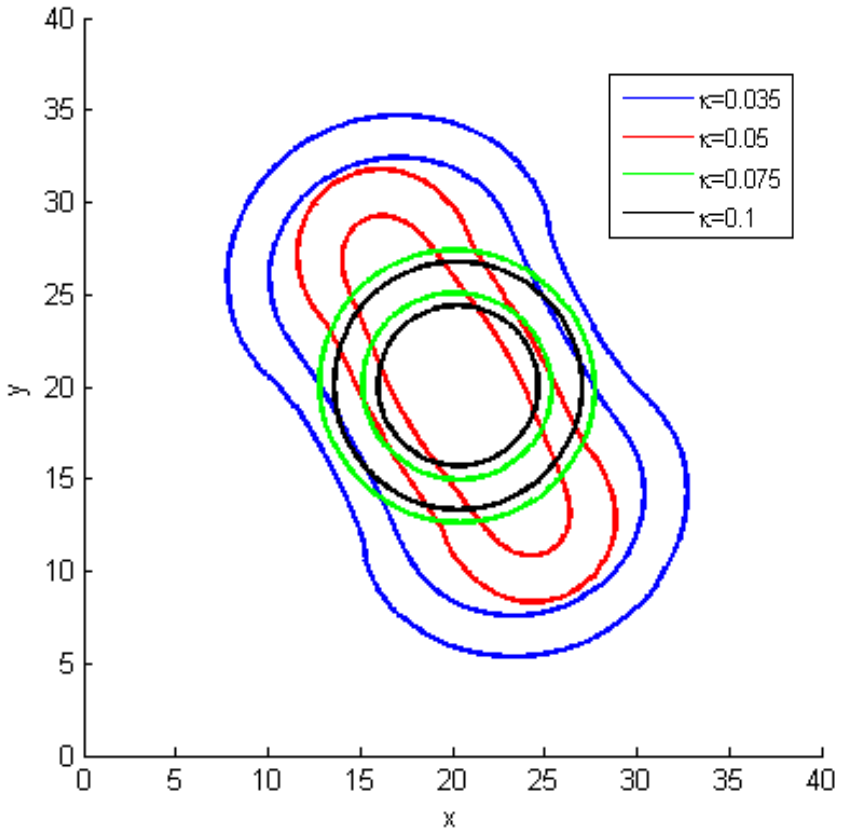

Figure C.26: Contours of the viable cells at $\phi_V = 0.5$ for $\bar{\phi}_W^H = 1.0$ with $\kappa = 0.035$ and $\kappa = 0.15$ at $t = 400$

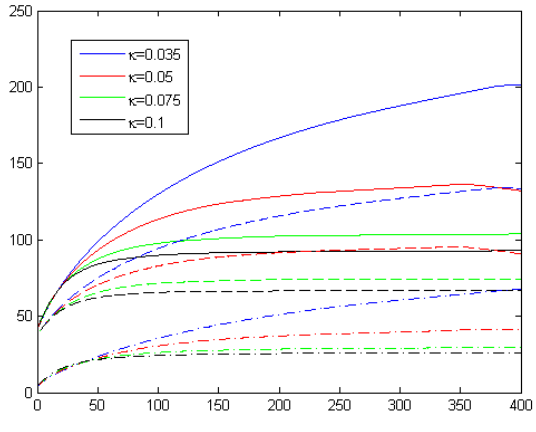

(a) ϕ_V (dashed line), ϕ_D (dash dot line), and ϕ_T (solid line)

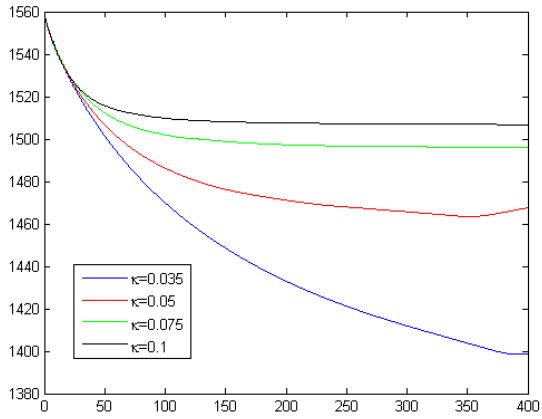

(b) water ϕ_W

Figure C.27: Total volume of $\bar{\phi}_W^H = 1.0$ with κ variations

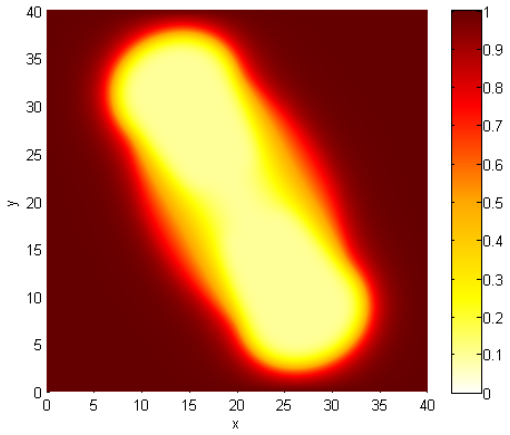

Figure C.28: nutrient concentration for $\bar{\phi}_W^H = 1.0$ with $\kappa = 0.035$ at $t = 400$

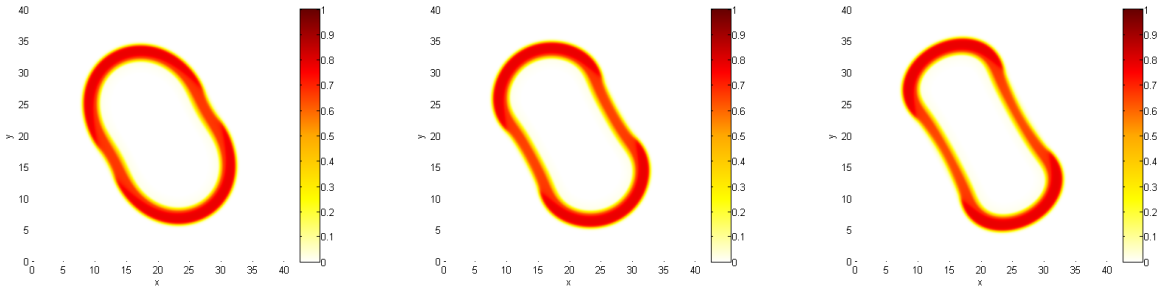

(a) viable cells ϕ_V, $t = 380$ (b) viable cells ϕ_V, $t = 400$ (c) viable cells ϕ_V, $t = 420$

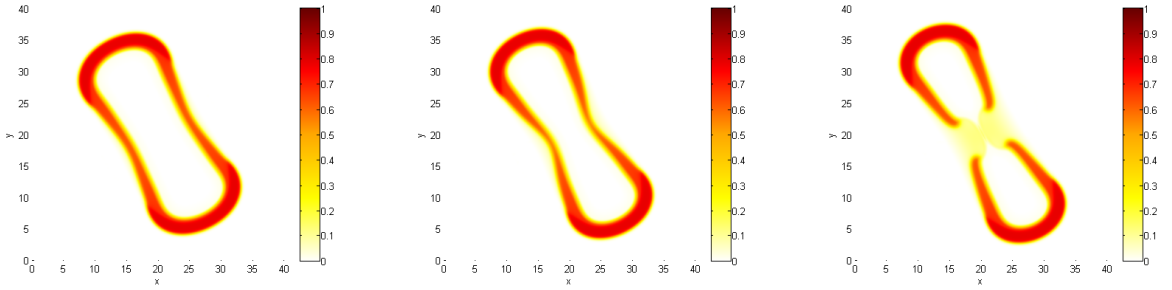

(d) viable cells ϕ_V, $t = 440$ (e) viable cells ϕ_V, $t = 460$ (f) viable cells ϕ_V, $t = 480$

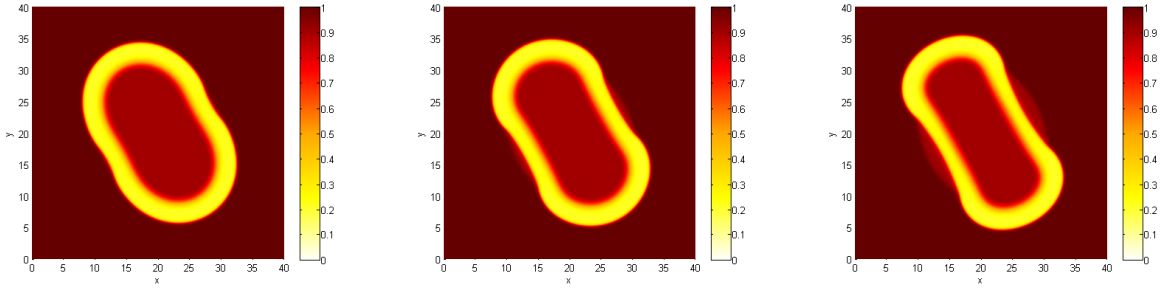

(g) water ϕ_W, $t = 380$ (h) water ϕ_W, $t = 400$ (i) water ϕ_W, $t = 420$

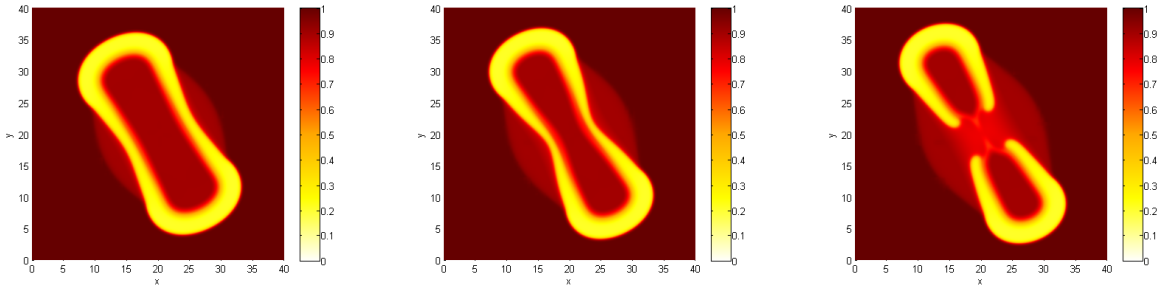

(j) water ϕ_W, $t = 440$ (k) water ϕ_W, $t = 460$ (l) water ϕ_W, $t = 480$

Figure C.29: viable cells and water for the vitro $\kappa = 0.035$ case

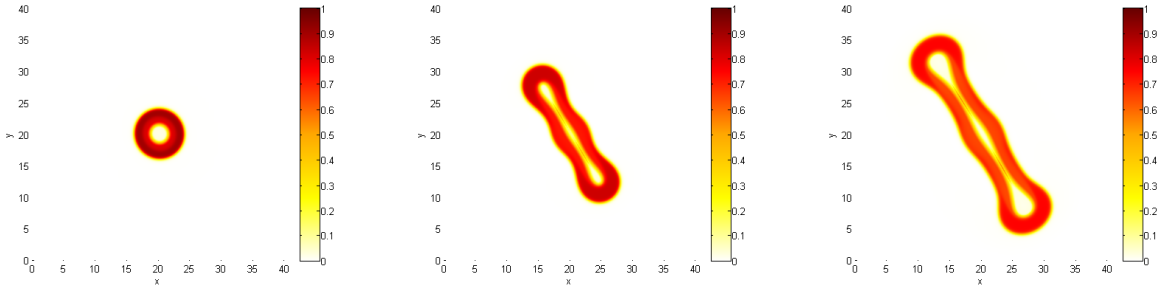

(a) viable cells ϕ_V, $\bar{\phi}_W^V = 0.1$ (b) viable cells ϕ_V, $\bar{\phi}_W^V = 0.2$ (c) viable cells ϕ_V, $\bar{\phi}_W^V = 0.3$

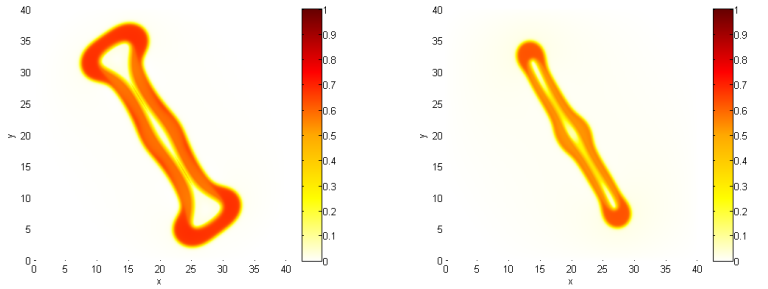

(d) viable cells ϕ_V, $\bar{\phi}_W^V = 0.4$ (e) viable cells ϕ_V, $\bar{\phi}_W^V = 0.5$

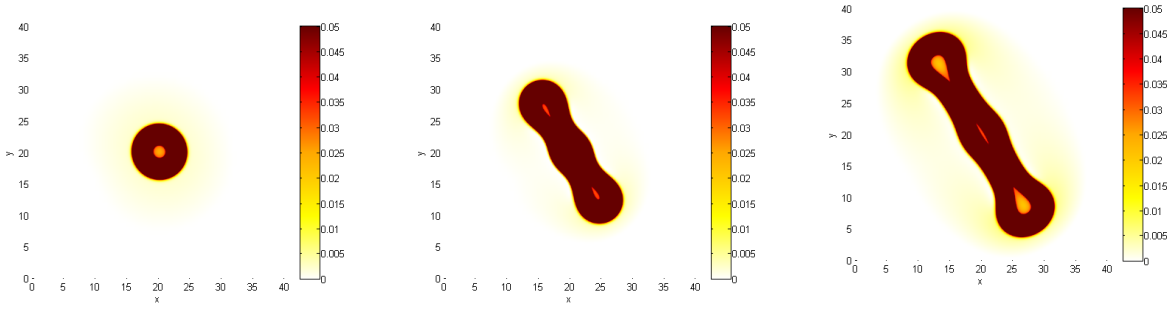

(f) viable cell shedding $\bar{\phi}_W^V = 0.1$(g) viable cell shedding $\bar{\phi}_W^V = 0.2$(h) viable cell shedding $\bar{\phi}_W^V = 0.3$

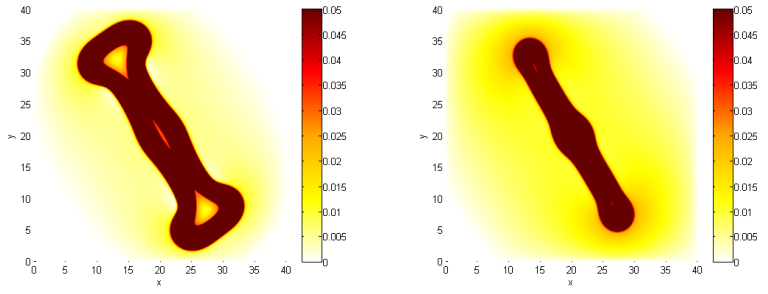

(i) viable cell shedding $\bar{\phi}_W^V = 0.4$(j) viable cell shedding $\bar{\phi}_W^V = 0.5$

Figure C.30: viable cells of $\bar{\phi}_W^V$ variations and the cell shedding at $t = 250$

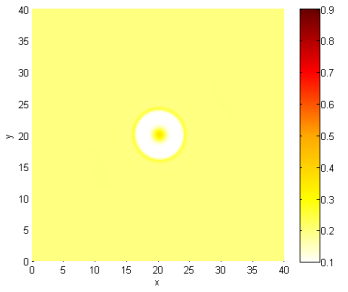

(a) water ϕ_W, $\bar{\phi}_W^V = 0.1$

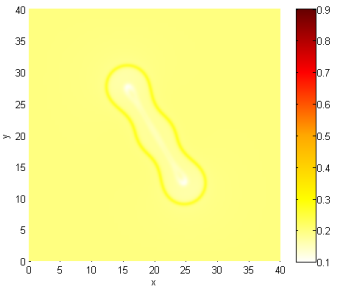

(b) water ϕ_W, $\bar{\phi}_W^V = 0.2$

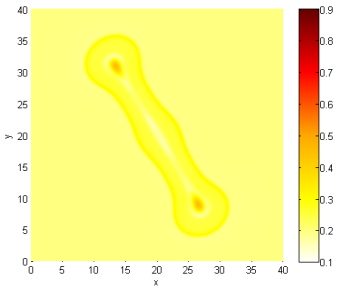

(c) water ϕ_W, $\bar{\phi}_W^V = 0.3$

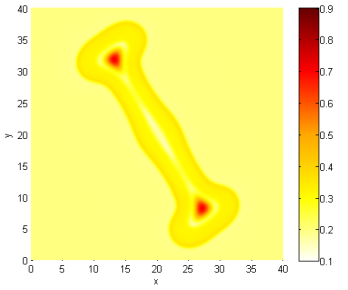

(d) water ϕ_W, $\bar{\phi}_W^V = 0.4$

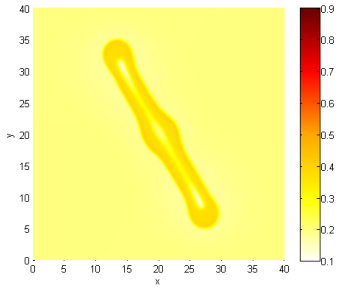

(e) water ϕ_W, $\bar{\phi}_W^V = 0.5$

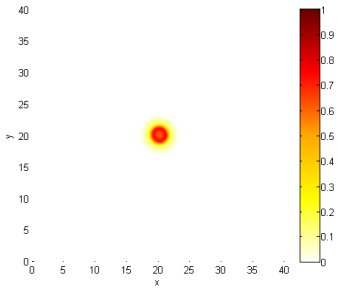

(f) dead cells ϕ_D, $\bar{\phi}_W^V = 0.1$

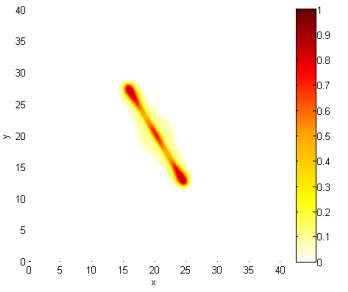

(g) dead cells ϕ_D, $\bar{\phi}_W^V = 0.2$

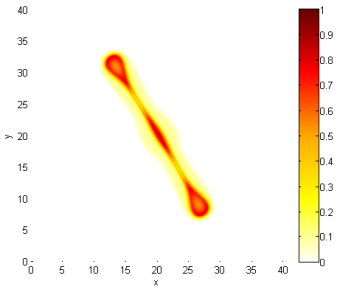

(h) dead cells ϕ_D, $\bar{\phi}_W^V = 0.3$

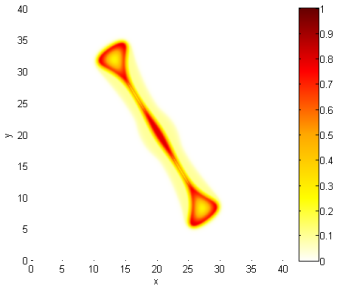

(i) dead cells ϕ_D, $\bar{\phi}_W^V = 0.4$

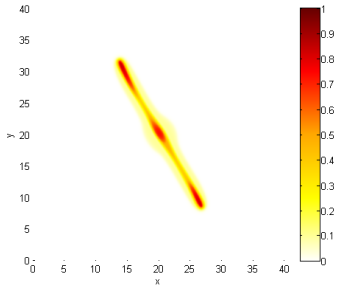

(j) dead cells ϕ_D, $\bar{\phi}_W^V = 0.5$

Figure C.31: water and dead cells of $\bar{\phi}_W^V$ variations at $t = 250$

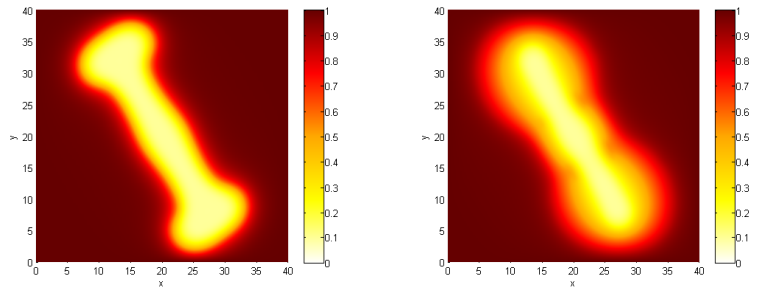

(a) nutrients C_0, $\bar{\phi}_W^V = 0.4$ (b) nutrients C_0, $\bar{\phi}_W^V = 0.5$

Figure C.32: nutrient levels of $\bar{\phi}_W^V = 0.4$ and $\bar{\phi}_W^V = 0.4$ at $t = 250$

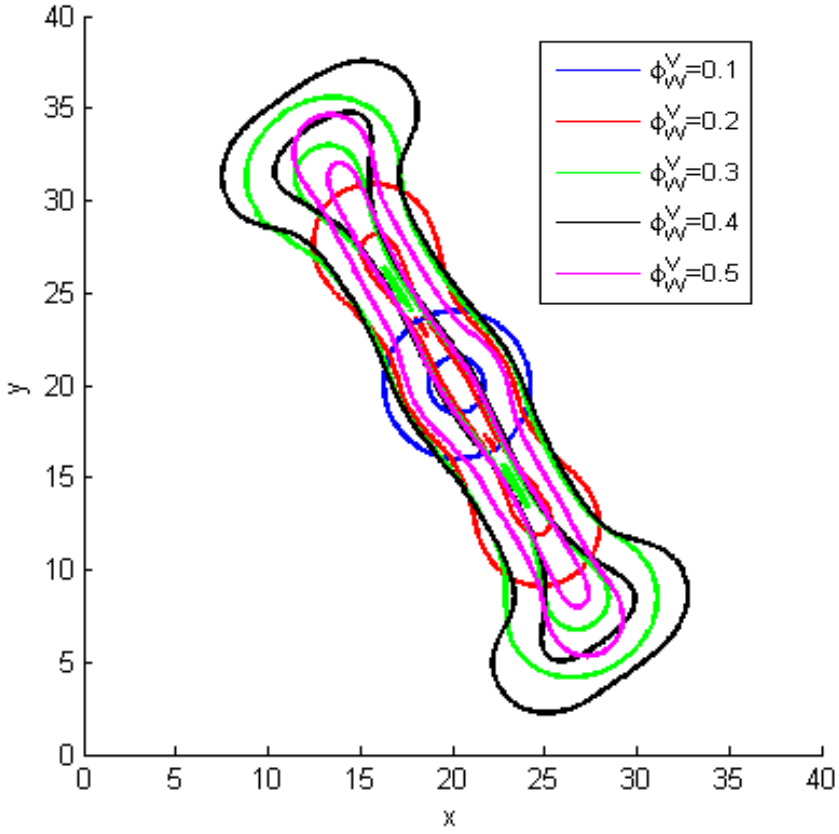

Figure C.33: Contours of the viable cells at $\phi_V = 0.5$ for $\bar{\phi}_W^V$ variations at $t = 250$

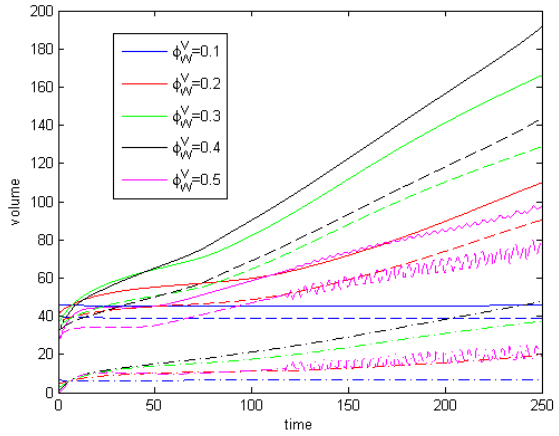

(a) ϕ_V (dashed line), ϕ_D (dash dot line), and ϕ_T (solid line)

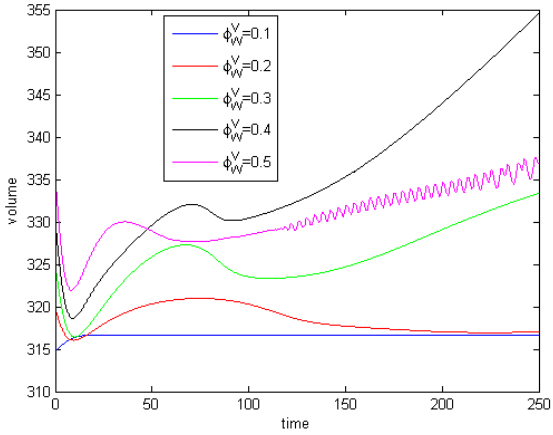

(b) water ϕ_W

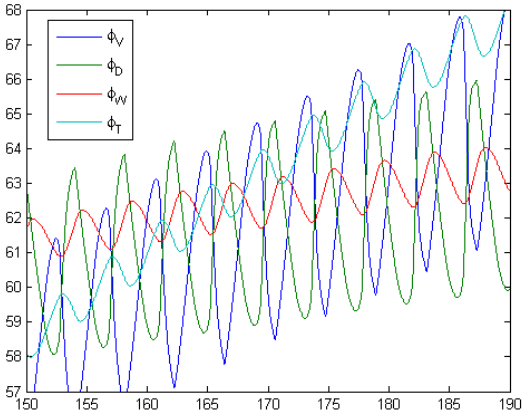

(c) total tumor volume closeup

Figure C.34: Total volume of $\bar{\phi}_W^V$ variations

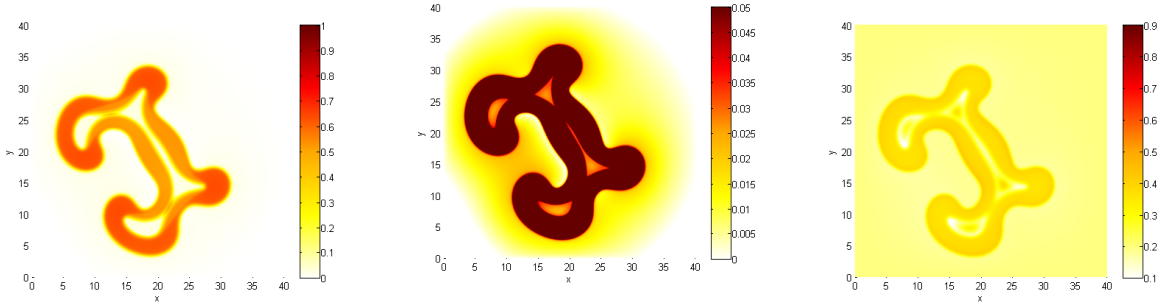

(a) viable cells ϕ_V, $\bar{\phi}_W^V = 0.5$ (b) viable cell shedding, $\bar{\phi}_W^V = 0.5$ (c) water ϕ_W, $\bar{\phi}_W^V = 0.5$

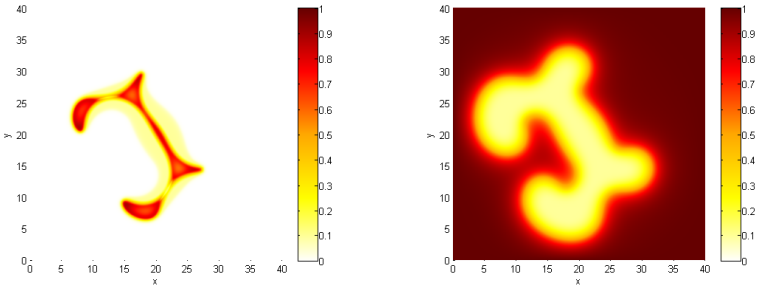

(d) dead cells ϕ_D, $\bar{\phi}_W^V = 0.5$ (e) nutrients ϕ_D, $\bar{\phi}_W^V = 0.5$

Figure C.35: $\bar{\phi}_W^V = 0.5$ at $t = 150$ with $Q(\phi_T) = 0.03$

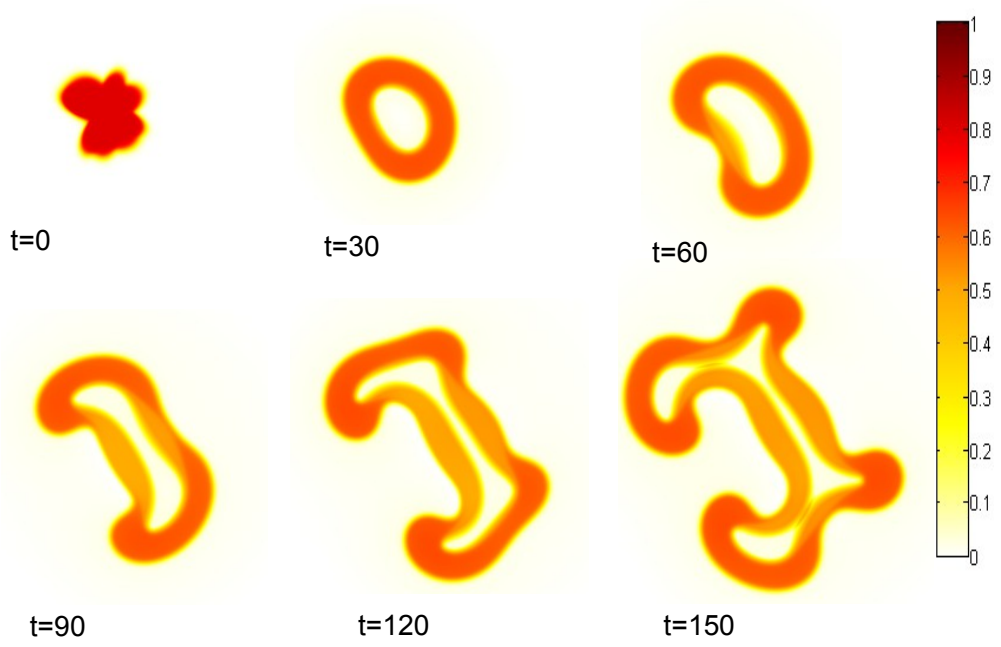

Figure C.36: evolution of viable cells for $\bar{\phi}_W^V = 5.0$ and $Q(\phi_T) = 0.03$

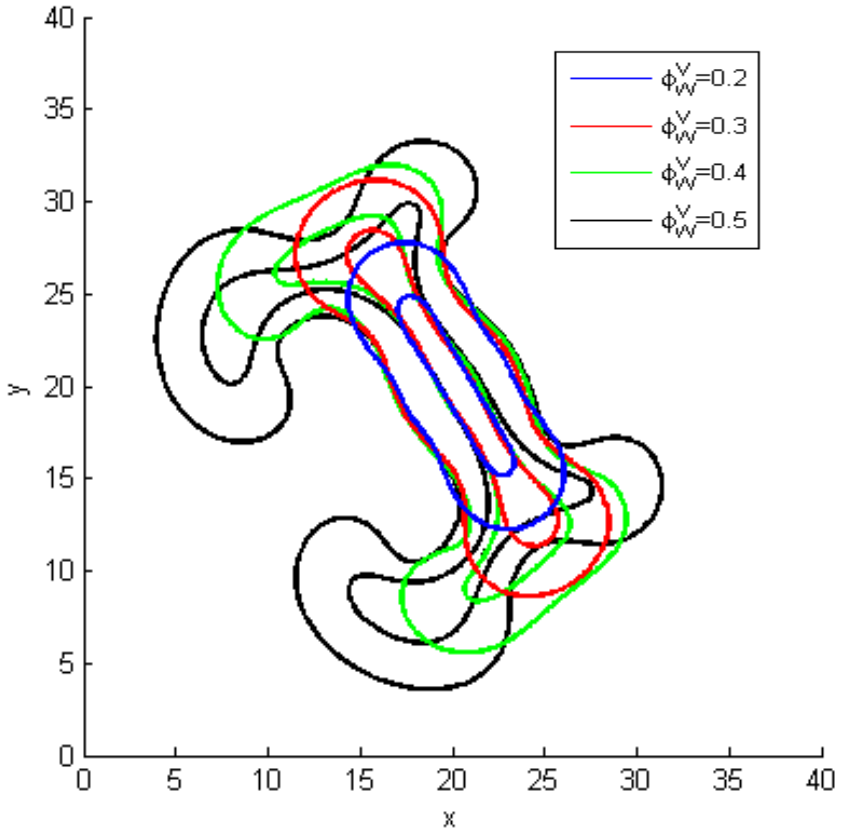

Figure C.37: Contours of the viable cells at $\phi_V = 0.5$ for $\bar{\phi}_W^V$ variations at $t = 150$

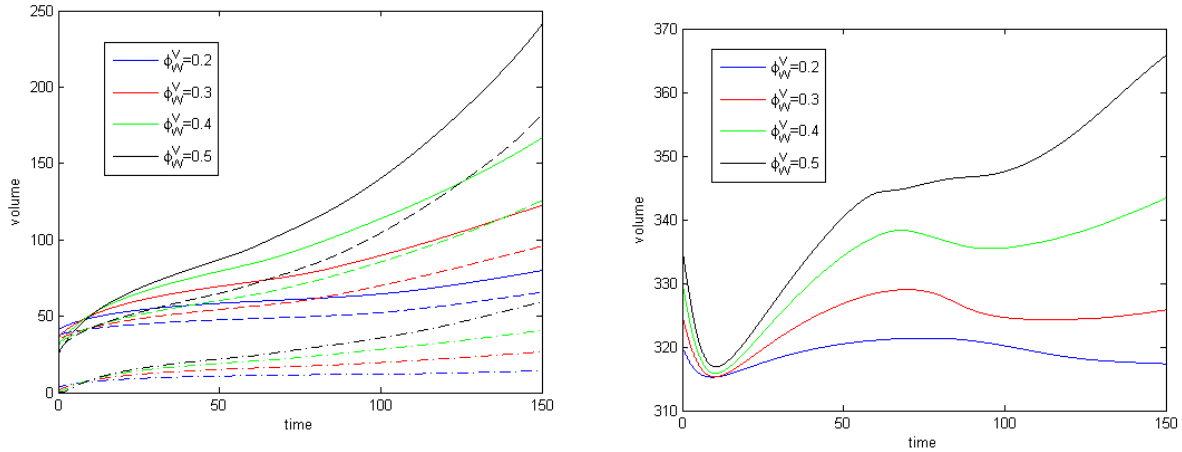

(a) ϕ_V (dashed line), ϕ_D (dash dot line), and ϕ_T (solid line)

(b) water ϕ_W

Figure C.38: Total volume of $\bar{\phi}_W^V$ variations

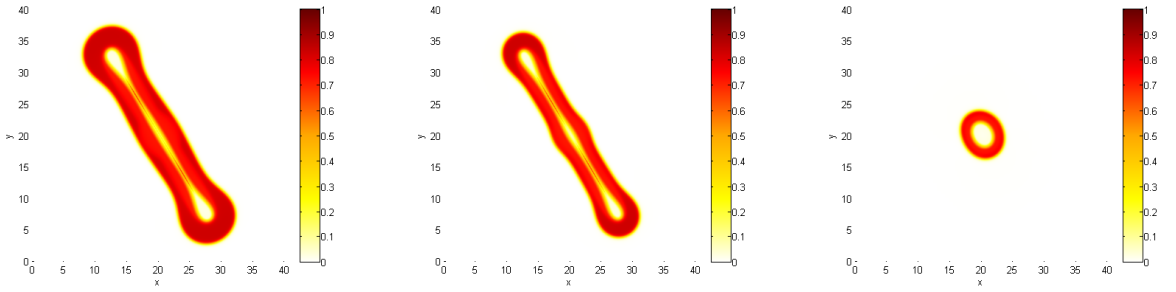

(a) viable cells ϕ_V, $\bar{C}_0 = 0.05$ (b) viable cells ϕ_V, $\bar{C}_0 = 0.10$ (c) viable cells ϕ_V, $\bar{C}_0 = 0.20$

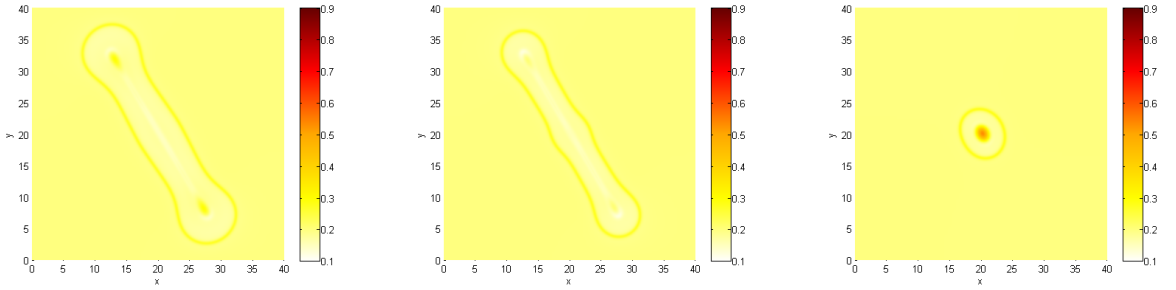

(d) water ϕ_W, $\bar{C}_0 = 0.05$ (e) water ϕ_W, $\bar{C}_0 = 0.10$ (f) water ϕ_W, $\bar{C}_0 = 0.20$

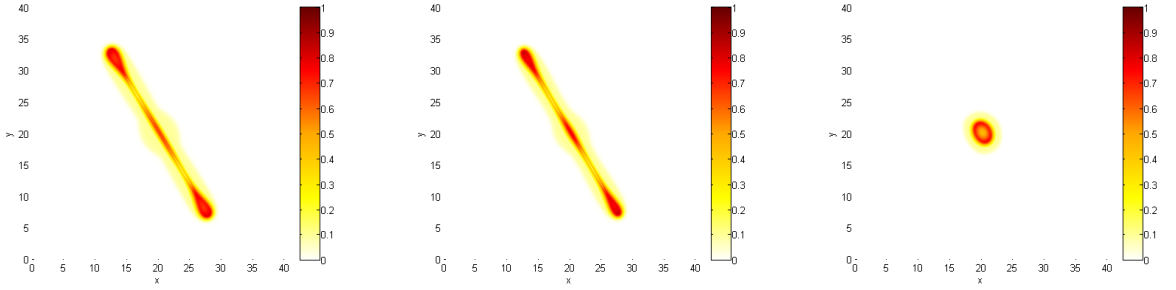

(g) dead cells ϕ_D, $\bar{C}_0 = 0.05$ (h) dead cells ϕ_D, $\bar{C}_0 = 0.10$ (i) dead cells ϕ_D, $\bar{C}_0 = 0.20$

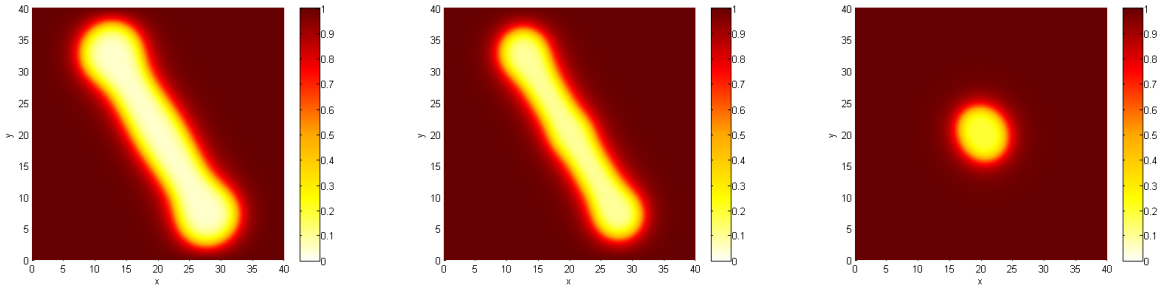

(j) nutrient level C_0, $\bar{C}_0 = 0.05$ (k) nutrient level C_0, $\bar{C}_0 = 0.10$ (l) nutrient level C_0, $\bar{C}_0 = 0.20$

Figure C.39: cell types of $\bar{C}_0$ variations at $t = 400$

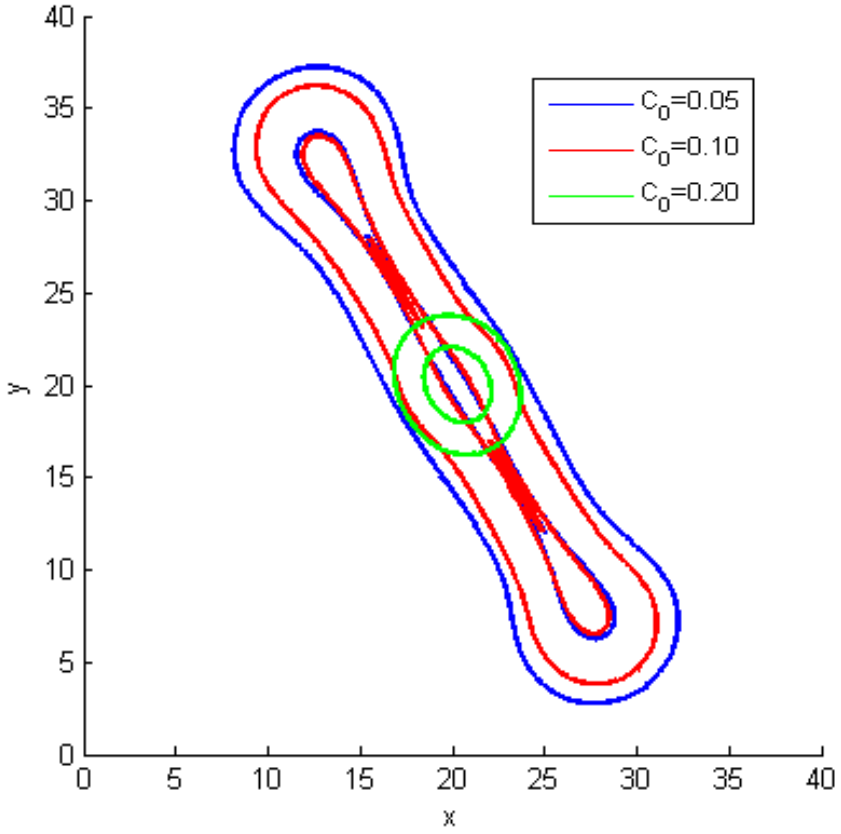

Figure C.40: Contours of the viable cells at $\phi_V = 0.5$ for $\bar{C}_0$ variations

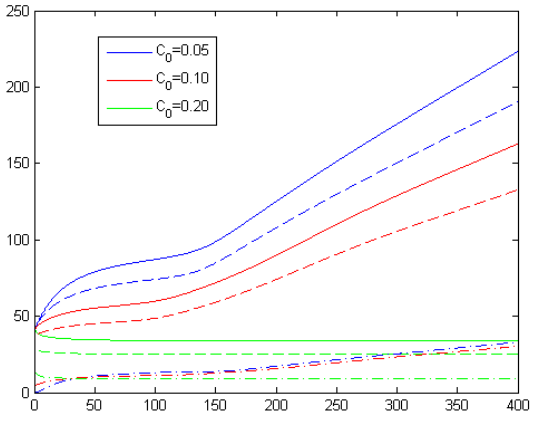

(a) ϕ_V (dashed line), ϕ_D (dash dot line), and ϕ_T (solid line)

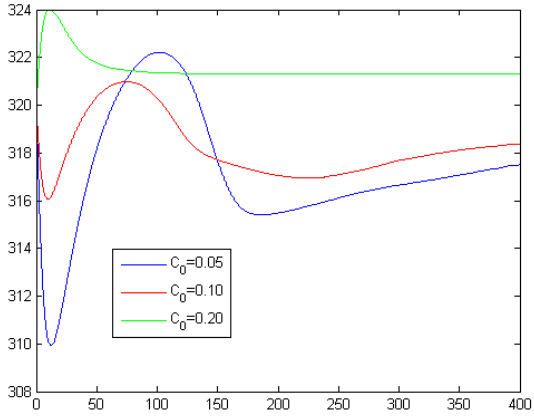

(b) water ϕ_W

Figure C.41: Total volume of $\bar{C}_0$ variations

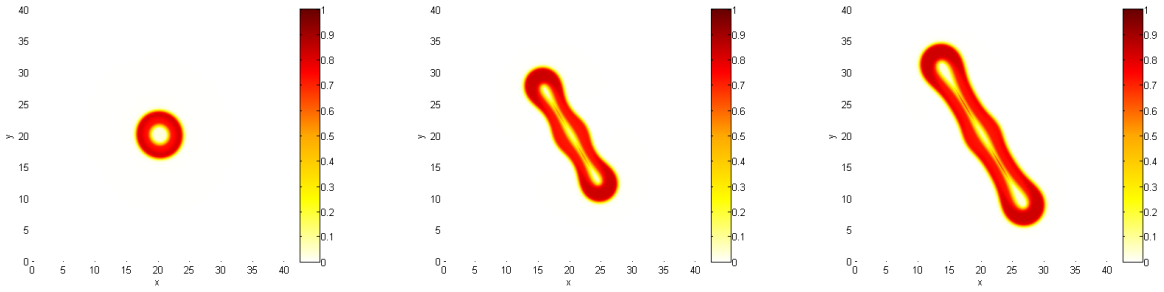

(a) viable cells ϕ_V, $\nu_{PO} = 0.1$ (b) viable cells ϕ_V, $\nu_{PO} = 0.25$ (c) viable cells ϕ_V, $\nu_{PO} = 0.5$

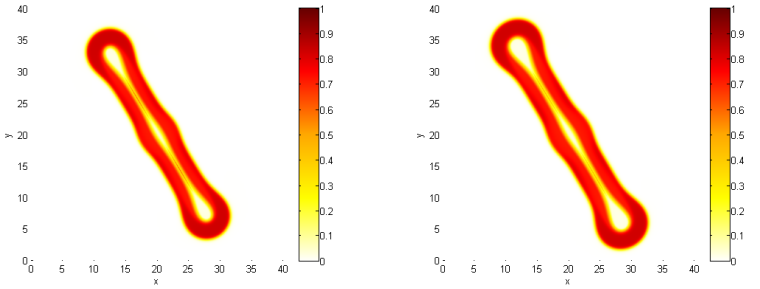

(d) viable cells ϕ_V, $\nu_{PO} = 1.0$ (e) viable cells ϕ_V, $\nu_{PO} = 2.0$

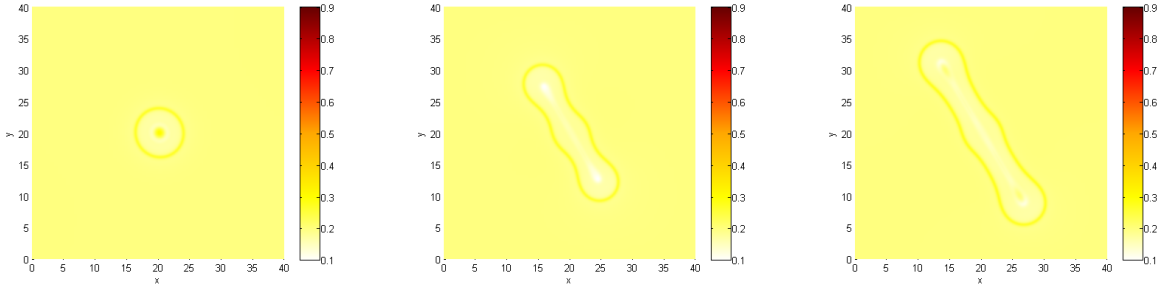

(f) water ϕ_W, $\nu_{PO} = 0.1$ (g) water ϕ_W, $\nu_{PO} = 0.25$ (h) water ϕ_W, $\nu_{PO} = 0.5$

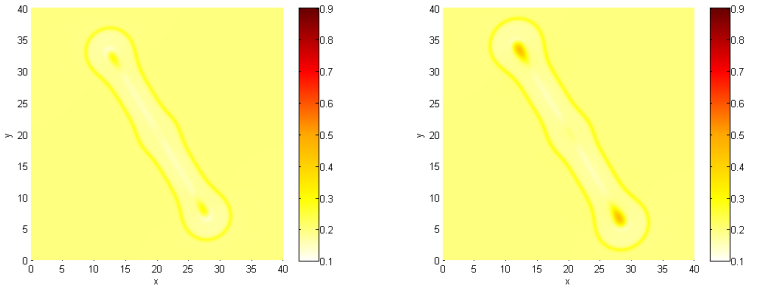

(i) water ϕ_W, $\nu_{PO} = 1.0$ (j) water ϕ_W, $\nu_{PO} = 2.0$

Figure C.42: water and viable cells of ν_{PO} variations at $t = 350$

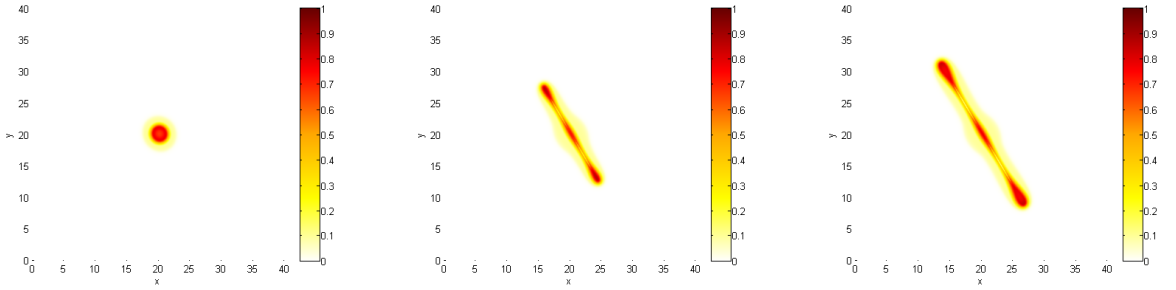

(a) dead cells ϕ_D, $\nu_{PO} = 0.1$ (b) dead cells ϕ_D, $\nu_{PO} = 0.25$ (c) dead cells ϕ_D, $\nu_{PO} = 0.5$

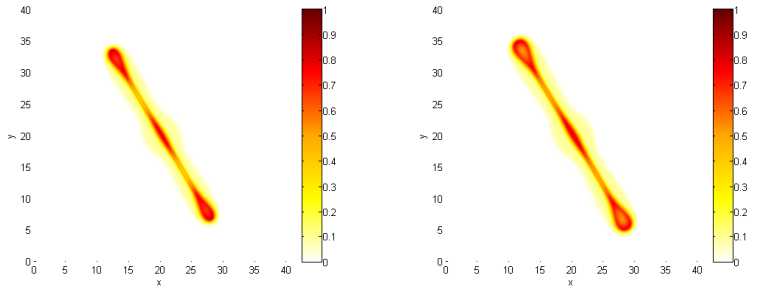

(d) dead cells ϕ_D, $\nu_{PO} = 1.0$ (e) dead cells ϕ_D, $\nu_{PO} = 2.0$

Figure C.43: dead cells of ν_{PO} variations at $t = 350$

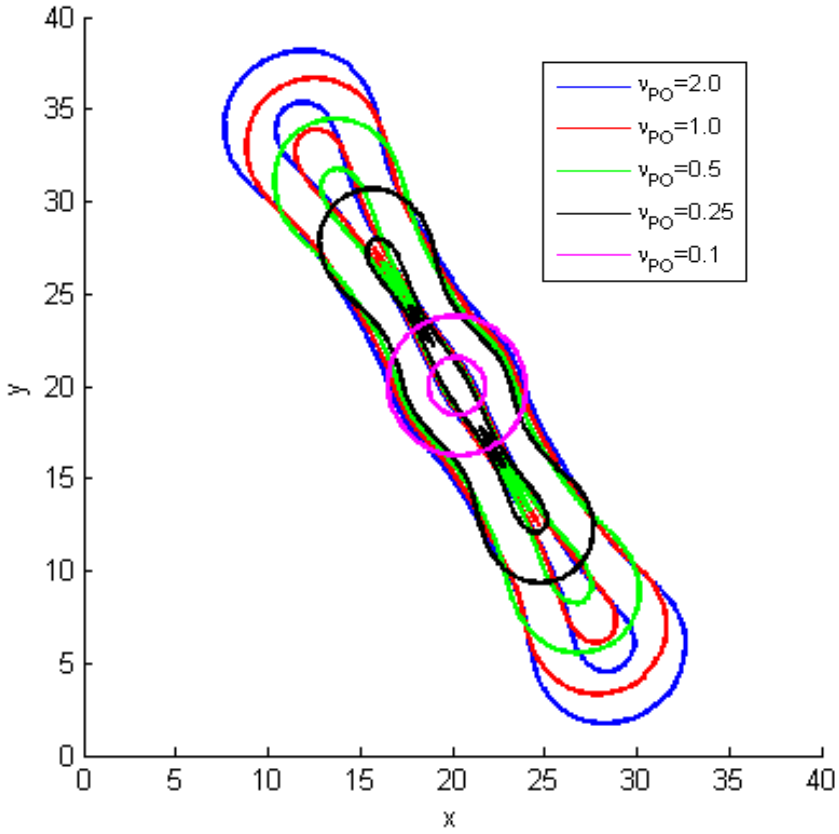

Figure C.44: Contours of the viable cells at $\phi_V = 0.5$ for ν_{PO} variations at $t = 350$

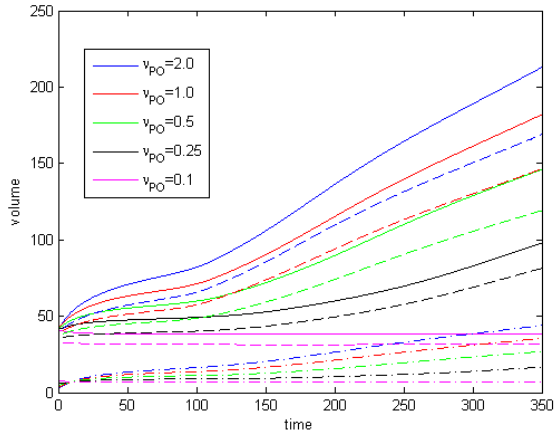

(a) ϕ_V (dashed line), ϕ_D (dash dot line), and ϕ_T (solid line)

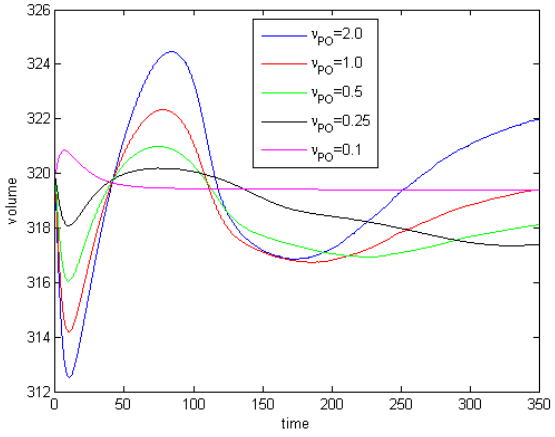

(b) water ϕ_W

Figure C.45: Total volume of ν_{PO} variations

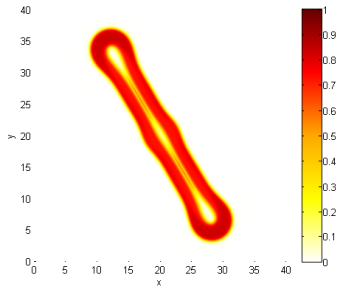

(a) viable cells ϕ_V, $M_W = 400$

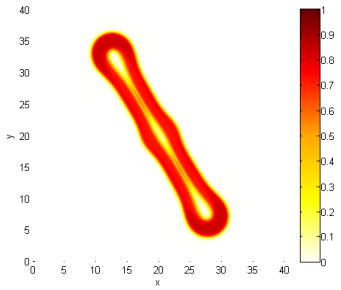

(b) viable cells ϕ_V, $M_W = 200$

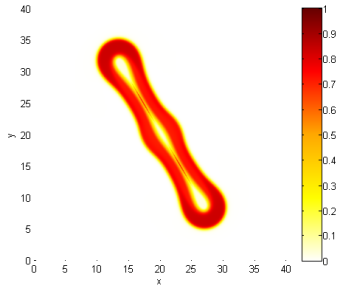

(c) viable cells ϕ_V, $M_W = 100$

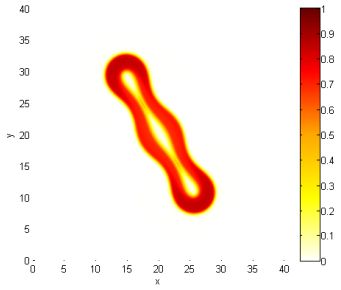

(d) viable cells ϕ_V, $M_W = 50$

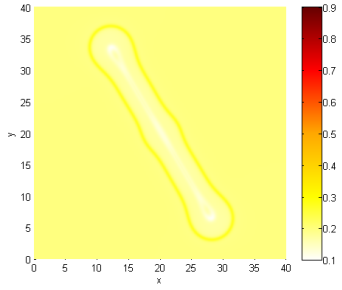

(e) water ϕ_W, $M_W = 400$

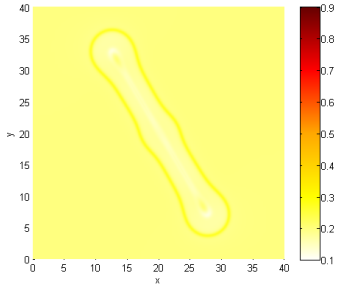

(f) water ϕ_W, $M_W = 200$

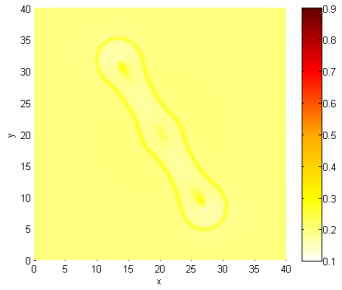

(g) water ϕ_W, $M_W = 100$

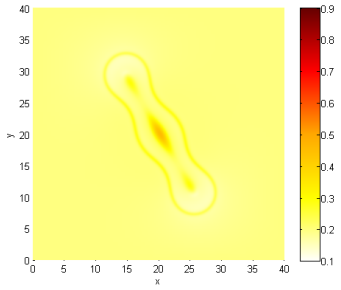

(h) water ϕ_W, $M_W = 50$

Figure C.46: water and viable cells of M_W variations at $t = 400$

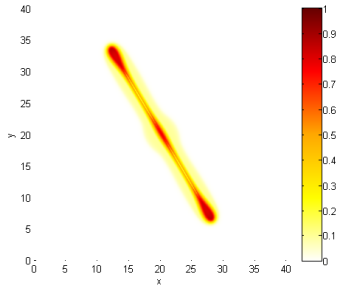

(a) dead cells ϕ_D, $M_W = 400$

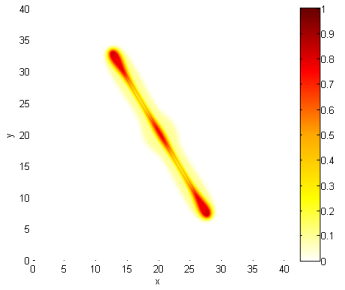

(b) dead cells ϕ_D, $M_W = 200$

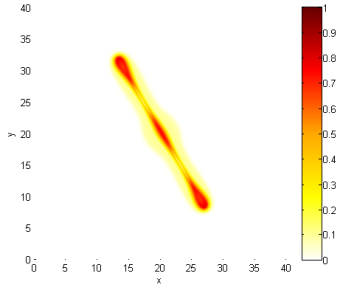

(c) dead cells ϕ_D, $M_W = 100$

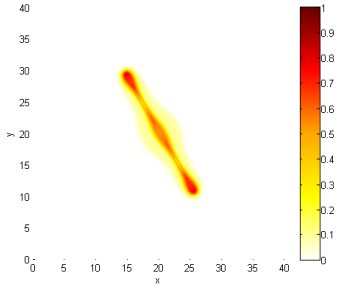

(d) dead cells ϕ_D, $M_W = 50$

Figure C.47: dead cells of M_W variations at $t = 400$

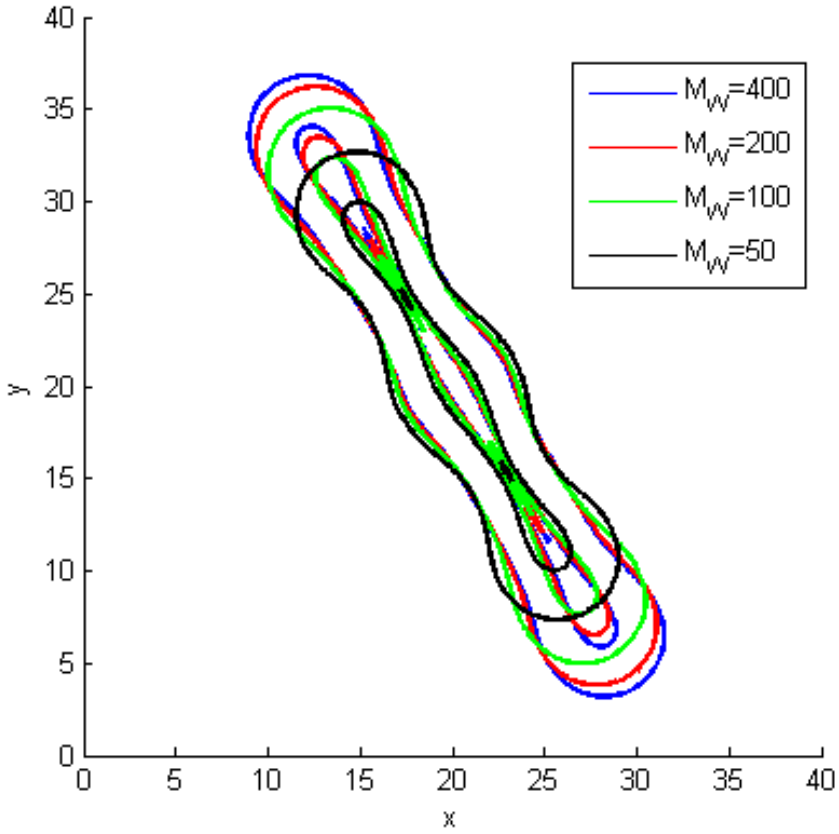

Figure C.48: Contours of the viable cells at $\phi_V = 0.5$ for M_W variations

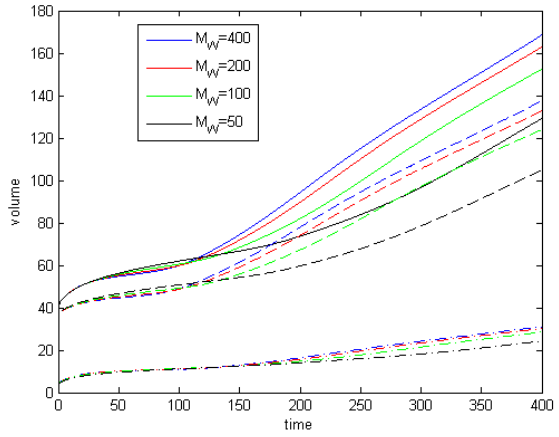

(a) ϕ_V (dashed line), ϕ_D (dash dot line), and ϕ_T (solid line)

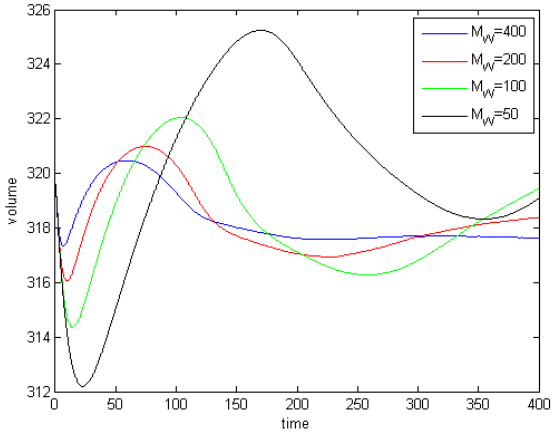

(b) water ϕ_W

Figure C.49: Total volume of M_W variations

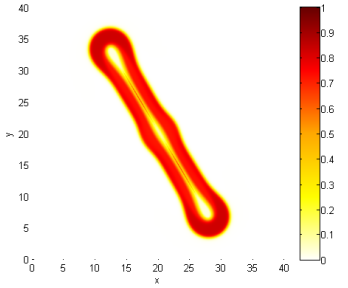

(a) viable cells ϕ_V, $\gamma = -0.5$

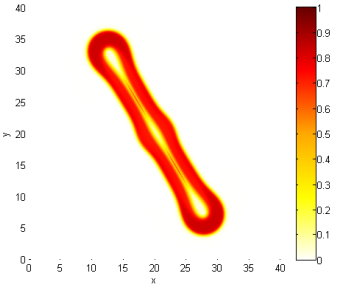

(b) viable cells ϕ_V, $\gamma = -0.1$

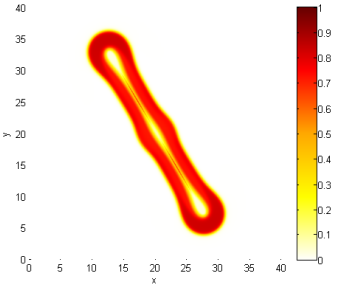

(c) viable cells ϕ_V, $\gamma = 0.0$

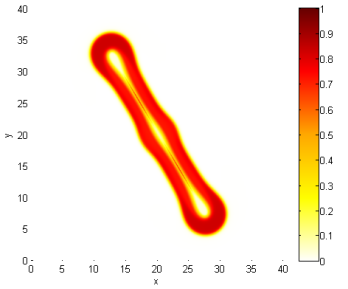

(d) viable cells ϕ_V, $\gamma = 0.1$

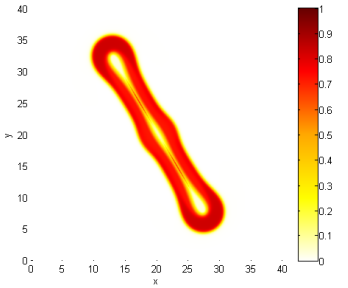

(e) viable cells ϕ_V, $\gamma = 0.5$

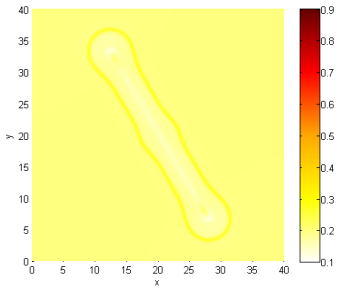

(f) water ϕ_W, $\gamma = -0.5$

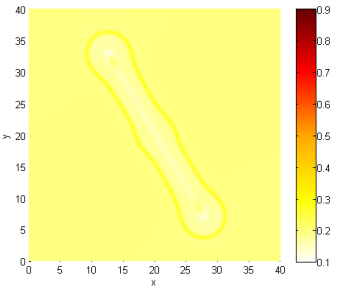

(g) water ϕ_W, $\gamma = -0.1$

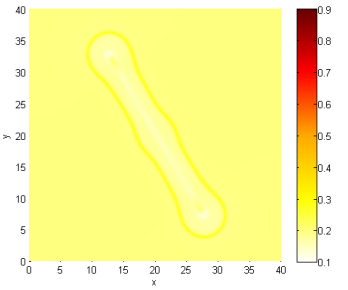

(h) water ϕ_W, $\gamma = 0.0$

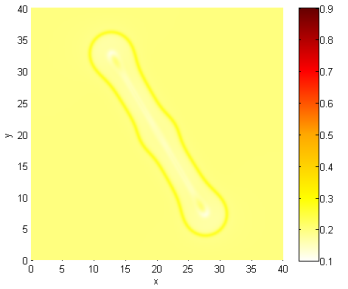

(i) water ϕ_W, $\gamma = 0.1$

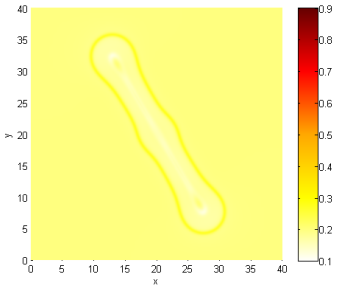

(j) water ϕ_W, $\gamma = 0.5$

Figure C.50: water and viable cells of γ variations at $t = 400$

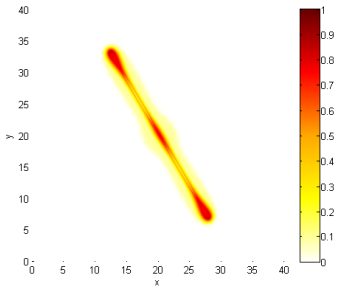

(a) dead cells ϕ_D, $\gamma = -0.5$

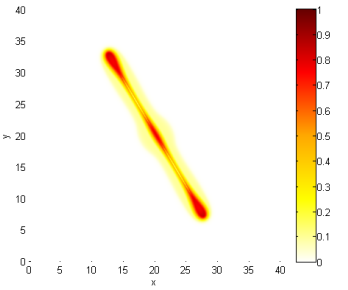

(b) dead cells ϕ_D, $\gamma = -0.1$

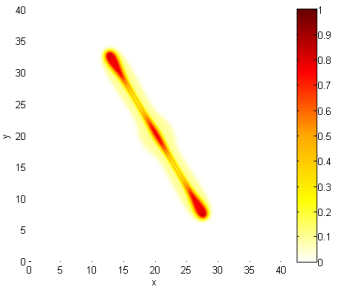

(c) dead cells ϕ_D, $\gamma = 0.0$

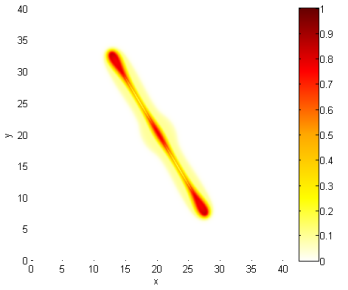

(d) dead cells ϕ_D, $\gamma = 0.1$

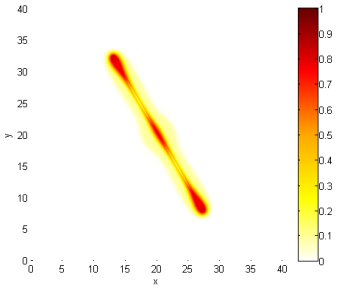

(e) dead cells ϕ_D, $\gamma = 0.5$

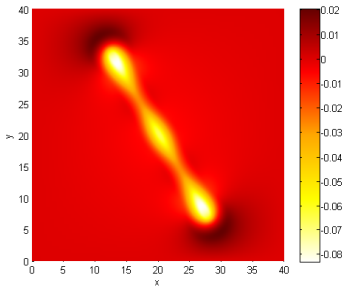

(f) pressure p, $\gamma = -0.5$

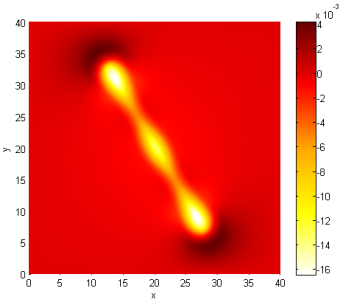

(g) pressure p, $\gamma = -0.1$

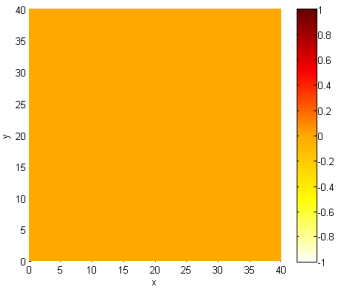

(h) pressure p, $\gamma = 0.0$

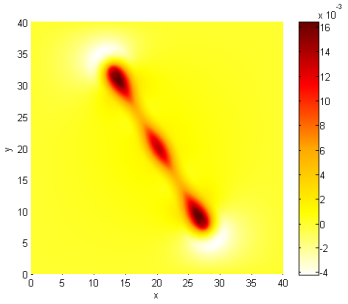

(i) pressure p, $\gamma = 0.1$

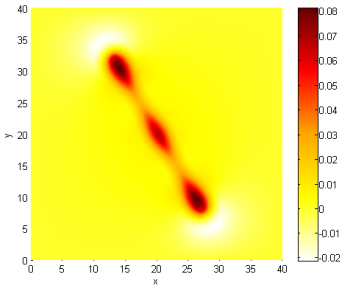

(j) pressure p, $\gamma = 0.5$

Figure C.51: dead cells and pressure for γ variations at $t = 400$

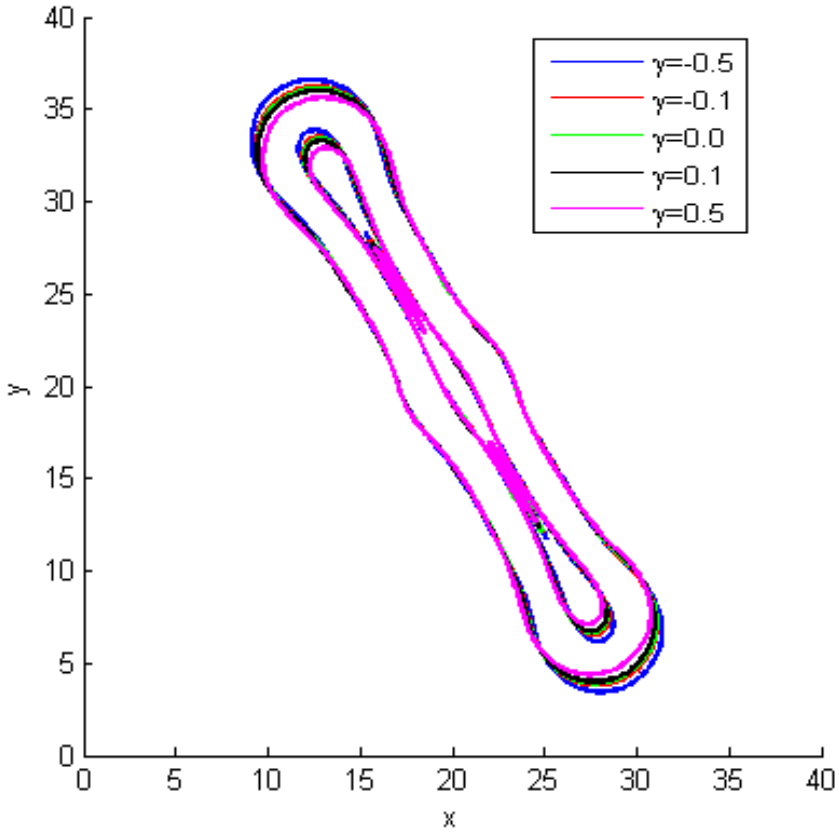

Figure C.52: Contours of the viable cells at $\phi_V = 0.5$ for γ variations at $t = 400$

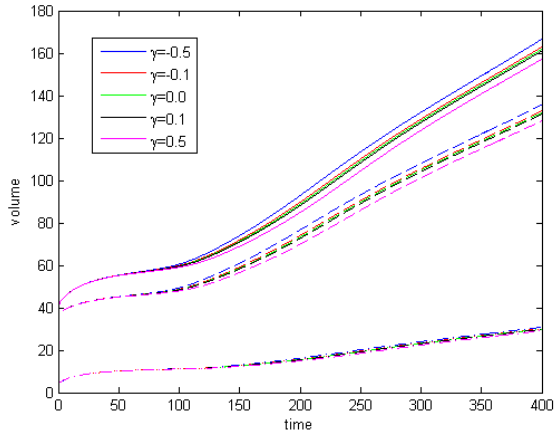

(a) ϕ_V (dashed line), ϕ_D (dash dot line), and ϕ_T (solid line)

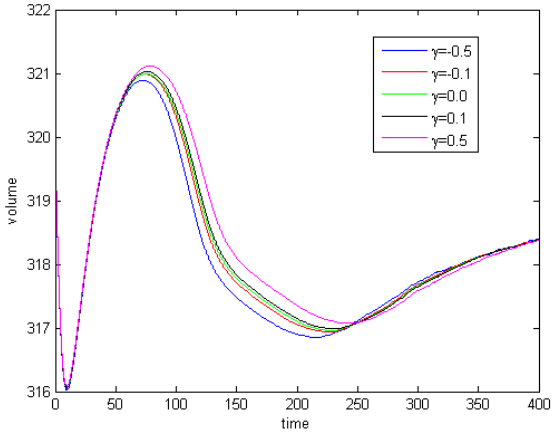

(b) water ϕ_W

Figure C.53: Total volume of γ variations

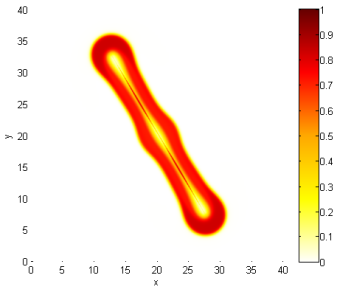

(a) viable cells ϕ_V, $\lambda_n = 25.0$

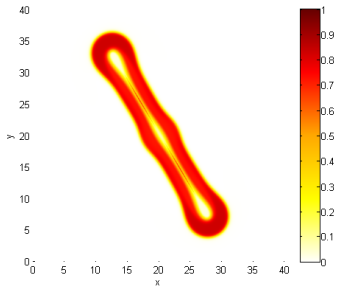

(b) viable cells ϕ_V, $\lambda_n = 5.0$

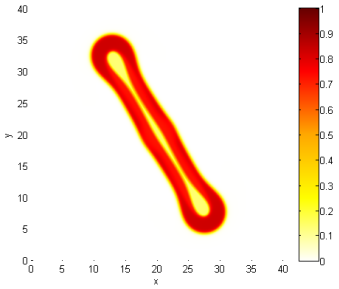

(c) viable cells ϕ_V, $\lambda_n = 1.0$

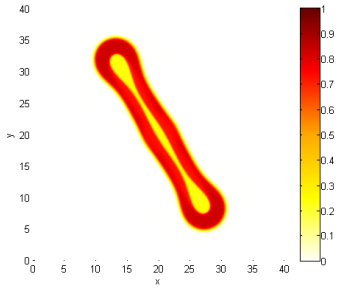

(d) viable cells ϕ_V, $\lambda_n = 0.5$

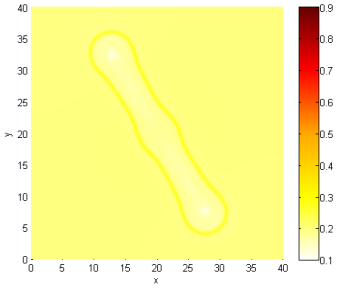

(e) water ϕ_W, $\lambda_n = 25.0$

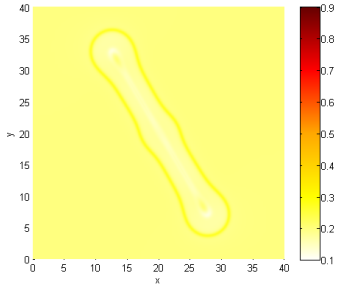

(f) water ϕ_W, $\lambda_n = 5.0$

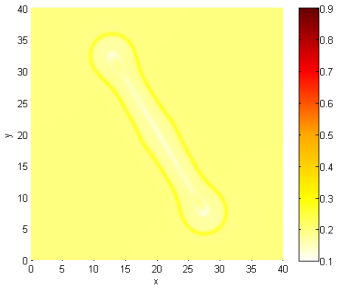

(g) water ϕ_W, $\lambda_n = 1.0$

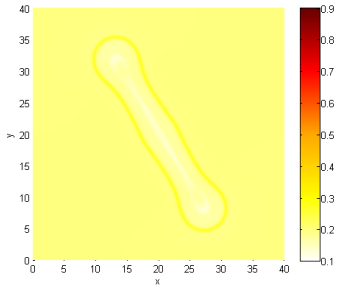

(h) water ϕ_W, $\lambda_n = 0.5$

Figure C.54: water and viable cells of λ_n variations at $t = 400$

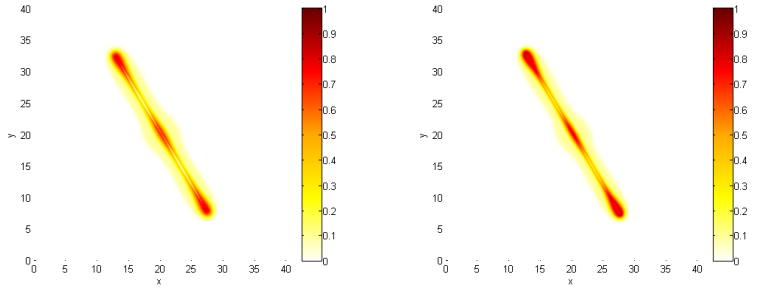

(a) dead cells ϕ_D, $\lambda_n = 25.0$ (b) dead cells ϕ_D, $\lambda_n = 5.0$

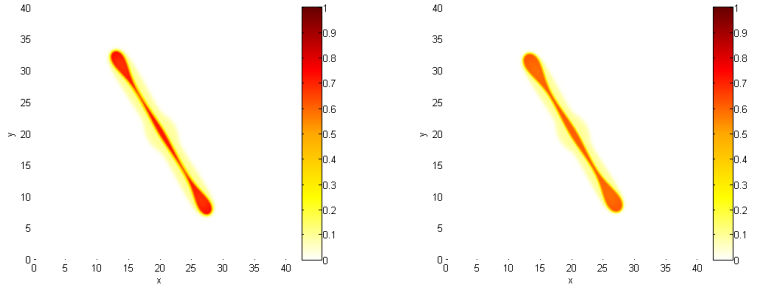

(c) dead cells ϕ_D, $\lambda_n = 1.0$ (d) dead cells ϕ_D, $\lambda_n = 0.5$

Figure C.55: dead cells of λ_n variations at $t = 400$

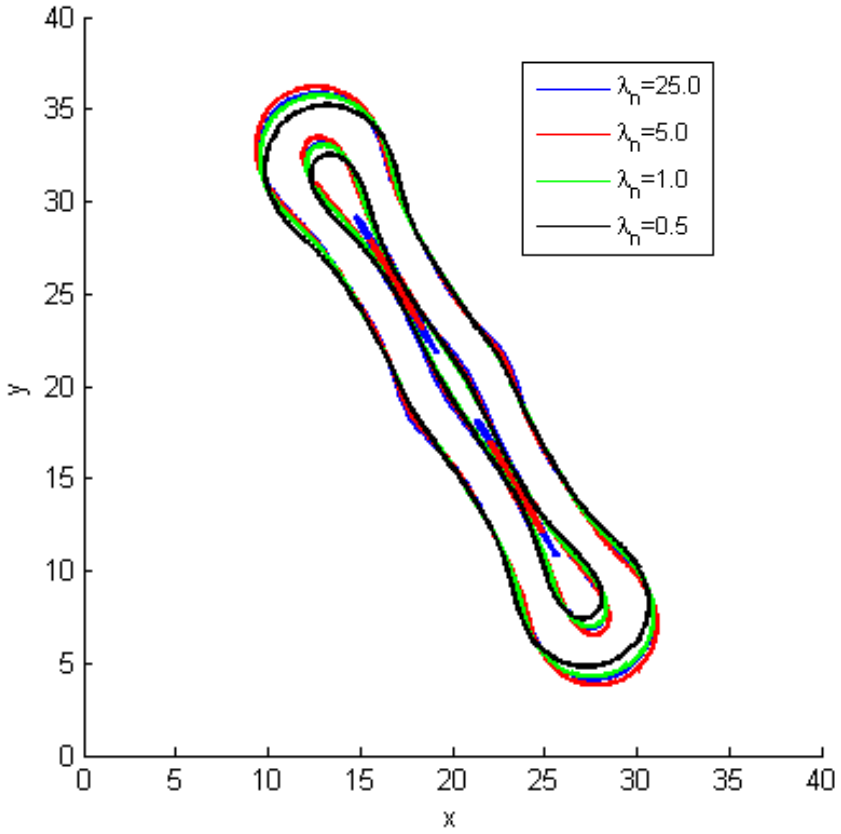

Figure C.56: Contours of the viable cells at $\phi_V = 0.5$ for λ_n variations

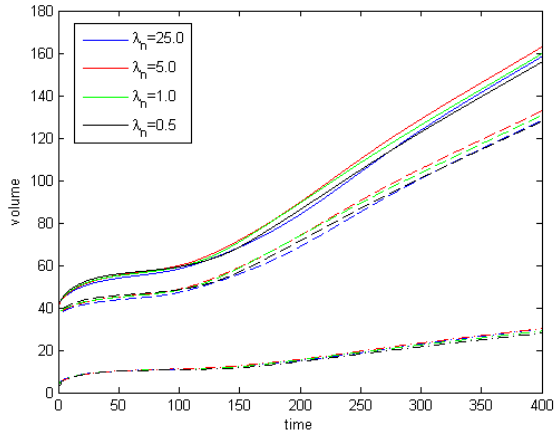

(a) ϕ_V (dashed line), ϕ_D (dash dot line), and ϕ_T (solid line)

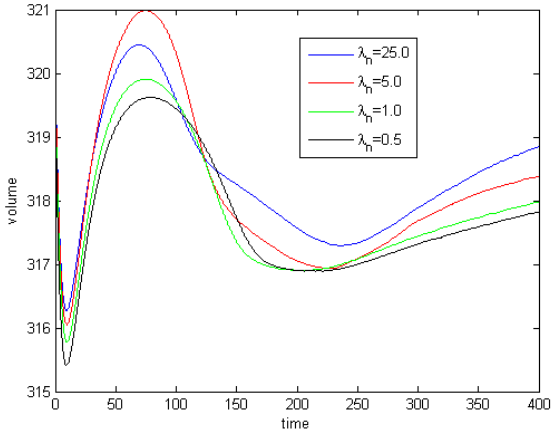

(b) water ϕ_W

Figure C.57: Total volume of λ_n variations

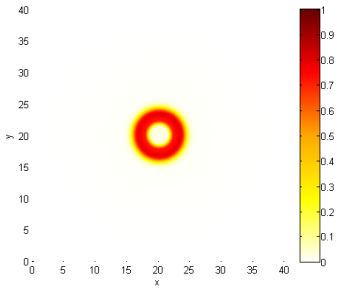

(a) viable cells ϕ_V, $\epsilon = 0.1$

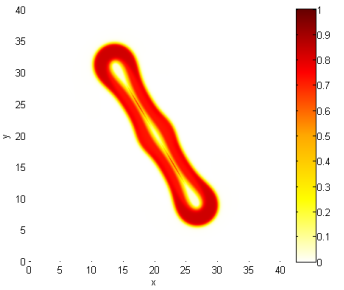

(b) viable cells ϕ_V, $\epsilon = 0.05$

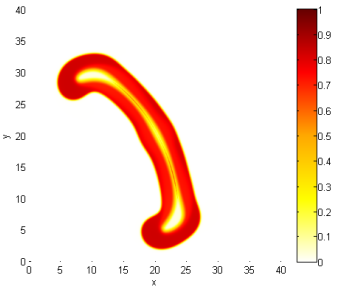

(c) viable cells ϕ_V, $\epsilon = 0.025$

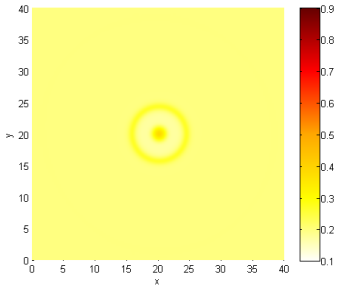

(d) water ϕ_W, $\epsilon = 0.1$

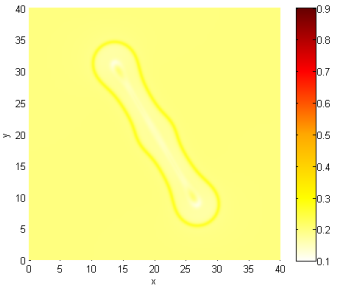

(e) water ϕ_W, $\epsilon = 0.05$

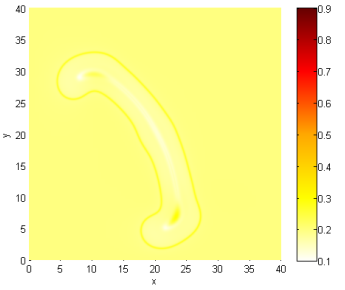

(f) water ϕ_W, $\epsilon = 0.025$

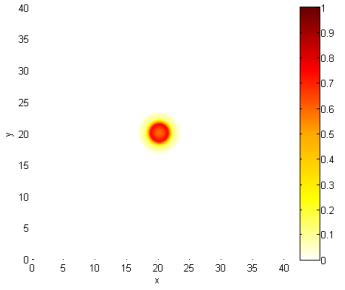

(g) dead cells ϕ_D, $\epsilon = 0.1$

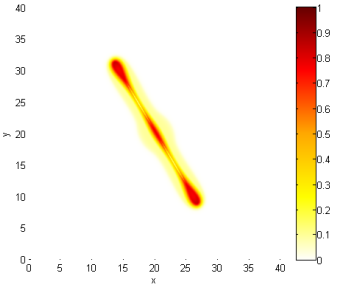

(h) dead cells ϕ_D, $\epsilon = 0.05$

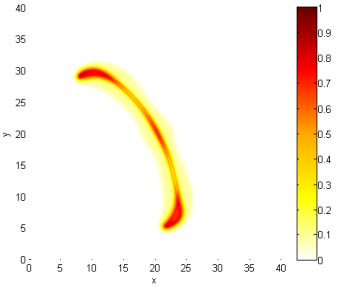

(i) dead cells ϕ_D, $\epsilon = 0.025$

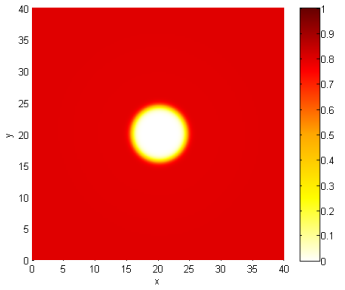

(j) host ϕ_H, $\epsilon = 0.1$

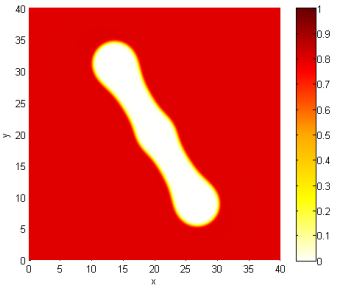

(k) host ϕ_H, $\epsilon = 0.05$

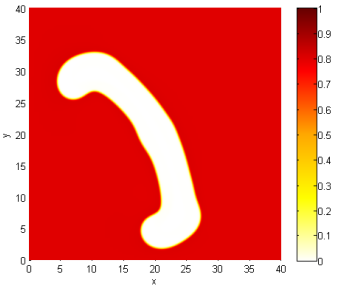

(l) host ϕ_H, $\epsilon = 0.025$

Figure C.58: cell types of ϵ variations at $t = 350$

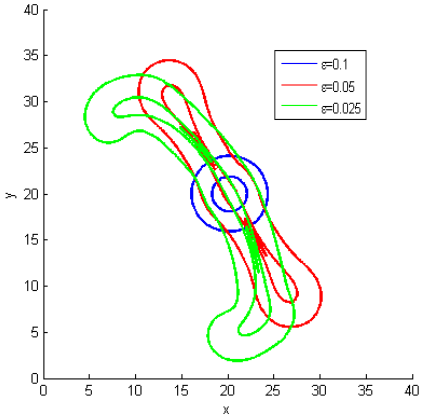

(a) contours for ϵ variation

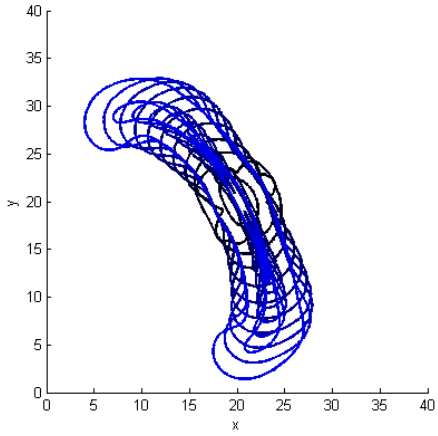

(b) contour evolution for $\epsilon = 0.025$, the contours are shown for every 40 time units. The contour go from black to blue as the tumor evolves.

Figure C.59: Contours of the viable cells at $\phi_V = 0.5$ for ϵ variations for $t = 350$

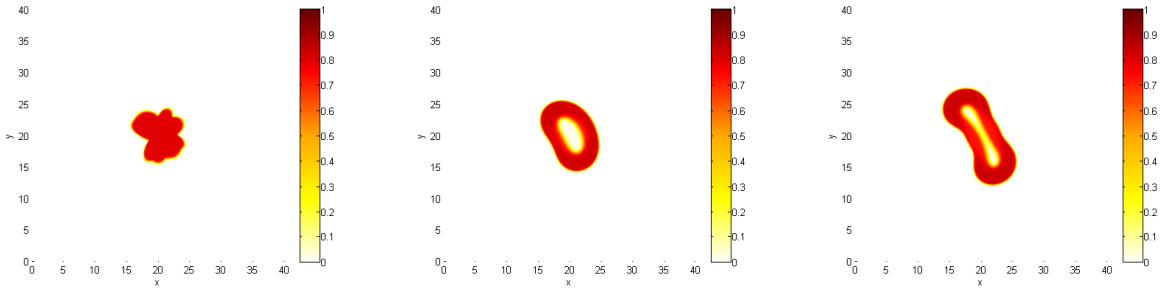

(a) $t = 0$ (b) $t = 50$ (c) $t = 100$

Figure C.60: viable cells of $\epsilon = 0.025$

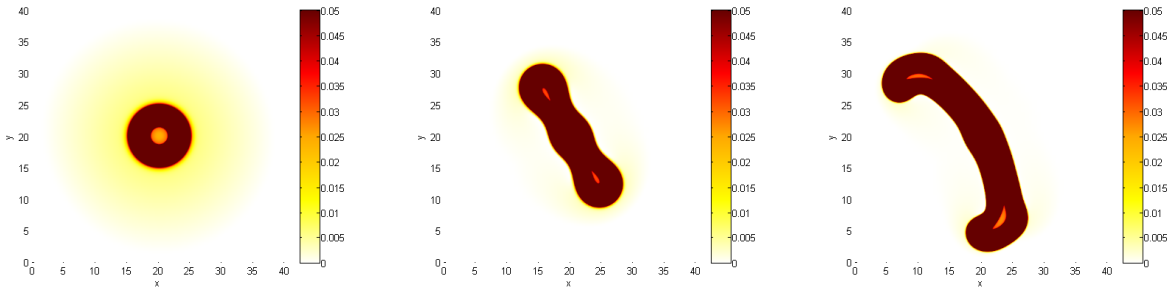

(a) $\epsilon = 0.1$ (b) $\epsilon = 0.05$ (c) $\epsilon = 0.025$

Figure C.61: viable cells shedding for ϵ variations at $t = 350$

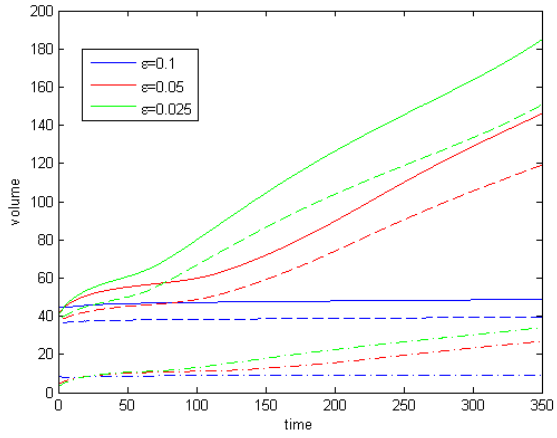

(a) ϕ_V (dashed line), ϕ_D (dash dot line), and ϕ_T (solid line)

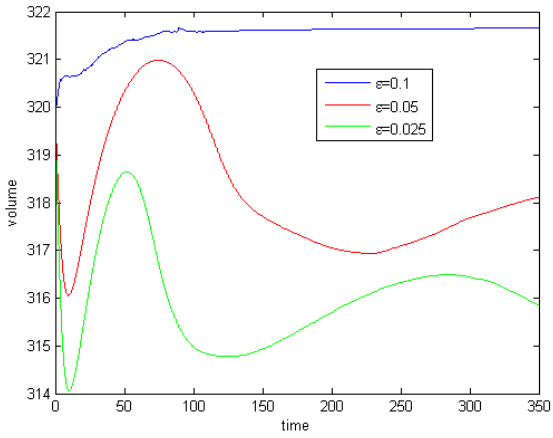

(b) water ϕ_W

Figure C.62: Total volume of ϵ variations

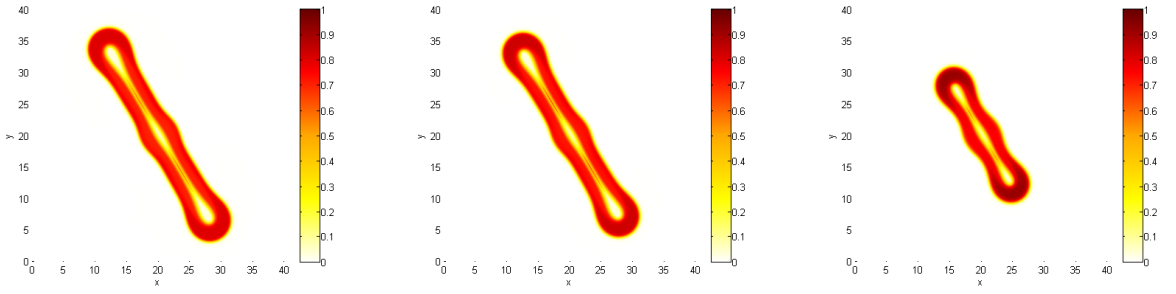

(a) viable cells ϕ_V, $\alpha_{VW} = 2.5$ (b) viable cells ϕ_V, $\alpha_{VW} = 0.25$ (c) viable cells ϕ_V, $\alpha_{VW} = 0.025$

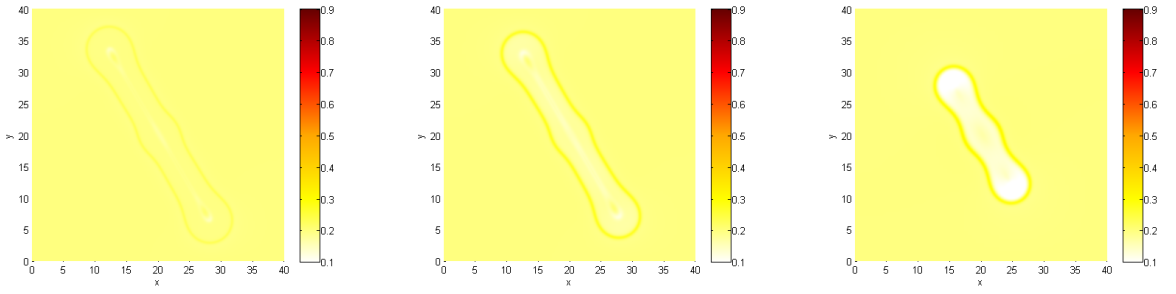

(d) water ϕ_W, $\alpha_{VW} = 2.5$ (e) water ϕ_W, $\alpha_{VW} = 0.25$ (f) water ϕ_W, $\alpha_{VW} = 0.025$

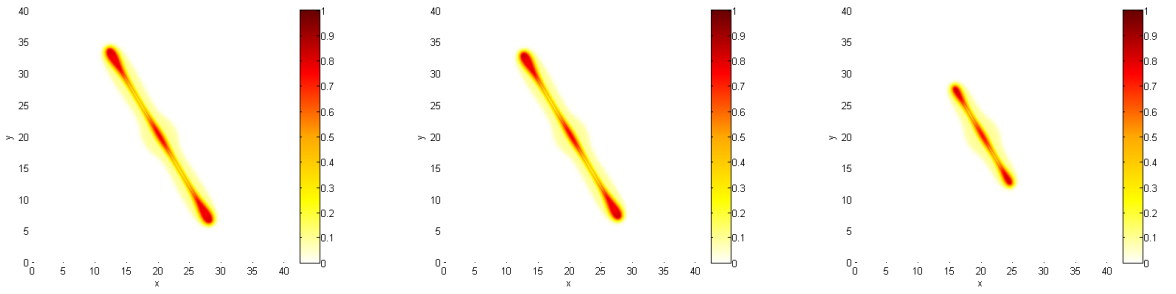

(g) dead cells ϕ_D, $\alpha_{VW} = 2.5$ (h) dead cells ϕ_D, $\alpha_{VW} = 0.25$ (i) dead cells ϕ_D, $\alpha_{VW} = 0.025$

Figure C.63: cell types of α_{VW} variations at $t = 400$

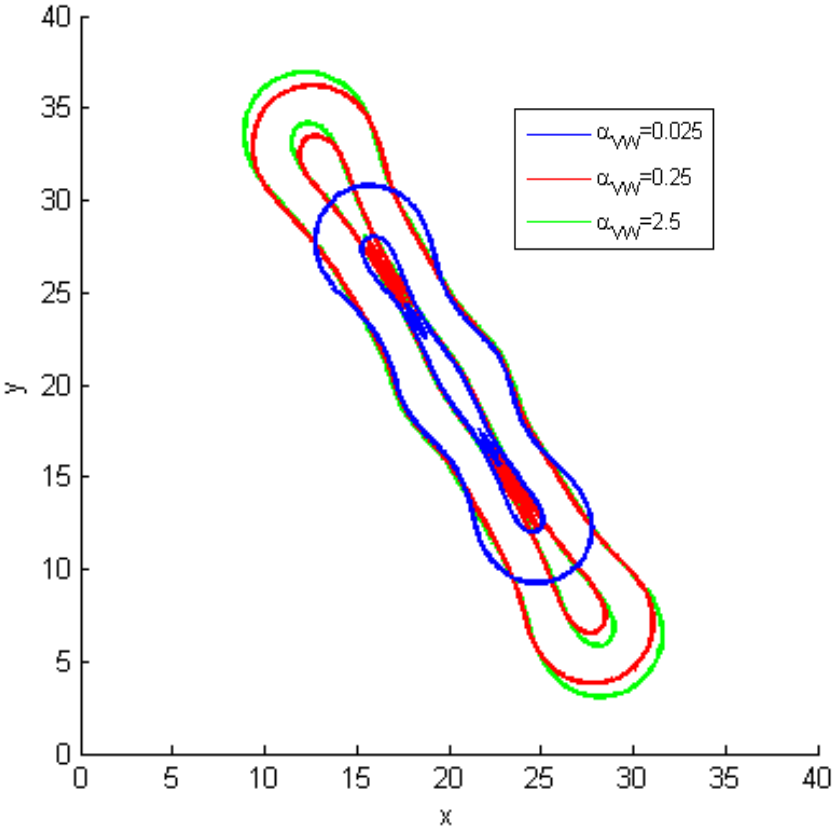

Figure C.64: Contours of the viable cells at $\phi_V = 0.5$ for α_{VW} variations

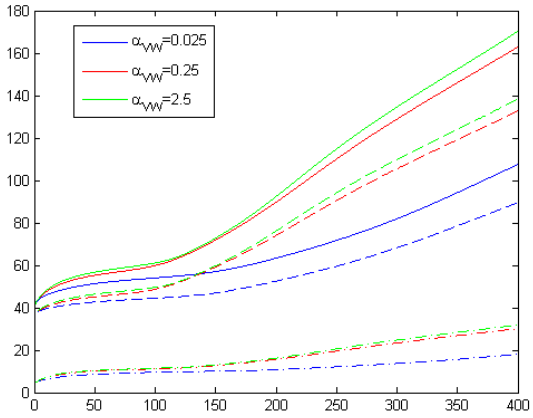

(a) ϕ_V (dashed line), ϕ_D (dash dot line), and ϕ_T (solid line)

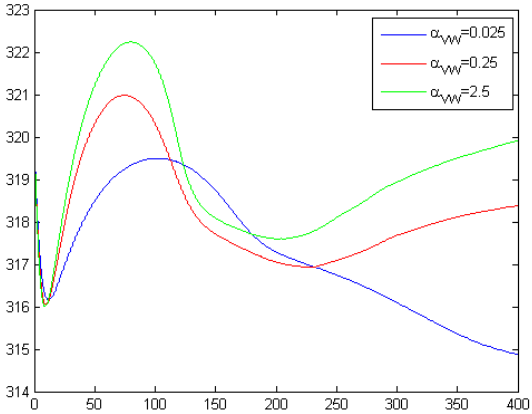

(b) water ϕ_W

Figure C.65: Total volume of α_{VW} variations

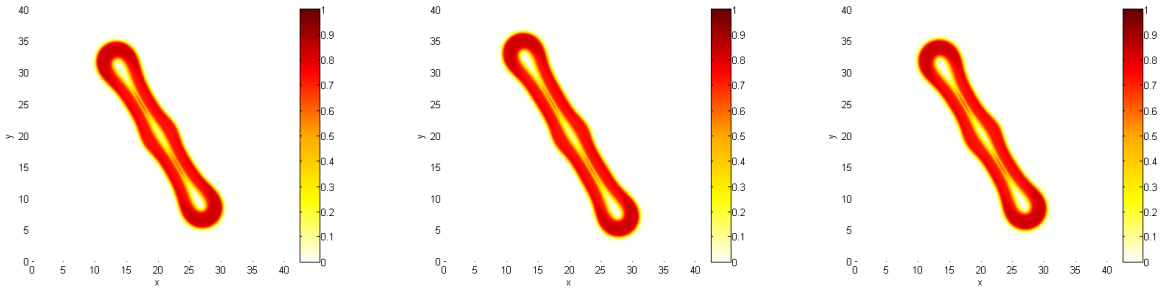

(a) viable cells ϕ_V, $\alpha_{WH} = 2.5$ (b) viable cells ϕ_V, $\alpha_{WH} = 0.25$ (c) viable cells ϕ_V, $\alpha_{WH} = 0.025$

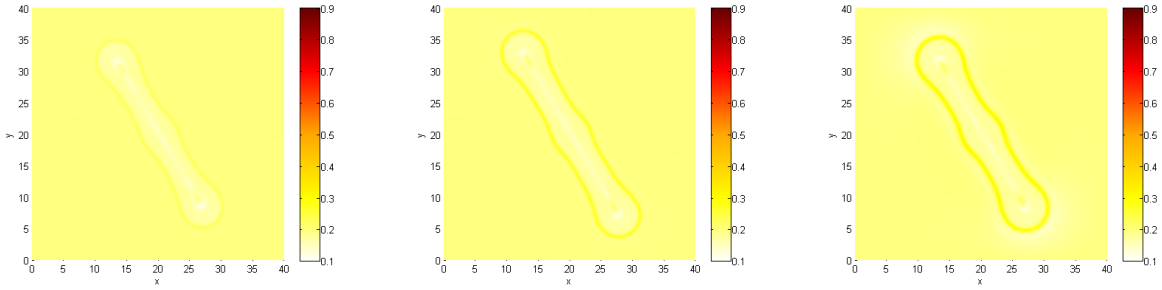

(d) water ϕ_W, $\alpha_{WH} = 2.5$ (e) water ϕ_W, $\alpha_{WH} = 0.25$ (f) water ϕ_W, $\alpha_{WH} = 0.025$

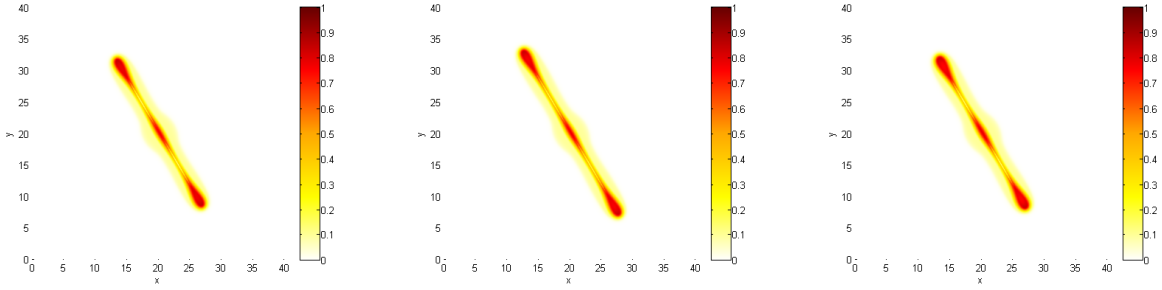

(g) dead cells ϕ_D, $\alpha_{WH} = 2.5$ (h) dead cells ϕ_D, $\alpha_{WH} = 0.25$ (i) dead cells ϕ_D, $\alpha_{WH} = 0.025$

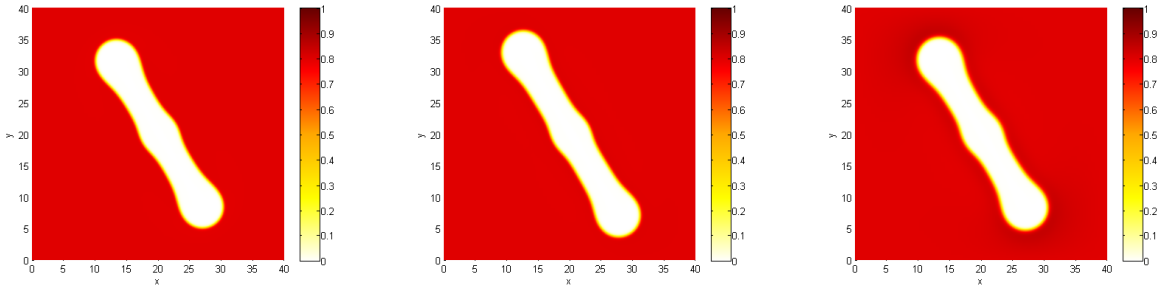

(j) host ϕ_H, $\alpha_{WH} = 2.5$ (k) host ϕ_H, $\alpha_{WH} = 0.25$ (l) host ϕ_H, $\alpha_{WH} = 0.025$

Figure C.66: cell types of α_{WH} variations at $t = 400$

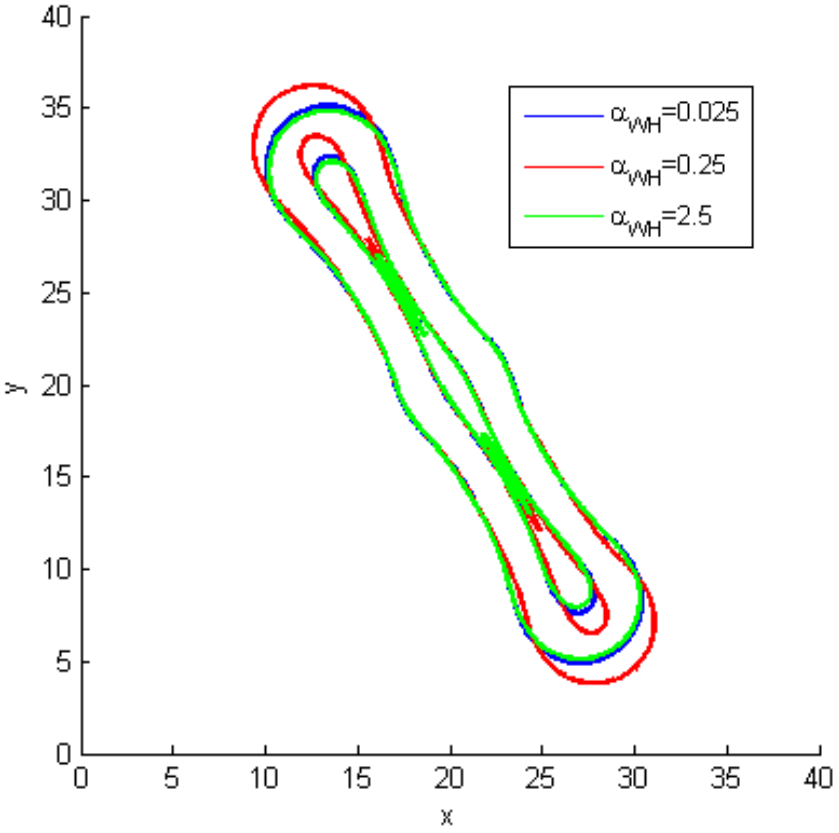

Figure C.67: Contours of the viable cells at $\phi_V = 0.5$ for α_{WH} variations

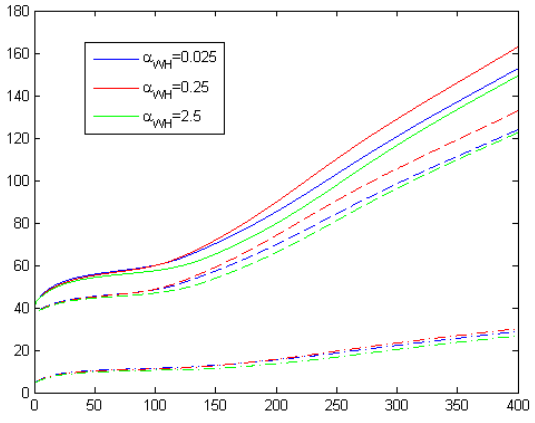

(a) ϕ_V (dashed line), ϕ_D (dash dot line), and ϕ_T (solid line)

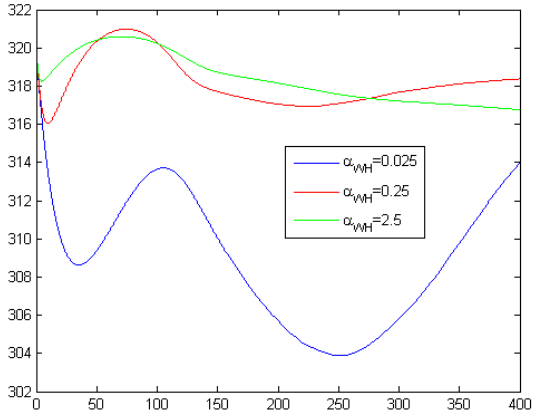

(b) water ϕ_W

Figure C.68: Total volume of α_{WH} variations

Appendix D

Symmetric Tumor with Stem Cells Parameter Study Slides

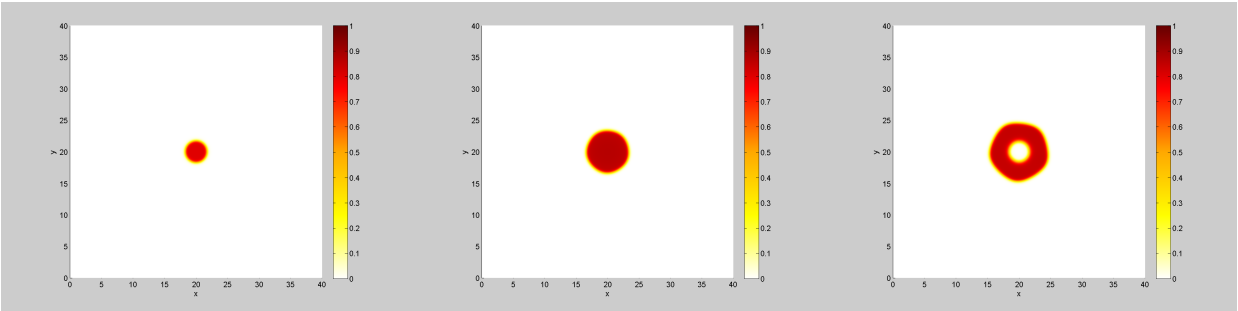

(a) $t = 0$ (b) $t = 20$ (c) $t = 40$

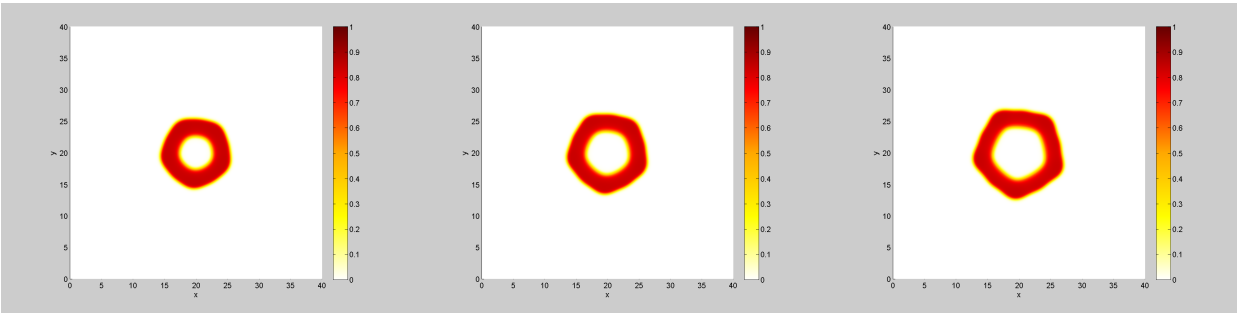

(d) $t = 60$ (e) $t = 80$ (f) $t = 100$

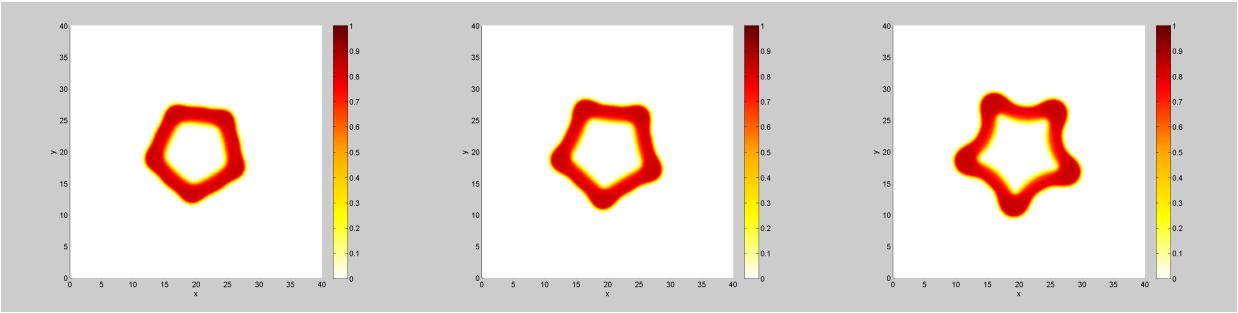

(g) $t = 120$ (h) $t = 140$ (i) $t = 160$

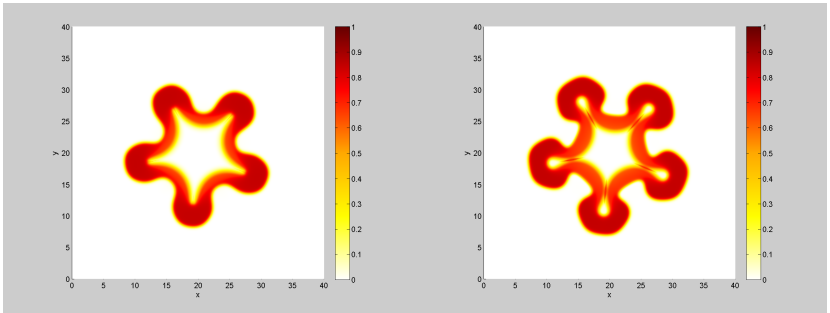

(j) $t = 180$ (k) $t = 200$

Figure D.1: viable cells ϕ_V for the base case

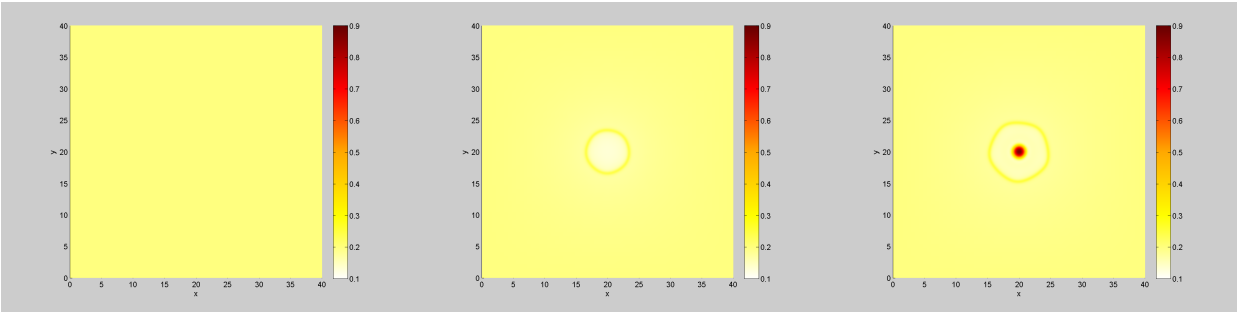

(a) $t = 0$ (b) $t = 20$ (c) $t = 40$

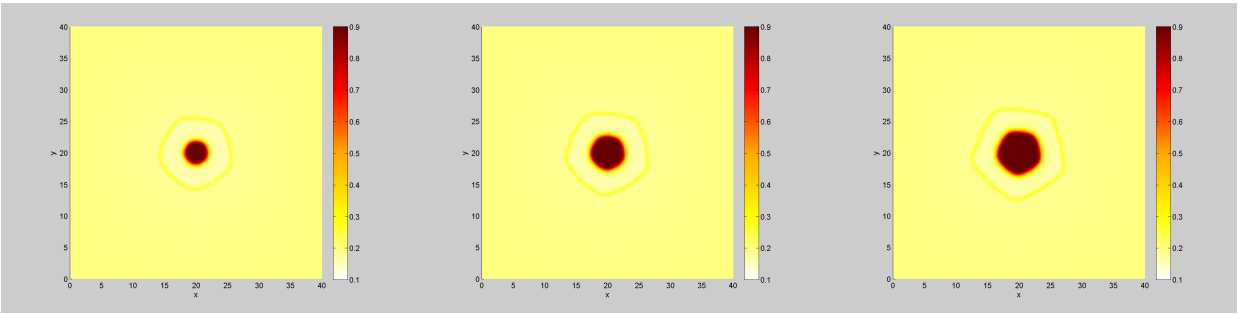

(d) $t = 60$ (e) $t = 80$ (f) $t = 100$

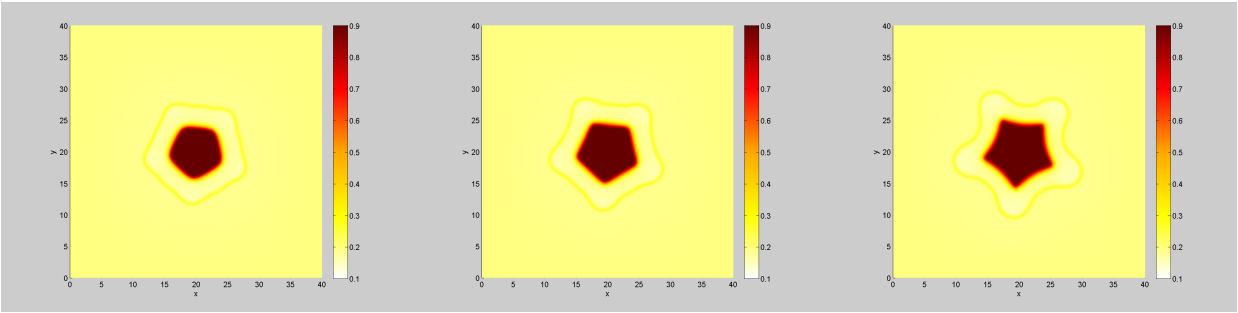

(g) $t = 120$ (h) $t = 140$ (i) $t = 160$

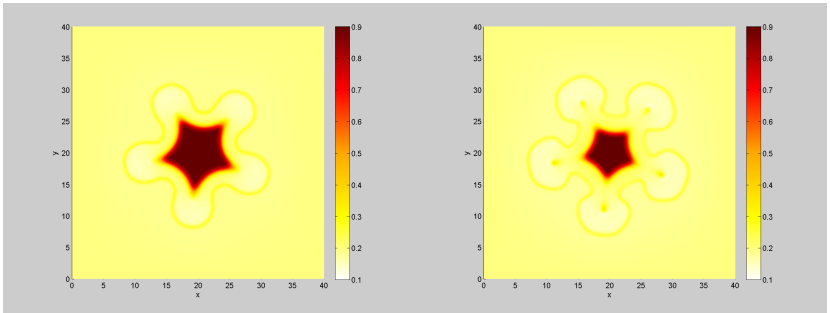

(j) $t = 180$ (k) $t = 200$

Figure D.2: water ϕ_W for the base case

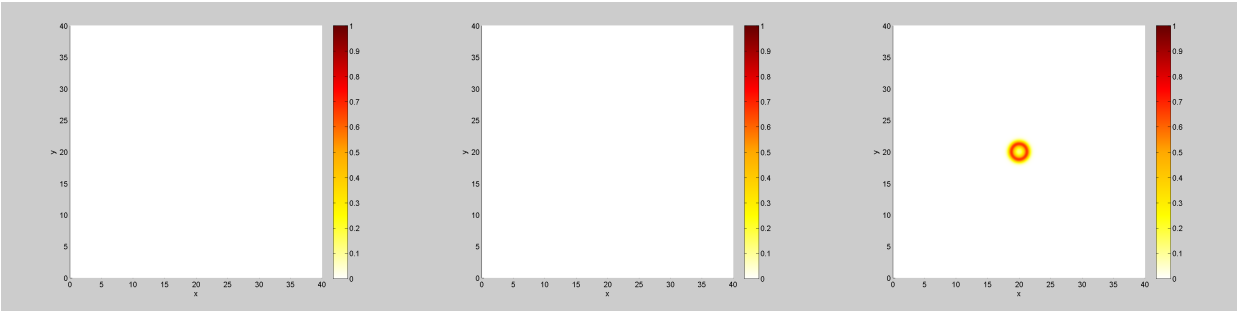

(a) $t = 0$ (b) $t = 20$ (c) $t = 40$

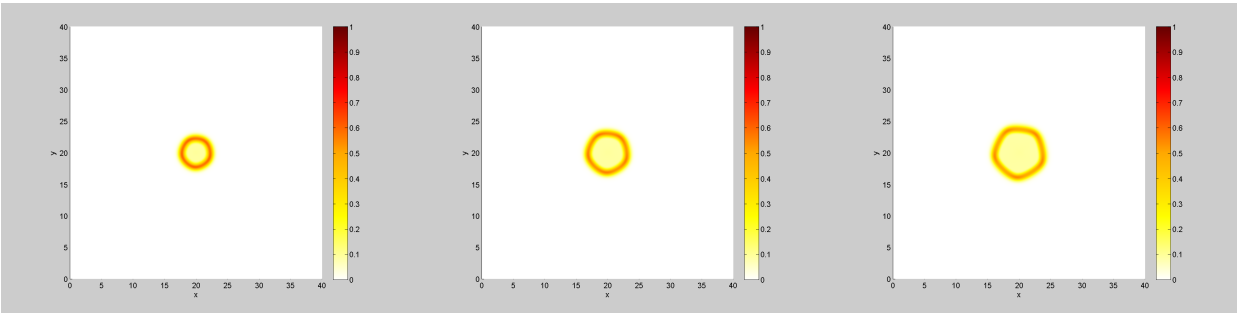

(d) $t = 60$ (e) $t = 80$ (f) $t = 100$

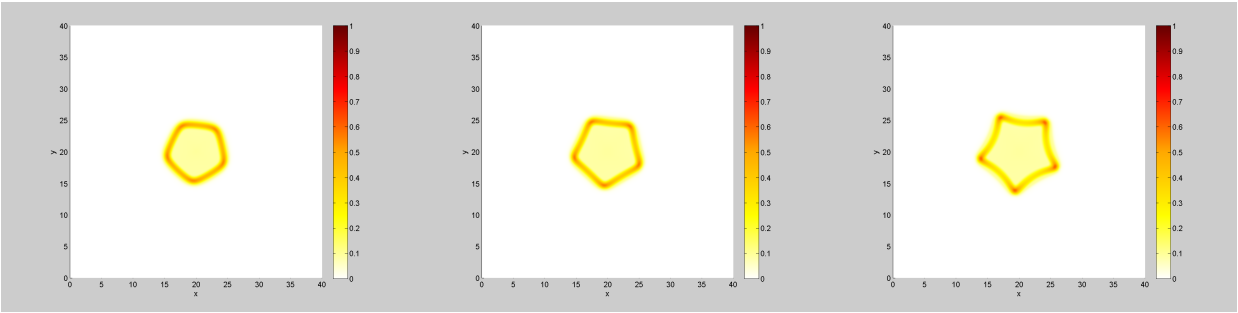

(g) $t = 120$ (h) $t = 140$ (i) $t = 160$

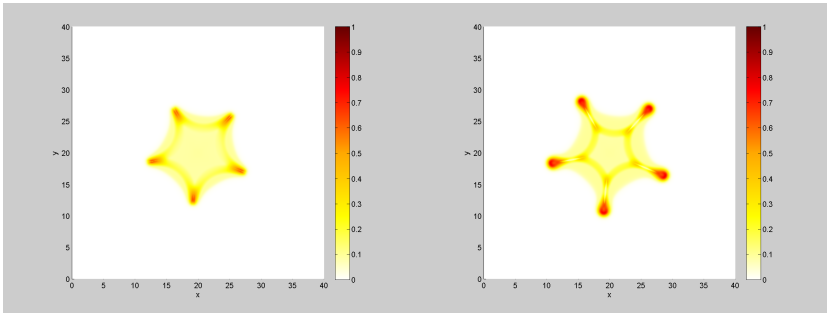

(j) $t = 180$ (k) $t = 200$

Figure D.3: dead cells ϕ_D for the base case

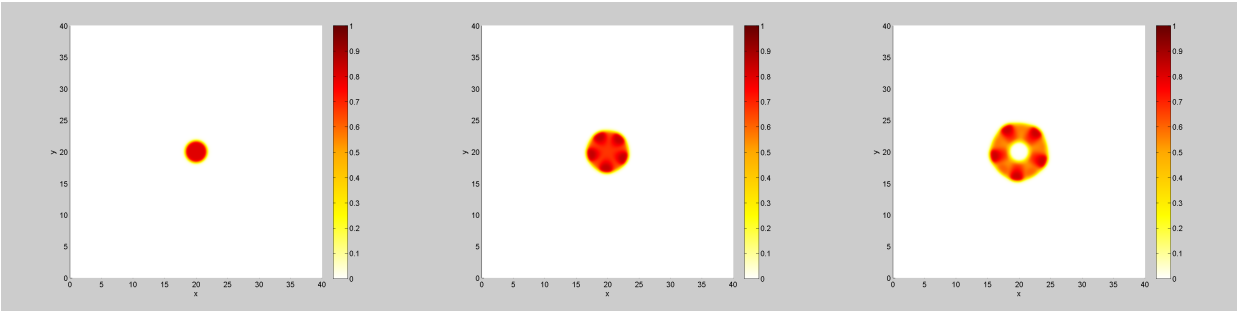

(a) $t = 0$ (b) $t = 20$ (c) $t = 40$

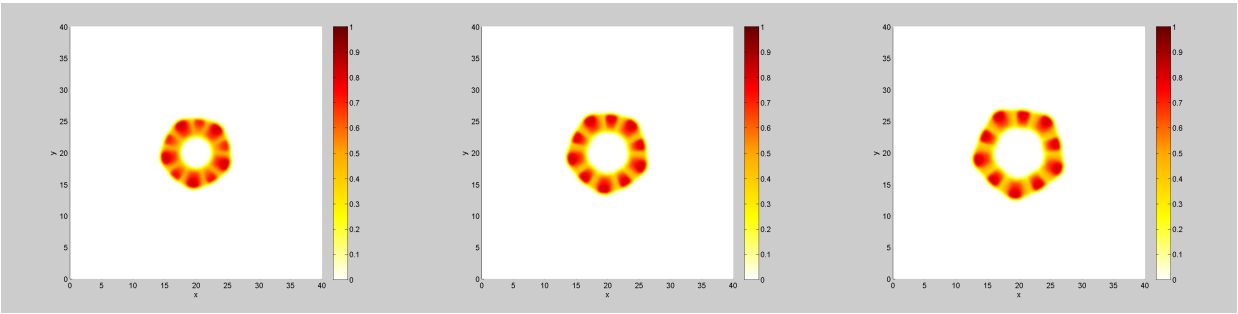

(d) $t = 60$ (e) $t = 80$ (f) $t = 100$

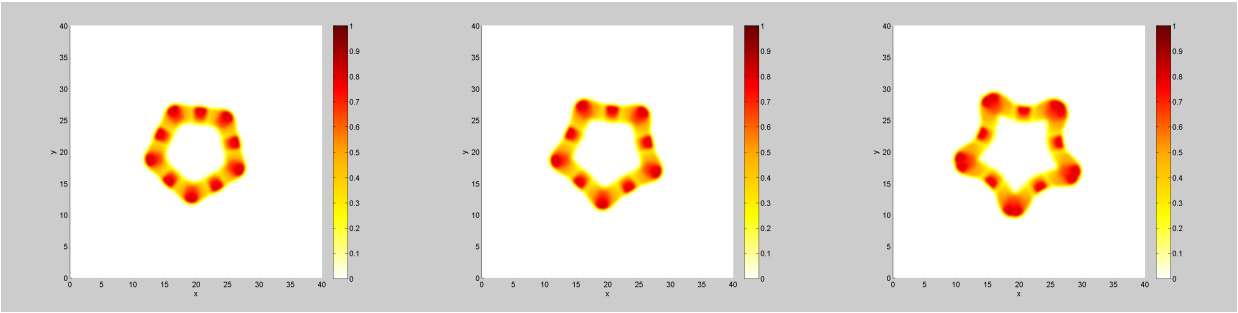

(g) $t = 120$ (h) $t = 140$ (i) $t = 160$

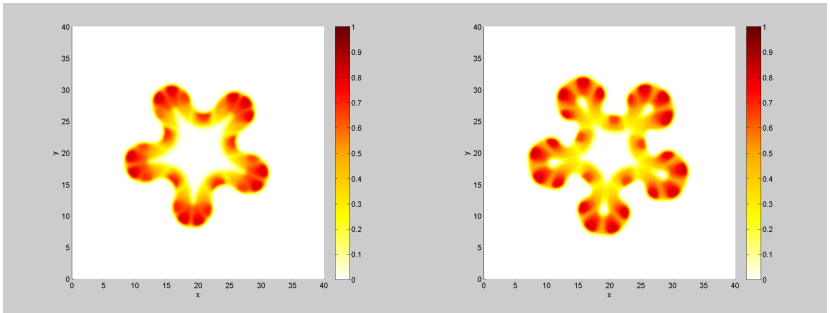

(j) $t = 180$ (k) $t = 200$

Figure D.4: stem cells ϕ_{SC} for the base case

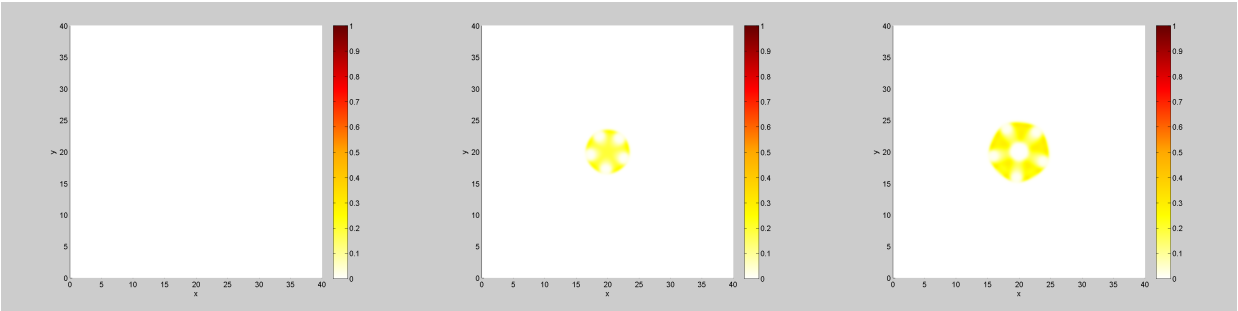

(a) $t = 0$ (b) $t = 20$ (c) $t = 40$

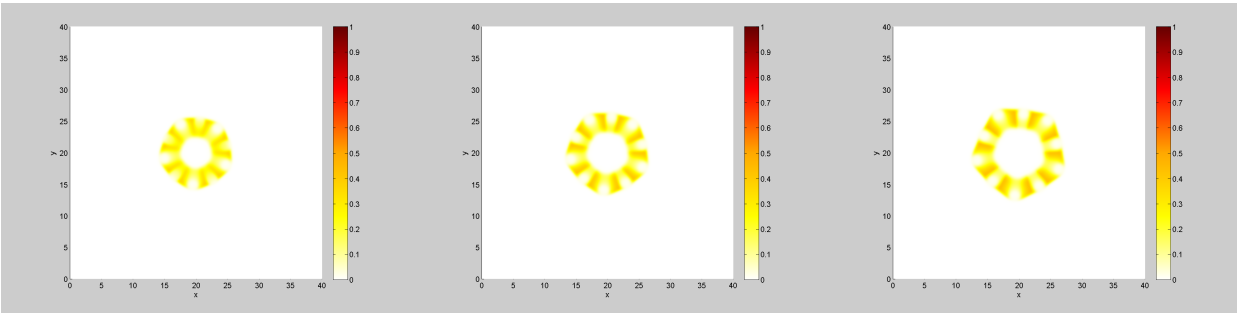

(d) $t = 60$ (e) $t = 80$ (f) $t = 100$

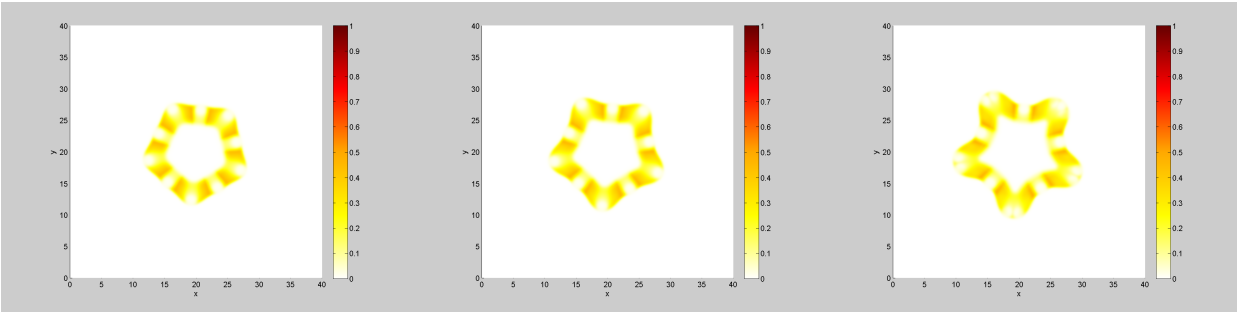

(g) $t = 120$ (h) $t = 140$ (i) $t = 160$

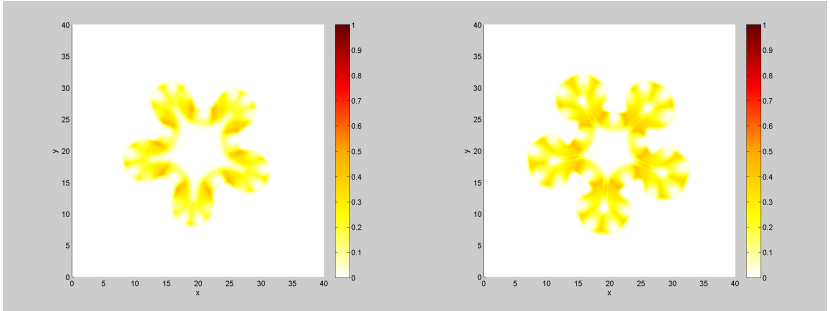

(j) $t = 180$ (k) $t = 200$

Figure D.5: terminal cells ϕ_{TC} for the base case

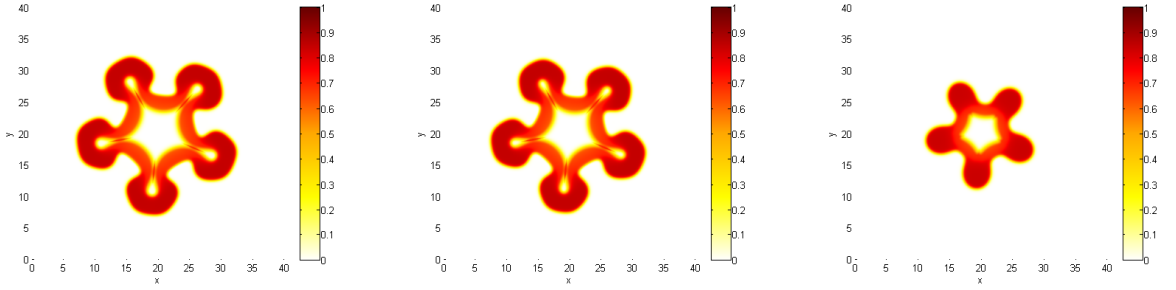

(a) viable cells ϕ_V, $\Phi = 0.01$ (b) viable cells ϕ_V, $\Phi = 0.1$ (c) viable cells ϕ_V, $\Phi = 0.5$

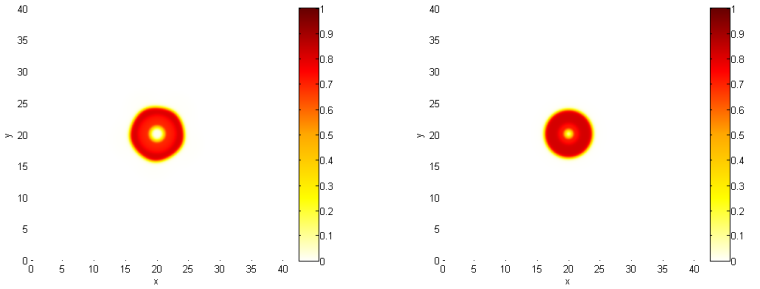

(d) viable cells ϕ_V, $\Phi = 1.0$ (e) viable cells ϕ_V, $\Phi = 10.0$

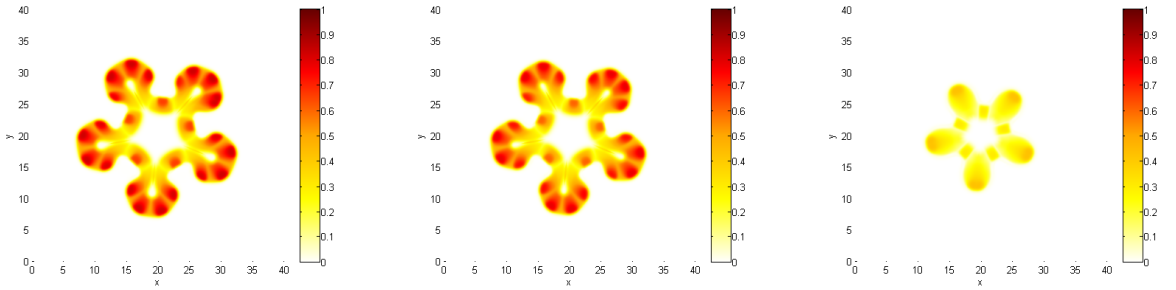

(f) stem cells ϕ_{SC}, $\Phi = 0.01$ (g) stem cells ϕ_{SC}, $\Phi = 0.1$ (h) stem cells ϕ_{SC}, $\Phi = 0.5$

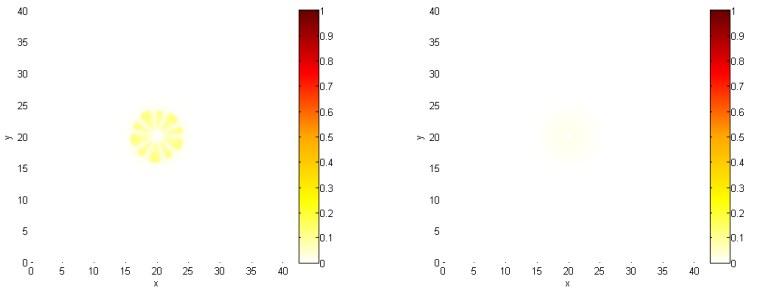

(i) stem cells ϕ_{SC}, $\Phi = 1.0$ (j) stem cells ϕ_{SC}, $\Phi = 10.0$

Figure D.6: viable cells and stems cells for Φ variations at $t = 200$

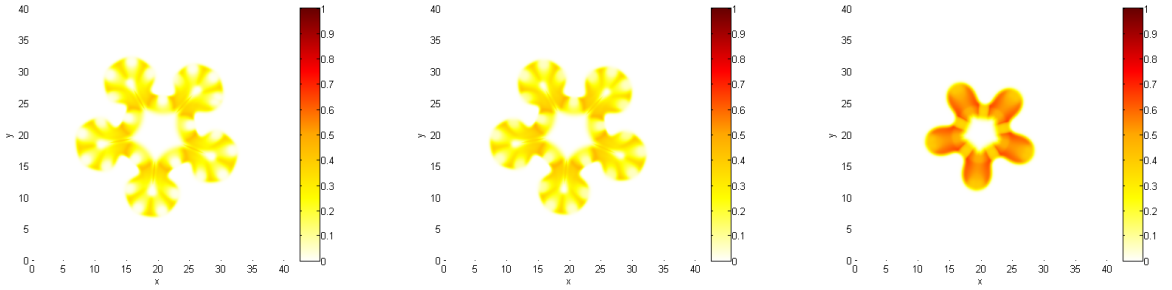

(a) terminal cells ϕ_{TC}, $\Phi = 0.01$ (b) terminal cells ϕ_{TC}, $\Phi = 0.1$ (c) terminal cells ϕ_{TC}, $\Phi = 0.5$

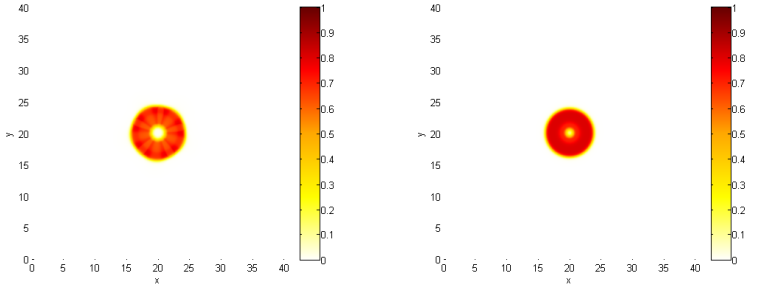

(d) terminal cells ϕ_{TC}, $\Phi = 1.0$ (e) terminal cells ϕ_{TC}, $\Phi = 10.0$

Figure D.7: terminal cells for Φ variations at $t = 200$

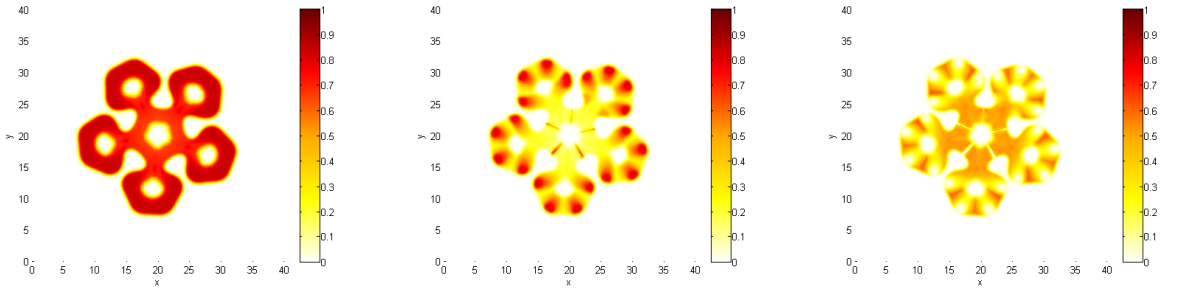

(a) viable cells ϕ_V, $\xi = 25$ (b) stem cells ϕ_{SC}, $\xi = 25$ (c) terminal cells ϕ_{TC}, $\xi = 25$

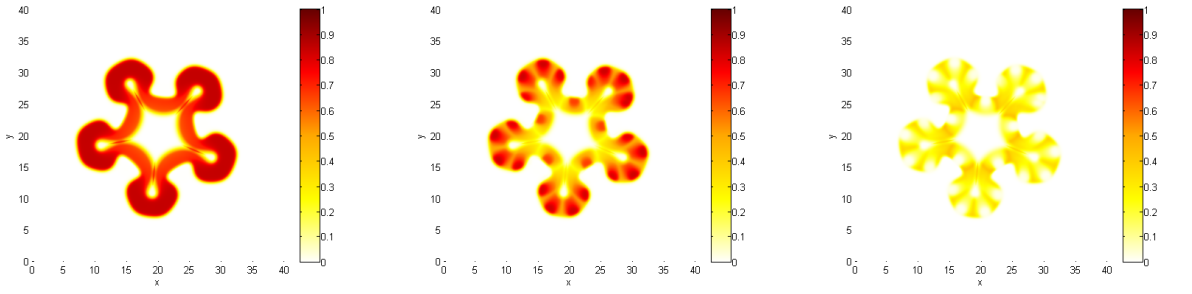

(d) viable cells ϕ_V, $\xi = 50$ (e) stem cells ϕ_{SC}, $\xi = 50$ (f) terminal cells ϕ_{TC}, $\xi = 50$

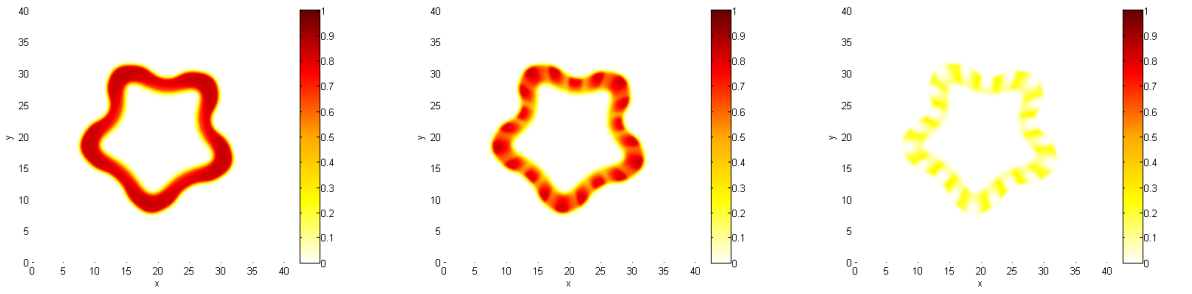

(g) viable cells ϕ_V, $\xi = 100$ (h) stem cells ϕ_{SC}, $\xi = 100$ (i) terminal cells ϕ_{TC}, $\xi = 100$

Figure D.8: viable cell species for ξ variations at $t = 200$

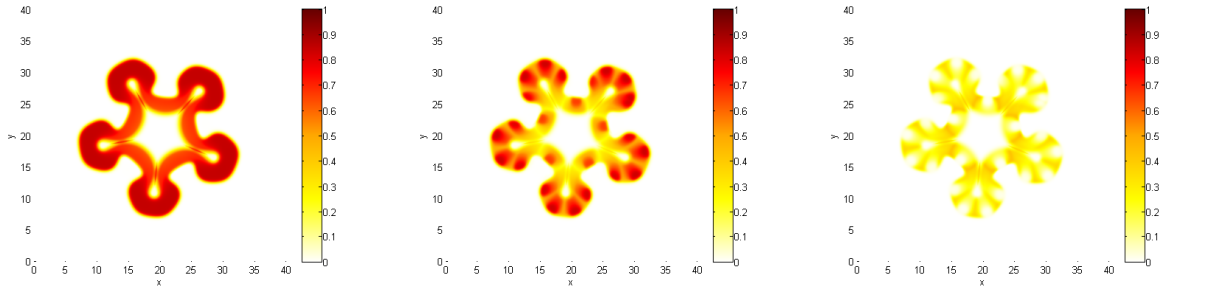

(a) viable cells ϕ_V, $M_V = 10$ (b) stem cells ϕ_{SC}, $M_V = 10$ (c) terminal cells ϕ_{TC}, $M_V = 10$

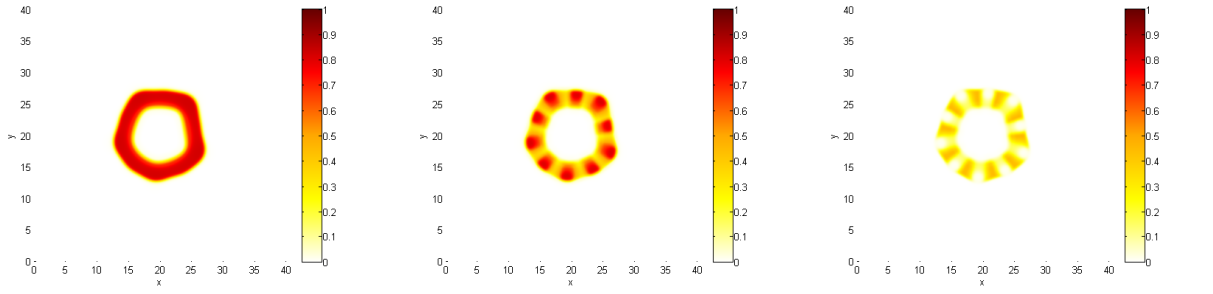

(d) viable cells ϕ_V, $M_V = 25$ (e) stem cells ϕ_{SC}, $M_V = 25$ (f) terminal cells ϕ_{TC}, $M_V = 25$

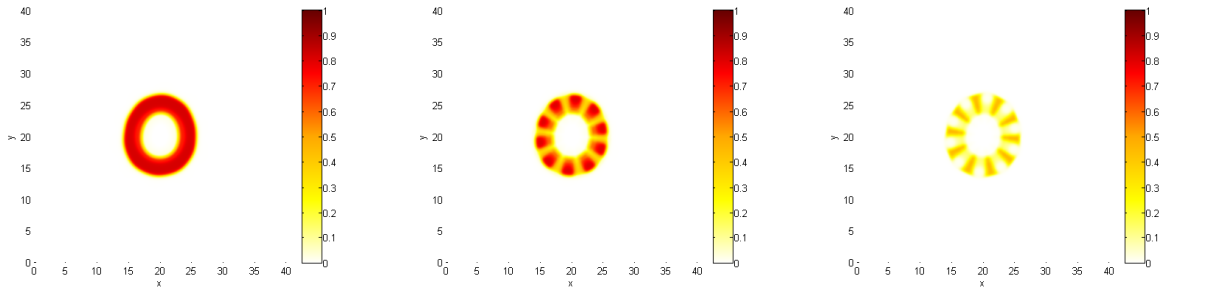

(g) viable cells ϕ_V, $M_V = 50$ (h) stem cells ϕ_{SC}, $M_V = 50$ (i) terminal cells ϕ_{TC}, $M_V = 50$

Figure D.9: viable cell species for M_V variations at $t = 200$

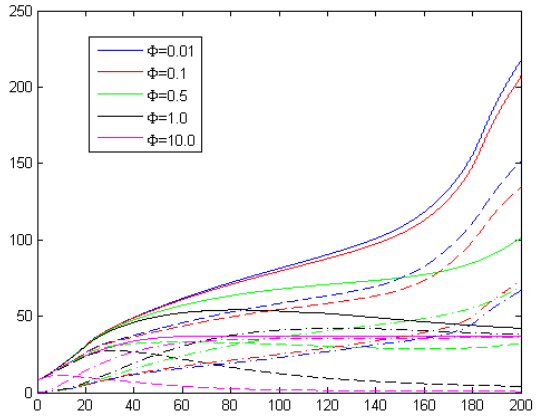

(a) Total volume of the viable cell species, ϕ_V (solid), ϕ_{SC} (dashed), ϕ_{TC} (dash-dotted)

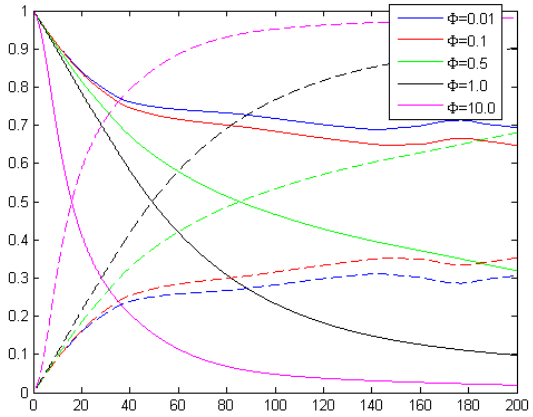

(b) stem cell and terminal cell percentage of the viable cells, ϕ_{SC} (solid), ϕ_{TC} (dashed)

Figure D.10: Φ variations

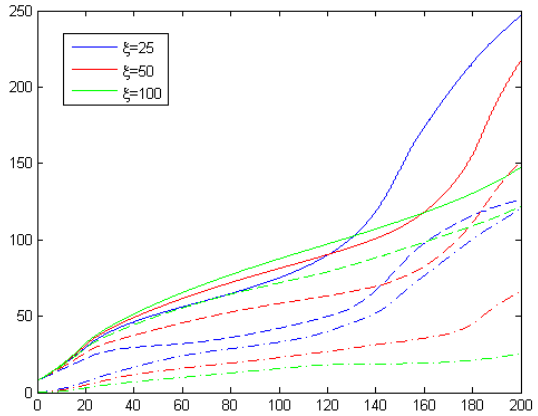

(a) Total volume of the viable cell species, ϕ_V (solid), ϕ_{SC} (dashed), ϕ_{TC} (dash-dotted)

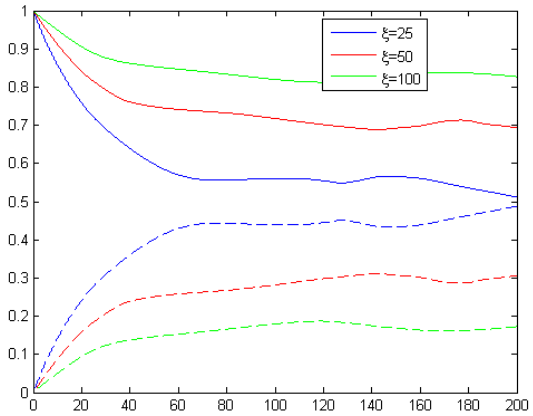

(b) stem cell and terminal cell percentage of the viable cells, ϕ_{SC} (solid), ϕ_{TC} (dashed)

Figure D.11: ξ variations

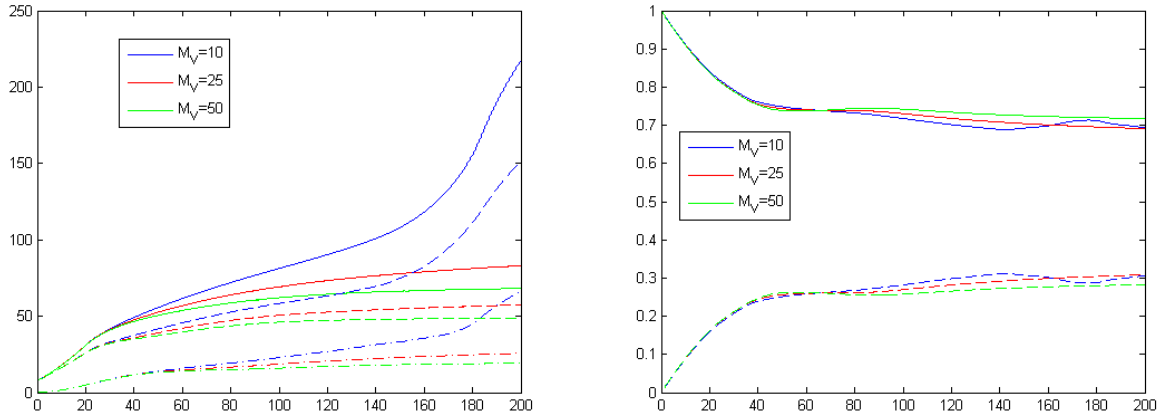

(a) Total volume of the viable cell species, ϕ_V (solid), ϕ_{SC} (dashed), ϕ_{TC} (dash-dotted)

(b) stem cell and terminal cell percentage of the viable cells, ϕ_{SC} (solid), ϕ_{TC} (dashed)

Figure D.12: M_V variations